BSD-TR-67-232

852 -2-Q

Copy_____

THE UNIVERSITY OF MICHIGAN

COLLEGE OF ENGINEERING
DEPARTMENT OF ELECTRICAL ENGINEERING
Radiation Laboratory

Investigation of Re-Entry Vehicle Surface Fields (U)

Quarterly Report No. 2

18 March-18 June 1967

By

R. F. GOODRICH, B. A. HARRISON, R. E. KLEINMAN
E. F. KNOTT and V. H. WESTON

July 1967

8525-2-Q = RL-2181

Contract F 04694-67-C-0055

Distribution Statement: In addition to security requirements which apply to this document and must be met, it may be further distributed by the holder only with specific prior approval of SAMSO, SMSDI, Air Force Station, Los Angeles, CA 90045

Contract With:

Hq. Space and Missile Systems Organization
Air Force Systems Command
Norton Air Force Base, California 92409

Administered through:

OFFICE OF RESEARCH ADMINISTRATION • ANN ARBOR

THE UNIVERSITY OF MICHIGAN

8525-2-Q

BSD-TR-67-232

Investigation of Re-entry Vehicle Surface Fields (U)

Quarterly Report No. 2
18 March - 18 June 1967

F 04694 67 C 0055

By

R. F. Goodrich, B. A. Harrison, R. E. Kleinman
E. F. Knott and V. H. Weston

July 1967

Prepared for

HQ, SPACE AND MISSILES SYSTEMS ORGANIZATION
AIR FORCE SYSTEMS COMMAND
NORTON AFB, CALIFORNIA

In addition to security requirements which apply to this document and must be met, it may be further distributed by the holder only with the specific prior approval of SAMSO, SMSDI, Air Force Station, Los Angeles, California 90045

——— THE UNIVERSITY OF MICHIGAN ———

8525-2-Q

FOREWORD

(U) This report, BSD-TR-67-232, was prepared by the Radiation Laboratory of the Department of Electrical Engineering of The University of Michigan under the direction of Dr. Raymond F. Goodrich, Principal Investigator and Burton A. Harrison, Contract Manager. The work was performed under Contract F 04694-67-C-0055, "Investigation of Re-entry Vehicle Surface Fields (SURF)". The work was administered under the direction of the Air Force Headquarters, Space and Missile Systems Organization, Norton Air Force Base, California 92409, by Capt. J. Wheatley, SMYSP, and was monitored by Mr. H.J. Katzman of the Aerospace Corporation.

(U) The studies presented herein cover the period 18 March 1967 through 18 June 1967.

(U) In addition to security requirements which must be met, this document is subject to special export controls and each transmittal to foreign governments or foreign nationals may be made only with prior approval of SAMSO, SMSDI, Air Force Station, Los Angeles, CA 90045.

(U) Information in this report is embargoed under the Department of State International Traffic in Arms Regulations. This report may be released to Foreign governments by departments or agencies of the U.S. Government subject to approval of Hq. Space and Missile Systems Organization (SMSDI), Air Forse Station, Los Angeles, Calif., 90045 or higher authority within the Department of the Air Force. Private individuals or firms require a Department of State export license.

(U) The publication of this report does not constitute Air Force approval of the report's findings or conclusions. It is published only for the exchange and stimulation of ideas.

SAMSO Approving Authority
William J. Schlerf BSYDR
Contracting Officer

ABSTRACT

(S) This is the Second Quarterly Report on Contract F 04694-67-C-0055 and covers the period 18 March to 18 June 1967. The report discusses work in progress on Project SURF and on a related short pulse investigation. Project SURF is a continuing investigation of the radar cross section of metallic cone-sphere shaped re-entry bodies and the effect on radar cross section of absorber and ablative coatings, antenna and rocket nozzle perturbations, changing the shape of the rear spherical termination, and of the plasma re-entry environment. The objective of the short pulse study is the determination of methods of modifying the short pulse signature of cone-sphere shaped re-entry bodies and of decoys. SURF investigations make use of experimental measurements in surface field and backscatter ranges to aid in the analytical formulation of mathematical expressions for the computation of radar cross section. A computer program for determining the radar cross section of any rotationally symmetric body is being developed.

SECRET

TABLE OF CONTENTS

Table of Contents (Cont'd)

I

INTRODUCTION

(S)   This is the Second Quarterly Report on Contract F 04694-67-C-0055, "Investigation of Re-entry Vehicle Surface Fields (Backscatter) (SURF)". It covers the period 18 March to 18 June 1967. Work under this program includes an investigation of methods to compute the radar cross section of cone-sphere shaped re-entry vehicles and a method for changing the short pulse discrimination characteristics of such re-entry vehicles and their decoys. These studies are monitored by Capt. J. Wheatley for the Space and Missile Systems Organization and by Mr. H. J. Katzman for the Aerospace Corporation.

(S)   The approach adopted in the SURF investigation makes use of experimental measurements of the surface fields induced on various scale models of re-entry bodies and related shapes to aid in the construction of a theory to explain radar scattering behavior and the formulation of mathematical expressions for the computation of radar cross section. In addition to the surface field measurements, backscatter measurements are relied on to furnish substantiation of the theory being developed or to guide the investigation in areas wherein surface field measurements alone do not provide adequate data. A digital computer program is being developed to aid in the study of cases of oblique incidence on the target and to provide supplementary data in cases where the very low backscatter from the target is difficult to measure accurately.

(S)   The SURF program is a comprehensive attempt to provide radar cross section formulas for such practical situations as may be expected to arise. They include formulas for the following:

(a) The metallic cone-sphere and the cone with non-spherical modifications to the cap.

(b) Modifications of the cone-sphere due to the addition of antennas and rocket nozzles.

(c) The addition of absorbing materials to the cone-sphere surface, and

(d) The effect of the re-entry plasma environment.

(S) Short pulse discrimination methods permit one to distinguish between a warhead and accompanying decoys by a simple numerical count of the pulses returned by each body. The short pulse investigation has been undertaken to determine methods for countering this discrimination method. The investigation in its early stages is principally mathematical so that the basic theory of short pulse scattering can be set forth. It application to re-entry shapes will follow. Experimental data made available by Lincoln Laboratory to the Radiation Laboratory via the Aerospace Corporation will be used as part of this analysis.

(S) During this quarter, surface field experiments were carried forward with measurements on coated objects in which the flushmounted tip and rear antenna were modeled. The measurements furnish data for analysis of both nose-on and oblique radar incidence. The newly installed L-band backscatter system was tested and data was obtained on indented rear models. Construction was begun on additional models for the study of the effect on radar cross section of the radius of curvature of the vehicle where the cone and spherical parts join. The re-entry plasma experiments revealed the need for a deeper study of curved surfaces so that the data to be obtained on cone-spheres could be meaningfully interpreted.

(S) Two principal items of analytical work were completed as part of the SURF theoretical investigation:

(a) The handbook section of the Final Report under Contract AF 04(694)683, dealing with radar cross section formulas for the computation of the radar return from metallic bodies with tip and rear antenna, rocket nozzle, and Mk-12 perturbations was completed.

(b) The comparison of theoretical and measured radar cross sections for re-entry shapes with rear concavity, with a ring type antenna and with a coating has been completed.

This work was done as an Agreement Item suggested at the March 1967 Technical Discussion meeting.

(U) An item of analytical work which continues to provide difficulties is the solution of the mathematical problems leading to the programming of the radar cross section of the rotationally symmetric reentry body. However, a new method is being incorporated in the programming and should provide substantial improvement in accuracy of the results.

II

TASK 2: EXPERIMENTAL INVESTIGATIONS

2.1 Introduction

(S) The surface field measurements and backscatter measurements on cone-sphere like objects continued with emphasis on obtaining data on coated models. In addition, oblique angle of incidence measurements were made on metallic models with annular antenna representations. These measurements are described in the sections which follow. Some preliminary observations are made of the data and the trends which appear. In support of the re-entry plasma environment study, radar cross section measurements and surface field measurements were made on flat plates covered by wire-grid representations of the plasma to determine whether the physical optics analysis for the radar cross section could be justified experimentally.

2.2 Surface Field Measurements for the Study of Flush Mounted Antenna Perturbations on Coated Cone-sphere. (Task 2.1.1 and 2.1.2)

(S) To furnish data to determine the effects of coatings on the surface fields of perturbed cone-sphere models, a series of measurements was carried out on models LSP and LSP. Model LSP, it will be recalled, is a cone-sphere whose tip is isolated from the rest of the object by a lucite spacer, and Model LSH contains a similar spacer just forward of the shadow boundary. The lucite spacers produce the annular discontinuity in the metallic cone-sphere surface which annular antennas would create at the same locations. These models, and plain, unperturbed ones as well, were sheathed in jackets of LS-22, LS-24, and LS-26 absorbing material and the surface fields thereon were measured for ka values of 1.1, 3.0, 5.0 and 8.0, where ka is the electrical circumference, in wavelengths, of the spherical base of the underlying metallic vehicle.

(S) Although the LS-22 coating was less effective than either LS-24 or LS-26 materials, the coatings in general have three effects: 1) they reduce the intensities of the forward and backward traveling waves on the conical portion of

the models, 2) they reduce the amplitude of the creeping wave, and 3) they either suppress or alter the perturbing effects of the lucite spacers underneath the coatings. The effects of the coatings are less dramatic for low than for high values of ka, and we have chosen ka = 5.0 for the purpose of illustration in Figs. 2-1 and 2-2.

(S) In Fig. 2-1 a comparison is drawn between the surface field behavior of the LSH cone-sphere model when bare and when coated with LS-26. The bare object exhibits the characteristic standing wave pattern along the conical surface, whose mean value arises to about the physical optics value of 2.0. Just beyond the join, however, there is a significant jump in intensity due to the spacer (thickness: 0.25 inch) and from there to the antipode the field decays as usual. We note that the amplitude of the standing wave pattern on the cone is substantial, suggesting a strong reflection arises near the join.

(S) When the coating is applied, the strong interference pattern is drastically suppressed in addition to a general depression of the fields which decays steadily as one advances from near the tip to the join. From the join rearward there is evidence of a creeping wave (i.e., the small perturbations) but its magnitude is substantially below that of the bare object. The sharp jump in field intensity near the lucite spacer has been markedly reduced, but a very small perturbation still exists.

(S) The fields shown in Fig. 2-2 are at once different from and similar to those of Fig. 2-1. Here the spacer is located not far from the cone tip and for the uncoated object there is a strong interference pattern between the tip and the spacer. Beyond the spacer, however, the field intensity is identical to that which would be measured on a plain cone-sphere having no spacers or other perturbations. The amplitude of the standing wave pattern is much smaller than that of the LSH Model in Fig. 2-1. When the model is coated,
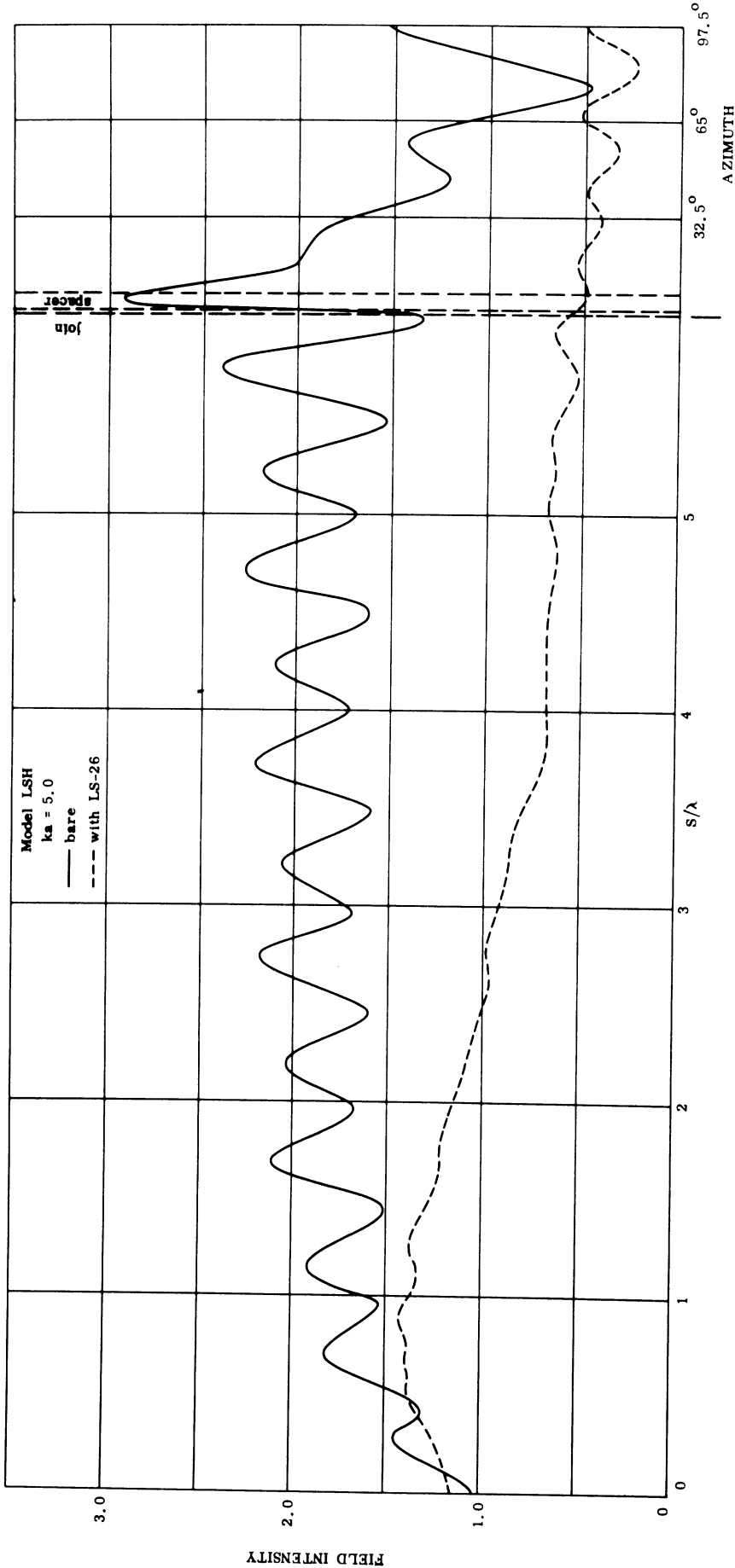
FIG. 2-1: THE ABSORBER COATING SUPPRESSES THE EFFECT OF THE SPACER AS WELL AS THE FIELDS OVER THE ENTIRE BODY.
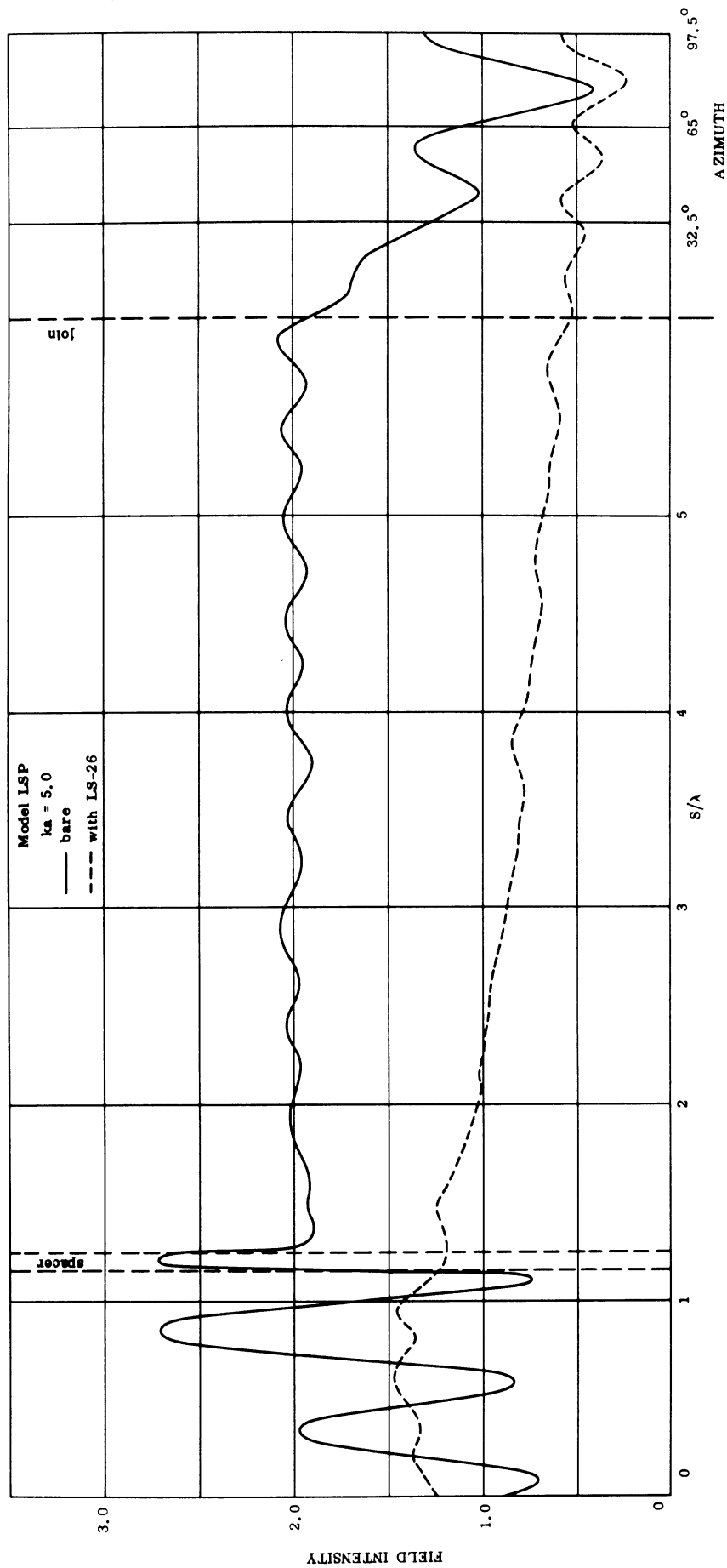
FIG. 2-2: THE LARGE PERTURBATIONS DUE TO THE SPACER HAVE BEEN
REMOVED BY THE ABSORBER COATING.

7

one finds practically the same rate of decay that occured for the LSH model (and a plain cone-sphere) and around the base of the model one can still see the creeping wave. Since there is no spacer near the join for this model, and since we see the same field structure around the back as we saw for the LSH model, we deduce that the small perturbations at the join in Fig. 2-1 were not due to the spacer. In Fig. 2-2 there are distinct wobbles in the fields of the coated model between tip and the spacer, but these are small. We conclude, then, that for the LSP model having the spacer near the tip the absorber coating does not totally remove the effect of the spacer, but that a marked suppression does occur.

(S) In addition to coated object measurements, data have been collected for the bare LSP model under conditions of oblique illumination. The data were obtained for ka values of 3.0 and 5.0 and the angle of incidence was varied from 0 degrees (nose-on) to 82.5 degrees in 7.5 degree intervals. Figures 2-3 through 2-5 are selections of data for incidence angles of 7.5, 45 and 82.5 degrees, respectively. Curves are sketched showing the field intensity on both the lit and shadowed sides and the spacer clearly has a strong effect, even in the shadow. Of interest is the interference pattern for the 82.5 degree angle of incidence, Fig. 2-5. On the lit side, the perturbations are spaced about λ apart, suggesting that on this side a wave travels from tip to join (or conversely); a wave of this kind, when added to the incident wave, produces a period of λ. On the shadowed side, however, the interference pattern shows a period of about $\lambda/2$, suggesting two waves are present, traveling in opposite directions. In the shadow, then, there is apparently a wave which travels from tip to join and another which runs from join to tip.

Model LSP
ka = 5.0
θ = 7½°
——— illuminated side
— — — shadow side

join

spacer

FIELD INTENSITY

AZIMUTH

s/λ

FIG. 2-3: OBLIQUE ANGLE INCIDENCE DATA FOR MODEL LSP; angle of incidence = 7.5°.
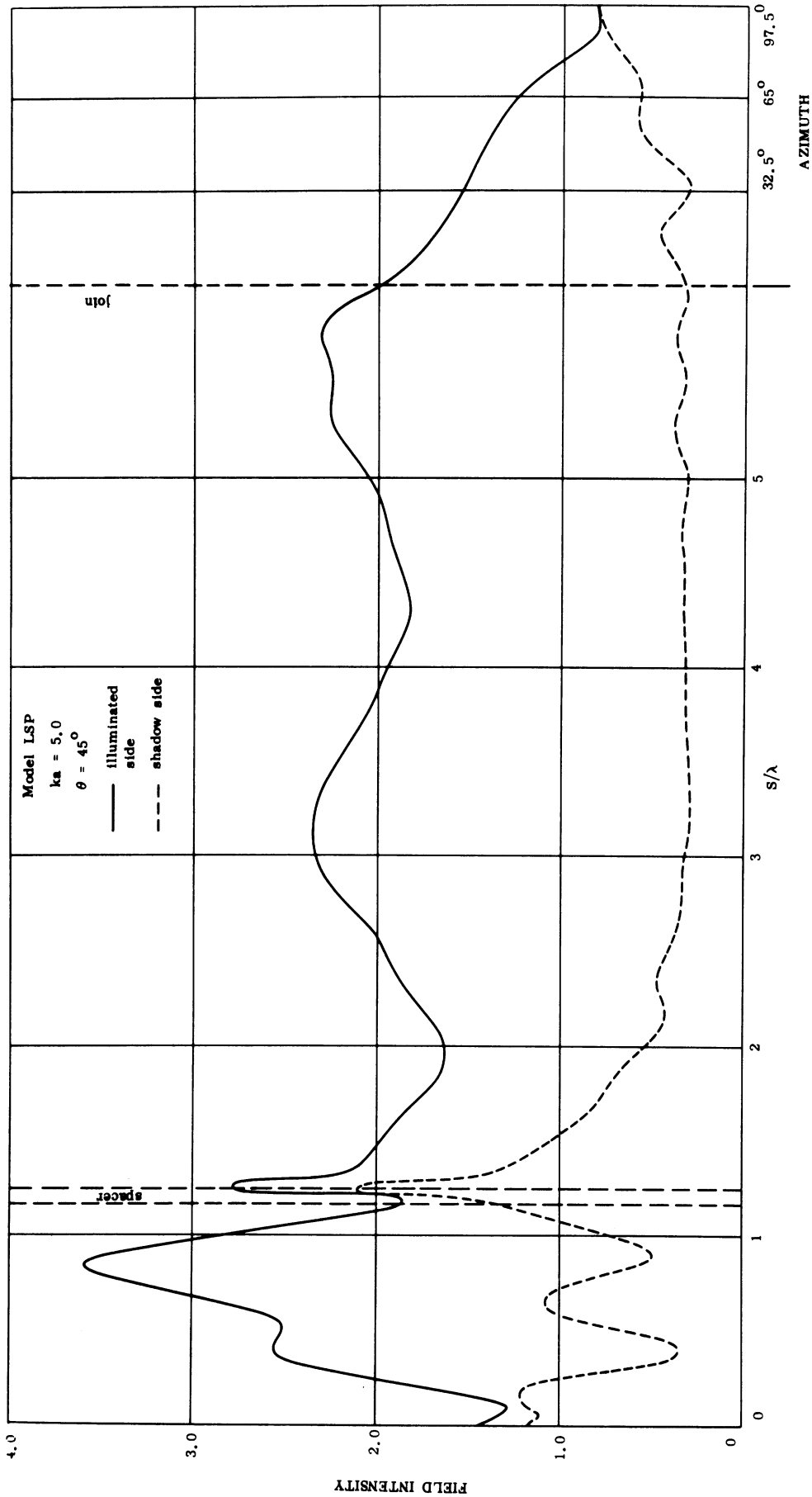
FIG. 2-4: OBLIQUE ANGLE INCIDENCE DATA FOR MODEL LSP; angle of incidence = 45°.

Model LSP

ka = 5.0

$\theta = 82.5^{o}$
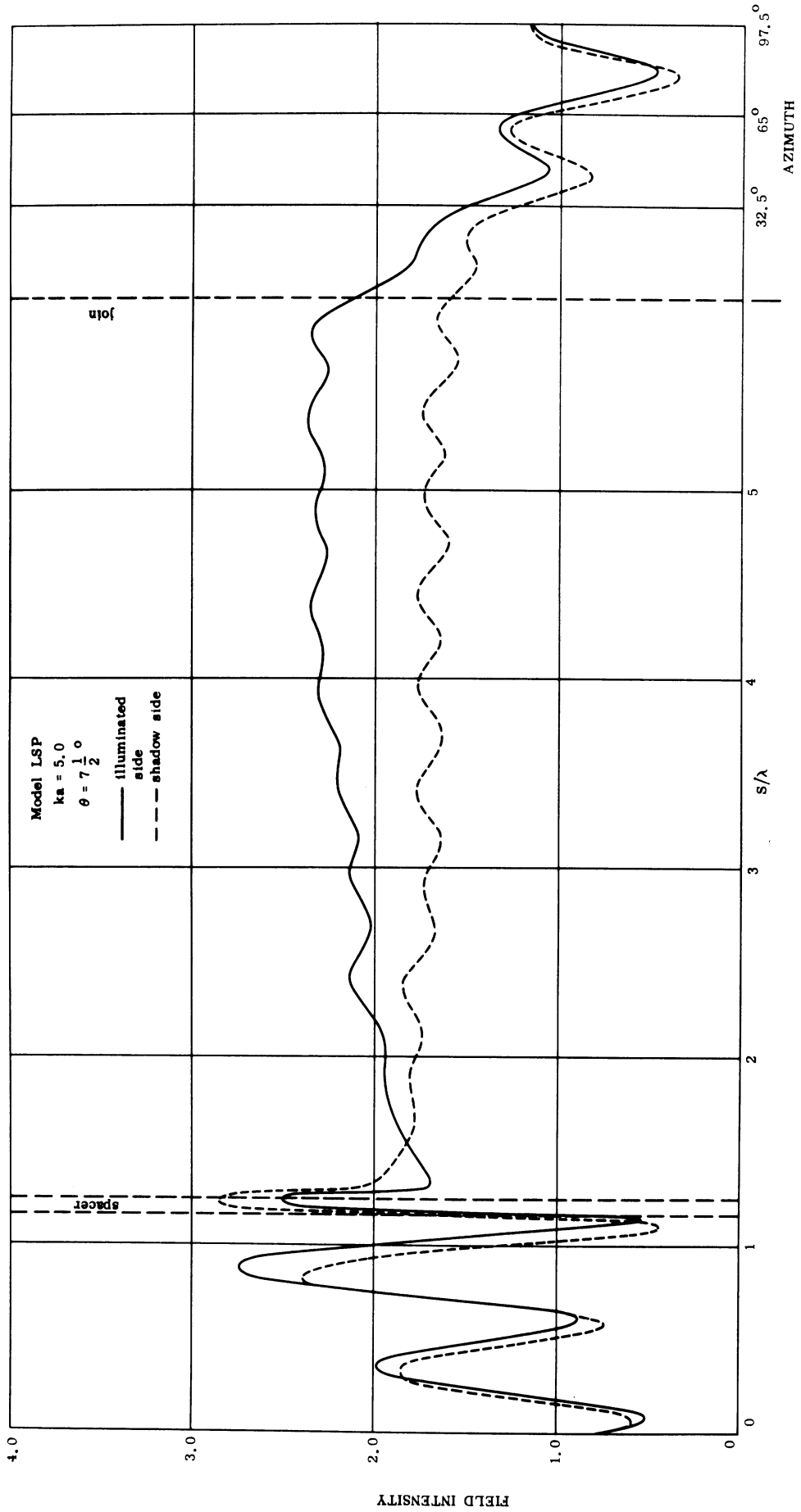
—— illuminated side

– – –shadow side

join

spacer

FIELD INTENSITY
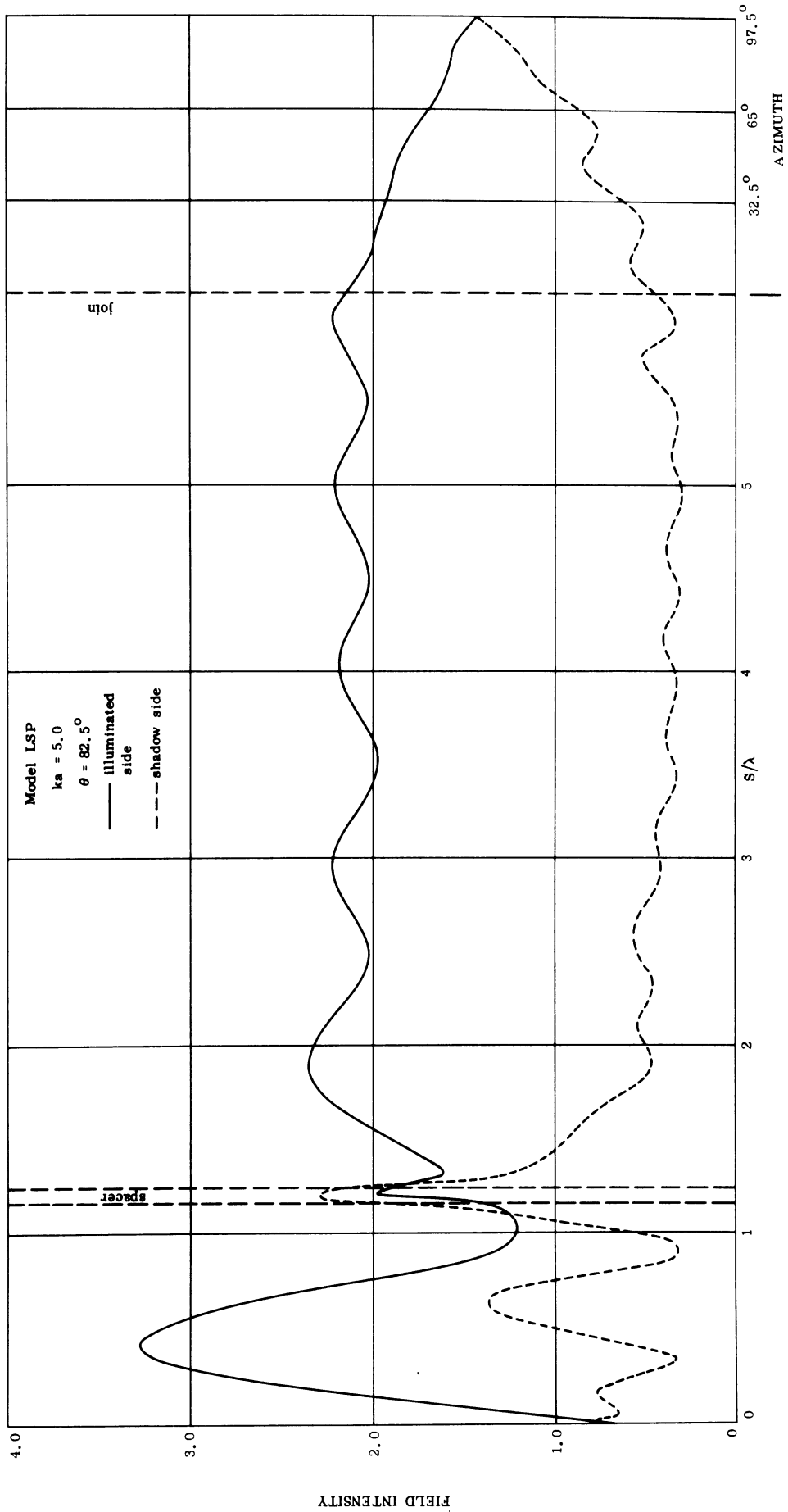
FIG. 2-5: OBLIQUE ANGLE INCIDENCE FOR MODEL LSP; angle of incidence = 82.5^{o}.

11

(S) In Fig. 2-4, the behavior is quite different (angle of incidence: 45 degrees). On the lit side the periodicity is about 2.2λ, and on the shadowed side there is no perturbation, save for those near the join or near the spacer. The cyclic disturbance seen on the lit side has the period one would expect of two waves propagating at an angle of 52.5 degrees from each other (45 + 7.5). One wave is the incident wave and the other runs along the side of the cone from tip to join.

(S) The perturbations of an indented base on the fields of a bare cone-sphere were studied in the second year's effort, but coatings have not yet been applied to these shapes. A series of experiments will soon be initiated in which such models will be coated and measured, but we have not yet decided how the coatings will be applied to the base.

2.3 Far Field Measurements (Backscatter) (Task 2.1.3)

(S) This task provides for a limited number of far-field measurements on coated perturbed shapes, but such targets have not yet been measured. However, a careful series of measurements were performed on a bare perturbed shape, in which a newly acquired L-band system was tested, and some enlightening data obtained. The model had an indented base (ID-2) and back-scattering measurements were obtained as a function of ka. The ka values obtained were $1.2 \leq ka \leq 1.8$ and $2.8 \leq ka \leq 4.5$ in steps of 0.1, and were split this way because the former values lay in L-band and the latter in S-band.

(S) Full 360 degree patterns were recorded with horizontal polarization, but results for three particular aspects (nose-on, tail-on, and specular flash) are presented in Fig. 2-6. The lines sketched in do not represent theory and are inteded only to lead the eye through a group of associated points. Note that the dip in the nose-on cross section occurs for ka = 3.3; the depth and position of this null is more characteristic of flat-backed cones than of cone-

spheres. It appears that the curvature of the radius near the join is small enough to make the model behave as though there were no indentation in the rear. We will refer to this observation again under Task 2.1.6.

2.4 Effect of Radius of Curvature Near Cone-sphere Join (Tasks 2.1.4 and 2.1.6).

(S) This task requires experimental study of the effect of the local radius of curvature near the join of the cone and spherical cap of a vehicle. The models required for this task are under construction and no measurements have been made. Four models are currently under construction which will permit us to study the effect of the radius of curvature just beyond the join. Although interest lies in shapes with indented bases, the study of the curvature in question can take place with flat-backed models. The data of Fig. 2-6, for example, suggest that the indented base model behaves much like one having a flat back. Additional data are presented in Fig. 2-7 in the form of surface field measurements. Here the probe trajectory was around the base of an indented model and was straight across the base, as though the base were flat and not indented. Two sets of data are presented; one is for a normal indented base while the other is for a flat base simulation obtained by stretching an aluminum foil disk across the indentation. The results show the fields are nearly the same in both cases, except that at the rear dead center, the intensity is slightly greater for the foil covered (flat base) model.

(S) Because of the minor role played by the concavity, as judged by Fig. 2-6 and 2-7, we have selected four radii of curvature to be constructed on four cone models with flat bases. The cone angle chosen was 18 degrees (total) and a sketch of the models is shown in Fig. 2-8. Table 2-I lists the model and full scale radii, and shows the available range in kr (r being the base corner radius) the models will provide.
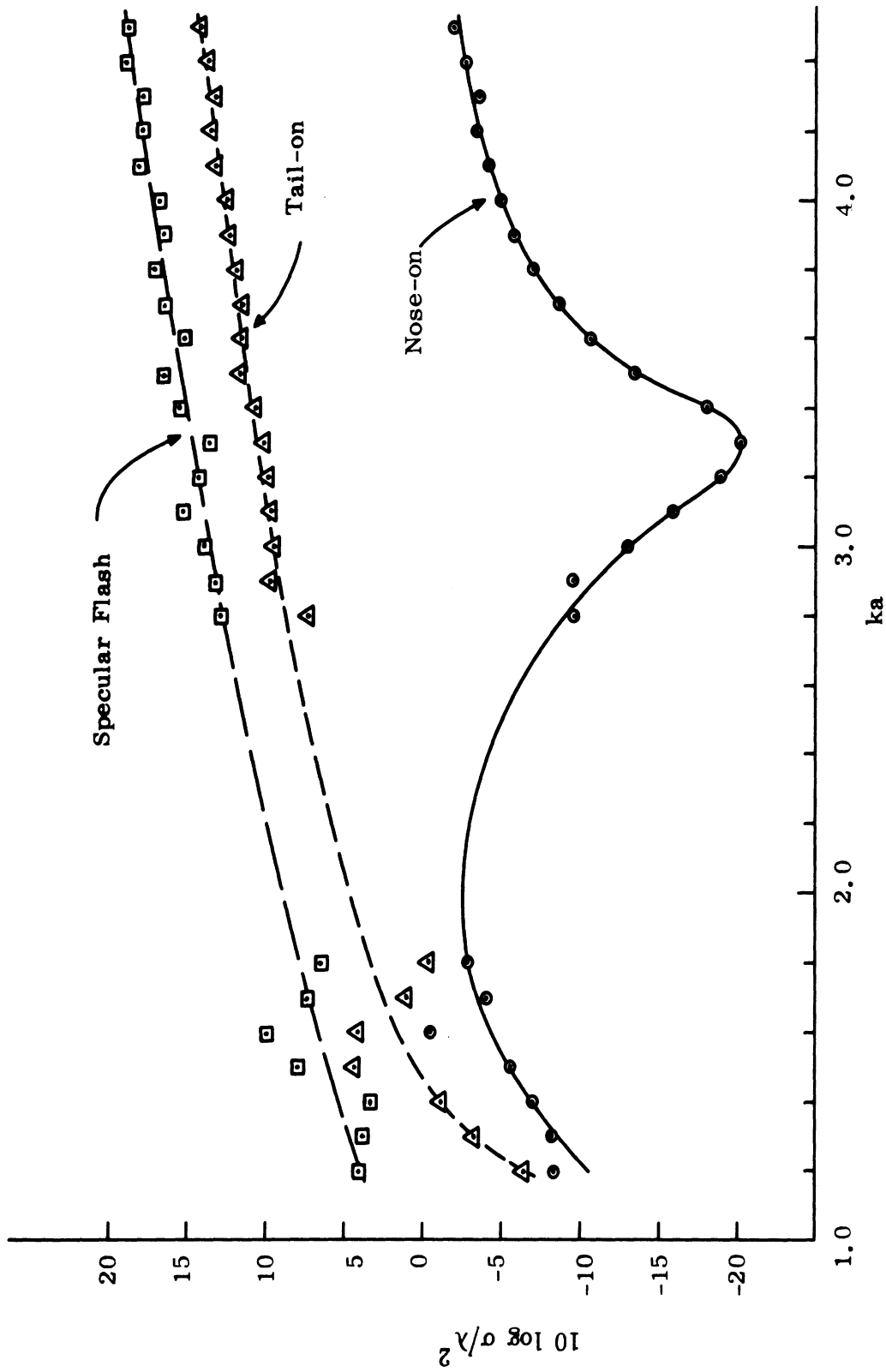
FIG. 2-6: BACKSCATTER DATA FOR AN INDENTED BASE MODEL SHOWS IT LOOKS MUCH LIKE A FLAT-BACKED CONE.

THE UNIVERSITY OF MICHIGAN
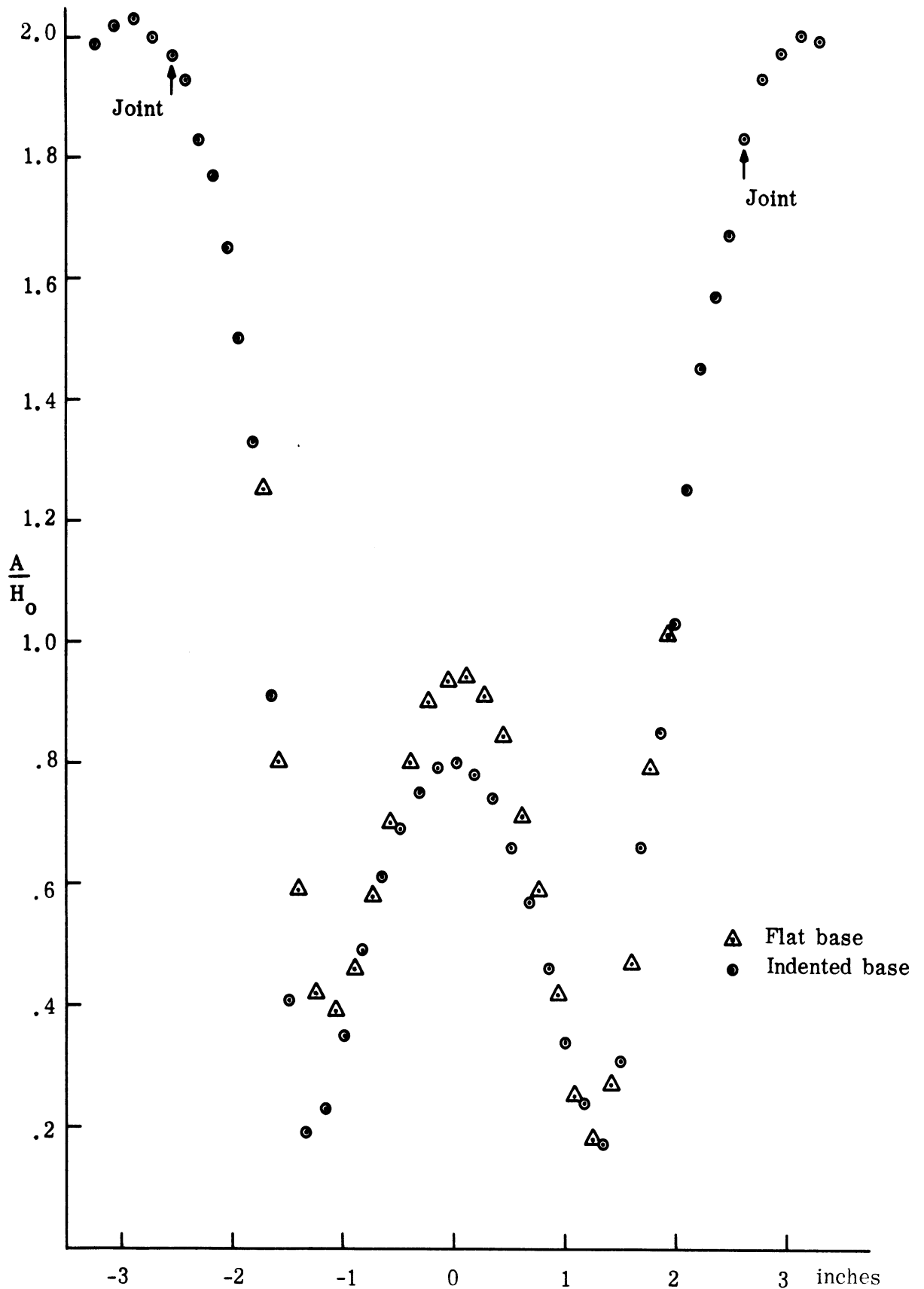
8525-2-Q

FIG. 2-7: MEASURED INTENSITIES AROUND THE BACK OF FLAT AND INDENTED BASE MODELS ARE NOT MUCH DIFFERENT FROM EACH OTHER.

0.188"R

12.077"

0.376"R

12.294"

0.564"R

12.511"

0.751"R

12.728"
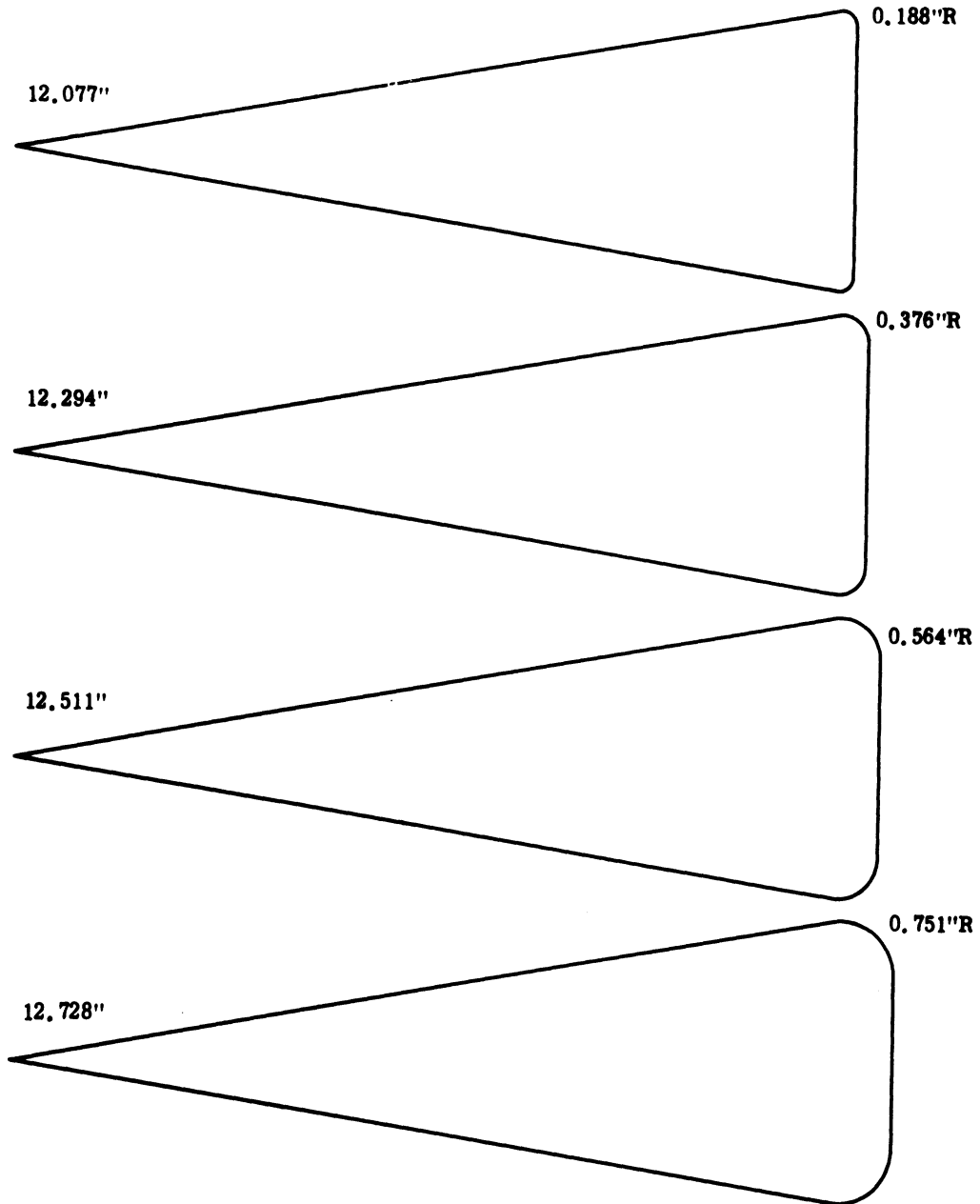
FIG. 2-8: THE FINAL APPEARANCE OF THE MODELS IS SHOWN IN THE
SKETCHES. Beside each is the total model length, assuming
a perfect tip (a point) and perfect tolerance. Cone base diameter
at point of tangency = 3.765" total cone angle = 18°.

TABLE 2-I:

Selected Model Radius, inches (r)	Simulated Full Scale Radius, inches	kr values for these ka:			
		ka = 1	ka = 3	ka = 5	ka = 8
0.188	1.075	0.1	0.3	0.5	0.8
0.376	2.15	0.2	0.6	1.0	1.6
0.564	3.22	0.3	0.9	1.5	2.4
0.751	4.30	0.4	1.2	2.0	3.2

2.5 Re-entry Plasma Experiments (Task 2.1.5)

2.5.1 Introduction

(S) Originally the experimental and the related analytical efforts for determining the RCS (radar cross section) of bodies covered by thin plasma sheaths were to be limited to the analysis of flat plates and cones. During the detailed investigation of the flat plate covered by a thin plasma sheath (simulated by a plane of wires) both experimental and analytical difficulties were encountered. Earlier, it had been anticipated that the flat plate problem would be straightforward and would be completed in a much shorter time.

(S) The investigation started with an examination to determine whether or not surface waves could be supported by a plasma coated surface with an air gap. It was found (J. R. Wait, 1960) that ordinary surface waves, which are attenuated away from and propagate parallel to the plasma-air interface, can indeed exist. In addition, when the air gap between the conducting plate and sheath is large enough, it was found that wavequide modes can be supported as

indicated by Wait (1960). A number of surface field measurements were made in search of these waves and modes, but none appeared to be excited in our experimental model. So far the measured surface fields show only an interference of the incident wave with the cylindrical waves scattered by the edges. This type of interference was observed with and without the wire structure present. The amplitude of the interference pattern was enhanced in the presence of the wires, but the periodic characteristics were constant and not related to the expected surface wave period.

(S) Meanwhile the physical optics analysis for the far field monostatic RCS was calculated and arrangements were made to measure it on the scattering range. Results from the RCS tests indicate that more than the ordinary physical optics model is necessary to explain the behavior of the fields scattered from the plasma coated plate. When the sheath is in the neighborhood of one half wavelength from the plate, a large gain appears in the HH polarization pattern (smaller gains in the VV polarization) in the aspect region between 30° and 60° from broadside. The location and amplitude of the gain seem to be related to the sheath surface impedance and the size of the air gap.

(S) Even though our first surface field measurements showed no sign of surface waves, it seems possible that the large gain off-broadside in the RCS patterns could be explained by the presence of leaky waves which are complex surface waves. Extensive research conducted at the Polytechnic Institute of Brooklyn during recent years indicates that over-dense plasma layers can support such waves. We are presently examining this problem and plan to make further surface field measurements to determine the behavior of the near fields which cause the gain in the RCS away from broadside.

(S)   Preliminary RCS tests made on the plasma cone borrowed from Aerospace - El Segundo indicate that there is as much or more return from the spacers that support the wire grid on the conducting cone as from the grid itself.   Since there is no mathematical analysis available for the coated cone problem, it is difficult to know how accurate our simulation is.   Besides the effects of curvature, the coated cone also produces coupling between the two polarizations, and these effects are not present in the flat plate problem.   Due to these preliminary cone difficulties and the nature of the flat plate problems, it seems more desirable and practical to investigate a plasma-coated circular cylinder of finite length before making any further measurements on the cone.   Both curvature and polarization coupling are produced in the coated cylinder problem, but in this case, it is believed that an approximate mathematical model can be formulated.   Therefore, with the cylinder study it should be possible to check our simulation as well as develop techniques for mounting wire grids on curved surfaces.   It is for these reasons that we propose to examine the cylinder in detail before the cone, although design work regarding modal analysis on a coated cone is still under-way.   With the added knowledge from the cylinder studies it should be easier to understand and follow the work on the cone, especially experimentally.

(U)   In the next section some results from the monostatic RCS measurement are discussed and typical patterns are presented for a flat plate covered with a plane of wires.

2.5.2   Radar Cross Section Measurements

(U)   The geometry related to the RCS measurements made on large (compared to a wavelength) flat aluminum plates with a plane of parallel wires set a distance ℓ away is shown in Fig. 2-9.   If the spacing h between adjacent

x

H

$E_y(\perp)$

R_0

$k(\perp) = -k_0 \; x \sin \theta(\perp) + z \cos \theta \, (\perp)$

$\theta(\perp)$

z

a

Region 2   Region 1

h

ℓ
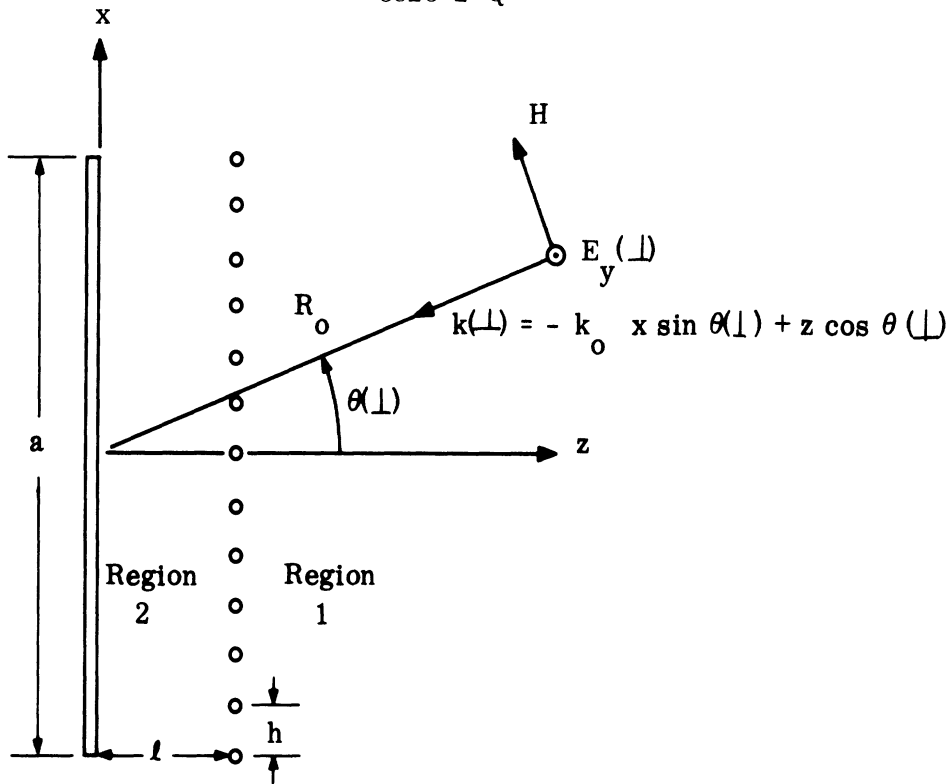
(a) Perpendicular or vertical polarization

y

$k(||) = -k_0 \; y \sin \theta(||) + z \cos \theta(||)$

$H_x(||)$

E

$\theta(||)$

z

Plasma sheath simulated by a plane of wires

Ground plane
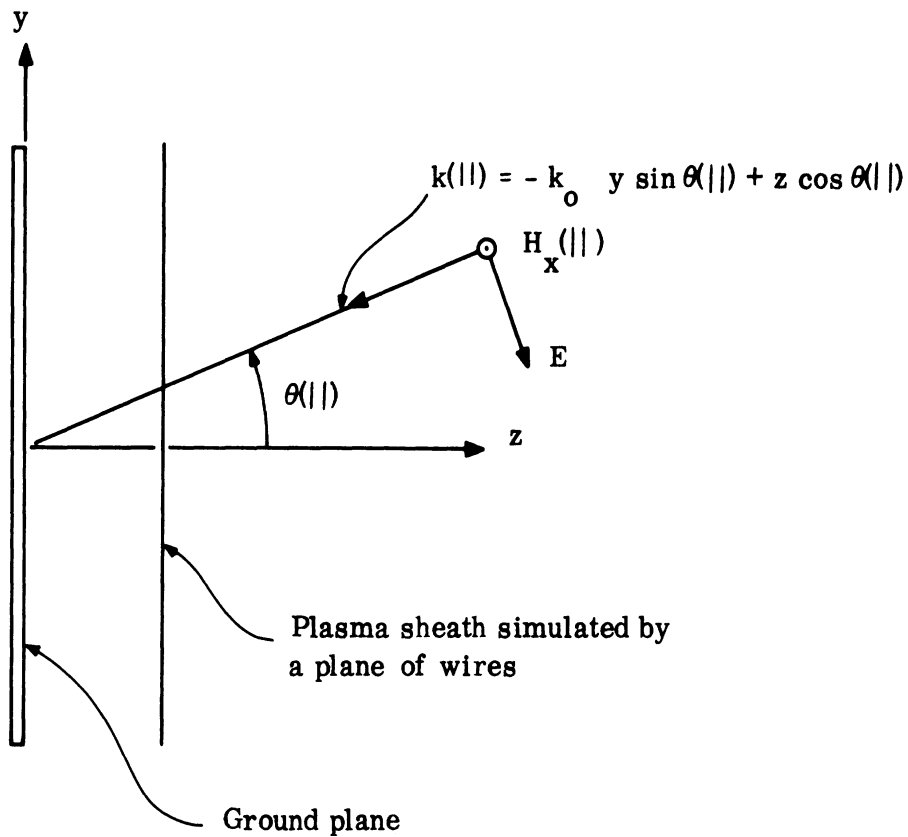
(b) Parallel or horizontal polarization

FIG. 2-9: GEOMETRY FOR RCS MEASUREMENTS.

20

wires is less than $\lambda_o/2$ and the internal resistance of the wires is negligible, the surface impedance is purely inductive

$$Z_s \simeq j Z_o h/\lambda_o \ln (h/\pi d) \tag{2.1}$$

where λ_o is the free space wavelength, $Z_o = \sqrt{\mu_o/\epsilon_o} = 377\Omega$, and d is the wire diameter.

(U)   All of our measurements are monostatic, that is, the transmitting and receiving antennas are located together in the far field. Two polarizations VV and HH are recorded and here V and H refer to the electric field being oriented in the vertical and horizontal planes. VV and HH polarizations are also refered to as perpendicular and parallel polarizations as indicated in Fig. 2-9. The wave vectors $k(\perp)$ and $k(\|)$ show the propagation direction of the incident fields as a function of the incident angles $\theta(\perp)$ and $\theta(\|)$. In the experiment the wires are directed along the y axis and there is no electric field component along the x axis. For the flat plate geometry no coupling is assumed between the two polarizations and the VV and HH cases are examined separately.

(U)   The boundary condition at the two surfaces $z = 0$ and $z = \ell$ are as follows:

$$\text{at } z = 0 \quad \hat{z} \times (\overline{E}_2) = 0 \tag{2.2}$$

$$\text{at } z = \ell \quad \hat{z} \times (\overline{E}_1 - \overline{E}_2) = 0$$

$$\hat{z} \times (\overline{H}_1 - \overline{H}_2) Z_s = \left[\overline{E}_1 - (\hat{z} \cdot \overline{E}_1) \hat{z} \right] \tag{2.3}$$

where z is the unit vector normal to the surface, Z_s is defined in Eq. (2.1), and the subscript 1 and 2 refer to the field in regions 1 and 2 (Fig. 2-9). An application of these conditions to the appropriate fields in the two regions

yields the reflection coefficients $\left[R(\perp) \text{ and } R(\|)\right]$ at the interface $z = \ell$ from region 1 back into region 1 and the transmission coefficients $\left[T(\perp) \text{ and } T(\|)\right]$ from region 1 into region 2 for both polarizations.

$\perp$ case

$$R(\perp) = e^{j2L} \left[\frac{Z_o \sin L - jZ_s \cos \theta(\perp) e^{-jL}}{Z_o \sin L - jZ_s \cos \theta(\perp) e^{jL}} \right].$$

$$T(\perp) = -j \, e^{jL} \left[\frac{Z_o \sin L}{Z_s \cos \theta(\perp)} - j \, e^{jL} \right]^{-1}$$

(2.4)

$\|$ case

$$R(\|) = e^{j2L} \left[\frac{Z_o \cos \theta(\|) \sin L - jZ_s e^{-jL}}{Z_o \cos \theta(\|) \sin L - jZ_s e^{jL}} \right]$$

$$T(\|) = -j e^{jL} \left[\frac{Z_o}{Z_s} \cos \theta(\|) \sin L - j \, e^{jL} \right]^{-1}.$$

(2.5)

In Eqs. (2.4) and (2.5) $L = k\ell \cos \theta(\perp) = k\ell \cos \theta(\|)$ depending on whether it is the $\perp$ or $\|$ case. $R(\perp)$ and $R(\|)$ are the same as the reflection coefficients discussed in the last Quarterly Report, but are in a different form.

(U) In the physical optics approach to determining RCS expressions, the Stratton-Chu equations, which are a vector form of the Kirchhoff-Huygens principle, are used to evaluate the scattered fields. Assuming time dependence of the form $e^{j\omega t}$, the scattered electric and magnetic fields $\overline{E}^S$ and $\overline{H}^S$ can be expressed in terms of tangential components of the fields $\overline{E}$ and $\overline{H}$ just outside

the scattering surface, (Johnson, 1965)

$$E^S = - \iint \left[(\hat{z} \times \bar{E}) \times \nabla G + (\hat{z} \cdot \bar{E}) \nabla G - jk_o Z_o G (\hat{z} \times \bar{H}) \right] dS \qquad (2.6)$$

$$H^S = - \iint \left[(\hat{z} \times \bar{H}) \times \nabla G + (\hat{z} \cdot \bar{H}) \nabla G + j \frac{k_o}{Z_o} (\hat{z} \times \bar{E}) \right] dS \qquad (2.7)$$

where S is the surface at $z = \ell^+$, $k_o = 2\pi/\lambda_o$, and G is the free space Green's function with the form

$$G = - \frac{e^{-j\hat{k} \cdot \hat{R}}}{4\pi R}$$

and in the far field

$$\nabla G = - jk \hat{R} G.$$

In the $\perp$ case

$$\hat{R}(\perp) = \hat{x} \sin \theta(\perp) + \hat{z} \cos \theta(\perp)$$

and in the $||$ case

$$\hat{R}(||) = \hat{y} \sin \theta(||) + \hat{z} \cos \theta(||).$$

(U) Only one field component is necessary for each case if the solutions are expressed in terms of $\bar{E}^S$ for the vertical polarization and $\bar{H}^S$ For the horizontal polarization. After a considerable amount of algebra and scattered fields may be represented as

$$E^S(\perp) = \hat{y} \iint \left[jk_o \cos \theta(\perp) E_y - \frac{\partial E_y}{\partial z} \right] G(\perp) \, dx \, dy \qquad (2.8)$$

$$H^S(||) = \hat{x} \iint \left[-j k_o \cos \theta(||) H_x + \frac{\partial H_x}{\partial z} \right] G(||) \, dx \, dy \qquad (2.9)$$

where

$$E_y = \left[e^{jk_o z \cos \theta(\perp)} + R(\perp)e^{-jk_o z \cos \theta(\perp)} \right] e^{jkx \sin \theta(\perp)} + E_p \qquad (2.10)$$

$$H_x = \left[e^{jk_o \cos \theta(||)} + R(||)e^{ihk z \cos \theta(||)} \right] e^{jky \sin \theta(||)} + H_p \quad . \qquad (2.11)$$

The reflections coefficients are given in Eqs. (2.4) and (2.5) and the Green's functions are listed above. E_p and H_1 represent possible complex surface waves which can exist on coated conducting bodies such as the one being considered here (Brekhovskikh, 1960). When the scattering body is a perfect conductor E_p and H_p are zero (for electrically large plates). We are still in the process of evaluating E_p and H_p for the problem at hand. These surface waves are related to the complex poles in the reflection coefficients.

(U) It is a straight forward calculation to find the radar cross section σ for a perfectly conducting flat plate

$$\sigma = 4\pi R^2 \left| \bar{E} \times \bar{H} \right| \quad . \qquad (2.12)$$

For both polarizations Eqs. (2.8) and (2.9) lead to the same result when substituted into Eq. (2.12)

$$\sigma = 4\pi \left(\frac{a^2}{\lambda_o} \right)^2 \left[\frac{\sin(ka \sin \theta)}{ka \sin \theta} \right]^2 \cos^2 \theta \qquad (2.13)$$

where a is the length of the flat plate. In the upper part of Fig. 2-10 the peaks and nulls of Eq. (2.12) are expressed as a function of $(ka \sin \theta)/\pi$ and in the lower part $\cos^2 \theta$ is shown as a function of θ. The $\cos^2 \theta$ term can be neglected in Eq. (2.12) for $\theta < 45^\circ$ with less than 3 db error. The purpose of Fig. 2-10 is to determine the magnitude and position of peaks and nulls; it is not intended to represent the complete pattern for Eq. (2.12).

(S) Eventhough our theoretical analysis is not complete for the geometry shown in Fig. 2-19, a number of experimental patterns have been recorded in the X and C frequency bands. Plates 18" x 18" and 9" x 9" have been tested with and without wires. The normalized surface inductance has ranges between

$$0.4 < \frac{X_s}{Z_o} < 1.2$$

while in all case R_s (related to collisions) has been zero. Air gap spacings have been between $\lambda/6$ and $3\lambda/2$.

(U) Examples of RCS patterns for VV and HH polarizations are given in Figs. 2-11 and 2-12 for the 9" x 9" plate with $\ell = 0.66"$, $h = 0.4"$, $d = 0.007"$ and $f = 9.46$ GHz. In both figures pattern (a) is for the flat alone, (b) flat plate with foam spacers $(\ell = 0.66")$, and (c) flat plate with spacers and wires. The parameters ℓ, h and d are explained in Fig. 2-9 and Eq. (2.1).

(S) A comparison between patterns (a) and (b) for both polarizations indicates that the foam spacers, used to hold the wires a distance ℓ away from the plate, cause no pattern disturbances. Also patterns (a) and (b) follow closely the theory expressed in Fig. 2-10 up to $\theta = 60^\circ$. Beyond 60° the effects due to the finite size of the plate begin to appear. Since the aspect range greater than 60° is beyond the range of interest in our model (the effect

THE   UNIVERSITY   OF   MICHIGAN
8525-2-Q

Peaks and nulls for first 11 lobes of $\left[\dfrac{\sin(ka\,\sin\theta)}{ka\,\sin\theta}\right]^2$
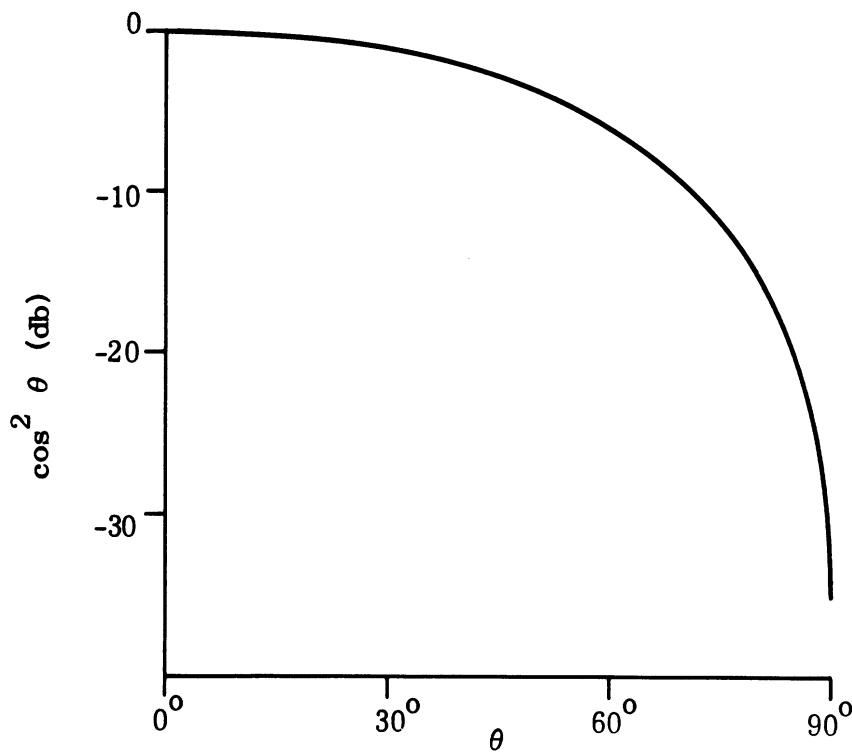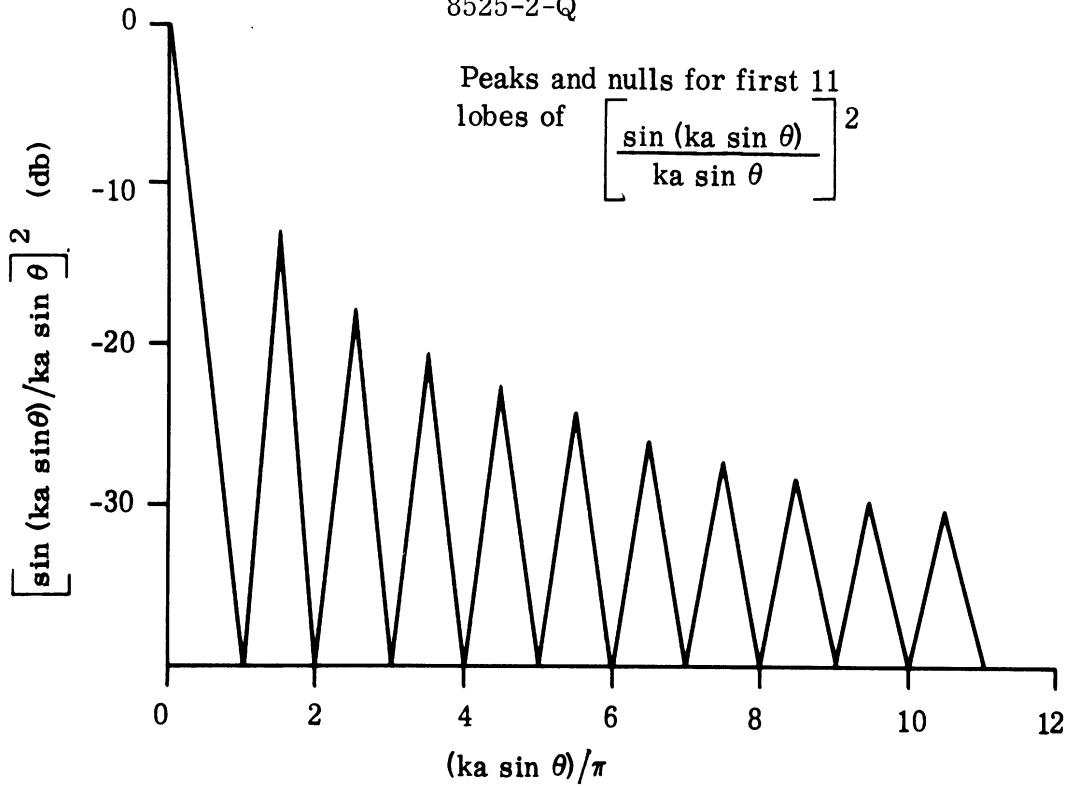
FIG. 2-10:   TWO CONSTITUENTS OF THE RCS PATTERN.

26
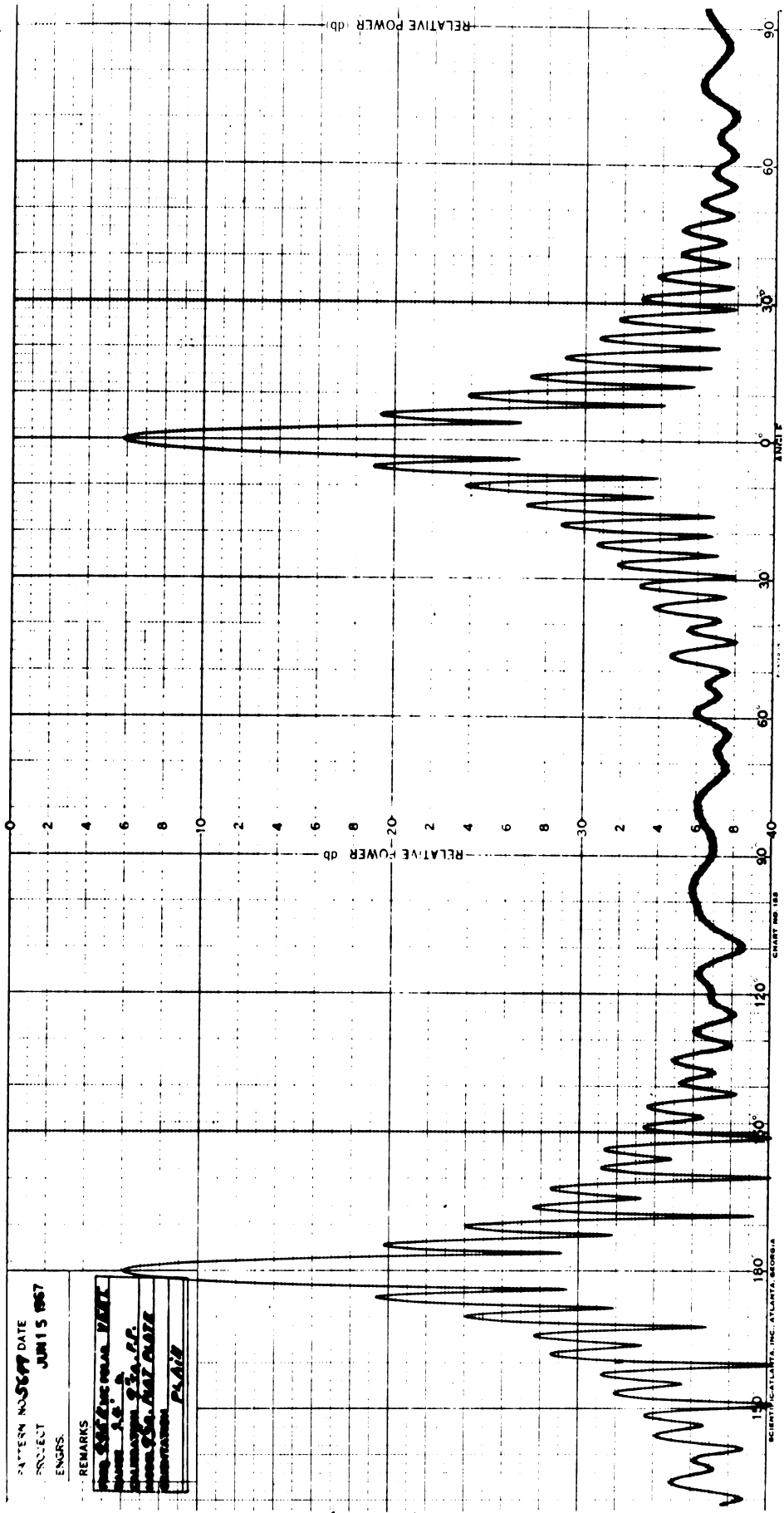
FIG. 2-11a: VV POLARIZATION, 9" x 9" FLAT PLATE.
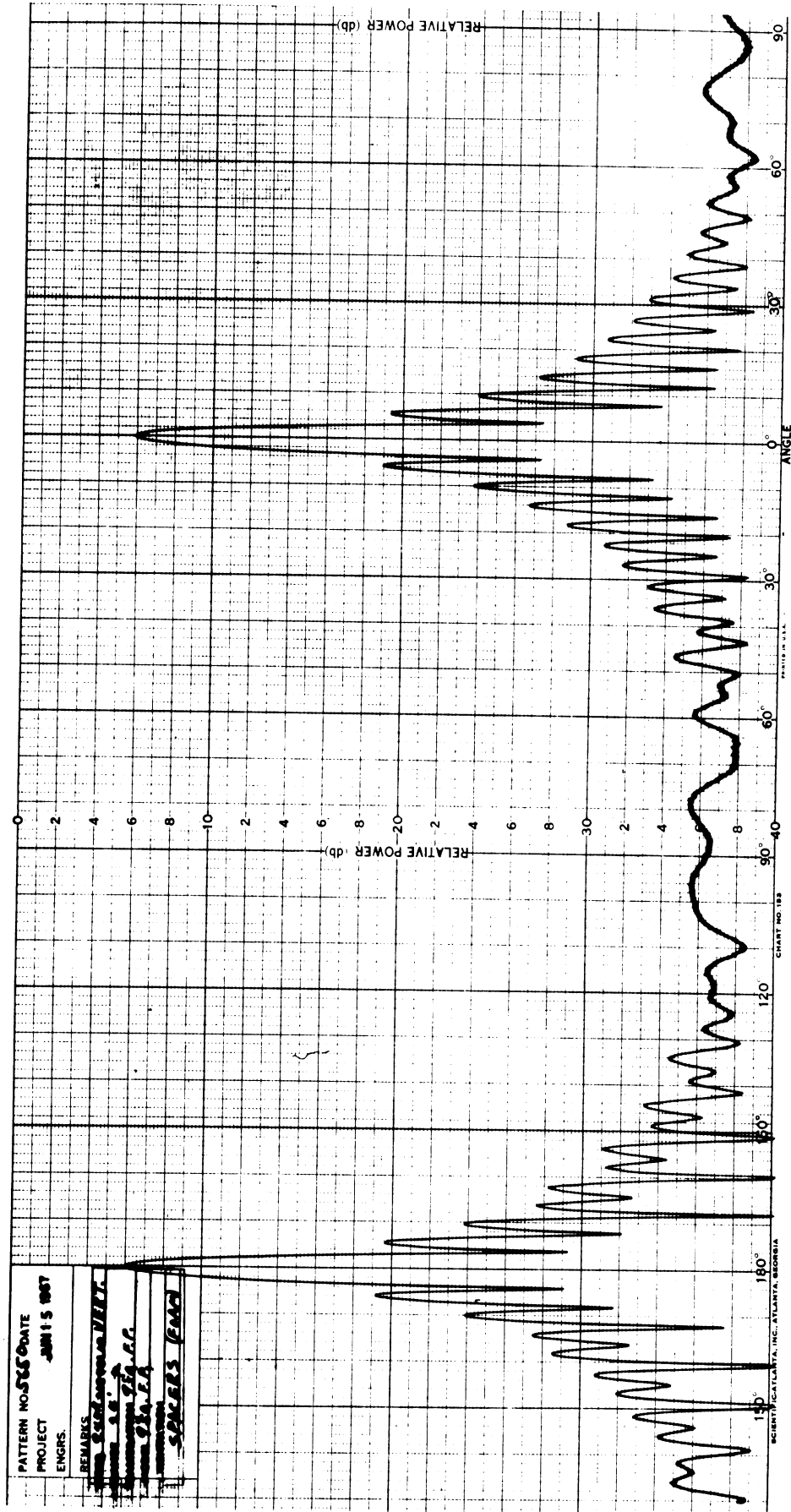
FIG. 2-11b: VV POLARIZATION 9" x 9" FLATE PLATE WITH FOAM SPACERS.

28
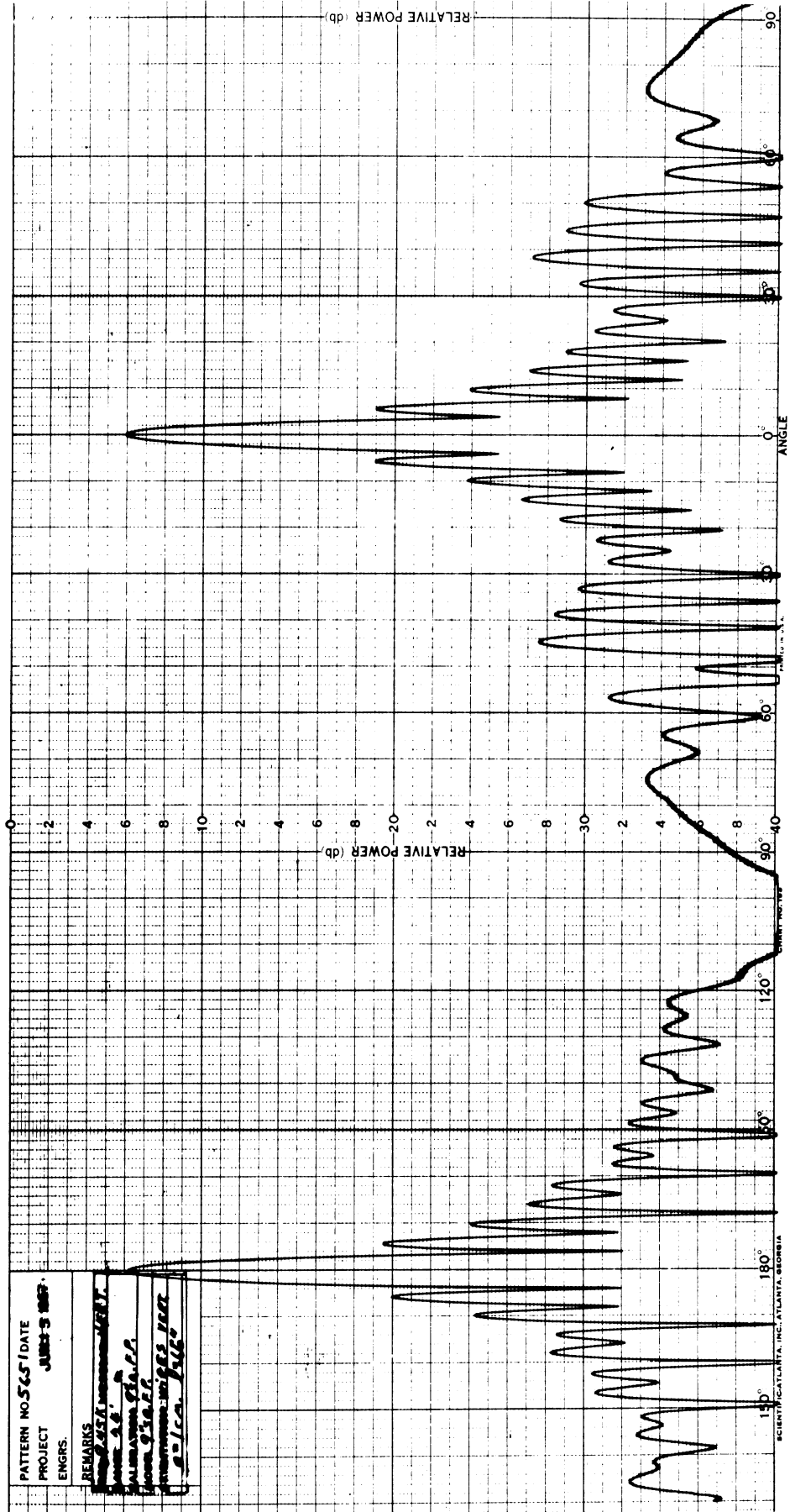
FIG. 2-11c: VV POLARIZATION, 9" x 9" FLAT PLATE WITH SPACERS AND WIRES.

29
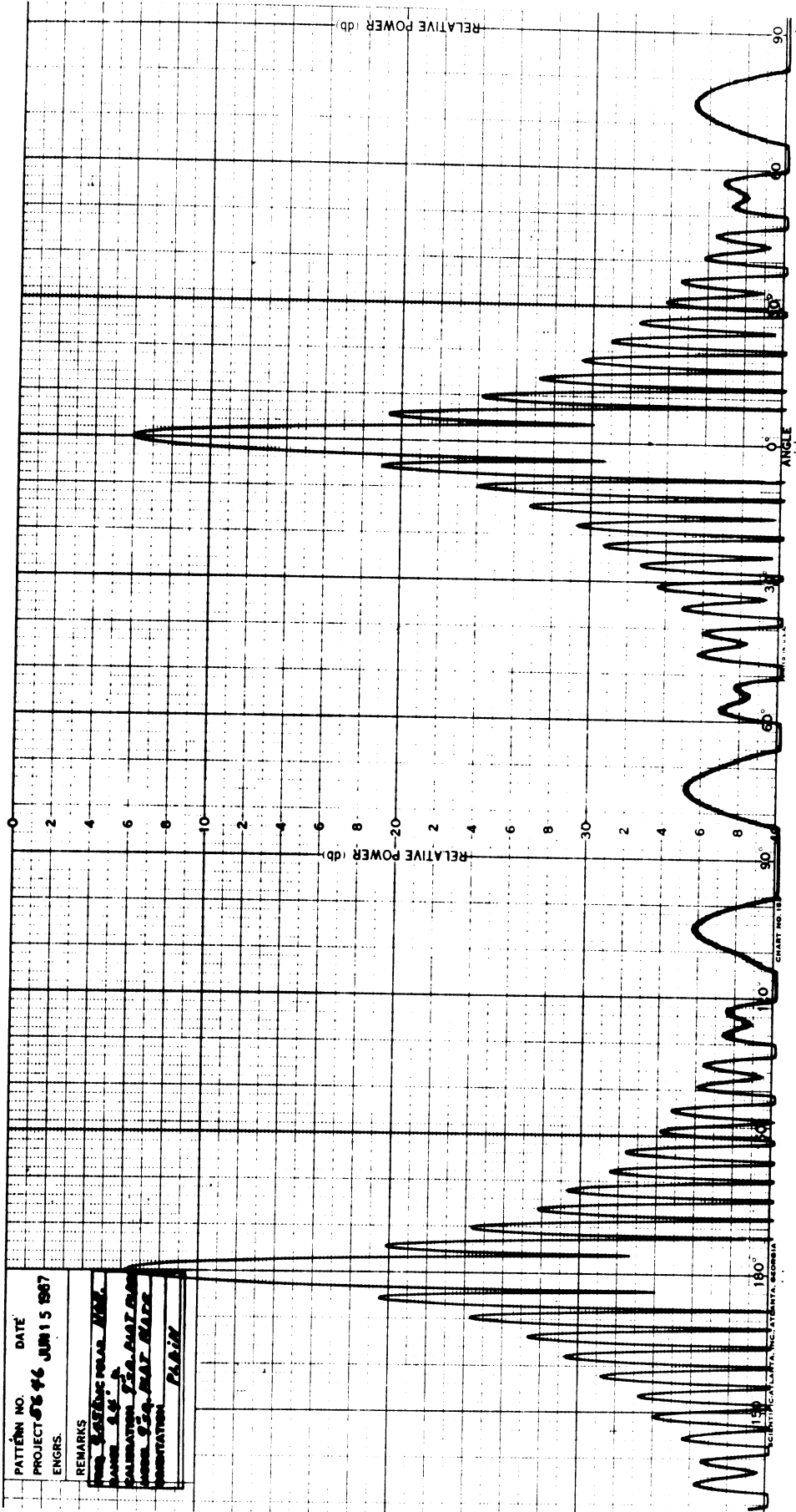
FIG. 2-12a: HH POLARIZATION, 9" x 9" FLAT PLATE.

30
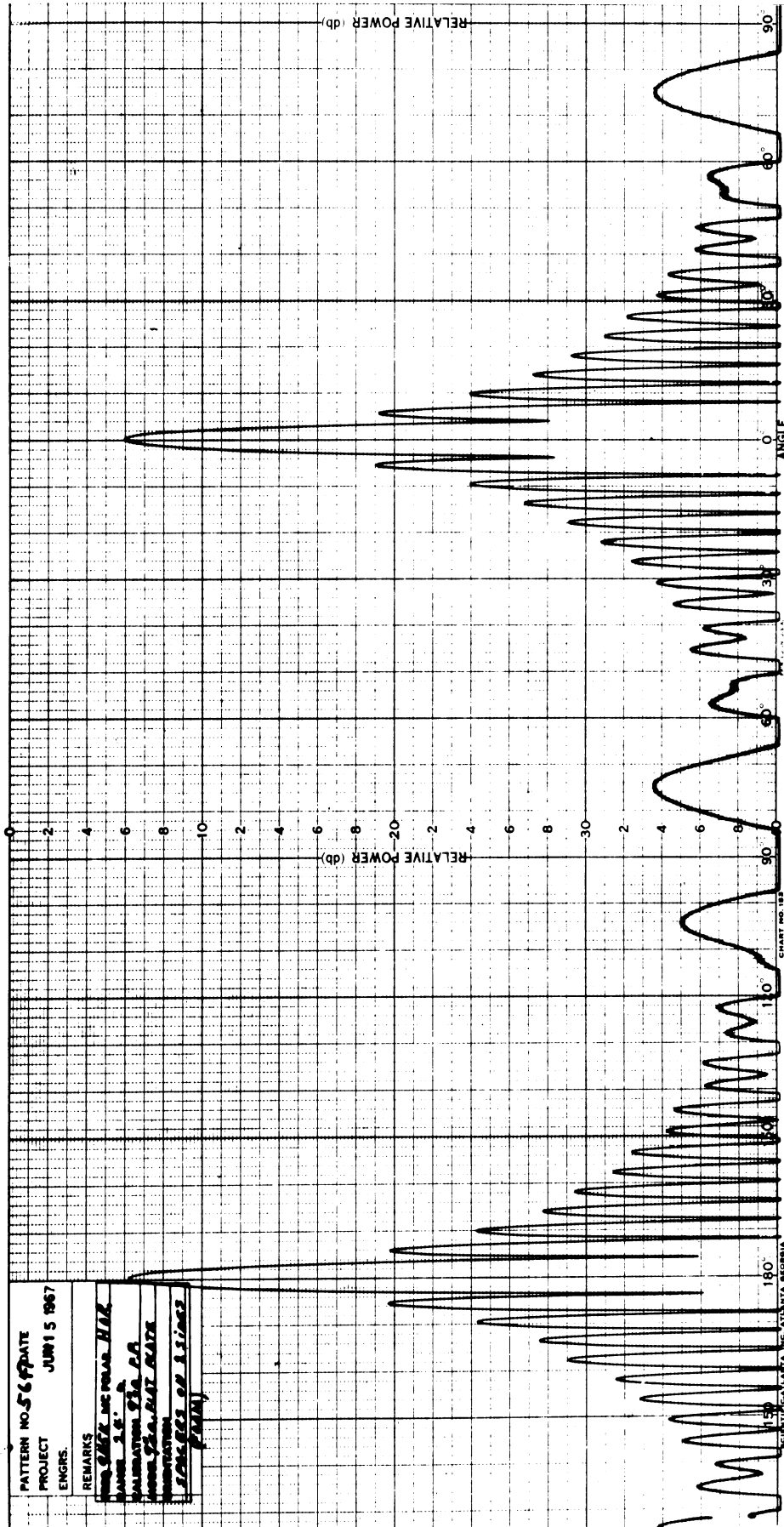
FIG. 2-12b: HH POLARIZATION, 9" x 9" FLAT PLATE WITH SPACERS.

31
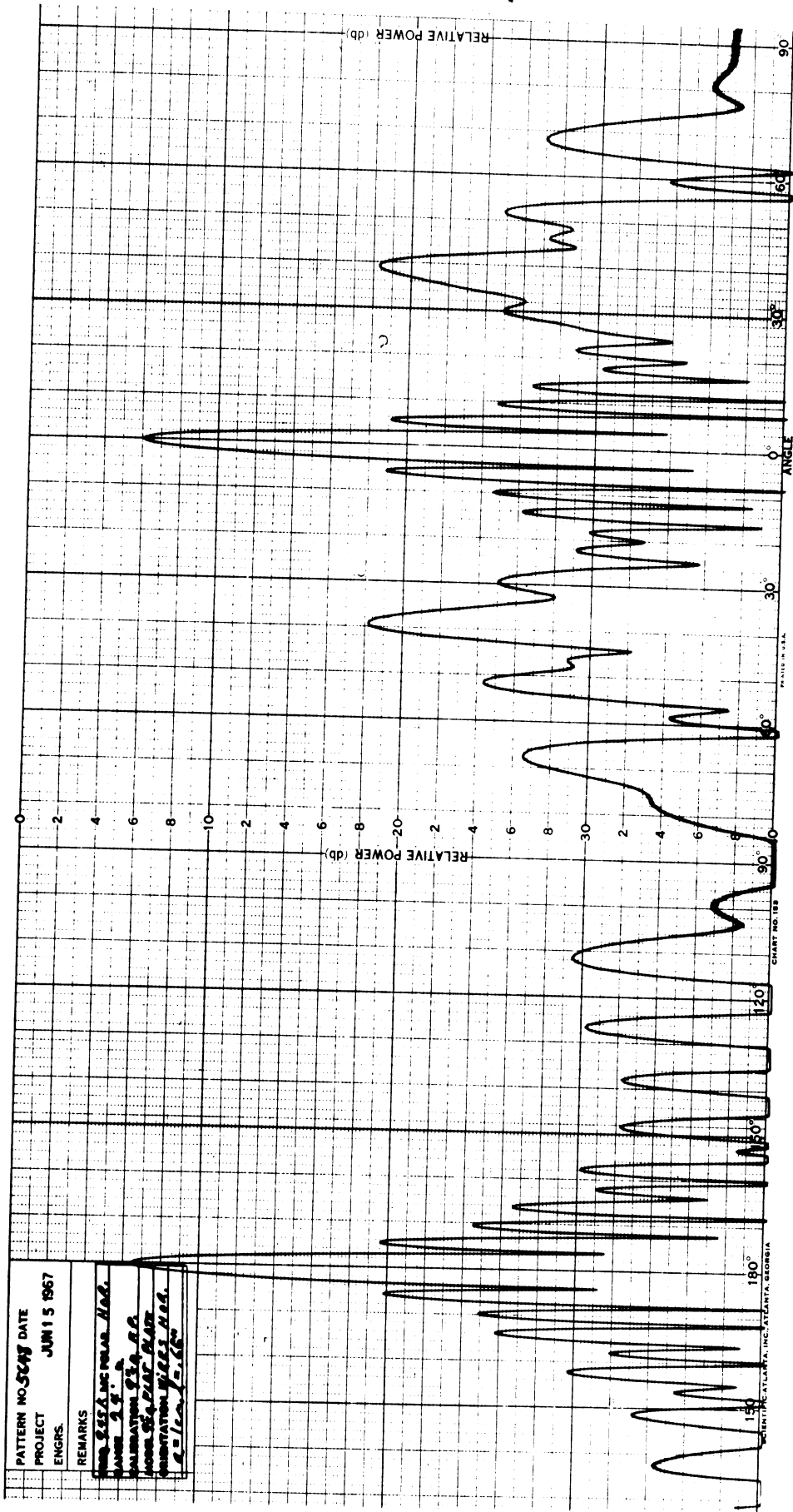
FIG. 2-12c: HH POLARIZATION, 9" x 9" FLAT PLATE WITH SPACERS AND WIRES.

32

of the wires is seen between 30° and 60°) this slight departure from theory should not cause trouble in our experiment. By general RSC range standards, all the (a) and (b) patterns are considered to be clean and acceptable for reference purposes.

(S) The effects of current sheath (plane of wires) is seen in Fig. 2-11c and 2-12c for VV and HH polarizations. The portion of the pattern centered about $\theta = 0^\circ$ (the right half of the figure) is the return from the front of the plate where the wires are set off a distance l from the plate. The left side of the pattern is the back return and can be used as a rough calabration reference for aspect angles $\pm 60^\circ$ away from $\theta = 180^\circ$. The HH pattern shows much stronger sheath effects compared to the VV case. Notice that the sheath causes little or no effect for θ up to 30° off broadside and that the effects of the sheath grow rapidly beyond 30°. It is this behavior which leads us to believe that leaky waves are causing these effects. Many different values of l/λ_o have been measured and in all cases no pattern distortions were introduced near broadside ($\theta = 0^\circ$).

(U) Photographs of the experimental models for the flat plate and cone are shown in Figs. (2-13) through (2-18). The first four photos depict an 18" x 18" flat plate with an attached plane of wires and covered with varying amounts of absorber. The last two figures are photos of the cone borrowed from Aerospace's Plasma Research Laboratory, Courtesy of K.E. Golden.

(S) Figure (2-13) shows the 18" x 18" flat plate with wires and plexiglass spacers totally exposed (no absorber). The wires are held taut by rubber bands on the back side of the plate. Without any absorber, there is a great deal of pattern distribution in the sidelobes away from broad side, with or without the wires present. The 4" wide absorber frame in Fig. 2-14 was introduced to
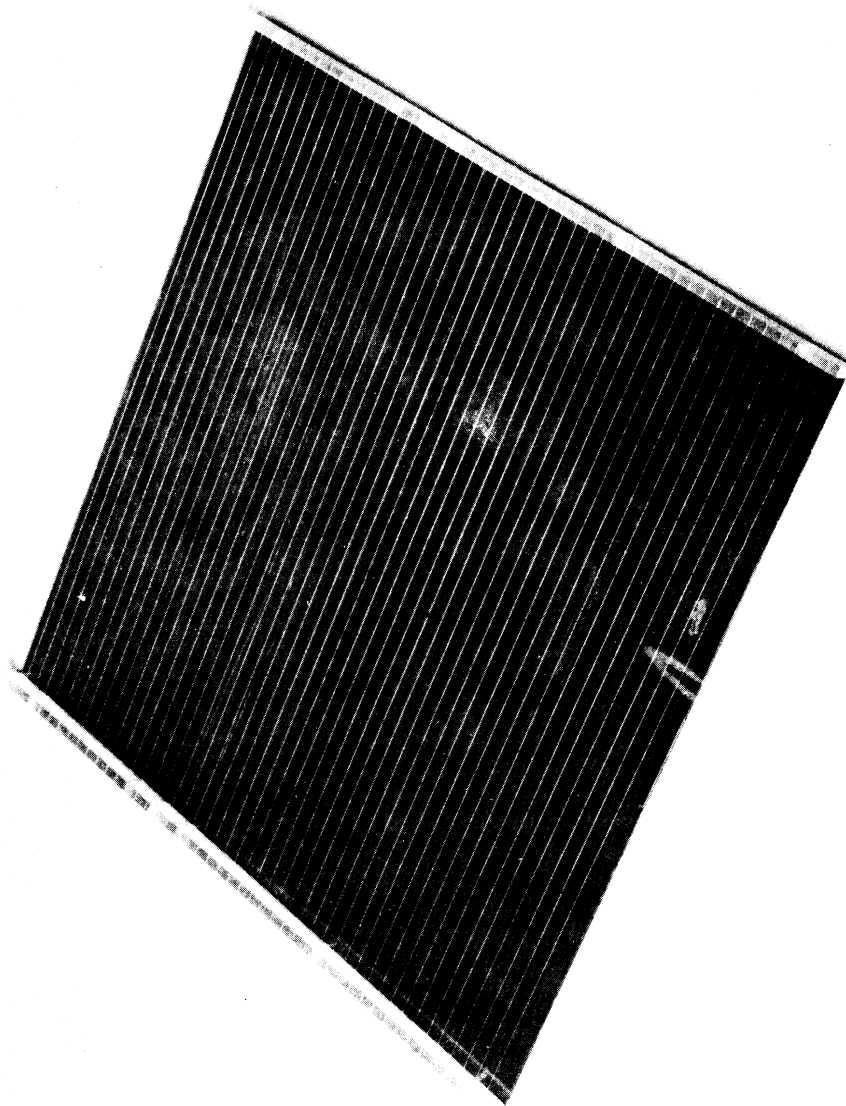
FIG. 2-13: 18" x 18" FLAT PLATE WITH PLEXIGLASS SPACERS
SUPPORTING THE WIRE GRID.
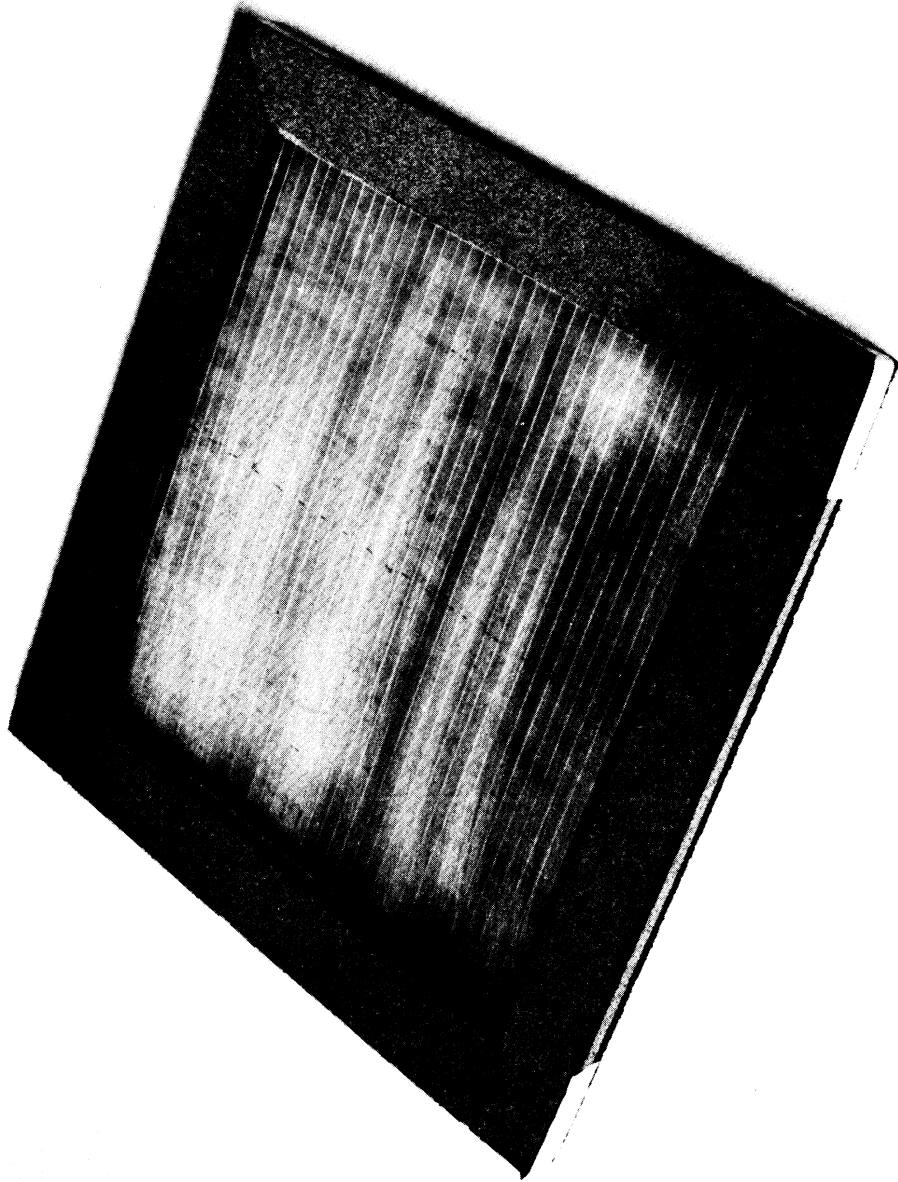
FIG. 2-14: 18" x 18" FLAT PLATE SURROUNDED BY A 4"
ABSORBER FRAME TO REDUCE EDGE EFFECTS.
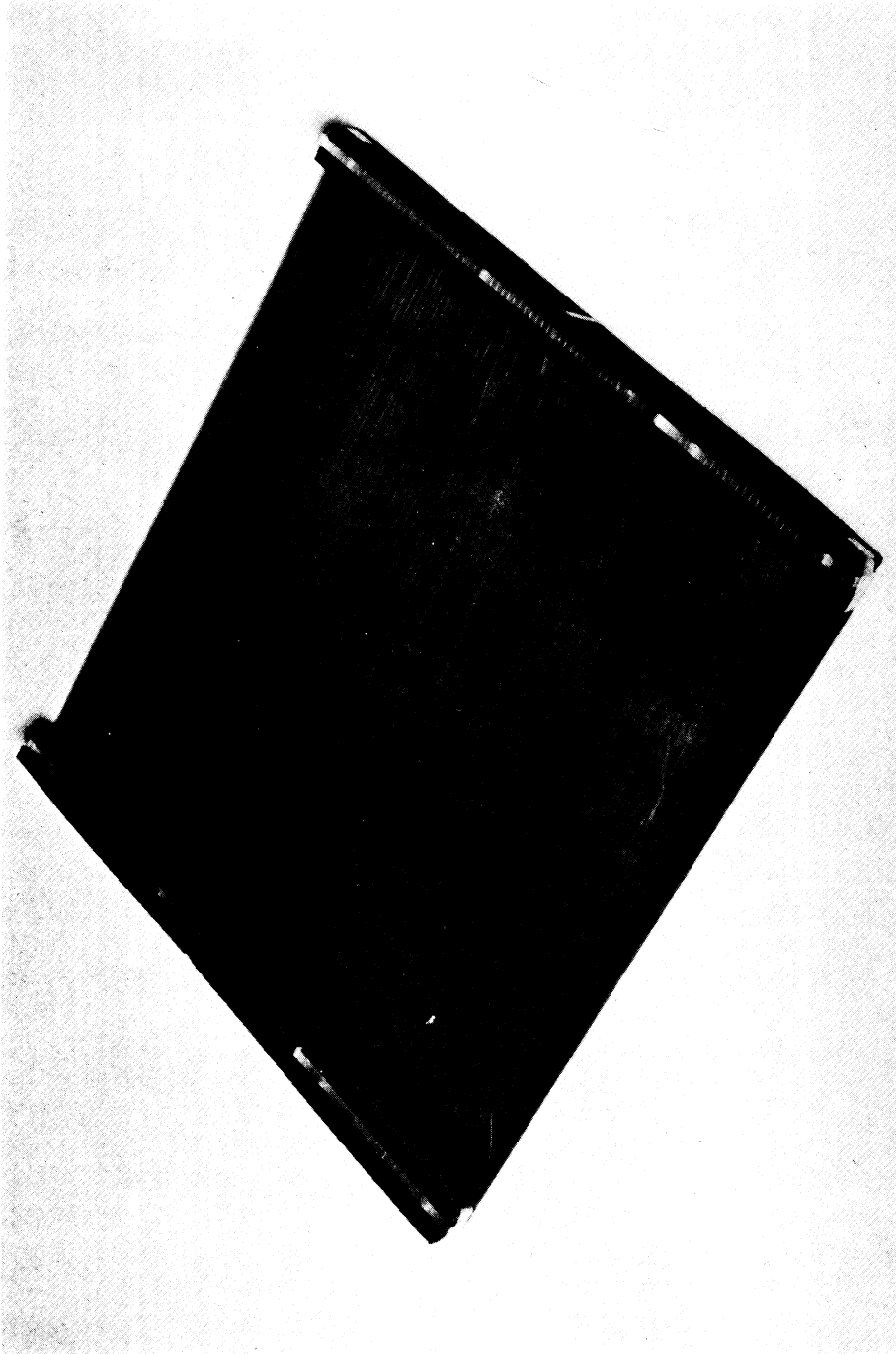
FIG. 2-15: 18" x 18" FLAT PLATE WITH ENOUGH ABSORBER TO ELIMINATE THE SCATTERING FROM THE PLEXIGLASS SPACERS.
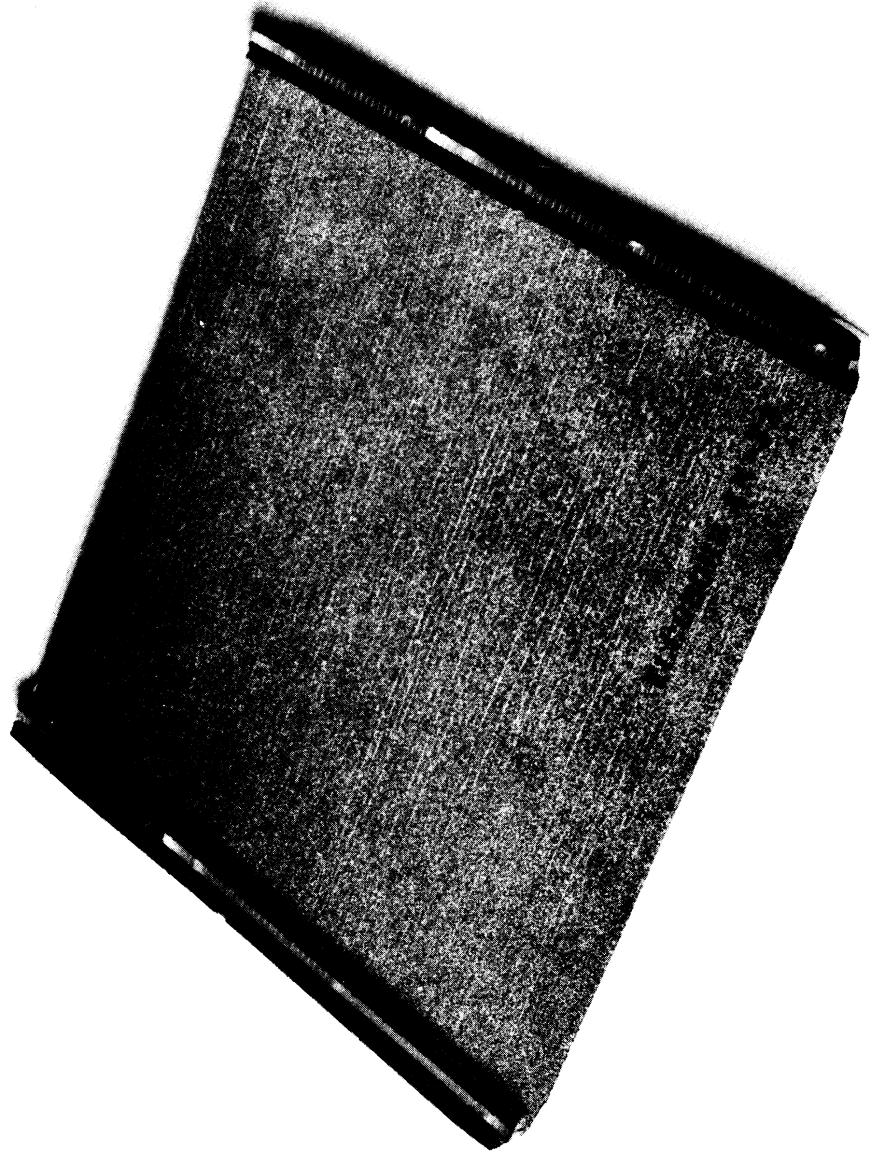
FIG. 2-16: 18" x 18" FLAT PLATE COVERED WITH NO. AN73
ABSORBER AND A PLANE OF WIRES.
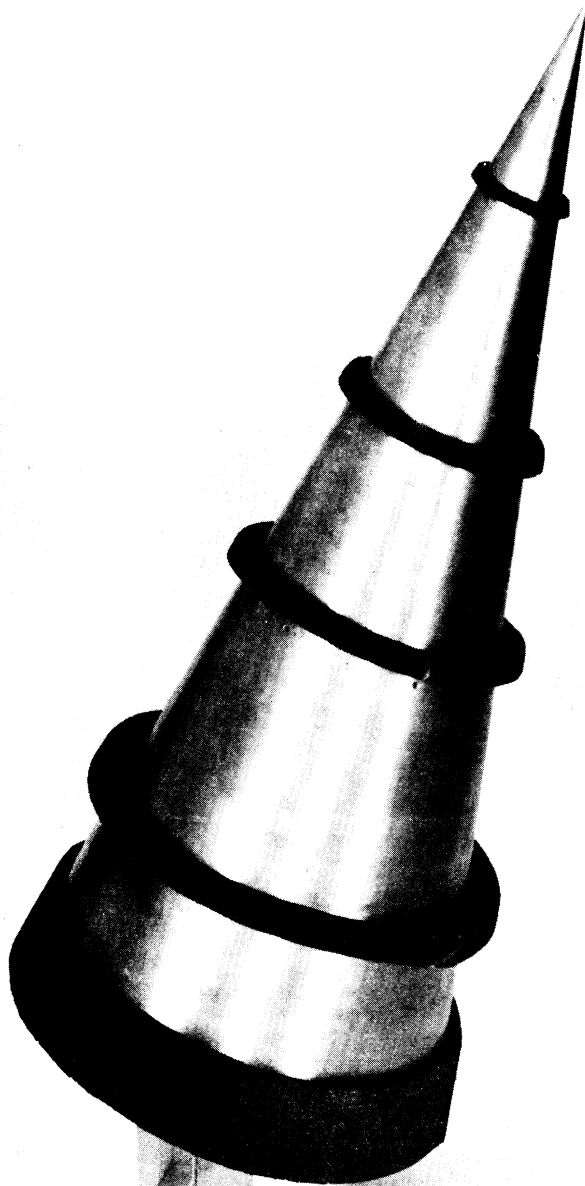
FIG. 2-17: 14° HALF ANGLE CONE WITH FOUR SPONGE LIKE SPACERS AND A RING OF ABSORBER AT THE CONE BASE.
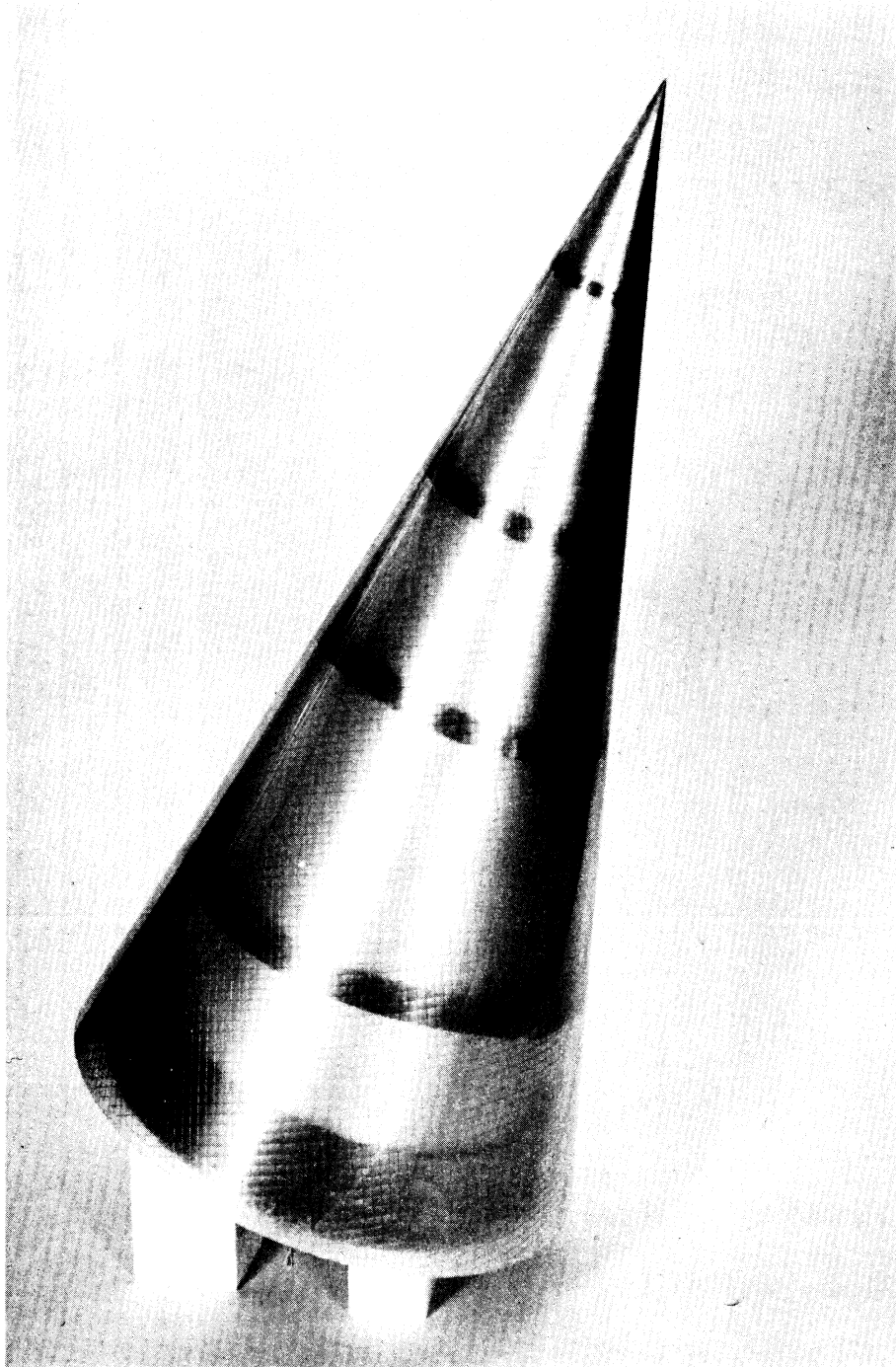
FIG. 2-18: CONICAL WIRE GRID (14.5° HALF CONE ANGLE) MOUNTED ON CONDUCTING CONE. The wire grid is supported by a mylar sheet.

cover up (reduce) edge effects and was found to be successful. Further tests with various amounts of absorber placed over different portions of the plate in an effort to locate more precisely the major cause of the scattering pattern distortions. The absorber scheme in Fig. 2-15 was found to eliminate nearly all of the distortions and it was therefore concluded that scattering from the plexiglass spacer was our major source of trouble. This discovery led us to use Styrofoam material in place of the plexiglass for spacers and now no absorber is necessary as demonstrated in the results of Fig. 2-10 and 2-11 which are RCS patterns for a 9" x 9" flat plate with Styrofoam spacers and no absorber. A few measurements were made with conducting plate completely covered with No. AN-73 absorber (Fig. 2-16) to study the effect of the wires alone.

(U) The 14° half angle aluminum cone is shown in Fig. 2-17 with 4 sponge like spacers and an absorber ring at the cone base. Figure 2-18 is a photo of the conical wire grid supported on the conducting cone by a sheet of mylar. Only limited tests have been made on the cone to date.

2.5.3 Conclusion

(S) Although our progress on the experimental plasma sheath program has been slower than originally expected, the RCS patterns presented here indicate that more than a physical optics model is necessary to explain even the flat plate results. It is one of the aims of this effort to determine the limitations of physical optics model for coated bodies and we found them earlier than hoped. At the present time it seems hopeful that we will be able to explain the flat plate behavior shortly and then move on the the coated cylinder.

III

TASK 3.0 THEORETICAL INVESTIGATIONS

3.1 Introduction

(U) In this section are reported the theoretical or analytic investigations which lead to the construction of formulas for the computer of radar cross section under a variety of conditions of interest. A discussion is given of the scattering from a re-entry shape with a rear concavity, a circumstance with direct practical importance. The analysis treats a metallic body. In order to understand the scattering from coated shapes, a study was made of the surface current on a curved surface, in this case a parabolic cylinder and a study was made of the field on an imperfectly conducting wedge. In Section 3.4, the work on the computer program for treating a general rotationally symmetric metallic shape is discussed. The present stage of the work involves the evaluation of several different approaches to a solution. In Section 3.5, the investigation of plasma sheathed bodies is discussed. The final part of Section III deals with a comparison of experimental theoretical data for shapes with indented rear terminations.

3.2 Scattering From Re-entry Shape with Rear Concavity (Task 3.1.4)

(U) From the shadow boundary on back to the central point at the rear, the profile of the body is composed of parts of two circles or radii b and c smoothly joined as shown in Fig. 3-1. When a and δ as indicated, the only constraint on a, b, c and δ such that the two circles are smoothly joined is provided by the relation

$$(a - b)^2 + (c + \delta)^2 = (c + b)^2 ,$$
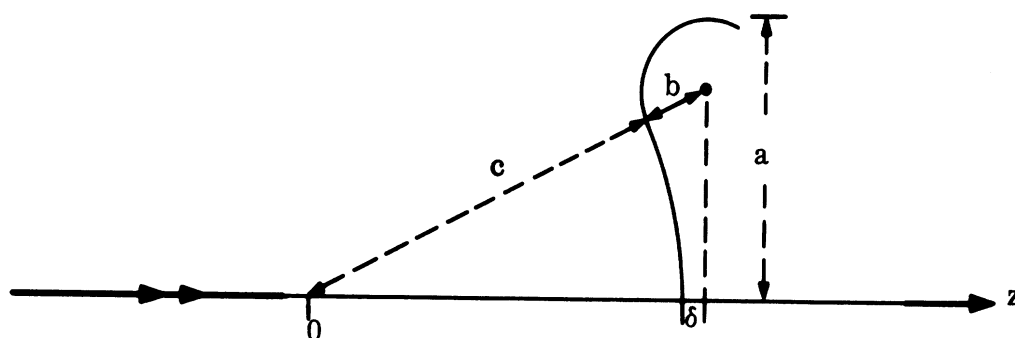
FIG. 3-1: COORDINATE SYSTEM FOR INDENTED REAR.

implying

$$b = \delta + \frac{(a - \delta)^2}{2(a + c)} \quad .$$

(U) If, now, the body is illuminated from the rear, the backscattering cross section according to physical optics is

$$\sigma = \frac{4\pi}{\lambda^2} \left| \int e^{2ikz} \frac{\partial A}{\partial z} \, dz \right|^2$$

when z is measured in the direction of propagation and $A = \pi \rho^2$. The integration is over the illuminated portion of the surface. Since the equation of the central (lower) circular arc is

$$z^2 + \rho^2 = c^2$$

and the equation of the upper arc is

42

$$\left\{ z - (c + \delta) \right\}^2 + \left\{ \rho - (a - b) \right\}^2 = b^2$$

it is convenient to break up the range of integration, with $\frac{\partial A}{\partial z}$ taking the following values:

$$z = \left(c, \ c \ \frac{c + \delta}{c + b} \right) : \ \frac{\partial A}{\partial z} = - 2 \pi z$$

$$z = \left(c \ \frac{c + \delta}{c + b} \ , \ c + \delta - b \right) :$$

$$z = (c + \delta - b, \ c + \delta) : \frac{\partial A}{\partial z} = -2\pi \left\{ z - (c + \delta) \right\} \left\{ 1 - \frac{a - b}{\sqrt{b^2 - (z - c + \delta)^2}} \right\} .$$

Using integration by parts,

$$\int_c^{c\Delta} (-2\pi z) e^{2ikz} dz + \left(\int_{c\Delta}^{c+\delta-b} + \int_{c+\delta-b}^{c+\delta} \right) \left(-2\pi \left\{ z - (c + \delta) \right\} \right) e^{2ikz} \ dz$$

$$= - \frac{ic\lambda}{2} \left\{ \left(1 - \frac{1}{2ikc} \right) e^{2ikc} - \frac{c + \delta}{c} e^{2ikc\Delta} + \frac{1}{2ikc} e^{2ik(c + \delta)} \right\}$$

where

$$\Delta = \frac{c + \delta}{c + b} \ .$$

The remaining integrals involving the factor $(a - b)$ can be broken up as

$$2 \int_{c + \delta}^{c + \delta - b} - \int_{c + \delta}^{c\Delta} .$$

To the first of these we put

$$z = c + \delta - b \sin \theta$$

to get

$$2\pi b(a - b) e^{2ik(c + \delta)} \int_0^\pi \sin \theta \, e^{-2ikb \sin \theta} \, d\theta,$$

and since the saddle point is $\theta = \pi/2$, as asymptotic calculation gives

$$2\pi (a - b) \sqrt{\frac{\pi b}{k}} \, e^{i\pi/4 + 2ik(c + \delta - b)}.$$

Similarly,

$$-\int_{c + \delta}^{c\Delta} = -2\pi b(a - b) e^{2ik(c + \delta)} \int_0^{\theta_0} \sin \theta \, e^{-2ikb \sin \theta} \, d\theta$$

where

$$\theta_0 = \sin^{-1} \frac{c + \delta}{c + b} \equiv \sin^{-1} \Delta$$

and since the saddle point is again $\theta = \pi/2$ (which lies outside the range of integration)

$$-\int_{c + \delta}^{c\Delta} \sim -2\pi b(a - b) e^{2ik(c + \delta)} \tan \theta_0 \int_0^{\theta_0} \cos \theta \, e^{-2ikb \sin \theta} \, d\theta$$

$$= -2\pi b(c + \delta) e^{2ik(c + \delta)} \left[\frac{e^{-2ikb \sin \theta}}{-2ikb} \right]_0^{\theta_0}$$

$$= \frac{i\lambda}{2}(c+\delta) e^{2ik(c+\delta)} \left\{ 1 - e^{-2ikb\Delta} \right\}$$

$$= \frac{i\lambda}{2}(c+\delta) \left\{ e^{2ik(c+\delta)} - e^{2ikc\Delta} \right\}.$$

(U) Adding up all the contributions, we now have

$$\int e^{2ikz} \frac{\partial A}{\partial z} dz \sim - \frac{ic\lambda}{2} \left(1 - \frac{1}{2ikc} \right) e^{2ikc}$$

$$+ 2\pi (a-b) \sqrt{\frac{b\lambda}{2}} e^{i\pi/4 + 2ik(c+\delta-b)}$$

$$- \frac{\lambda^2}{8\pi} \left\{ 1 - 2ik(c+\delta) \right\} e^{2ik(c+\delta)} .$$

The last of these has a phase factor appropriate to the shadow boundary contribution; as such the term is known to be in error and will be omitted. We shall likewise omit the connection term in the first contribution, and thereby obtain

$$\frac{\sigma}{\lambda^2} = \left\{ k(a-b) \right\}^2 (kb) \left| 1 - \frac{c}{a-c} \frac{e^{i\pi/4 + 2ik(b-\delta)}}{2\sqrt{\pi kb}} \right|^2 .$$

(U) The first (dominant) term is attributable to the specular return from the annular ring provided by the upper circle, and we note that the result could have been computed by using the cross section of the infinite circular cylinder $\left[\sigma = kb\ell^2 \right]$ and giving ℓ the value $2\pi(a-b)$ corresponding to the "length" of the ring. The second (smaller) term in the above cross section arises from the lower circle in the profile.

(U) To illustrate the behavior of the above cross section, consider the case

$$c = a$$

$$b = a/4$$

(implying $\delta = 0$), corresponding (approximately) to model ID-2. Then

$$\frac{\sigma}{\lambda^2} = \frac{9}{64} (ka)^3 \left| 1 - \frac{4}{3} \frac{e^{i\pi/4 + i ka/2}}{\sqrt{\pi ka}} \right|^2$$

and some computed values are as follows:

ka	σ/λ^2(db)	ka	σ/λ^2(db)
1	-7.9	3	8.2
$\pi/2$	-1.3	3.5	10.4
2	2.3	4	12.2
2.5	5.6	$3\pi/2$	14.3

Note that ka $= \pi/2$ finds the two contributions in quadrature, whereas ka $= 3\pi/2$ finds then in-phase (and therefore corresponds to a local maximum in the cross section). The above values are in excellent agreement with the measured tail-on data discussed in Section 2.3 and illustrated in Fig. 2-6.

3.3 Absorber Coated Configuration (Task 3.1.2)

3.3.1 Introduction

(U) No suitable techniques exist for determining the surface field induced on a coated cone-sphere. However, the problem can be approached by developing a method of solution for a similar shape which exhibits the same fundamental characteristics as the cone-sphere and then extending that solution to the cone-sphere. The formula for the surface field and for radar cross section which would result from such an approach can then be checked by experimental methods. In section 3.3.2 the surface field on a cylindrical surface is studied and in Section 3.3.3 and Appendix A the surface field on a wedge is studied.

3.3.2 <u>Surface Current in the Shadow Region on a Parabolic Cylinder</u>

(U) A surface current in the shadow region excited by a plane wave on the surface of a perfectly conducting parabolic cylinder is obtained when the focal length is comparable to the incident wavelength. The current is expressed by the residue series which represents creeping waves propagating along the surface. Results are compared with those of the half-plane and large parabolic cylinder.

(U) a) <u>Integral Representation for the Surface Current</u>. Let us consider a perfectly conducting parabolic cylinder $x^2 = 4h(h - y)$ with the focal length h and the focus at the origin of coordinates (Fig. 3-1). In parabolic coordinates
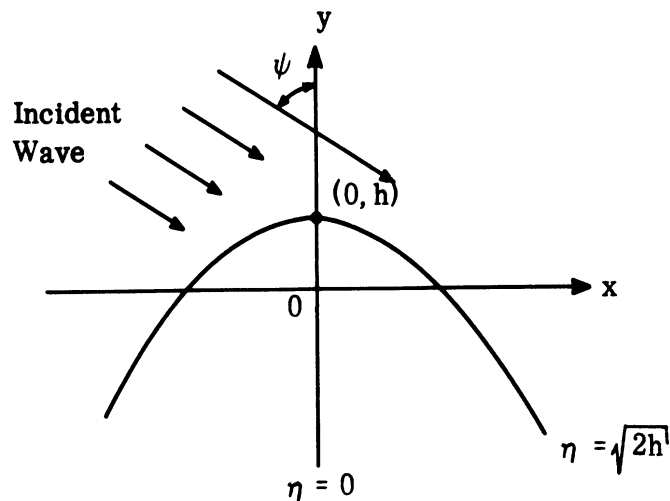
$$x = \xi\eta$$
$$y = \frac{1}{2}(\eta^2 - \xi^2)$$

(3.1)

FIG. 3-1: THE SURFACE OF THE PARABOLIC CYLINDER $x^2 = 4h(h - y)$.

the given parabolic cylinder is a coordinate surface $\eta = \sqrt{2h} \geq 0$. When $\eta = 0$ the cylinder reduces to the half-plane $x = 0$, $y \leq 0$. In the variables ξ, η the wave equation takes the form

$$\frac{\partial^2 u}{\partial \xi^2} + \frac{\partial^2 u}{\partial \eta^2} + k^2 (\xi^2 + \eta^2) u = 0. \tag{3.2}$$

By separation of variables in this equation, solutions are expressed in terms of Hermite functions.

(U) Following Rice's (1954) notation, special solutions of (3.2) are defined by contour integrals of the form

$$W_n(x) = \frac{1}{2\pi i} \int_W e^{f(t)} dt, \tag{3.3}$$

$$U_n(z) = \frac{1}{2\pi i} \int_U e^{f(t)} dt, \tag{3.4}$$

where

$$f(t) = t^2 + 2zt - (n + 1)\ln t. \tag{3.5}$$

The path of integration for $W_n(z)$ runs for $+\infty$ to $-\infty$ where $\arg t = -\pi$, and the path for $U_n(z)$ comes in from $-\infty$ where $\arg t = -\pi$, encircles the origin counterclockwise and runs out to $-\infty$ with $\arg t = \pi$ in the complex t-plane shown in Fig. 3-2.

(U) The Wronskian of these functions is

$$W'_n U_n - U'_n W_n = i \frac{2^n e^{z^2}}{\sqrt{\pi}\, \Gamma(n + 1)}. \tag{3.6}$$

t - plane

cut

U

W

t_i

t_r
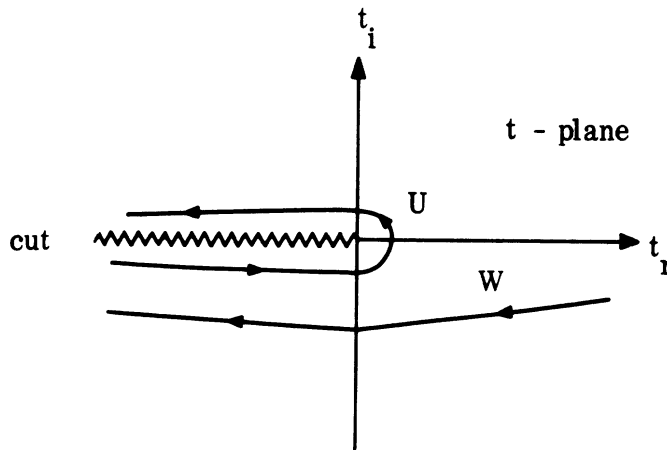
FIG. 3-2: PATHS OF INTEGRATION FOR THE FUNCTION
$U_n(z)$ AND $W_n(z)$.

(U) The Dirichlet problem and the Neumann problem will be solved for the wave equation (3.2) by assuming an incident plane wave $u_o = e^{-ik(x \sin\psi - y \cos\psi)}$ and omitting the time factor $e^{i\omega t}$. Then the solution takes the form $u_o = u_o + u_s$; here u_s is the wave scattered from the cylinder and satisfying the radiation conditions. For the Dirichlet problem, the solution satisfies the boundary condtion $u|_{\eta = \eta_o} = 0$ on the cylinder, and it satisfies $\partial u / \partial \eta |_{\eta = \eta_o} = 0$ for the Neumann problem.

(U) The expansion of the plane wave in Hermite functions is well known:

$$u_o = e^{-ik(x \sin\psi - y \cos\psi)}$$

$$= e^{iky} \sec \frac{\psi}{2} \sum_0^\infty n! \left(-\frac{i}{2} \tan\frac{\psi}{2}\right)^n U_n(z)U_n(z'), \quad 0 < |\psi| < \frac{\pi}{2} \qquad (3.7)$$

where

$$z = \sqrt{ik}\,\xi, \qquad z' = \sqrt{-ik}\,\eta \qquad (3.8)$$

(U) Expressing the scattered field u_s in the form of the superposition of the function $e^{iky} U_n(z) W_n(z')$ satisfying the radiation conditions as $\eta \to \infty$, the solution of the Dirichlet problem is obtained as

$$u_D = e^{iky} \sec \frac{\psi}{2} \sum_{n=0}^{\infty} n! \left(-\frac{i}{2} \tan \frac{\psi}{2} \right)^n U_n(z) \left[U_n(z') \right.$$

$$\left. - \frac{U_n(z'_0)}{W_n(z'_0)} W_n(z') \right] \tag{3.9}$$

where

$$z'_0 = \sqrt{-ik'}\, \eta_0 = \sqrt{-2ikh} = \sqrt{-i}\, \rho \quad . \tag{3.10}$$

Similarly the solution for the Neumann problem is

$$u_N = e^{iky} \sec \frac{\psi}{2} \sum_{n=0}^{\infty} n! \left(-\frac{i}{2} \tan \frac{\psi}{2} \right)^n U_n(z) \left[U_n(z') \right.$$

$$\left. - \frac{'U_n(z'_0)}{'W_n(z'_0)} W_n(z') \right] \tag{3.11}$$

where

$$'W_n(z) = -z W_n(z) + \frac{\partial}{\partial z} W_n(z)$$

$$\tag{3.12}$$

$$'U_n(z) = -z U_n(z) + \frac{\partial}{\partial z} U_n(z) \quad .$$

Series in (3.9) and (3.11) converge, if $\left| \tan \frac{\psi}{2} \right| < 1$. Correspondingly, surface currents are obtained for the Dirichlet problem as

$$J_D = \frac{1}{\sqrt{\eta^2 + \xi^2}} \frac{\partial u_D}{\partial \eta}\bigg|_{\eta = \eta_0}$$

$$= \sqrt{\frac{ik}{2\pi r}} e^{-ikr} \sec \frac{\psi}{2} \sum_{n=0}^{\infty} \left(-i \tan \frac{\psi}{2}\right)^n \frac{U_n(z)}{W_n(z'_0)} \tag{3.13}$$

and for the Neumann problem as

$$J_N = u_N\bigg|_{\eta = \eta_0}$$

$$= i \frac{1}{\sqrt{\pi}} e^{-ikr} \sec \frac{\psi}{2} \sum_{n=0}^{\infty} \left(-i \tan \frac{\psi}{2}\right)^n \frac{U_n(z)}{'W_n(z'_0)} \tag{3.14}$$

where

$$r = \frac{1}{2}(\xi^2 + \eta_0^2) = \frac{1}{2}(\xi^2 + 2h) \ .$$

(U) By Watson's transformation, the series can be converted into contour integrals with n as the complex veriable of integration. Thus expressions (3.13) and (3.14) are transformed respectively into

$$J_D = \sqrt{\frac{k}{2\pi ri}} \frac{e^{-ikr}}{2} \sec \frac{\psi}{2} \int_{C_1} \frac{\left(i \tan \frac{\psi}{2}\right)^n}{\sin \pi n} \frac{U_n(z)}{W_n(z'_0)} dn \tag{3.15}$$

and

$$J_N = \frac{1}{\sqrt{\pi}} \frac{e^{-ikr}}{2} \sec \frac{\psi}{2} \int_{C_1} \frac{\left(i \tan \frac{\psi}{2}\right)^n}{\sin \pi n} \frac{U_n(z)}{'W_n(z'_0)} dn \ . \tag{3.16}$$

with the path of integration C_1 shown in Fig. 3-3.
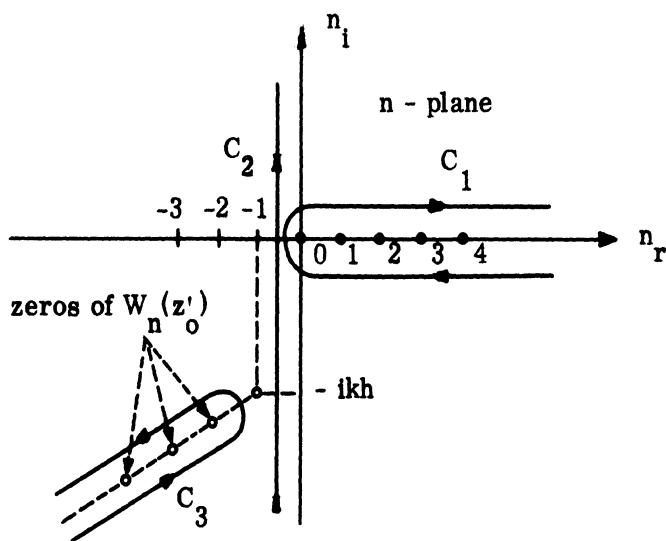
FIG. 3-3: PATHS OF INTEGRATION IN THE COMPLEX n-PLANE.

(U) Since all zeros of both functions $W_n(z'_0)$ and $'W_n(z'_0)$, are located in the third quadrant of the n-plane, while the points n = -1, -2, -3, ... are not singular (Rice, 1954), the contour C_1 may be deformed into C_2. In the shadow region the asymptote of the integral over C_2 is defined by the poles of the integrand located to the left of C_2. In this case C_2 may be deformed into C_3. For the shadow region we obtain

$$J_D = \sqrt{\frac{ik\pi}{2r}} \, e^{-ikr} \sec \frac{\psi}{2} \sum_{s=1}^{\infty} \left[\frac{\left(i \tan \frac{\psi}{2}\right)^n U_n(z)}{\sin \pi n \, \frac{\partial}{\partial n} W_n(z'_0)} \right]_{n=n_s} \tag{3.17}$$

$$J_N = i\sqrt{\pi} \, e^{-ikr} \sec \frac{\psi}{2} \sum_{s=0}^{\infty} \left[\frac{\left(i \tan \frac{\psi}{2}\right)^n U_n(z)}{\sin \pi n \, \frac{\partial}{\partial n} 'W_n(z'_0)} \right]_{n=n'_s} \tag{3.18}$$

here n_s and n'_s are zeros of functions $W_n(z'_0)$ and $'W_n(z'_0)$ respectively.

(U) Now currents are expressed by the sum of the residues at the poles which in turn represent creeping waves launched from the shadow boundary and traveling along the surface of the parabolic cylinder.

(U) b) The Saddle-point Method. The saddle-point method of approximate integration is used to obtain asymptotic expressions for the functions $W_n(z)$ and $U_n(z)$. Let the integrand of the integral of (3.3) be

$$f(t) = -t^2 + 2zt - m \ell nt, \qquad m = n + 1, \tag{3.19}$$

then we have

$$W_n(z) = \frac{1}{2\pi i} \int_W e^{f(t)} dt. \tag{3.20}$$

The saddle points of the integrand are located at points t_0 and t_1 in the complex t-plane where $f'(t) = 0$. Solving this equation we have

$$t_0 = (1/2) \left(z + \sqrt{z^2 - 2m} \right) \tag{3.21}$$

$$t_1 = (1/2) \left(z - \sqrt{z^2 - 2m} \right) \tag{3.22}$$

$$t_0^2 - zt_0 = -\frac{m}{2} \tag{3.23}$$

$$t_0 + t_1 = z \tag{3.24}$$

$$2t_0 t_1 = m \tag{3.25}$$

(U) Let the path of integration W of (3.20) be deformed so as to pass through a saddle point t_0 along a path of steepest descent. In the vicinity of the saddle point, a Taylor expansion gives

$$f(t) = f(t_o) + \frac{1}{2} \left. \frac{d^2 f}{dt^2} \right|_{t = t_o} (t - t_o)^2 + \ldots . \tag{3.26}$$

(U) If

$$\left. \frac{d^2 f}{dt^2} \right|_{t = t_o} = b \neq 0,$$

the main contribution to the value of the integral comes from the vicinity of t_o as expressed by

$$W_n(z) \approx \frac{e^{f(t_o)}}{i \sqrt{2\pi b}} \tag{3.27}$$

where

$$b = \frac{2(t_o - t_1)}{t_o} .$$

The sign of $(2\pi b)^{-1/2}$ is chosen so that the argument of the right hand side of (3.27) is equal to arg (dt) at $t = t_o$ on the path of steepest descent. The values of these quantities at the saddle point t_1 may be obtained by interchanging t_o and t_1. Similarly we can obtain the asymptotic expression of the function $U_n(z)$ as (3.27).

(U) c) <u>The Path of Steepest Descent.</u> The path of steepest descent which passes through t_o is that branch of the curve

$$\text{Im} \left[f(t) - f(t_o) \right] = 0$$

and

$$\text{Re} \left[f(t) - f(t_o) \right] \leq 0 \tag{3.28}$$

for which t_o is the highest point.

(U) The path of steepest descent may be shown to have the following properties:

(1) If z is regarded as fixed and t_o, t_1 are functions of m defined by (3.21) and (3.22), the equation

$$\text{Im}\left[f(t_o) - f(t_1)\right] = 0 \tag{3.29}$$

defines a critical boundary in the complex m-plane. On this boundary the steepest descent contour passes through two saddle points, t_o and t_1, in the complex t-plane. In this case, both saddle points will contribute to the asymptotic expression of the functions $W_n(z)$ and $U_n(z)$. In general, this critical boundary defines a region in the complex m-plane within which a function is approximately evaluated from two saddle points (Fig. 3-4).

(2) If m is such that the path of integration for a particular function, say $W_n(z)$, must be deformed along the steepest descent contour to pass both saddle points, each one will contribute to the value of $W_n(z)$. Furthermore, if m is such that

$$\text{Re}\left[f(t_o) - f(t_1)\right] = 0 \tag{3.30}$$

t_o and t_1 have the same height and the two contributions have a chance of cancelling each other and giving a value of zero for $W_n(z)$. Thus (3.30) defines the line in the complex m-plane along which zeros of $W_n(z)$ are asymptotically distributed (Fig. 3-5).

(3) The lines in the complex m-plane defined by (3.29) and (3.30) may be obtained by the following transformation

$$w = \ell n \, (t_o/t_1) = u + iv \quad . \tag{3.31}$$
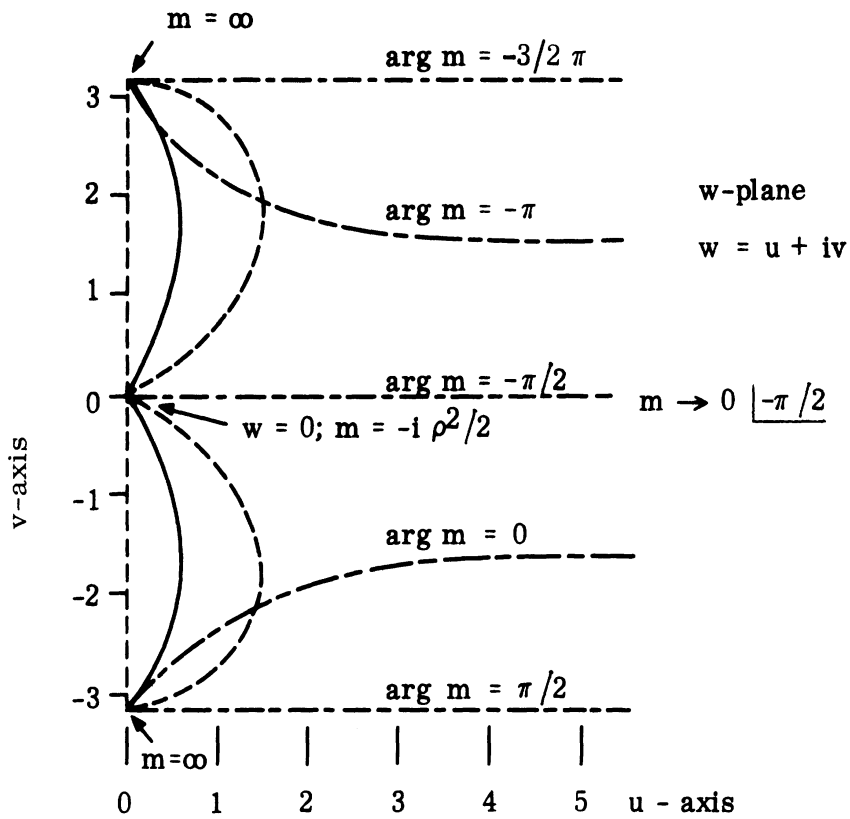
FIG. 3-4: THE w-PLANE WHEN $z = \sqrt{-i}\ \rho$; $\rho = \sqrt{2kh}$.

$$m = -i\,\rho^2/2$$

m-plane

$$m = n + 1$$

m_i

m_r

0
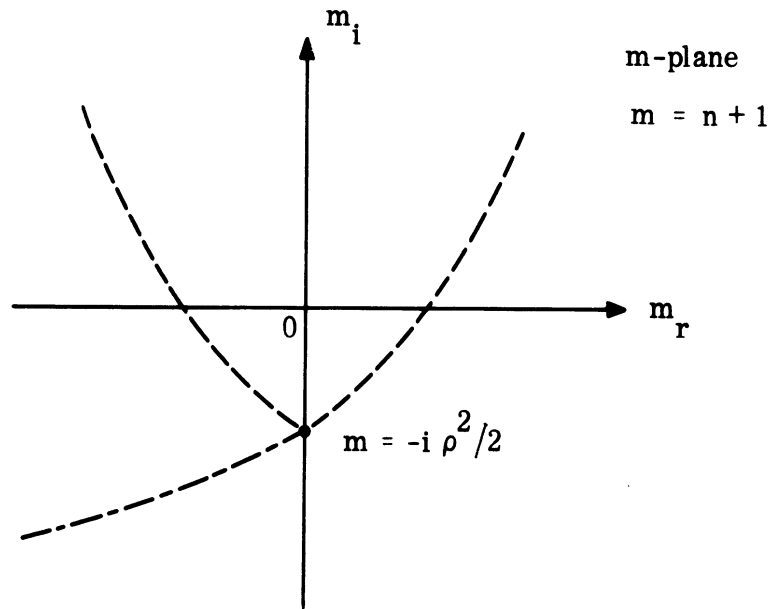
---- Zeros of $W_n(z)$

$$R_e\left[f(t_0) - f(t_1)\right] = 0$$

--- Boundary of

$$I_m\left[f(t_0) - f(t_1)\right] = 0$$

FIG. 3-5: LINE OF ZEROS FOR THE FUNCTION $W_n(z)$ WHEN $z = \sqrt{-i}\ \rho$.

From this transformation we obtain

$$m = \frac{z^2}{\cosh w + 1} \tag{3.32}$$

$$f(t_0) - f(t_1) = m(\sinh w - w) = \frac{z^2 (\sinh w - w)}{\cosh w + 1} \tag{3.33}$$

Since $\left| t_0 \right| \geq t_1$ and $\left| \arg t_0 - \arg t_1 \right| \leq \pi$ we have $u \geq 0$ and $|v| \leq \pi$ for mapping. The w-plane is shown in Fig. 3-4.

(4) For the special case $z = \sqrt{-2ikh} = \sqrt{-i}\,\rho = \rho\, e^{-i\pi/4}$, (3.33) gives

$$(\cosh u + \cos v - v \sin v) \sinh u = (\cosh u \cos v + 1) u \tag{3.34}$$

$$(\cos v + \cosh u + u \sinh u) \sin v = (\cosh u \cos v + 1) v \tag{3.35}$$

respectively for $\text{Im}\left[f(t_0) - f(t_1) \right] = 0$ and $\text{Re}\left[f(t_0) - f(t_1) \right] = 0$. These equations are plotted in Fig. 3-4 and 3-5.

(U) d) <u>Zeros of $W_n(z'_0)$</u>. The zeros of $W_n(z'_0)$, regarded as function n, occur when the contribution from two saddle points cancel each other. Thus the zeros will distribute very nearly $\text{Re}\left[f(t_0) - f(t_1) \right] = 0$ in the m-plane (Fig. 3-5).

(U) When $z'_0 = \sqrt{-2ikh} = \sqrt{-i}\,\rho$, the asymptotic expression of $W_n(z'_0)$ for the case in which the path of integration passes through two saddle points t_0 and t_1 is

$$W_n(z'_0) = A_0 - A_1 \tag{3.36}$$

where

$$A_0 = \frac{\sqrt{t_0}\; e^{f(t_0)}}{-2i\sqrt{\pi}\; (-i\rho^2 - 2m)^{1/4}}$$

$$A_1 = \frac{\sqrt{t_1}\ e^{f(t_1)}}{2\sqrt{\pi}\ (-i\rho^2 - 2m)^{1/4}}$$

$$t_o = \frac{1}{2}\left[\sqrt{-i}\ \rho + \sqrt{-i\rho^2 - 2m}\right]$$

$$t_1 = \frac{1}{2}\left[\sqrt{-i}\ \rho - \sqrt{-i\rho^2 - 2m}\right]$$

$$f(t_o) = \frac{m}{2}\left(1 - \ln\frac{m}{2} - \ln\frac{t_o}{t_1}\right) + \sqrt{-i}\ \rho\ t_o$$

$$f(t_1) = \frac{m}{2}\left(1 - \ln\frac{m}{2} - \ln\frac{t_1}{t_o}\right) + \sqrt{-i}\ \rho\ t_1$$

$$m = n + 1$$

$$-3\pi/2 \leq \arg m < \pi/2$$

$$-3\pi/2 \leq \arg (-i\rho^2 - 2m) < \pi/2$$

$$-3\pi/4 \leq \arg t_o < \pi/4$$

$$-5\pi/4 \leq \arg t_1 < 3\pi/4$$

therefore zeros of $W_n(\sqrt{-i}\ \rho)$ are located at

$$W_n(\sqrt{-i}\rho) = A_o - A_1 = 0 \tag{3.37}$$

or

$$\exp\left[f(t_o) - f(t_1)\right] = \frac{1}{i\sqrt{t_o/t_i}} \tag{3.38}$$

(U) Using the transformation (3.31) and (3.33) we obtain

$$\exp\left[f(t_0) - f(t_1)\right] = \exp\left\{(z'_0)^2\left[\frac{\sinh w - w}{\cosh w + 1}\right]\right\}, \tag{3.39}$$

and

$$\frac{1}{i\sqrt{t_0/t_1}} = \frac{1}{\exp\left[i(\frac{\pi}{2} - 2s\pi)\right]e^{w/2}} \tag{3.40}$$

where $s = 1, 2, 3, \ldots,$

$$(z'_0)^2 = -i\rho^2$$

$$w = u + iv .$$

From (3.39) and (3.40), zeros are located by the following equation

$$-i\rho^2\frac{\sinh w - w}{\cosh w + 1} = -\left[\frac{w}{2} + i\frac{\pi}{2}(1 - 4s)\right] \tag{3.41}$$

By separating the real part and the imaginary part of (3.41), we obtain two simultaneous equations

$$\rho^2\left[(\cos v + \cosh u + u\sinh u)\sin v - (\cosh u \cos v + 1)v\right] =$$

$$= -\frac{1}{2}u\left[(\cosh u \cos v + 1)^2 + (\sinh u \sin v)^2\right] \tag{3.42}$$

$$\rho^2\left[(\cos v + \cosh u - v\sin v)\sinh u - (\cosh u \cos v + 1)u\right] =$$

$$= \frac{1}{2}\left[v + (1 - 4s)\pi\right]\left[(\cosh u \cos v + 1)^2 + (\sinh u \sin v)^2\right] \tag{3.43}$$

Let (3.42) be divided by (3.43), we obtain

$$\frac{(\cos v + \cosh u + u \sinh u)\sin v - (\cosh u \cos v + 1)v}{(\cos v + \cosh u + v \sin v)\sinh u - (\cosh u \cos v + 1)u} =$$

$$= \frac{-u}{v - (1 - 4s)\pi} \cdot \qquad (3.44)$$

This equation is independent of the parameter ρ. Setting $s = 1$, we calculate the first zero as the following:

(U) Equation (3.44) may be approximated by a circle in the w-plane as

$$\left[u - (r - a)\right]^2 + \left[v - \frac{\pi}{2}\right]^2 = r^2 \qquad (3.45)$$

where

$$r = \frac{a^2 + (\pi/2)^2}{2a}$$

$$a = u\big|_{v = \pi/2} = 0.575, \quad s = 1$$

$$0 < u < a < 1 \quad .$$

For $u < 1$, (3.43) can be evaluated approximately by

$$-\rho^2 uv \sin v = \frac{1}{2}(v - 3\pi)\left[(\cos v + 1)^2 + (u \sin v)^2\right] \quad . \qquad (3.46)$$

The location of zeros may be obtained by graphical means. If we plot (3.45) and (3.46) on the w-plane, the points of intersection between the two curves determine the zeros of $W_n(z'_o)$. A typical plot is given in Fig. 3-6. Mapping the zeros of $W_n(z'_o)$ from the auxilliary w-plane with the help of $m = -i\rho^2/$ (cosh $w + 1$) gives the location of zeros on the m-plane. If we consider ρ as the variable parameter, the locus of the first zero in the m-plane is expressed approximately by

FIG. 3-6: GRAPHICAL SOLUTION FOR ZEROS OF $W_n(z)$ WHEN $z = \sqrt[n]{-i}\,\rho$.

$$m_p = -\frac{1}{2}\left[(\rho + 2.8) + i(\rho^2 + \rho + 1.4)\right] \qquad (3.47)$$

where we limit the range of ρ as $0 < \rho < 10$. Re m_p and Im m_p are plotted in Fig. 3-7. Similarly, loci for $s = 2, 3, 4\ldots,$ may be obtained by the graphical method.

(U) e) $\underline{\text{Zeros of } {}'W_n(z'_o).}$ In Neumann's problem we define the function

$$'W_n(z'_o) = -z'_o W_n(z'_o) + \frac{\partial}{\partial z'_o} W_n(z'_o) . \qquad (3.48)$$

Here

$$W'_n(z'_o) = \frac{\partial}{\partial z'_o} W_n(z'_o)$$

has the asymptotic expression

$$W'_n(z'_o) \simeq 2t_o\left[\text{contribution of } t_o \text{ to } W_n(z'_o)\right] +$$

$$+ 2t_1\left[\text{contribution of } t_1 \text{ to } W_n(z'_o)\right] \qquad (3.49)$$

from the saddle points t_o and t_1. If the path of integration does not pass through a particular saddle point, its contribution to (3.49) is zero. Upon replacing t_o and t_1 by their expressions and subtracting the corresponding expression for $z'_o W_n(z'_o)$ we obtain

$$'W_n(z'_o) \simeq \sqrt{(z'_o)^2 - 2m}\left\{\left[t_o \text{ contribution to } W_n(z'_o)\right] - \right.$$

$$\left. - \left[t_1 \text{ contribution to } W_n(z'_o)\right]\right\} . \qquad (3.50)$$

(U) When $z'_o = \sqrt{-2ikh} = \sqrt{-i}\,\rho$, the asymptotic expression of $'W_n(z'_o)$ for the case that the path of integration passes through two saddle points t_o and t_i is
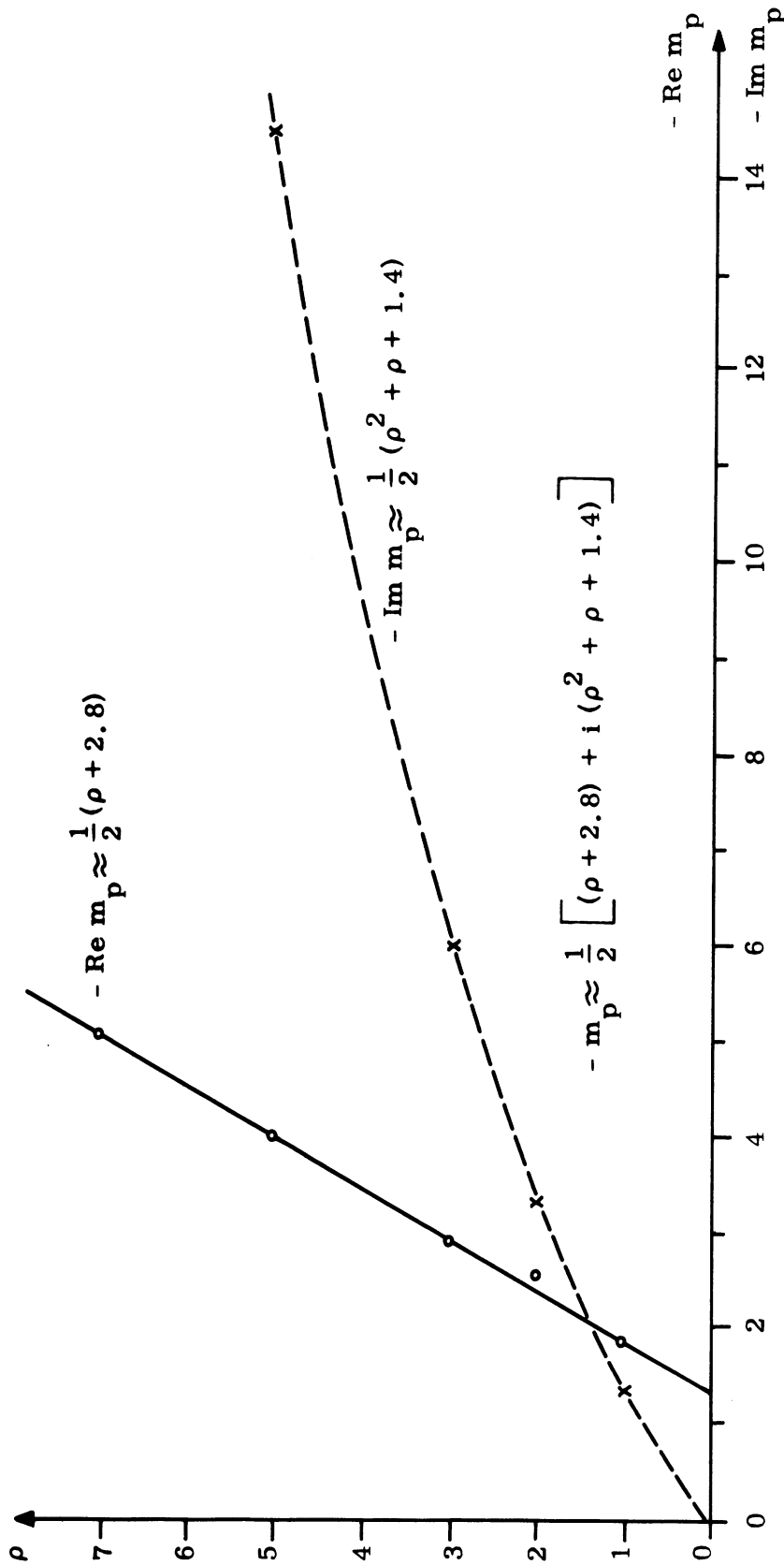
$$- \text{Re}\, m_p \approx \frac{1}{2}(\rho + 2.8)$$

$$- \text{Im}\, m_p \approx \frac{1}{2}(\rho^2 + \rho + 1.4)$$

$$- m_p \approx \frac{1}{2}\left[(\rho + 2.8) + i(\rho^2 + \rho + 1.4)\right]$$

FIG. 3-7: LOCUS OF THE FIRST ZERO OF $W_n(z)$ IN THE m-PLANE WHEN $z = \sqrt{-i}\; \rho.$

64

$$'W_n(z'_o) = \sqrt{-i\rho^2 - 2m}\,\left[A_o + A_1\right] , \tag{3.51}$$

where A_o and A_1 are expressed by (3.36).

(U) Therefore, the zeros of $'W_n(z)$ are located at

$$A_o + A_1 = 0 \tag{3.52}$$

or

$$\exp\left[f(t_o) - f(t_1)\right] = \frac{i}{\sqrt{t_o/t_1}} \quad ; \tag{3.53}$$

here t_o, t_1, $f(t_o)$ and $f(t_1)$ are also expressed by (3.36).

(U) Using the transformation $w = \ln(t_o/t_1) = u + iv$, we obtain

$$-i\rho^2\,\frac{\sinh w - w}{\cosh w + 1} = i\,\frac{\pi}{2}\,(1 + 4s) - \frac{w}{2} \tag{3.54}$$

where $s = 0, 1, 2, 3, \ldots$. By separating the real part and the imaginary part of (3.54) we obtain two simultaneous equations

$$\rho^2\left[(\cos v + \cosh u + u \sinh u) \sin v - (\cosh u \cos v + 1)v\right]$$
$$= -\frac{1}{2}\,u\left[(\cosh u \cos v + 1)^2 + (\sinh u \sin v)^2\right] \tag{3.55}$$

$$\rho^2\left[(\cos v + \cosh u - v \sin v) \sinh u - (\cosh u \cos v + 1)u\right]$$
$$= \frac{1}{2}\left[v - \pi(1 + 4s)\right]\left[(\cosh u \cos v + 1)^2 + (\sinh u \sin v)^2\right] \tag{3.56}$$

Dividing (3.55) by (3.56) we have

$$\frac{(\cos v + \cosh u + u \sinh u)\sin v - (\cosh u \cos v + 1)v}{(\cos v + \cosh u + v \sin v)\sinh u - (\cosh u \cos v + 1)u} =$$
$$= \frac{-u}{v - \pi(1 + 4s)} \tag{3.57}$$

Setting $s = 0$, (3.57) may be approximated by a circle in the w-plane

$$\left[u - (r - a)\right]^2 + \left[v - \frac{\pi}{2}\right]^2 = r^2 \tag{3.58}$$
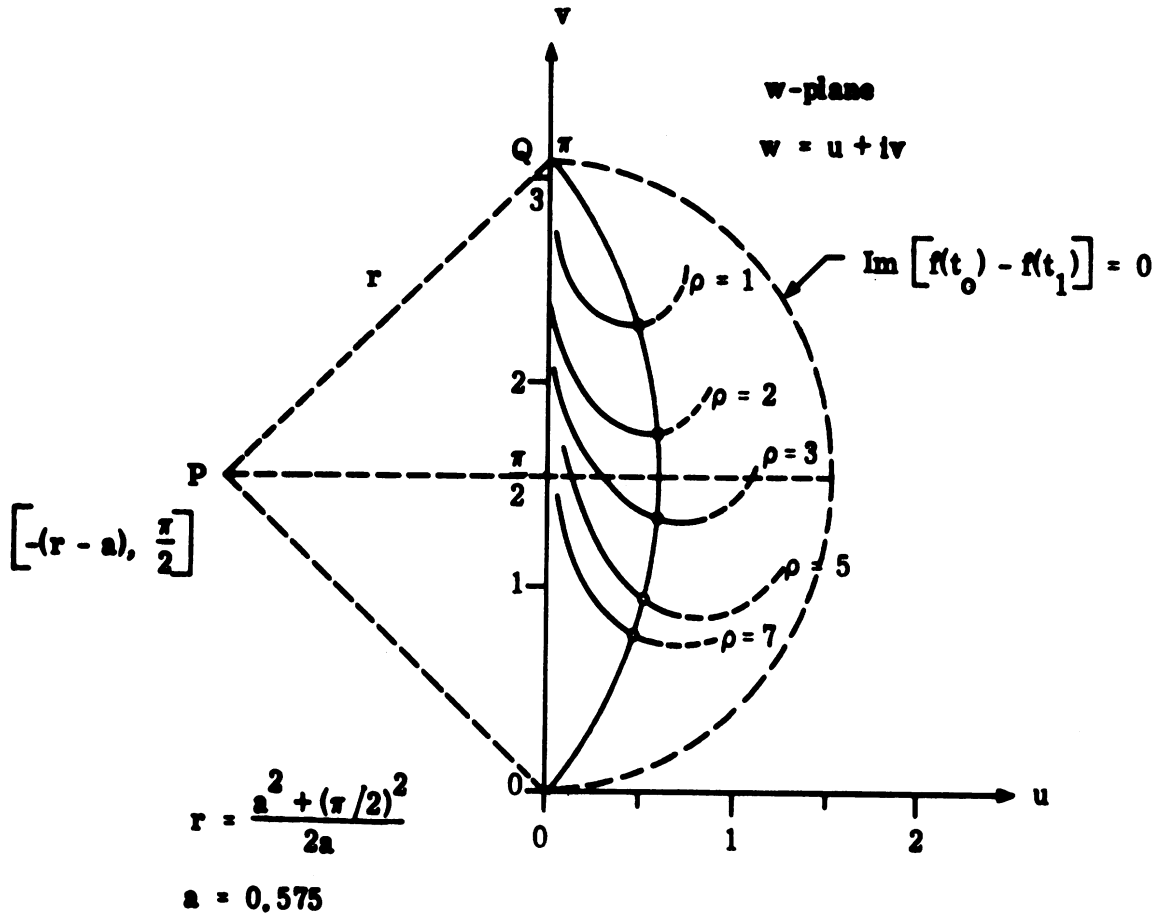
where

$$r = \frac{a^2 + (\pi/2)^2}{2a}$$

$$a = u\Big|_{v = \pi/2} = 0.48$$

$$0 < u < a < 1.$$

For $u < 1$, (3.56) may be approximated by

$$-\rho^2 uv \sin v = \frac{1}{2}(v - \pi)\left[(\cos v + 1)^2 + (u \sin v)^2\right] . \tag{3.59}$$

The location of zeros are determined by the graphical method from (3.58) and (3.59). A typical plot is shown in Fig. 3-8. Mapping the zeros from the w-plane to m-plane gives approximately the locus of the first zero as

$$m'_p = -(\frac{1}{\pi}\rho + \frac{1}{10}) - i\frac{1}{2}\rho(\rho + 1) \tag{3.60}$$

where ρ is limited in the range $0 < \rho < 10$. Re m'_p and Im m'_p are plotted in Fig. 3-9. Similarly, loci for $s = 1, 2, 3, \ldots$, may be obtained by the graphical method.

(U) f) The Value of the Functions $\frac{\partial}{\partial n} W_n(z'_o)$ and $\frac{\partial}{\partial n} {}'W_n(z'_o)$ Evaluated at Zeros. The function $W_n(z'_o)$ is defined by

$$W_n(z'_o) = \frac{1}{2\pi i}\int_W e^{f(t)} dt \tag{3.61}$$

where

$$f(t) = -t^2 + 2z'_o t - (n + 1)\ln t . \tag{3.62}$$
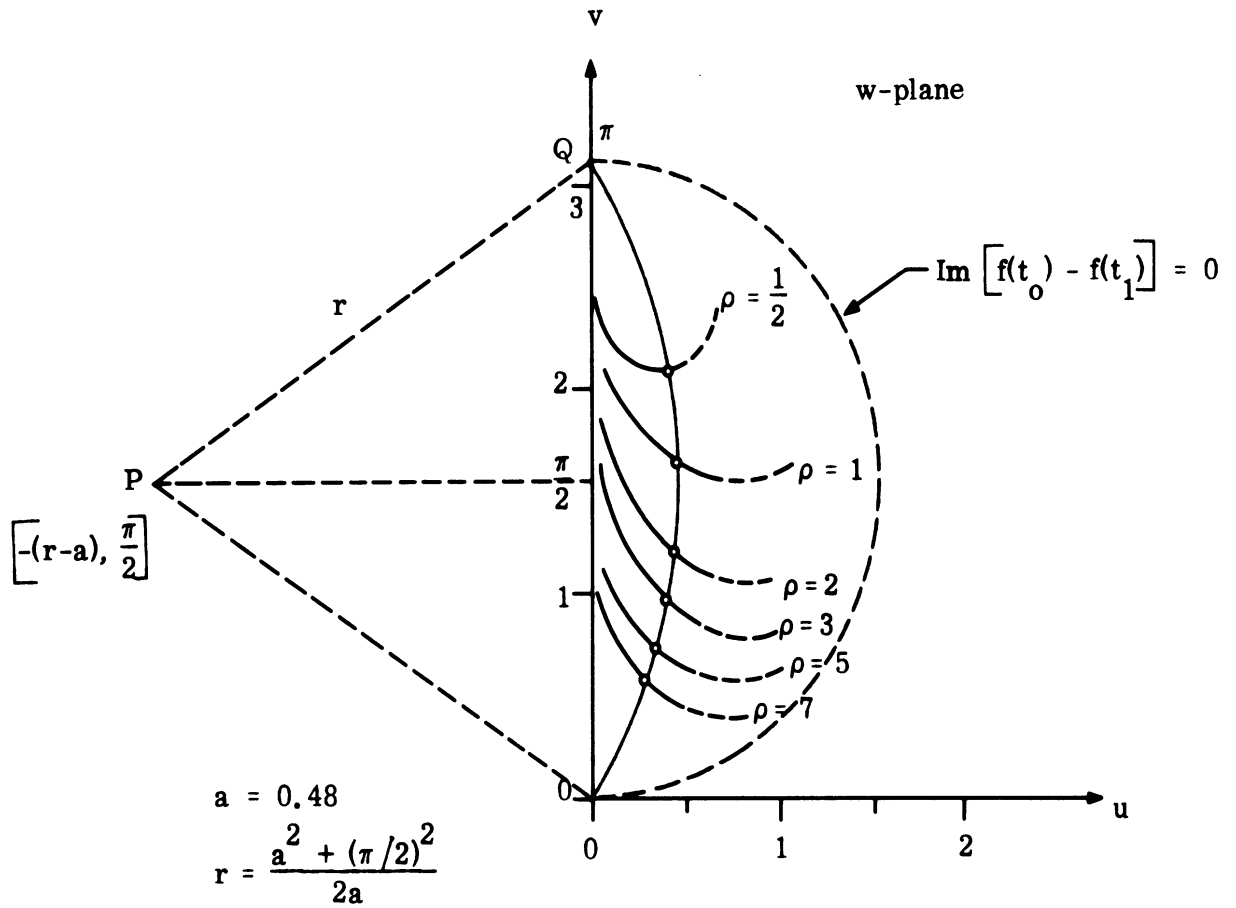
FIG. 3-8: GRAPHICAL SOLUTION FOR ZEROS OF
$W_n(z)$ WHEN $z = \sqrt{-i}\, \rho$.
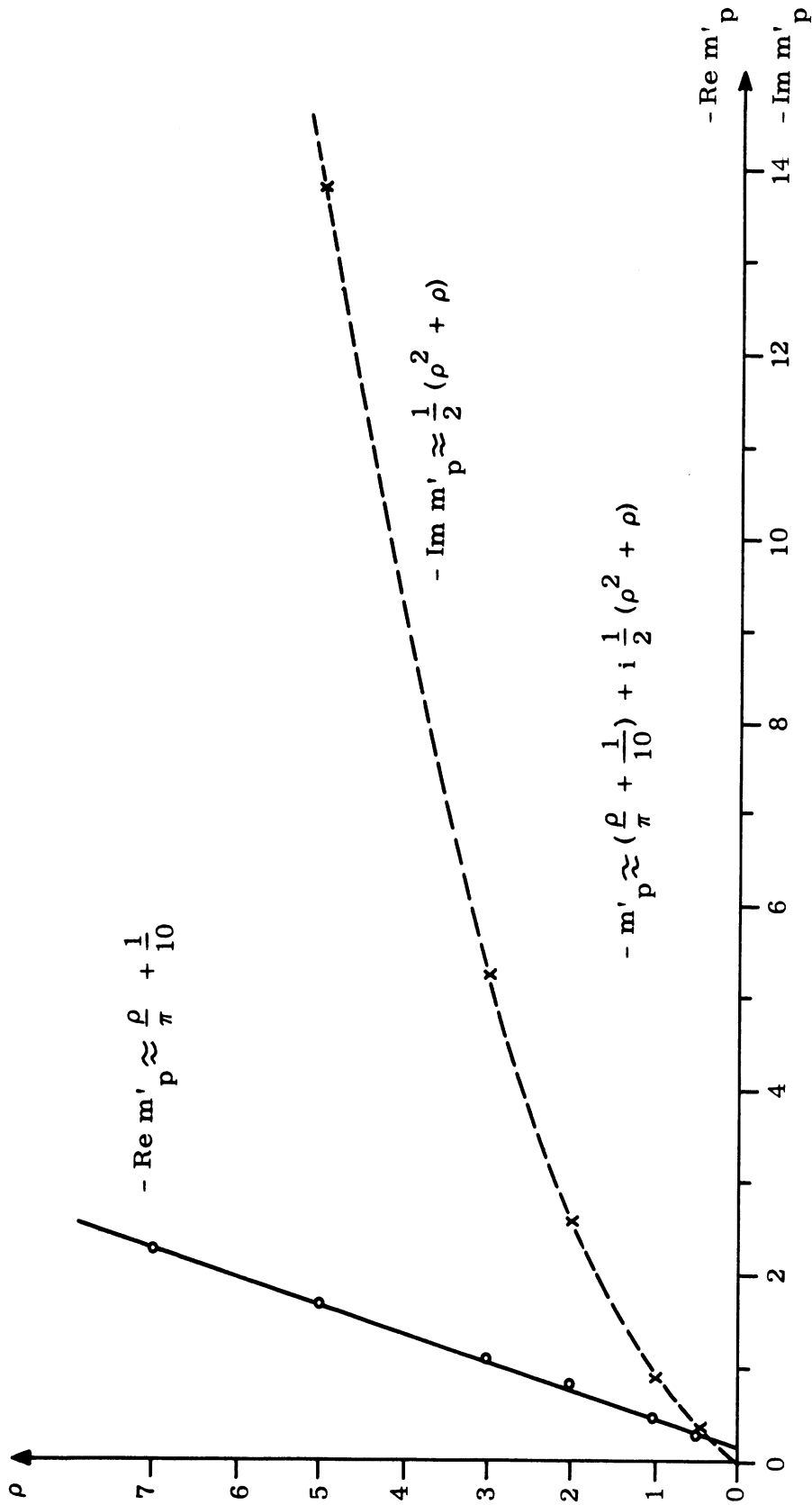
67

$$-\operatorname{Re} m'_p \approx \frac{\rho}{\pi} + \frac{1}{10}$$

$$-\operatorname{Im} m'_p \approx \frac{1}{2}(\rho^2 + \rho)$$

$$-m'_p \approx (\frac{\rho}{\pi} + \frac{1}{10}) + i\frac{1}{2}(\rho^2 + \rho)$$

FIG. 3-9: LOCUS OF THE FIRST ZERO OF $'W_n(z)$ IN THE m-PLANE WHEN $z = \sqrt{-i}\,\rho$.

68

Differentiating (3.61) we obtain the function $\frac{\partial}{\partial n} W_n(z'_o)$ as

$$\frac{\partial}{\partial n} W_n(z'_o) = -\frac{1}{2\pi i} \int_W (\ell nt) \, e^{f(t)} \, dt \tag{3.63}$$

If we assume the path of integration W does not pass through the point $t = 0$, the function $\ell n(t)$ may be considered as a slowly varying function in comparison with the integrand and put outside the integration sign at the saddle point. Therefore the saddle-point method may be applied to evaluate the asymptotic expression as the following

$$\frac{\partial}{\partial n} W_n(z'_o) \simeq -(\ell nt_o) \left[\text{contribution of } t_o \text{ to } W_n(z)\right] -$$

$$- (\ell nt_1) \left[\text{contribution of } t_1 \text{ to } W_n(z)\right]$$

$$= -\left[(\ell nt_o) A_o - (\ell nt_1) A_1\right] \tag{3.64}$$

where A_o and A_1 are expressed by (3.36) and $z'_o = \sqrt{-2ikh} = \sqrt{-i\rho}$. At the zero, $A_o - A_1 = 0$, the asymptotic expression gives

$$\frac{\partial}{\partial n} W_n(z'_o) \bigg|_{n = n_s} = -\left[\ell n (t_o/t_1)\right] A_o \tag{3.65}$$

where n_s is the sth zero of $W_n(z)$ in the n-plane.

(U) Next let us consider the definition

$$'W_n(z'_o) = -z'_o W_n(z'_o) + \frac{\partial}{\partial z'_o} W_n(z'_o) . \tag{3.66}$$

By a similar consideration as before, we obtain the asymptotic expression for $\frac{\partial}{\partial n} 'W_n(z'_o)$ as

$$\frac{\partial}{\partial n} \, 'W_n(z'_0) \cong -z'_0 \left[-(\ell n t_0)A_0 + (\ell n t_1)A_1 \right] +$$

$$+ 2 \left[- (\ell n t_0)t_0 A_0 + (\ell n t_1)t_1 A_1 \right]$$

$$= -\sqrt{(z'_0)^2 - 2m} \left[(\ell n t_0)A_0 + (\ell n t_1)A_1 \right] \tag{3.67}$$

At the zero, $A_0 + A_1 = 0$, we obtain

$$\frac{\partial}{\partial n} \, 'W_n(z'_0) \bigg|_{n = n'_s} = -\sqrt{(z'_0)^2 - 2m'_p} \left[\ell n(t_0/t_1) \right] A_0 \tag{3.68}$$

where n'_s is the sth zero of $'W_n(z)$ in the n-plane, and

$$z'_0 = \sqrt{-2ikh} = \sqrt{-i} \; \rho$$

$$m'_p = - (\frac{1}{\pi}\rho + \frac{1}{10}) - i \frac{1}{2} \rho (\rho + 1) = n'_s + 1 \; .$$

(U) g) <u>Surface Currents in the Shadow Region.</u> The asymptotic expression of the function $U_n(z)$ at zeros of the functions $W_n(\sqrt{-i}\rho)$ and $'W_n(\sqrt{-i} \; \rho)$ was obtained by Rice (1954) as

$$U_n(z) = (1 - i^{4n}) \, A'_1 \tag{3.69}$$

where

$$A'_1 = \frac{\sqrt{t'_1} \; \exp f(t'_1)}{2\sqrt{\pi} \; (z^2 - 2m)^{1/4}} \tag{3.70}$$

$$z = \sqrt{ik} \; \xi$$

$$f(t'_1) = - t'^2_1 + 2zt'_1 - (n + 1) \, \ell n t'_1$$

$$t'_1 = \frac{1}{2}\left[\sqrt{ik}\,\xi - \sqrt{ik\xi^2 - 2m}\right]$$ (3.71)

$$m = n + 1$$

$$= m_p \text{ for Dirichlet's problem}$$

$$= m'_p \text{ for Neumann's problem .}$$

Substituting the asymptotic expressions from previous derivations into (3.17) and (3.18), we obtain surface currents expressed in the form of a residue series. Assume a plane wave impinges upon the parabolic cylinder at an angle $\psi = \pi/2$. If we consider the leading terms of the residue series, the surface current for the Dirichlet problem becomes

$$J_D \approx k\sqrt{\frac{\pi}{kri}}\, e^{-ikr}\, \frac{(i)^n(1 - i^{4n})\sqrt{t'_1}(-i\rho^2 - 2m_p)^{1/4}}{\sin \pi n(ik\xi^2 - 2m_p)^{1/4}\ln(t_o/t_1)\sqrt{t_o}}\, \exp\left[f(t'_1) - f(t_o)\right]$$

$$= -i2k\sqrt{\frac{\pi}{kr}}\left[\frac{1}{\ln(t_o/t_1)}\right]\left[\frac{-i\rho^2 - 2m_p}{ik\xi^2 - 2m_p}\right]^{1/4}$$

$$\exp\left\{(m_p - \frac{1}{2})\ln\left[\frac{\sqrt{k}\,\xi + \sqrt{k\xi^2 + 2im_p}}{\sqrt{-2im_p}}\right] - i\frac{\sqrt{k}\,\xi}{2}\sqrt{k\xi^2 + 2im_p} + \right.$$

$$\left. + (m_p - \frac{1}{2})\ln\left[\frac{\rho + \sqrt{\rho^2 - 2im_p}}{\sqrt{-2im_p}}\right] + i\frac{\rho}{2}\sqrt{\rho^2 - 2im_p}\right\}$$ (3.72)

where

$$n = m_p - 1$$

$$\rho = \sqrt[4]{2kh}$$

$$t_o = \left[\sqrt{-i}\,\rho + \sqrt{-i\rho^2 - 2m_p}\,\right] \Big/ 2$$

$$t_1 = \left[\sqrt{-i}\,\rho - \sqrt{-i\rho^2 - 2m_p}\,\right] \Big/ 2$$

$$t'_1 = \left[\sqrt{ik}\,\xi - \sqrt{ik\xi^2 - 2m_p}\,\right] \Big/ 2$$

$$m_p = -\frac{1}{2}\left[(\rho + 2.8) + i\,(\rho^2 + \rho + 1.4)\right] \ .$$

(U) Similarly, we obtain the surface current for the Neumann problem as following:

$$J_N \approx \sqrt{2\pi}\ e^{-ikr}\ \frac{(i)^n(1 - i^{4n})\sqrt{t'_1}\ \exp\left[f(t'_1) - f(t_o)\right]}{\sin \pi n \ell n(t_o/t_1)(ik\xi^2 - 2m'_p)^{1/4}(-i\rho^2 - 2m'_p)^{1/4}\sqrt{t_o}}$$

$$= -\frac{2\sqrt{2\pi}\ i^{3/2}}{\ell n(t_o/t_1)\left[(ik\xi^2 - 2m'_p)(-i\rho^2 - 2m'_p)\right]^{1/4}}$$

$$\exp\left\{(m'_p - \frac{1}{2})\ell n\left[\frac{\sqrt{k}\,\xi + \sqrt{k\xi^2 + 2im'_p}}{\sqrt{-2im'_p}}\right] - i\,\frac{\sqrt{k}\,\xi}{2}\sqrt{k\xi^2 + 2im'_p} + \right.$$

$$\left. + (m'_p - \frac{1}{2})\ell n\left[\frac{\rho + \sqrt{\rho^2 - 2im'_p}}{\sqrt{-2im'_p}}\right] + i\,\frac{\rho}{2}\sqrt{\rho^2 - 2im'_p}\right\} \qquad (3.73)$$

where

$$n = m'_p - 1$$

$$\rho = \sqrt{2kh}$$

$$t_0 = \left[\sqrt{-i}\,\rho + \sqrt{-i\rho^2 - 2m'_p}\right]\Big/2$$

$$t_1 = \left[\sqrt{-i}\,\rho + \sqrt{-i\rho^2 - 2m'_p}\right]\Big/2$$

$$t'_1 = \left[\sqrt{ik}\,\xi - \sqrt{ik\xi^2 - 2m'_p}\right]\Big/2$$

$$m'_p = -\left(\frac{\rho}{\pi} + 0.1\right) - i\frac{\rho}{2}(\rho + 1) \quad.$$

(U) The surface current density at the crest is plotted as a function of ρ in Fig. 3-10. Since at the crest $\xi = 0$, there are two numbers having the same magnitude involved in subtraction in the exponent of (3.72) and (3.73) the accurate surface current density may be obtained by solving the location of zeros of functions $W_n(z)$ and $'W_n(z)$ exactly, otherwise the error is large. In general, this is not necessary in obtaining the attenuation factor for the surface current beyond the crest due to the fact of additions in the exponent. The graphical solution is quite satisfactory in this case. Here the attenuation factor is defined as:

$$\left|J_D/k\right| = A\,e^{-\alpha(\xi)} \tag{3.74}$$

$$\left|J_N\right| = A'\,e^{-\alpha'(\xi)} \tag{3.75}$$

where A and A' express the surface current density at the crest $\xi = 0$; $\alpha(\xi)$ and $\alpha'(\xi)$ are the attenuation factor as a function of the parabolic coordinate ξ.

(U) In Fig. 3-11a,b the attenuation factor is plotted as a function $\sqrt{k}\,\xi$. From these figures we see that the attenuation factor of a large cylinder increases more rapidly than for a small one in the deep shadow region, i.e. the larger the cylinder the darker it is. In general it is much darker behind a parabolic cylinder than behind a half-plane.
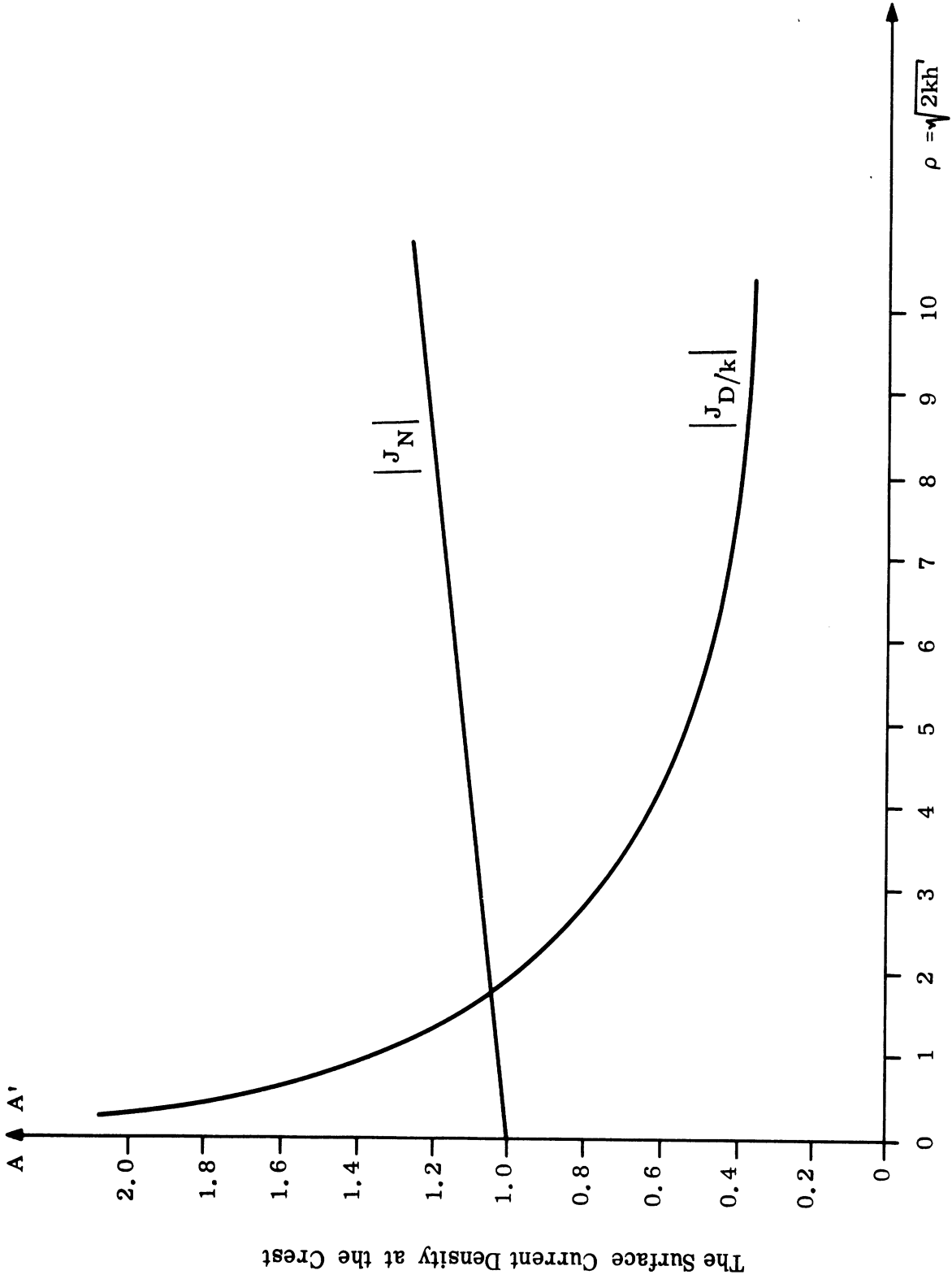
FIG. 3-10: THE SURFACE CURRENT DENSITY AT THE CREST, $\xi = 0$.
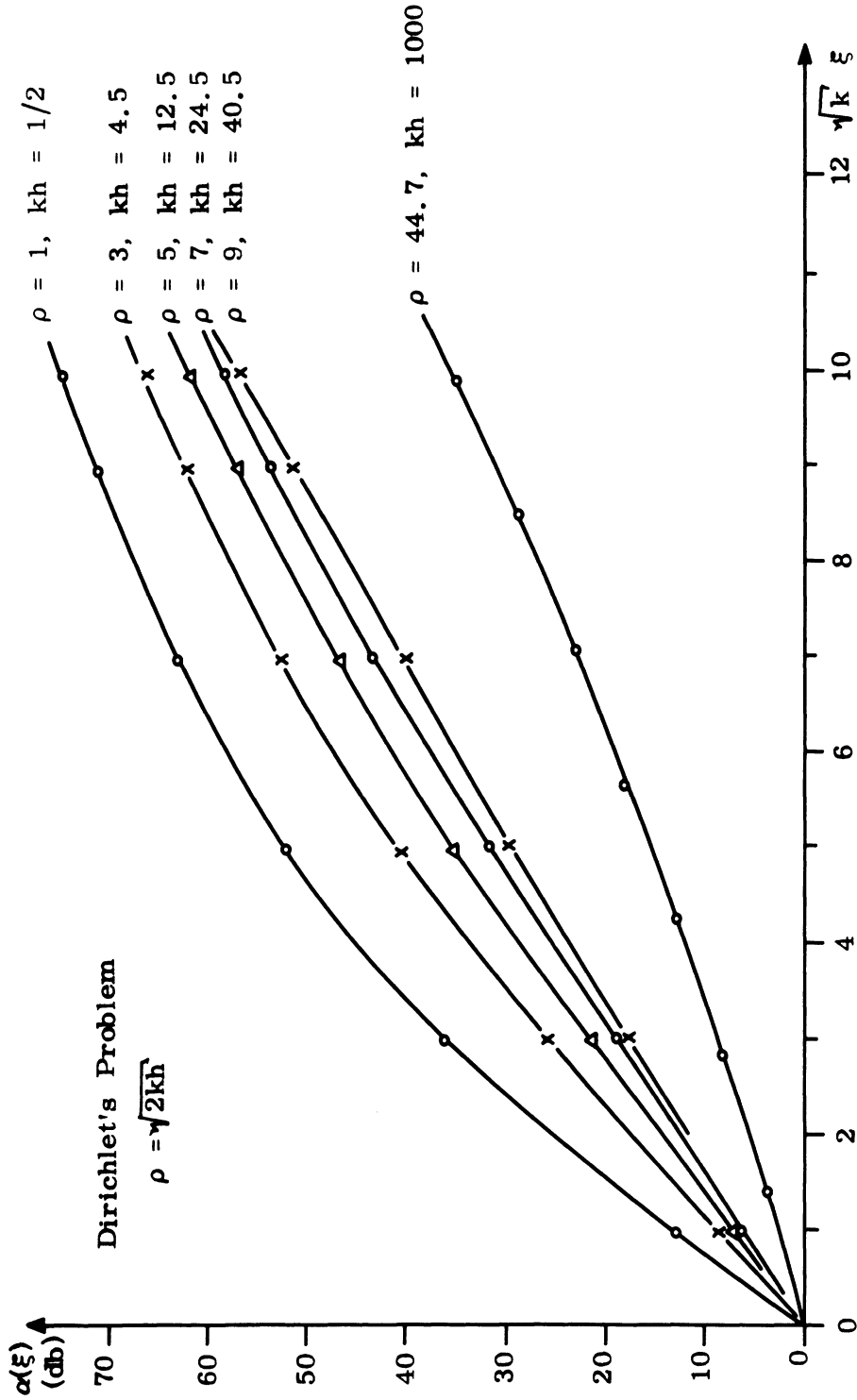
FIG. 3-11a: ATTENUATION FACTOR FOR THE SURFACE CURRENT J_D.

75
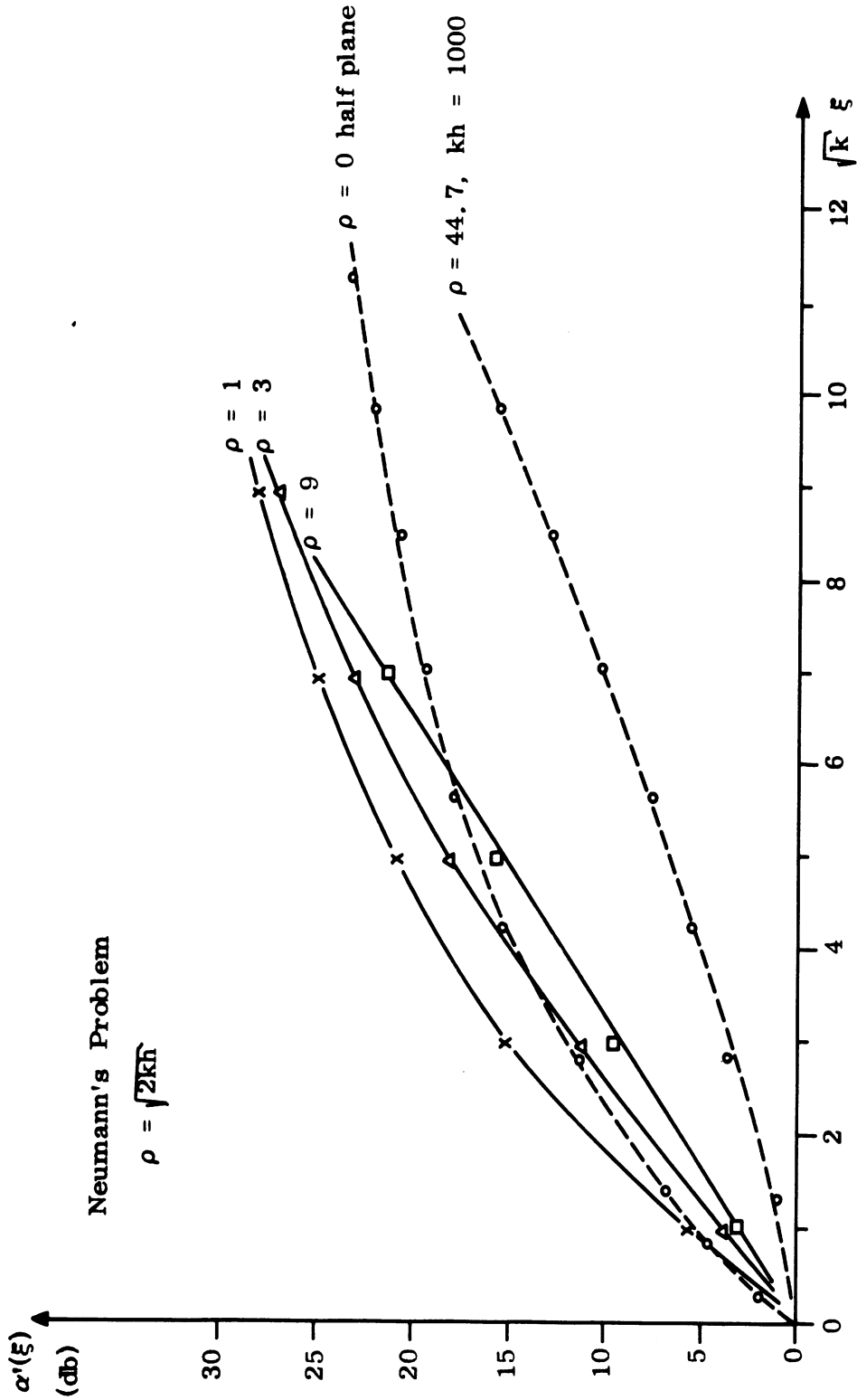
FIG. 3-11b: ATTENUATION FACTOR FOR THE SURFACE CURRENT J_N.

(U)   Figure 3-12 and 3-13 show the attenuation factor as a function of the arc length along the parabolic cylinder.   It is seen that the surface current density in Dirichlet's problem attenuates more rapidly than does that in Neumann's problem.   For instance, for ρ = 7 in Dirichlet's problem, the creeping wave will propagate one wavelength along the parabolic cylinder before it is attenuated at 6 db, but it will propagate two wavelengths on the same cylinder before it reaches 6 db attenuation in Neumann's problem.

(U)   Figure 3-14 shows the constant attenuation contour on parabolic cylinders.   Once again it shows that the larger the cylinder the more wavelengths the creeping wave will propagate along the cylinder, but the larger the cylinder the darker it is.   The wavelength λ of the incident plane wave is plotted against parabolic cylinders for scaling.

(U)   h) Results as Compared with Those of a Large Cylinder.   The asymptotic expressions obtained may be interpreted in terms of the "geometric theory of diffraction" (Keller, 1956).   Let the length of the arc of the parabola between the points ξ = 0 and ξ = ξ be

$$S = \int_0^\xi \sqrt{\xi^2 + 2h} \, d\xi = \frac{\xi}{2} \sqrt{\xi^2 + 2h} + h\ell n \left[\frac{\xi + \sqrt{\xi^2 + 2h}}{2h} \right] , \quad (3.76)$$

and the radius of curvature of the parabola at the point with coordinates (ξ, 2h) is

$$R(\xi) = \frac{(\xi^2 + 2h)^{3/2}}{\sqrt{2h}} . \qquad (3.77)$$

Finally let us express the integral over the arc of the parabola as
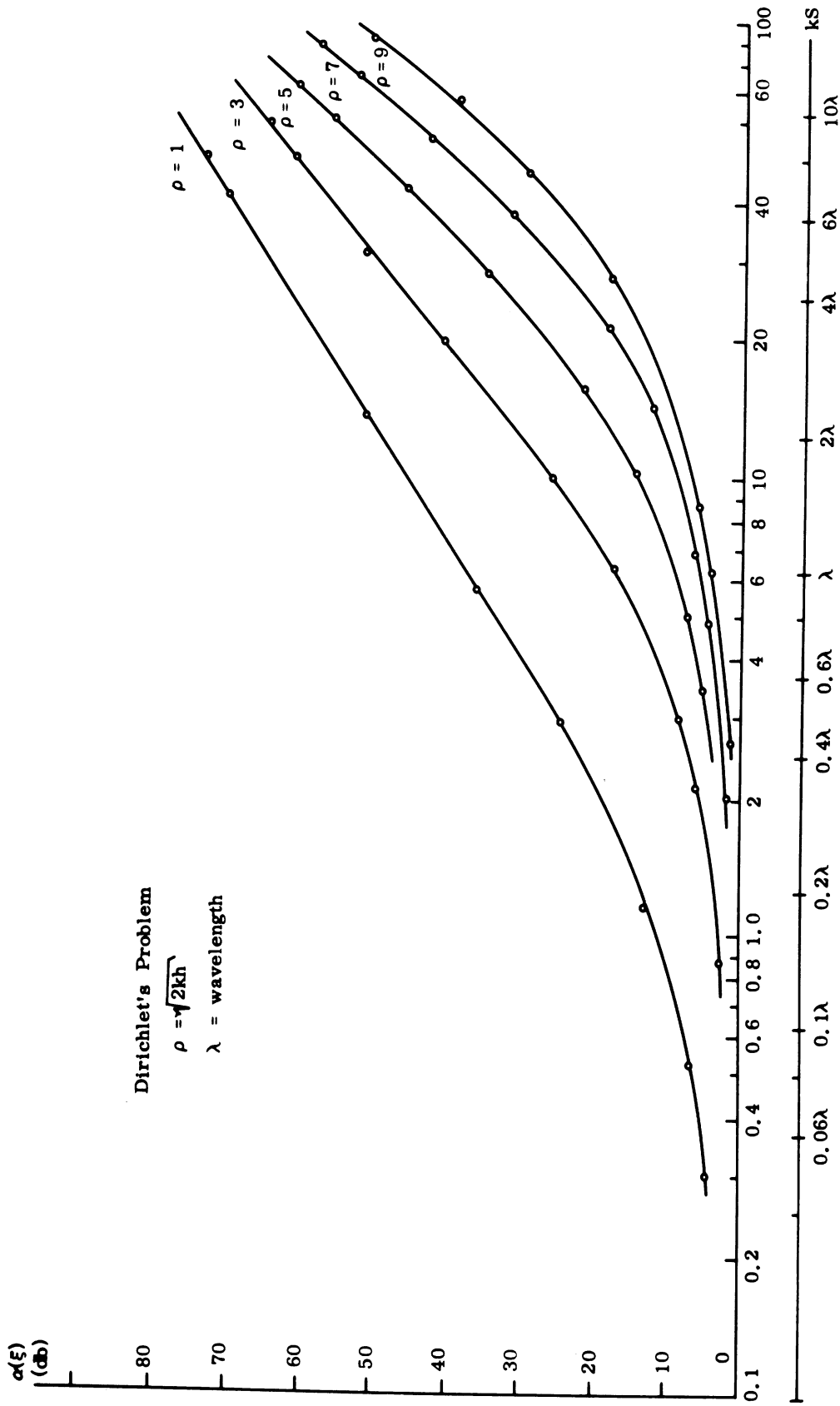
FIG. 3-12: ATTENUATION FACTOR FOR THE SURFACE CURRENT J_D VS THE ARC LENGTH ALONG THE PARABOLA.

78
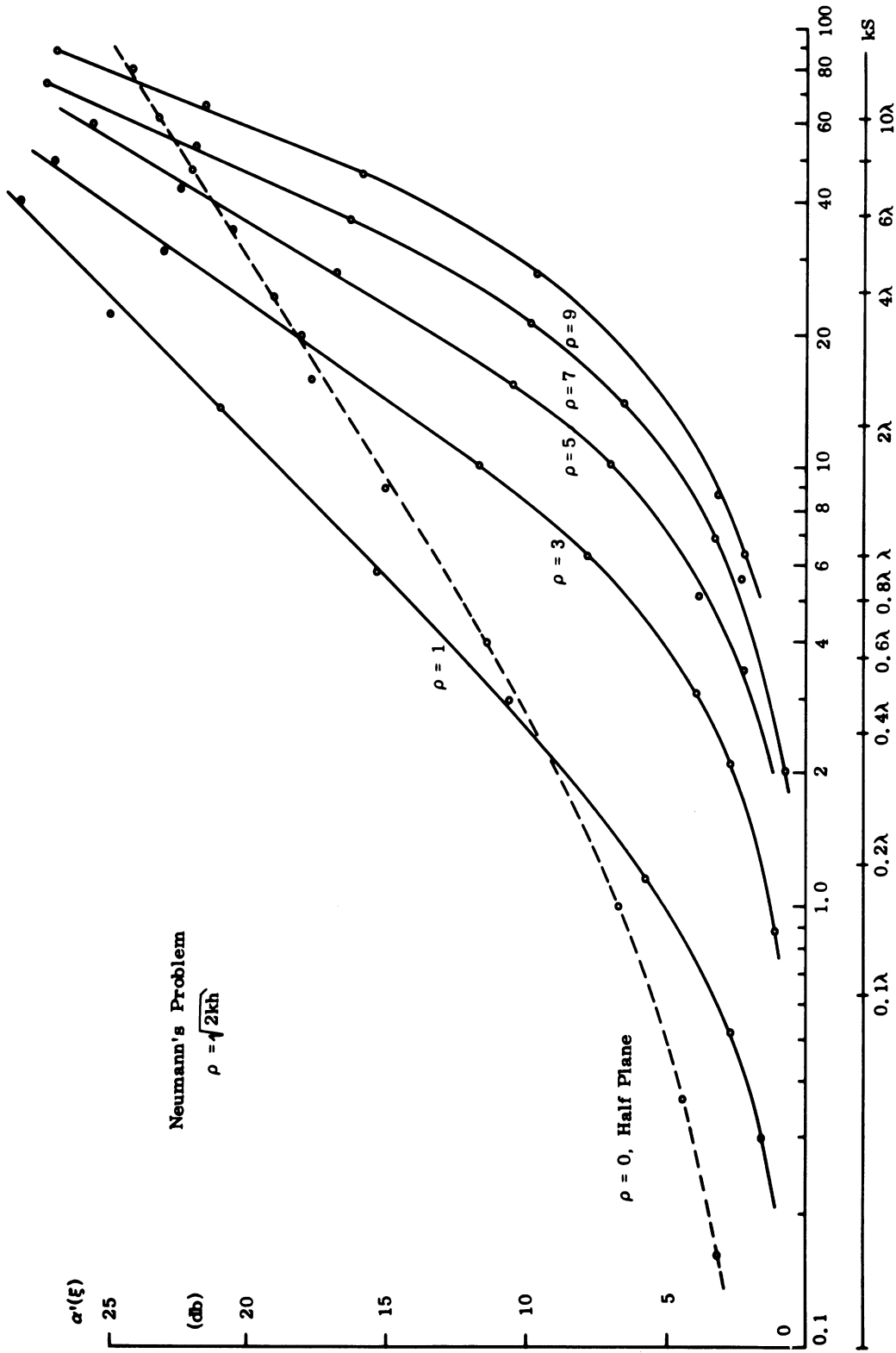
FIG. 3-13: ATTENUATION FACTOR FOR THE SURFACE CURRENT J_N
VS THE ARC LENGTH ALONG THE PARABOLA.
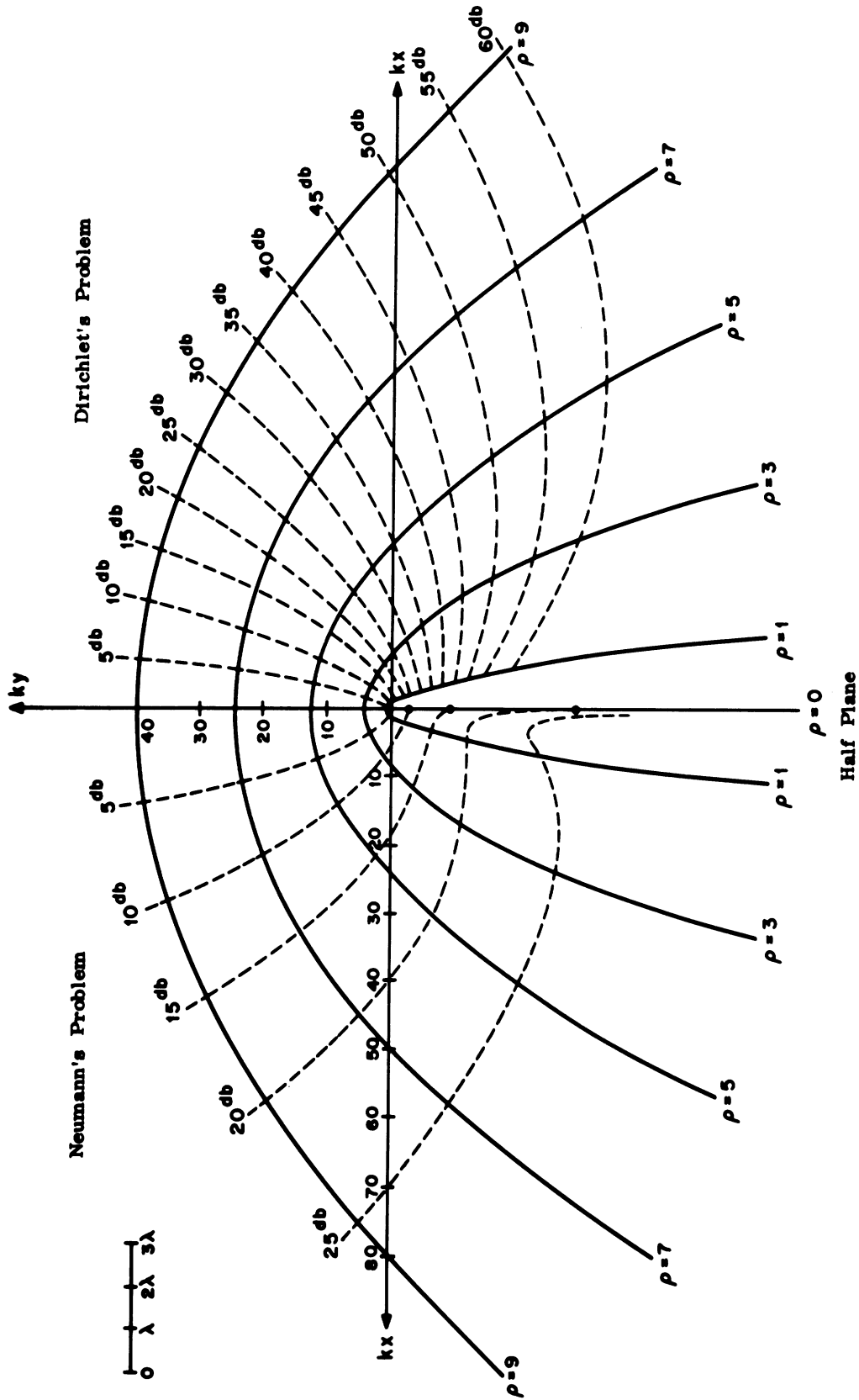
FIG. 3-14: ATTENUATION FACTORS ON PARABOLIC CYLINDERS.

$$D = \int_0^s \frac{ds}{\left[R(s)\right]^{2/3}} = (2h)^{1/3} \int_0^\xi \frac{d\xi}{(\xi^2 + 2h)^{1/3}}$$

$$= (2h)^{1/3} \ln \frac{\xi + \sqrt{\xi^2 + 2h}}{\sqrt{2h}} \quad . \tag{3.78}$$

Comparing these expressions with formulae (3.72) and (3.73), we obtain the asymptotic surface current in the forms

$$\frac{J_D}{k} \sim A(\rho) \frac{1}{\sqrt{kr}} \left[R(\xi)\right]^{-1/6} \exp\left\{ -ikS - \frac{k^{1/3}}{2} \left[(\rho + 3.8) + i(\rho + 1.4)\right] \frac{D}{\rho^{2/3}} \right\} \tag{3.79}$$

$$J_N \sim A'(\rho) \left[R(\xi)\right]^{-1/6} \exp\left\{ -ikS - \frac{k^{1/3}}{2} \left[(\frac{2\rho}{\pi} + 1.2) + i\rho\right] \frac{D}{\rho^{2/3}} \right\} \tag{3.80}$$

where $A(\rho)$ and $A'(\rho)$ express amplitude functions which are a function of ρ only. Here $\rho = 2kh$.

(U) Formulae (3.79) and (3.80) have the same expression as the results of Keller and Levy (1959). Therefore it is clear that the creeping wave theory may be extended into the region where the radius of curvature is comparable to the incident wavelength. The only place needing modification is the coefficient of D in the exponent of (3.79) and (3.80) where the coefficient is expressed as a function of the focal length $\rho = \sqrt{2kh}$. For large cylinders these coefficients are equal to $2.338e^{i\pi/6}$ and $1.0188e^{i\pi/6}$ for Dirichlet's and Neumann's problems respectively (Ivanov, 1960). In our case these coefficients are

$\left[(\rho + 3.8) + i(\rho + 1.4)\right]/2\rho^{2/3}$ and $\left[(\frac{2\rho}{\pi} + 1.2) + i\rho\right]/2\rho^{2/3}$ in Dirichlet's and Neumann's problems respectively.

(U) When the focal length of the parabolic cylinder is large compared to an incident wavelength, the asymptote of the function $W_n(z)$ may be expressed by Fock type formulae, i.e. the function can be expressed in terms of the Airy function (Rice, 1954; Ivanov, 1960). This is due to the fact that the asymptotic expressions given by the saddle-point method fail when m_p and m'_p are near $-ikh$, i.e. zeros of $W_n(z)$ are very close to $-(ikh + 1)$. In this case two saddle points t_0 and t_1 coincide, and $f''(t_0)$ vanishes in (3.26), Taylor expansion of the function $f(t)$. Therefore the unvanished terms will start from the third derivative of the function $f(t)$, and the asymptotic formulae may be expressed in terms of Airy integrals. In the case of the short focal length compared to the incident wavelength, the locations of zeros of the function $W_n(z)$ are not closed to $-(ikh + 1)$. Therefore the saddle-point method may be applied to evaluate the asymptotic expressions. This is what we used to obtain the asymptotic formulae for surface currents in (3.72) and (3.73).

(U) For the large cylinder, Fock (1946) defined the width of the penumbra region as

$$d = \sqrt[3]{\frac{2R^2}{k}} \qquad (3.81)$$

and the quantity

$$\gamma = \frac{\ell}{d} = \sqrt[3]{\frac{k}{2R^2}}\,\ell \qquad (3.82)$$

where R is the radius of curvature of the cylinder by the plane of incidence, and the distance ℓ is measured from the geometrical boundary of the shadow. For large positive values of γ, the surface current density is proportional to $e^{-\alpha\gamma}$. Here α is a positive constant.

(U) From (3.79) and (3.80) we may obtain the similar quantities defined by Fock by considering the region $\xi < 2h$ or $k\xi < \rho$, within which D can be approximated by

$$D \approx \frac{\xi}{(2h)^{1/6}} = \frac{x}{(2h)^{2/3}} = \frac{k^{2/3} x}{\rho^{4/3}} \quad . \tag{3.83}$$

For the Dirichlet problem, we obtain

$$\alpha\gamma = \left(\frac{\rho + 3.8}{2\rho^2}\right) kx \quad . \tag{3.84}$$

Similarly we have

$$\alpha'\gamma' = \left(\frac{\frac{\rho}{\pi} + 0.6}{k}\right) kx \tag{3.85}$$

for the Neumann problem.

(U) From these expressions, we find the definition of the width of the penumbra region as

$$
\begin{aligned}
d &= \sqrt[3]{\frac{2R^2}{k}} &\quad \text{for} \quad \sqrt{kR} \gg 1 \\
&= \sqrt[2]{\frac{R}{k}} &\quad \text{for} \quad \sqrt{kR} > 1 \\
&= R &\quad \text{for} \quad \sqrt{kR} < 1 \quad .
\end{aligned}
\tag{3.86}
$$

From (3.86) it is interesting to see that d is proportional to the radius of the curvature and almost independent of the incident wavelength when $\sqrt{kR} < 1$.

3.3.3 Tangential Magnetic Field on the Surface of an Imperfectly Conducting Wedge.

(S) a) Introduction . The aim of this section is to investigate the tangential magnetic field on the surface of an imperfectly conducting wedge. The results and method then obtained is to be applied to the coated cone-sphere. We assume that on that surface, the electromagnetic fields satisfy the boundary condition

$$\underline{E} - (\hat{n} \cdot \underline{E}) \, \hat{n} = \eta \, Z_o \, \hat{n} \times \underline{H} \, . \tag{3.87}$$

In Eq. (3.87) $\hat{n}$ denotes the outward normal of the wedge surface, Z_o is the free space intrinsic impedance and η is related to the permeability and permittivity of the material making up the wedge. For convenience of analysis, we employ the cylindrical coordinates (ρ, ϕ, z) where the z-axis coincides with the edge of the wedge. The time convention $e^{-j\omega t}$ is assumed. We further assume that the wedge occupies the space $(a \le \rho \le \infty, \ \alpha \le \phi \le 2\pi, \ -\infty < z < \infty)$ and is excited by a magnetic line source at a position $(a, \beta, -\infty < z < \infty)$ with $0 < \beta < \alpha$. From Maxwell's equations and the above geometrical configuration, one can easily see that the non-zero field components will be H_z, E_ρ and E_ϕ, i.e.,

$$\underline{H} = \hat{z} \, H_z$$
$$\underline{E} = \hat{\rho} \, E_\rho + \hat{\phi} \, E_\phi \tag{3.88}$$

where $\hat{z}, \hat{\rho}, \hat{\phi}$ are the unit vectors along the respective coordinates.

(U) It has been shown (Den 1967, Appendix A) that if the tangential electric field and magnetic field on a surface S of a scatterer satisfy Eq. (3.87) then one has

$$\frac{1}{2} \, \underline{F}_o(\underline{r}') - \oiint_S (\nabla g_o \times \underline{F}_o) \times \hat{n}' \, ds = - \underline{H}_o(\underline{r}') \times \hat{n}' \tag{3.89}$$

84

and

$$\frac{1}{2} \underset{\rightarrow n}{F}(\underrightarrow{r}') - \oiint_S (\nabla g_o \times \underset{\rightarrow n}{F}) \times \hat{n}' \, ds$$

$$= -\frac{1}{ik} \hat{n}' \times \left[\nabla' \times \oiint_S \nabla g_o \times (\hat{n} \times \underset{\rightarrow n-1}{F}) \, ds \right] . \tag{3.90}$$

Where F_o, F_1, F_2 ... are defined by

$$\underset{\rightarrow}{F} = \hat{n} \times \underset{\rightarrow}{H} = \underset{\rightarrow 0}{F} + \eta \underset{\rightarrow 1}{F} + \eta^2 \underset{\rightarrow 2}{F} + \ldots \tag{3.91}$$

$\underset{\rightarrow 0}{H}(\underrightarrow{r}')$ represents the incident magnetic field and g_o denotes the free space Green's function

$$g_o = \frac{1}{4\pi} \frac{e^{jk|\underrightarrow{r} - \underrightarrow{r}'|}}{|\underrightarrow{r} - \underrightarrow{r}'|} . \tag{3.92}$$

Moreover one may note that in (3.89) and (3.90) one integrates with respect to the unprimed system.

(U) In the section b, recognizing the surface S in (3.89) and (3.90) as the wedge surface and inserting (3.88) in (3.87), from (3.89) and (3.90) we will obtain a set of integral equations for the surface magnetic field. In sections c and **d**, solutions of the integral equations are obtained. In section e, we discuss the possible ways that one may apply a similar method to a cone diffraction problem.

(U) b) <u>Formulation of the Integral Equations</u>. To the two lateral surfaces of the wedge, $\phi = 0$ and $\phi = \alpha$, the unit normal $\hat{n}$ becomes

$$\hat{n} = \hat{\phi} \quad \text{for} \quad \phi = 0$$

and

$$\hat{n} = -\hat{\phi} \quad \text{for} \quad \phi = \alpha . \tag{3.93}$$

Moreover, if one lets H_z^a and H_z^b denote the tangential magnetic field on the surface $\phi = 0$ and $\phi = \alpha$ respectively, then from (3.91) one has

$$\underrightarrow{F} = \hat{r}\ H_z^a \quad \text{for } \phi = 0$$

and

$$\underrightarrow{F} = -\ \hat{r}\ H_z^b \quad \text{for } \phi = \alpha. \tag{3.94}$$

Now we express H_z^a and H_z^b in perturbed form as indicated by

$$H_z^a = H_{z0}^a + \eta\ H_{z1}^a + \eta^2\ H_{z2}^a + \ldots \ ,$$

and

$$H_z^b = H_{z0}^b + \eta\ H_{z1}^b + \eta^2\ H_{z2}^b + \ldots \ , \tag{3.95}$$

and from Eq. (3.92) we obtain

$$\underrightarrow{F}_n = \hat{r}\ H_{zn}^a \quad \text{for } \phi = 0,$$

$$= -\ \hat{r}\ H_{zn}^b \quad \text{for } \phi = \alpha. \tag{3.96}$$

Upon substituting (3.93) to (3.96) in (3.89) and (3.90), on the surface $\phi' = 0$, the integral on the left had side of (3.89) and (3.90) becomes

$$I_1 = \oiint_S (\nabla g_0 \times \underrightarrow{F}_n) \times \hat{n}'\ ds = \hat{r}' \left[\int_0^\infty \int_{-\infty}^\infty \frac{H_{zn}^a}{\rho} \frac{\partial}{\partial \phi} g_0\ dz\ d\rho \right.$$

$$\left. + \int_0^\infty \int_{-\infty}^\infty \frac{H_{zn}^b}{\rho} \frac{\partial}{\partial \phi} g_0\ dz\ d\rho \right], \quad n = 0, 1, 2, \ldots \tag{3.97}$$

One may note that on the right hand side of (3.97), in the first integral we integrate on the wall $\phi = 0$ and in the second integral we integrate on the other wall of the wedge $\phi = \alpha$. Since H_{zn} is independent of z, we have

$$\int_{-\infty}^{\infty} \frac{H_{zn}^{a,b}}{\rho} \frac{\partial}{\partial \phi} g_0 \, dz = \frac{H_{zn}^{a,b}}{\rho} \frac{\partial}{\partial \phi} \int_{-\infty}^{\infty} g_0 \, dz \quad . \tag{3.98}$$

But

$$\int_{-\infty}^{\infty} g_0 \, dz = \frac{i}{4} H_0^{(1)}(k\rho_{PQ}) \tag{3.99}$$

where

$$\rho_{PQ} = \sqrt{\rho^2 + \rho^2 - 2\rho\rho' \cos(\phi - \phi')}. \tag{3.100}$$

It has been shown (Oberhettinger, 1954) that

$$H_0^{(1)}(k\rho_{PQ}) = \frac{4i}{\pi^2} \int_0^{\infty} K_{i\lambda}(\gamma\rho) K_{i\lambda}(\gamma\rho') \cosh\left[\lambda\left(\pi - |\phi - \phi'|\right)\right] d\lambda \tag{3.101}$$

where $\gamma = -ik$ and $K_{i\lambda}(\gamma\rho)$ is the modified Bessel function of second kind. Applying the operator $\partial/\partial\phi$ to (3.101), for $\phi' = 0$, we have

$$\frac{\partial}{\partial\phi} H_0^{(1)}(k\rho_{PQ}) = -\frac{4i}{\pi^2} K^a(\rho, \rho') \quad \text{when } \phi \to 0,$$

$$= -\frac{4i}{\pi^2} K^b(\rho, \rho') \quad \text{when } \phi \to \alpha \quad , \tag{3.102}$$

where

$$K^a(\rho, \rho') = \int_0^{\infty} \lambda K_{i\lambda}(\gamma\rho) K_{i\lambda}'(\gamma\rho') \sinh \pi \lambda \, d\lambda \quad , \tag{3.103}$$

and

87

$$K^b(\rho, \rho') = \int_0^\infty \lambda \, K_{i\lambda}(\gamma\rho) \, K_{i\lambda'}(\gamma\rho') \, \sinh \lambda \, (\pi - \alpha) \, d\alpha \; . \qquad (3.104)$$

Similarly, for the case $\phi' = \alpha$

$$\frac{\partial}{\partial \phi} \, H_0^{(1)}(k\rho_{PQ}) = \frac{4i}{\pi^2} \, K^b(\rho, \rho') \quad \text{when} \quad \phi \to 0, \qquad (3.105)$$

$$= \frac{4i}{\pi^2} \, K^a(\rho, \rho') \quad \text{when} \quad \phi \to \alpha \; . \qquad (3.106)$$

For the convenience of further analysis, based on the integral representation (3.101), we also introduce the notations

$$G^a(\rho') = \int_0^\infty K_{i\lambda}(\gamma a) \, K_{i\lambda}(\gamma\rho') \, \cosh \lambda \, (\pi - \beta) \, d\lambda \; , \qquad (3.107)$$

$$G^b(\rho') = \int_0^\infty K_{i\lambda}(\gamma a) \, K_{i\lambda}(\gamma\rho') \, \cosh \lambda \, (\pi - \alpha + \beta) \, d\lambda, \qquad (3.108)$$

$$M^a(\rho, \rho') = \int_0^\infty K_{i\lambda}(\gamma\rho) \, K_{i\lambda}(\gamma\rho') \, \cosh \lambda \, \pi \, d\lambda, \qquad (3.109)$$

and

$$M^b(\rho, \rho') = \int_0^\infty K_{i\lambda}(\gamma\rho) \, K_{i\lambda}(\gamma\rho') \, \cosh \lambda \, (\pi - \alpha) \, d\lambda \; . \qquad (3.110)$$

From (3.98) to (3.104), one may reduce I_1 to a form as shown

$$I_1 = \frac{1}{\pi^2} \hat{r}' \left[\int_0^\infty \rho^{-1} H_{zn}^a K^a (\rho, \rho') \, d\rho + \right.$$

$$\left. + \int_0^\infty \rho^{-1} H_{zn}^b K^b (\rho, \rho') \, d\rho \right] . \tag{3.111}$$

Similarly on the other surface of the wedge, $\phi' = \alpha$, following the same procedure and using formulas (3.105) and (3.106) the integral on the left hand side of (3.89) can be reduced to

$$I_1 = - \frac{1}{\pi^2} \hat{r}' \left[\int_0^\infty \rho^{-1} H_{zn}^a K^b (\rho, \rho') \, d\rho \right.$$

$$\left. + \int_0^\infty \rho^{-1} H_{an}^b K^a (\rho, \rho') \, d\rho \right] . \tag{3,112}$$

The primary field due to the magnetic line source can be written as

$$\underline{H}_0(\underline{r}') = \hat{z} \, H_0^{(1)} \left(k \sqrt{\rho'^2 + a^\beta - 2a\rho' \cos (\phi' - \beta)} \right)$$

where (a, β) indicates the radial and azimuth coordinates of the source. On the surfaces of the wedge, in terms of the notations given by (3.107) and (3.108), the primary field is of the form

$$\underline{H}_0(\underline{r}') = \hat{z}' \, \frac{4i}{\pi^2} \, G^a(\rho') \quad \text{for } \phi = 0$$

$$= \hat{z}' \, \frac{4i}{\pi^2} \, G^b(\rho') \quad \text{for } \alpha = \alpha. \tag{3.113}$$

Substituting (3.111), (3.112) and (3.113) in (3.89), on the surface $\phi' = 0$, the integral equation can be reduced to the following form

$$
H_{zo}^a - \frac{2}{\pi^2} \left\{ \int_0^\infty \rho^{-1} H_{zo}^a (\rho, \rho') \, d\rho \right.
$$

$$
\left. + \int_0^\infty \rho^{-1} H_{zo}^b K^b (\rho, \rho') \, d\rho \right\} = \frac{8i}{\pi} G^a(\rho') \ , \tag{3.114}
$$

Similarly, for the surface $\phi' = \alpha$, one may obtain an integral equation as shown

$$
H_{zo}^b - \frac{2}{\pi^2} \left\{ \int_0^\infty \rho^{-1} H_{zo}^a K^b (\rho, \rho') \, d\rho \right.
$$

$$
\left. + \int_0^\infty \rho^{-1} H_{zo}^b K^a(\rho, \rho') \, d\rho \right\} = \frac{8i}{\pi} G^b(\rho') \ . \tag{3.115}
$$

Equation (3.114) and (3.115) are coupled integral equations. We note that their unknown functions H_{zo}^a and H_{zo}^b represent the magnetic fields on the surfaces $\phi' = 0$ and $\phi' = \alpha$ respectively when the surface impedance ηZ_o approaches to zero.

(U) Now we turn our attention to the right hand side of (3.90). Since

$$
\nabla g_o \times (\hat{n} \times \underline{F}_{n-1}) = -\nabla g_o \times \hat{z} \, H_{z, n-1}^{a, b}
$$

$\nabla = -\nabla'$ and $\hat{z} = \hat{z}'$, we have

$$I_2 = -\frac{1}{ik} \hat{n}' \times \left[\nabla' \oiint_S \nabla g_0 \times (\hat{n} \times \underline{F}_{n-1}) \, dS \right]$$

$$= \frac{1}{ik} n' \times \left\{ \int_0^\infty \int_{-\infty}^\infty \nabla' \times (\nabla' g_0 \times \hat{z}' H^a_{z,n-1}) dz \, d\rho \right.$$

$$\left. + \int_0^\infty \int_{-\infty}^\infty \nabla' \times (\nabla' g_0 \times \hat{z}' H^b_{z,n-1}) \, dz \, d\rho \right\} \quad . \tag{3.116}$$

As we point out in the early paragraphs that $H^{a,b}_{z,n-1}$ are independent of z, using the well known formula (3.99), I_2 can be reduced to

$$I_2 = \frac{1}{4k} \hat{n}' \times \left\{ \int_0^\infty \nabla' \times \left[\nabla' H_0^{(1)}(k\rho_{PQ}) \times z' H^a_{z,n-1} \right] d\rho \right.$$

$$\left. + \int_0^\infty \nabla' \times \left[\nabla' H_0^{(1)}(k\rho_{PQ}) \times \hat{z}' H^b_{z,n-1} \right] d\rho \right\} \quad , \tag{3.117}$$

where ρ_{PQ} is given by (3.100). It is of importance to recall that in the first integral $\phi = 0$, and in the second one $\phi = \alpha$. For the case $\phi' = 0$, i.e., on the lower surface of wedge, employing Eq. (3.109), we may reduce (3.117) to a form as shown

$$I_2 = \frac{i}{\pi^2 k} \hat{\phi}' \times \left\{ \int_0^\infty \nabla' \times \left[\nabla' M^a(\rho, \rho') \times \hat{z}' H^a_{z,n-1} \right] d\rho \right.$$

$$\left. + \int_0^\infty \nabla' \times \left[\nabla' M^b(\rho, \rho') \times z' H^b_{z,n-1} \right] d\rho \right\} \quad . \tag{3.118}$$

It can be shown that

$$\nabla' \times \left[\nabla' M^{a,b}(\rho, \rho') \times \hat{z}\, \xi \right] = -\hat{z}'\, k^2\, \xi\, M^{a,b}(\rho, \rho') \qquad (3.119)$$

where ξ is a scalar function of the unprimed system only. Substituting (3.119) in (3.118), we immediately obtain

$$I_2 = -\frac{ik}{\pi^2}\, \hat{r}' \cdot \left\{ \int_0^\infty H^a_{z,\,n-1}\, M^a(\rho, \rho')\, d\rho \right.$$

$$\left. + \int_0^\infty H^b_{z,\,n-1}\, M^b(\rho, \rho')\, d\rho \right\} . \qquad (3.120)$$

On the upper surface $\phi' = \alpha$, employing (3.110) and (3.119) we have

$$I_2 = \frac{ik}{\pi^2}\, \hat{r}' \left\{ \int_0^\infty H^a_{z,\,n-1}\, M^b(\rho, \rho')\, d\rho \right.$$

$$\left. + \int_0^\infty H^b_{z,\,n-1}\, M^b(\rho, \rho')\, d\rho \right\} . \qquad (3.121)$$

Thus for the surface $\phi' = 0$, if we substitute (3.111) and (3.120) in Eq. (3.90), we obtain an integral equation of the form

$$H^a_{zn} - \frac{2}{\pi^2} \left\{ \int_0^\infty \rho^{-1} H^a_{zn} K^a(\rho, \rho')\, d\rho + \int_0^\infty \rho^{-1} H^b_{zn} K^b(\rho, \rho')\, d\rho \right\}$$

$$= -\frac{ik}{\pi^2} \left\{ \int_0^\infty H^a_{z,\,n-1} M^a(\rho, \rho')\, d\rho + \int_0^\infty H^b_{z,\,n-1} M^b(\rho, \rho')\, d\rho \right\} , \quad (3.122)$$

$$n = 1,\, 2,\, \ldots$$

Similarly for $\phi' = \alpha$, one can obtain the following equation

$$H_{zn}^b - \frac{2}{\pi^2}\left\{\int_0^\infty \rho^{-1} H_{zn}^a K^b(\rho, \rho')\, d\rho + \int_0^\infty \rho^{-1} H_{zn}^b K^a(\rho, \rho')\, d\rho\right\}$$

$$= -\frac{ik}{\pi^2}\left\{\int_0^\infty H_{z,n-1}^a M^b(\rho, \rho')d\rho + \int_0^\infty H_{z,n-1}^b M^a(\rho, \rho')d\rho\right\}, \quad (3.123)$$

$$n = 1, 2, \ldots,$$

from (3.90). Equation (3.122) and (3.123) are also coupled integral equations and their free terms depend on the solutions of previous order or integral equations.

(U) In section c, method of solutions for (3.114) and (3.115) are investigated. In section d, we will apply the method employed in the previous section to (3.122) and (3.123) and obtain the solutions for the first order integral equations, i.e., the case $n = 1$.

(U) c) <u>Solutions for the Zeroth Order Equations.</u> In a study of the form (3.101) of the primary wave due to the magnetic line source, we may assume that H_{zo}^a and H_{zo}^b are of the forms

$$H_{zo}^a = \frac{4i}{\pi^2} \int_0^\infty K_{i\lambda}(\gamma\rho)\, f_o^a(\lambda)\, d\lambda \qquad (3.124)$$

and

$$H_{zo}^b = \frac{4i}{\pi^2} \int_0^\infty K_{i\lambda}(\gamma\rho)\, f_o^a(\lambda)\, d\lambda \qquad (3.125)$$

respectively. Substitution of (3.124) and (3.125) in (3.114) and (3.115), the

later equations become

$$\int_0^\infty K_{i\lambda}(\gamma\rho')f_o^a(\lambda)\,d\lambda - \frac{2}{\pi^2}\left\{\int_0^\infty d\rho\rho^{-1}K^a(\rho,\rho')\int_0^\infty K_{i\lambda'}(\gamma\rho)f_o^a(\lambda')\,d\lambda'\right.$$

$$\left. + \int_0^\infty d\rho\rho^{-1}K^b(\rho,\rho')\int_0^\infty K_{i\lambda'}(\gamma\rho)f_o^b(\lambda')\,d\lambda'\right\}$$

$$= 2\int_0^\infty K_{i\lambda}(\gamma a)K_{i\lambda}(\gamma\rho')\cosh\lambda\,(\pi-\beta)\,d\lambda, \qquad (3.126)$$

and

$$\int_0^\infty K_{i\lambda}(\gamma\rho')f_o^b(\lambda)\,d\lambda - \frac{2}{\pi^2}\left\{\int_0^\infty d\rho\rho^{-1}K^b(\rho,\rho')\int_0^\infty K_{i\lambda'}(\gamma\rho)f_o^a(\lambda')\,d\lambda'\right.$$

$$\left. + \int_0^\infty d\rho\,\rho^{-1}K^a(\rho,\rho')\int_0^\infty K_{i\lambda'}(\gamma\rho)f_o^b(\lambda')\,d\lambda'\right\}$$

$$= 2\int_0^\infty K_{i\lambda}(\gamma a)K_{i\lambda}(\gamma\rho')\cosh\lambda\,(\pi-\alpha+\beta)\,d\lambda \qquad (3.127)$$

where $K^a(\rho,\rho')$ and $K^b(\rho,\rho')$ are given by (3.103) and (3.104). If one inserts the later equations in (3.126) and (3.127) and reverses the order of integration, one arrives at

$$f_o^a(\lambda) - \frac{2}{\pi^2}\Bigg\{ \lambda \sinh \pi\lambda \int_0^\infty d\rho \rho^{-1} K_{i\lambda}(\gamma\rho) \int_0^\infty K_{i\lambda'}(\gamma\rho) f_o^a(\lambda') \, d\lambda'$$

$$+ \lambda \sinh \lambda (\pi - \alpha) \int_0^\infty d\rho \rho^{-1} K_{i\lambda}(\gamma\rho) \int_0^\infty K_{i\lambda'}(\gamma\rho) f_o^b(\lambda') \, d\lambda' \Bigg\}$$

$$= 2 K_{i\lambda}(\gamma a) \cosh \lambda (\pi - \beta) \, , \qquad (3.128)$$

and

$$f_o^b(\lambda) - \frac{2}{\pi^2}\Bigg\{ \lambda \sinh \lambda (\pi - \alpha) \int_0^\infty d\rho \rho^{-1} K_{i\lambda}(\gamma\rho) \int_0^\infty K_{i\lambda'}(\gamma\rho) f_o^a(\lambda') d\lambda'$$

$$+ \lambda \sinh \pi\lambda \int_0^\infty d\rho \rho^{-1} K_{i\lambda}(\gamma\rho) \int_0^\infty K_{i\lambda'}(\gamma\rho) f_o^b(\lambda') \, d\lambda' \Bigg\}$$

$$= 2 K_{i\lambda}(\gamma a) \cosh \lambda (\pi - \alpha + \beta) \, . \qquad (3.129)$$

For the moment, we assume that in Eqs. (3.128) and (3.129), the order of integration are interchangeable, then we reduce (3.128) and (3.129) to the forms

$$f_o^a(\lambda) - \frac{2}{\pi^2}\Bigg\{ \lambda \sinh \lambda\pi \int_0^\infty f_o^a(\lambda) N(\lambda, \lambda') d\lambda'$$

$$+ \lambda \sinh \lambda (\pi - \alpha) \int_0^\infty f_o^b(\lambda') N(\lambda, \lambda') d\lambda' \Bigg\}$$

$$= 2 K_{i\lambda}(\gamma a) \cosh \lambda (\pi - \beta) \, , \qquad (3.130)$$

$$f_0^b(\lambda) - \frac{2}{\pi^2}\left\{ \lambda \sinh \lambda(\pi - \alpha) \int_0^\infty f_0^a(\lambda) N(\lambda, \lambda') d\lambda' \right.$$

$$\left. + \lambda \sinh \lambda \pi \int_0^\infty f_0^b(\lambda') N(\lambda, \lambda') d\lambda' \right\}$$

$$= 2 K_{i\lambda}(\gamma a) \cosh \lambda (\pi - \alpha + \beta) \tag{3.131}$$

respectively where

$$N(\lambda, \lambda') = \int_0^\infty \rho^{-1} K_{i\lambda}(\gamma\rho) K_{i\lambda'}(\gamma\rho) d\rho \quad . \tag{3.132}$$

One notes that the integral $N(\lambda, \lambda')$ behaves as the kernel of the last two integral equations, therefore it deserves more investigation.

(U) It has been shown (Luke, 1962) that

$$I(\mu, \nu, \xi; a, b) = \int_0^\infty t^{-\xi} K_\mu(at) K_\nu(bt) dt$$

$$= \frac{(\frac{a}{2})^{\xi-1}(\frac{a}{2})^\nu \Gamma\left(\frac{1+\nu+\mu-\xi}{2}\right)\Gamma\left(\frac{1+\nu-\mu-\xi}{2}\right)\Gamma\left(\frac{1-\nu-\mu-\xi}{2}\right)\Gamma\left(\frac{1-\nu-\mu-\xi}{2}\right)}{8\Gamma(1-\xi)}$$

$$x_2 F_1\left[\frac{1+\nu+\mu-\xi}{2}, \frac{\xi+\nu-\mu-\xi}{2}, 1-\xi; 1-(b/a)^2\right] \tag{3.133}$$

if $R(1 - \xi \pm \mu \pm \nu) > 0$ and $R(a+b) > 0$. We let $a = b$, $\mu = i\lambda$ and $\nu = i\lambda'$ then the last integral becomes

$$I(i\lambda, i\lambda', \xi; a, a) = \left(\frac{a}{2}\right)^{\xi-1} \Gamma\left(\frac{1 + i\lambda + i\lambda' - \xi}{2}\right)\Gamma\left(\frac{1 - i\lambda + i\lambda' - \xi}{2}\right)$$

$$\times \frac{\Gamma\left(\frac{1 + i\lambda - i\lambda' - \xi}{2}\right)\Gamma\left(\frac{1 - i\lambda - i\lambda' - \xi}{2}\right)}{8\Gamma(1 - \xi)} . \qquad (3.134)$$

Since Gamma function $\Gamma(z)$ is analytic for all z except for z equal to zero and negative integers where $\Gamma(z)$ has simple poles. Therefore from (3.134) we observe that when $\xi \rightarrow 1$, for the case $\lambda' \neq \lambda$

$$I(i\lambda, i\lambda', \xi; a, a) \rightarrow 0 \qquad (3.135)$$

and for $\lambda' = \lambda$

$$I(i\lambda, i\lambda', \xi; a, a) \rightarrow \frac{2\pi}{\lambda' \sinh \lambda'\pi} \Gamma\left(\frac{1 - \xi}{2}\right) , \qquad (3.136)$$

$$R(2a) > 0 .$$

The above properties (3.135) and (3.136) imply that $I(i\lambda, i\lambda', 1^-; a, a)$ behaves like a delta function divided by the function $\lambda' \sinh \lambda'\pi$, i.e.,

$$I(i\lambda, i\lambda', 1; a, a) = \frac{C_m}{\lambda' \sinh \lambda'\pi} \delta(\lambda' - \lambda) \qquad (3.137)$$

where C_m is a numerical constant to be determined. If we integrate Eq. (3.137) with respect to λ' then the right hand side is

$$\int_0^\infty \frac{C_m}{\lambda' \sinh \lambda'\pi} \delta(\lambda' - \lambda) \, d\lambda' = \frac{C_m}{\lambda \sinh \lambda'\pi} , \qquad (3.138)$$

and the left hand sides, upon interchanging the order of integration, becomes

$$\int_0^\infty I(i\lambda, i\lambda', \xi; a, a) d\lambda' = \int_0^\infty \left[\frac{1}{t\xi} K_{i\lambda}(at) \int_0^\infty K_{i\lambda'}(at) d\lambda' \right] dt, \quad (3.139)$$

$$\xi \to 1.$$

By definition of Lebedev transform (Oberhettinger and Higgins, 1961), we obtain

$$\int_0^\infty I(i\lambda, i\lambda', 1^-; a, a) \, d\lambda = \frac{\pi^2}{2} \frac{1}{\lambda \sinh \lambda \pi} \quad . \quad (3.140)$$

Equating (3.138) to (3.140), we can easily arrive at

$$C_m = \pi^2/2 \ . \quad (3.141)$$

(U) Returning to Eq. (3.132), if we assume that the medium in the space between two wedge surfaces is slightly lossy, i.e., $R(\gamma) > 0$, then we may let $\gamma = a$ and

$$N(\lambda, \lambda') = \frac{\pi^2}{2} \frac{1}{\lambda' \sinh \lambda' \pi} \delta(\lambda' - \lambda). \quad (3.142)$$

Upon substituting (3.142) and (3.141), one obtains immediately the following results:

$$f_0^a(\lambda) = - \frac{2 \sinh \lambda \pi \cosh \lambda (\pi - \alpha + \beta)}{\sinh \lambda (\pi - \alpha)} K_{i\lambda}(\gamma a) \ , \quad (3.143)$$

and

$$f_0^b(\lambda) = - \frac{2 \sinh \lambda \pi \cosh \lambda (\pi - \beta)}{\sinh \lambda (\pi - \alpha)} K_{i\lambda}(\gamma a) \ . \quad (3.144)$$

The zeroth order solution for the tangential magnetic field on the surfaces $\phi' = 0$ and $\phi' = \alpha$ can be written as

$$H^a_{zo} = -\frac{8i}{\pi^2} \int_0^\infty K_{i\lambda}(\gamma\rho)K_{i\lambda}(\gamma a) \frac{\sinh\lambda\pi \cosh\lambda(\pi - \alpha + \beta)}{\sinh\lambda(\pi - \alpha)} d\lambda \qquad (3.145)$$

and

$$H^b_{zo} = -\frac{8i}{\pi^2} \int_0^\infty K_{i\lambda}(\gamma\rho)K_{i\lambda}(\gamma a) \frac{\sinh\lambda\pi \cosh\lambda(\pi - \beta)}{\sinh\lambda(\pi - \alpha)} d\lambda \qquad (3.146)$$

respectively. Using the identities

$$K_{i\lambda}(z) = \frac{\pi}{2} \frac{I_{-i\lambda}(z) - I_{i\lambda}(z)}{i \sinh \lambda\pi} \quad , \qquad (3.147)$$

and

$$K_{-\nu}(z) = K_{\nu}(z) \qquad (3.148)$$

Eqs. (3.145) and (3.146) can be transformed into the forms

$$H^a_{zo} = -\frac{4}{\pi} \int_{-\infty}^\infty K_{i\lambda}(\gamma\rho)I_{-i\lambda}(\gamma a) \frac{\cosh \lambda(\pi - \alpha + \beta)}{\sinh \lambda(\pi - \alpha)} d\lambda \quad , \qquad (3.149)$$

and

$$H^b_{zo} = -\frac{4}{\pi} \int_{-\infty}^\infty K_{i\lambda}(\gamma\rho)I_{-i\lambda}(\gamma a) \frac{\cosh \lambda(\pi - \beta)}{\sinh \lambda(\pi - \alpha)} d\lambda \qquad (3.150)$$

respectively if $\rho > a$ and the origin is indented by a small semi-circle in the upper half λ-plane. Last two expressions are also valid for the case $\rho < a$ with ρ and a interchanged.

(U) d) <u>Solutions for the First Order Equations.</u> Upon substituting Eqs. (3.109) and (3.110) in the free term of the integral equation (3.122) for the case n = 1 and reversing the order of integration, then the free term will be of the form

$$-\frac{ik}{\pi^2}\left\{\int_0^\infty K_{i\lambda}(\gamma\rho')\left[\cos\lambda\pi\int_0^\infty H_{zo}^a K_{i\lambda}(\gamma\rho)\,d\rho\right.\right.$$

$$\left.\left.+\cosh\lambda(\pi-\alpha)\int_0^\infty H_{zo}^b K_{i\lambda}(\gamma\rho)\,d\rho\right]d\lambda\right\}\,. \qquad (3.151)$$

Analogous to Eqs. (3.124) and (3.125), we assume that H_{z1}^a and H_{z1}^b are of the following integral representations

$$H_{z1}^a = \frac{4i}{\pi^2}\int_0^\infty K_{i\lambda}(\gamma\rho')\,f_1^a(\lambda)\,d\lambda\,, \qquad (3.152)$$

and

$$H_{z1}^b = \frac{4i}{\pi^2}\int_0^\infty K_{i\lambda}(\gamma\rho')\,f_1^b(\lambda)\,d\lambda \qquad (3.153)$$

respectively. If we substitute the last two expressions in the left hand side of (3.122) we can write the integral equation in a new form as shown

$$f_1^a(\lambda)-\frac{2}{\pi^2}\left\{\lambda\sinh\lambda\pi\int_0^\infty d\rho\rho^{-1}K_{i\lambda}(\gamma\rho)\int_0^\infty K_{i\lambda'}(\gamma\rho)f_1^a(\lambda')\,d\lambda'\right.$$

$$\left.+\lambda\sinh\lambda(\pi-\alpha)\int_0^\infty d\rho\rho^{-1}K_{i\lambda}(\gamma\rho)\int_0^\infty K_{i\lambda'}(\gamma\rho)f_1^b(\lambda')\,d\lambda'\right\}$$

$$= -\frac{k}{4}\left\{\cosh \lambda \, \pi \int_0^\infty H_{zo}^a K_{i\lambda} (\gamma\rho) \, d\rho \right.$$

$$\left. + \cosh \lambda \, (\pi - \alpha) \int_0^\infty H_{zo}^b K_{i\lambda} (\gamma\rho) \, d\rho \right\} . \qquad (3.154)$$

The left hand side of (3.154) has the same form as (3.128), therefore following the steps from (3.128) to (3.144), we obtain

$$f_1^b(\lambda) = \frac{k}{4} \frac{\sinh \lambda \pi}{\sinh \lambda \, (\pi - \alpha)} \left\{ \cosh \lambda \pi \int_0^\infty H_{zo}^a K_{i\lambda} (\gamma\rho) \, d\rho \right.$$

$$\left. + \cosh \lambda \, (\pi - \alpha) \int_0^\infty H_{zo}^b K_{i\lambda} (\gamma\rho) \, d\rho \right\} . \qquad (3.155)$$

Similarly, using (3.109), (3.110), (3.152) and (3.153), one may reduce Eq. (3.123) to a form as shown

$$f_1^a(\lambda) = \frac{k}{4} \frac{\sinh \lambda \, \pi}{\sinh \lambda \, (\pi - \alpha)} \left\{ \cosh\lambda \, (\pi - \alpha) \int_0^\infty H_{zo}^a K_{i\lambda} (\gamma\rho) \, d\rho \right.$$

$$\left. + \cosh \lambda \, \pi \int_0^\infty H_{zo}^b K_{i\lambda} (\gamma\rho) \, d\rho \right\} . \qquad (3.156)$$

It is seen from last two equations that a knowledge of the integral

$$A(\lambda) = \int_0^\infty H_{zo}^a K_{i\lambda} (\gamma\rho) \, d\rho \quad \text{and} \quad B(\lambda) = \int_0^\infty H_{zo}^b K_{i\lambda} (\gamma\rho) \, d\rho ,$$

will be crucial to the solutions of (3.155) and (3.156).

(U) Substituting (3.145) and (3.146) in the integrals $A(\lambda)$ and $B(\lambda)$ respectively and reversing the order of integration, we have

$$A(\lambda) = -\frac{8i}{\pi^2} \int_0^\infty d\lambda' K_{i\lambda'}(\gamma a) \frac{\sinh \lambda' \pi \cosh \lambda' (\pi - \alpha + \beta)}{\sinh \lambda' (\pi - \alpha)}$$

$$\cdot \int_0^\infty K_{i\lambda'}(\gamma\rho) K_{i\lambda}(\gamma\rho) \, d\rho \quad , \tag{3.157}$$

and

$$B(\lambda) = -\frac{8i}{\pi^2} \int_0^\infty d\lambda' K_{i\lambda'}(\gamma a) \frac{\sinh \lambda' \pi \cosh \lambda' (\pi - \beta)}{\sinh \lambda' (\pi - \alpha)}$$

$$\cdot \int_0^\infty K_{i\lambda'}(\gamma\rho) K_{i\lambda}(\gamma\rho) \, d\rho \quad . \tag{3.158}$$

But from (3.133), one knows that

$$\int_0^\infty K_{i\lambda'}(\gamma\rho) K_{i\lambda}(\gamma\rho) \, d\rho = \frac{1}{4\gamma} \Gamma(\tfrac{1}{2} + ix) \Gamma(\tfrac{1}{2} - ix)$$

$$\cdot \Gamma(\tfrac{1}{2} + iy) \Gamma(\tfrac{1}{2} - iy) \tag{3.159}$$

where $x = (\lambda + \lambda')/2$ and $y = (\lambda' - \lambda)/2$. Employing the well known formula (Abramowitz and Stegun, 1964)

$$\Gamma(\tfrac{1}{2} + iz) \Gamma(\tfrac{1}{2} - iz) = \frac{\pi}{\cosh \pi z} \tag{3.160}$$

Eq. (3.159) yields to the form

$$\int_0^\infty K_{i\lambda'}(\gamma\rho)\, K_{i\lambda}(\gamma\rho)\, d\rho = \frac{\pi^2}{4\gamma}\, \frac{1}{\cosh \pi x \cosh \pi y}\, .$$

Consequently, we arrive at

$$\int_0^\infty K_{i\lambda'}(\gamma\rho)\, K_{i\lambda}(\gamma\rho)\, d\rho = \frac{\pi^2}{2\gamma}\, \frac{1}{\cosh \pi\lambda + \cosh \pi\lambda'}\, .$$

Substituting the last equation in the integrals $A(\lambda)$ and $B(\lambda)$, we obtain the following forms

$$A(\lambda) = -\frac{4i}{\gamma} \int_0^\infty \frac{\sinh \lambda' \pi}{\sinh \lambda' (\pi - \alpha)}$$

$$\cdot \frac{\cosh \lambda' (\pi - \alpha + \beta)}{\cosh \pi \lambda + \cosh \pi \lambda'}\, K_{i\lambda'}(\gamma a)\, d\lambda' \qquad (3.161)$$

and

$$B(\lambda) = -\frac{4i}{\gamma} \int_0^\infty \frac{\sinh \lambda' \pi}{\sinh \lambda' (\pi - \alpha)}$$

$$\cdot \frac{\cosh \lambda' (\pi - \beta)}{\cosh \pi \lambda + \cosh \pi \lambda'}\, K_{i\lambda'}(\gamma a)\, d\lambda' \qquad (3.162)$$

Because of the identity (3.147),, we may transform $A(\lambda)$ and $B(\lambda)$ into two-side integrals as shown

$$A(\lambda) = \frac{2\pi}{\gamma} \int_{-\infty}^\infty \frac{I_{i\lambda'}(\gamma a)}{\sinh \lambda' (\pi - \alpha)}\, \frac{\cosh \lambda' (\pi - \alpha + \beta)}{\cosh \pi \lambda + \cosh \pi \lambda'}\, d\lambda'\, , \qquad (3.163)$$

and

$$B(\lambda) = \frac{2\pi}{\gamma} \int_{-\infty}^{\infty} \frac{I_{i\lambda'}(\gamma a)}{\sinh \lambda' (\pi - \alpha)} \frac{\cosh \lambda' (\pi - \beta)}{\cosh \pi \lambda + \cosh \pi \lambda'} \, d\lambda' \qquad (3.164)$$

respectively if the origin is indented by a small semicircle in the upper half λ-plane. Last two integrals can be written in series form if we close the contour of integration in the upper half plane. From (3.163) and (3.164), one observes that $A(\lambda)$ and $B(\lambda)$ are even functions of λ and they are inversely proportional to γ.

(U) Substituting (3.156) and (3.155) in (3.152) and (3.153) we have

$$H_{z1}^a = \frac{ki}{\pi^2} \int_0^{\infty} \frac{\sinh \lambda \pi}{\sinh \lambda (\pi - \alpha)} \left[A(\lambda) \cosh \lambda (\pi - \alpha) \right.$$

$$\left. + B(\lambda) \cosh \lambda \pi \right] K_{i\lambda} (\gamma \rho) \, d\lambda \quad , \qquad (3.165)$$

and

$$H_{z1}^b = \frac{ki}{\pi^2} \int_0^{\infty} \frac{\sinh \lambda \pi}{\sinh \lambda (\pi - \alpha)} \left[A(\lambda) \cosh \lambda \pi \right.$$

$$\left. + B(\lambda) \cosh \lambda (\pi - \alpha) \right] K_{i\lambda} (\gamma \rho) \, d\lambda \qquad (3.166)$$

respectively. Last two integrals can be also transformed into two-sided integrals as we obtain (3.163) from (3.161). The resulting integral representations for H_{z1}^a and H_{z1}^b can be written as

$$H_{z1}^a = \frac{k}{2\pi} \int_{-\infty}^{\infty} \frac{I_{-i\lambda}(\gamma \rho)}{\sinh \lambda (\pi - \alpha)} \left[A(\lambda) \cosh \lambda (\pi - \alpha) \right. +$$

$$\left. + B(\lambda) \cosh \lambda \pi \right] d\lambda \quad , \qquad (3.167)$$

$$H^b_{z1} = \frac{k}{2\pi} \int_{-\infty}^{\infty} \frac{I_{-i\lambda}(\gamma\rho)}{\sinh \lambda (\pi - \alpha)} \left[A(\lambda) \cosh \lambda \pi \right.$$

$$\left. + B(\lambda) \cosh \lambda (\pi - \alpha) \right] d\lambda \qquad (3.168)$$

respectively.

(U) e) <u>Discussion and Suggestions for Further Work.</u> In the last two sections, the zeroth order and first order equations are solved. We represent the results in integral forms. As we point out that those integral represent-ations can be transformed into series forms if one carefully studies the nature of the poles and the position of poles in the upper half λ-plane. Examining Eqs. (3.149), (3.150), (3.163), (3.164), (3.167) and (3.168), it seems that there are only simple poles occuring at

$$\sinh \lambda (\pi - \alpha) = 0.$$

(U) Although in this section, we only treat the zeroth order and first order equations, however, the method developed in c and d can be used to tackle the equations of order higher than unity (n > 1). One may expect that the solutions of nth order equations will be of the form

$$H^{a,b}_{zn} = \frac{k}{2\pi} \int_{-\infty}^{\infty} \frac{I_{-i\lambda}(\gamma\rho)}{\sinh \lambda (\pi - \alpha)} \left[\qquad \right] d\lambda , \qquad (3.169)$$

where the expression inside the square bracket depends on λ and a the same as the expression inside square bracket of (3.167) and (3.168). However, it will be much more complicated in comparison with that of (3.167) and (3.168).

(U) One may note that the sequence of thought in section c is the conjunction with that of Magnus' work (1941) on the diffraction of electromagnetic wave by a perfectly conducting half plane. He began with an integral equation whose kernel a is Hankel function of zeroth order. The free term of that equation is related to the incident wave. For the half plane, he expanded the incident wave and kernel into a series of Bessel functions of integer order and in the meantime, he assumed that the surface current is of a similar series form. Then he reduced the original integral equation into a system of an infinite number of linear algebraic equations. Introducing an auxilliary function, he solved the infinite system so that the orininal integral equation is solved. Paralleling to Magnus' method, in section c we choose an integral representation due to Oberhettinger (1954) for the Hankel function of zeroth order which may be used with either incident wave and the kernel of the integral Eq. (3.89). Denoting the surface current on the walls of the wedge by an integral form similar to the incident wave we can reduce the original integral equations to a new integral equation which corresponds to Magnus' linear algebraic equations. It is shown that the kernel of the new integral equation behaves as the delta function so that the solutions of the integral equations can be obtained immediately.

(U) It is of some practical interest to investigate the tangential magnetic field on the surface of a coated cone. One may tackle the problem by using the perturbation technique (Den, 1967, see Appendix A). As a result of the applications of that technique, a set of integral equations which govern the above tangential magnetic field will be obtained from (3.89) and (3.90). We may wish to extend the ideal described in the last paragraph to solve this set of integral equations. According to the previous discussions, one observes that the crucial point will be the choice of a proper integral representation for the

free space Green's function. It seems that

$$\frac{e^{-\gamma R}}{R} = \frac{2}{\pi} \frac{1}{\sqrt{r\,r'}} \int_0^\infty \lambda \, \tanh \pi\lambda \, P_{i\lambda - 1/2} (-\cos \theta)$$

$$\cdot \, K_{i\lambda}(\gamma r) \, K_{i\lambda}(\gamma r') \, d\lambda \, , \qquad 0 \le \theta \le 2\pi \, , \qquad (3.170)$$

will be the prospective form in which

$$R = \sqrt{r^2 + r'^2 - 2r\,r' \cos \theta} \, .$$

(U) In section c and d, we assume that the source of excitation is a magnetic line source. If that source is replaced by an electric line source then the non-zero field components becomes

$$\underline{E} = \hat{z} \, E_z$$

$$\underline{H} = \hat{r} \, H_r + \hat{\phi} \, H_\phi \, .$$

We may apply the method described in previous sections to determine the field components H_r on the surfaces of the wedge.

3.4 Computer Program for Rotationally Symmetric Re-entry Body (Task 3.1.3)

(S) The objective of the development under this Task is to write a computer program for computing the surface current and radar cross section of rotationally symmetric re-entry bodies. The groundwork for this development was laid in the previous year's SURF study (Castellanos 1966). It was our intention to write a computer program for a metallic cone-sphere and extend it by theoretically feasible computations to coated cone spheres with antenna and indented rear cap perturbations. The analytic development, which is simple in conception, has proven to be difficult in execution and is taking considerably longer to complete than had been supposed. In order to provide the required accuracy, it has been found necessary to discard some of the earlier methods for computing the matrix elements and to use a method of Gaussian quadratures.

(U) The calculation has been completely recast using Gaussian quadratures where we exploit the explicit form of the integrand incorporating all singular behavior in weight functions. This results in the need to evaluate a number of different schemes which are described below.

(U) a) <u>Computation of the Matrix Elements T_{ij}</u>. The computation of the matrix elements is done in terms of integrations over cells of the form

$$I_{ab} = \int_a^{a+h} \int_b^{b+h} F(s, t)\, G_m\, (s, t)\, ds\, dt \qquad (3.171)$$

where

$$G_m = \int_0^\pi \frac{e^{ik\widetilde{R}}}{KR}\, \cos m\, \theta\, d\theta \qquad (3.172)$$

$$\widetilde{R} = \left| \vec{r}' - \vec{r} \right|$$

$$= \left[(\Delta z)^c + \rho^2(s) + \rho^2(t) - 2\rho(s)\, \rho(t)\, \cos\theta \right]^{1/2}$$

and $F(s, t)$ is "well behaved". Using the parameterization

$$z(t) = f_2(t)\, C$$

$$\rho(t) = f_1(t)\, C \qquad (3.173)$$

$$C = 1/2 \text{ circumference} \ .$$

Then

$$K\widetilde{R} = \Gamma \left\{ \left[f_2(t) - f_2(s) \right]^2 + f_1^2(t) + f_1^2(s) - 2f_1(t)f_1(s)\, \cos\theta \right\}^{1/2} \qquad (3.174)$$

where

$$\Gamma = KC \ .$$

Let $\theta - 2\phi$ then

$$K\tilde{R} = \int \left[(\Delta f_2)^2 + (\Delta f_1)^2 + 4f_1(s) \, f_1(t) \, \sin^2 \phi \right]^{1/2}$$

$$= \int (R_o^2 + 4 \, R_1^2 \, \sin^2 \phi)^{1/2} \qquad (3.175)$$

and

$$G_m = 2 \int_0^{\pi/2} \frac{e^{i\int (R_o^2 + 4R_1^2 \, \sin^2 \phi)^{1/2}}}{\int (R_o^2 + 4R_1^2 \, \sin^2 \phi)^{1/2}} \cos 2m\phi \; d\phi \qquad (3.176)$$

Let

$$k^2 = \frac{4R_1^2}{R^2} \quad \text{and let} \quad \phi \to \pi/2 - \phi$$

$$G_m = 2(-i)^m \int_0^{\pi/2} \frac{e^{i\int R \sqrt{1 - k^2 \, \sin^2 \phi}}}{\int R \sqrt{1 - k^2 \, \sin^2 \phi}} \cos 2m\phi \; d\phi \qquad (3.177)$$

where

$$R^2 = R_o^2 + 4R_1^2 \quad .$$

On going to elliptic functions by the change in variable

$$u = \int_0^\phi \frac{d\psi}{\sqrt{1 - k^2 \, \sin^2 \psi}} \qquad (3.178)$$

and noting that $\cos 2m\phi$ is the Chebychev polynomial of the first kind

$$\cos 2m\phi = T_{2m} (\cos \phi) , \qquad (3.179)$$

we find

$$G_m = \frac{2}{\Gamma R}(-i)^m \int_0^K e^{i\Gamma dn\, u}\, T_{2m}(\text{sn}\, u)\, du \qquad (3.180)$$

where $k = u(\pi/2)$ or on putting

$$u = Kx\,;$$

$$G_m = \frac{2K}{R}\,(i)^m \int_0^1 e^{i\Gamma dn(Kx)}\, T_{2m}\left[\text{cn}(Kx)\right]\, dx\,. \qquad (3.181)$$

The function G_m now has its singularity explicit in the factor $K(k)$. The numerical problem at this stage is the valuation of

$$g_m \equiv \int_0^1 e^{i\Gamma dn\, Kx}\, T_{2m}(\text{cn}\, Kx)\, dx\,. \qquad (3.182)$$

This evaluation will appear below (b) using a Gauss-Legendre method.

(U) In order to examine the singular behavior of G_m we note that for $k \sim 1$

$$K(k) \sim \ln \frac{4}{\sqrt{1 - k^2}}\,.$$

This obtains for $R_o \sim 0$ or for $s \sim t$, indeed, for this case,

$$R_o = \left|s - t\right| + O\left(\left|s - t\right|^3\right)\,. \qquad (3.183)$$

In terms of the integration (3.171) this can occur for $a = b$ or $a = b \pm h$.
Hence, in these cases the integration must take into account the logarithmic
singularity.

(U) The second case of singular behavior occurs for $R \rightarrow 0$. This obtains only in the two cells $a = b = 0$ and $a = b = 1 - h$ since for $a = b = 0$,

$$R = (s + t) + O\left[(s + t)^2\right] \quad ;$$

for $a = b = 1 - h$,

$$R = \left[2 - (s + t)\right] + O\left\{\left[2 - (s + t)\right]^2\right\} \quad .$$

This behavior leads to singularities of the forms

$$\frac{1}{s + t} \, \ell n \, \frac{|s - t|}{s + t} \quad \text{and} \quad \frac{1}{s + t}$$

where we put $s = 1 - s'$ and $t = 1 - t'$ in the case $a = b = 1 - h$. Therefore the integration scheme used for these two cells must take into account these singularities.

(U) We now develop general methods for treating the singular integrands and then exhibit the explicit formulas for the computation of the matrix elements.

(U) b) <u>Gaussion Methods for the Singular Integrands</u>. We consider the integral

$$I'_{aa} = \int\int_{a}^{a + h} F(s, t) \, \ell n \, |s - t| \, ds \, dt \qquad (3.184)$$

and make the transformation

$$s = a + h/2 + \frac{u - v}{\sqrt{2}}$$

$$t = a + h/2 + \frac{u + v}{\sqrt{2}} \qquad (3.185)$$

so that with $F(s, t) = G(u, v)$

$$I'_{aa} = \int_{-h/\sqrt{2}}^{0} dv \int_{-(v+h/\sqrt{2})}^{v+h/\sqrt{2}} du \; G(u,v) \ln\sqrt{2} \; |v|$$

$$+ \int_{0}^{h/\sqrt{2}} dv \int_{-(h/\sqrt{2}-v)}^{h/\sqrt{2}-v} du \; G(u,v) \ln\sqrt{2} \; |v| \tag{3.186}$$

where

$$G(u,v) = F\left(s + \frac{h}{2} + \frac{u-v}{\sqrt{2}}, \; t + \frac{h}{2} + \frac{u+v}{\sqrt{2}}\right).$$

In the first term of (3.186) we let $v \rightarrow -v$ and

$$I'_{aa} = \int_{0}^{h/\sqrt{2}} dv \int_{-(h/\sqrt{2}-v)}^{h/\sqrt{2}-v} du \; G(u,v) + G(u,-v) \ln\sqrt{2} \; v \tag{3.187}$$

Now let

$$v = h/\sqrt{2} \; x$$

$$u = h/\sqrt{2} \; (1-x) y \tag{3.188}$$

and (3.187) becomes

$$I^1_{aa} = \frac{h^2}{2} \int_0^1 dx \, (1-x) \ln hx \int_{-1}^1 dy \cdot \left\{ G\left[\frac{h}{\sqrt{2}}(1-x)y, \frac{h}{\sqrt{2}} x\right] \right.$$

$$\left. + G\left[\frac{h}{\sqrt{2}}(1-x)y, -\frac{h}{\sqrt{2}} x\right] \right\}$$

$$I^1_{aa} = \frac{h^2}{2} \int_0^1 dx \, (1-x) \, \ln hx \int_{-1}^1 dy \cdot \left\{ F\left[s(x,y), \, t(x,y)\right] \right.$$

$$\left. + \; F\left[t(x,y), \, s(x,y)\right] \right\} \tag{3.189}$$

where

$$s(x,y) = \frac{h}{2} (1-x)(1+y) + a$$

$$\tag{3.190}$$

$$t(x,y) = \frac{h}{2} \left[(1-x)y + x + 1 + a\right].$$

(U) The y-integration is to be done using a Gauss-Legendre scheme; the x-integration using a Gauss scheme with the weight $(1-x) \ln hx$. The result of the x-integration is of the form

$$I^1_{aa} = \frac{h^2}{2} \sum_{\substack{i=1 \\ j=1}}^{\substack{j=M \\ i=N}} A_{ij} \left[F(s_{ij}, \, t_{ij}) + F(t_{ij}, \, s_{ij}) \right]. \tag{3.191}$$

(U) For $b = a - h$ we need consider the integral

$$I^1_{a, \, a-h} = \int_a^{a+h} ds \int_{a-h}^a dt \, F(s,t) \ln \left| s - t \right|. \tag{3.192}$$

we make the transformation

$$s = a + \frac{u - v}{\sqrt{2}} \qquad\qquad t = a + \frac{u + v}{\sqrt{2}} \tag{3.193}$$

$$\left| s - t \right| = \sqrt{2} \, |v|$$
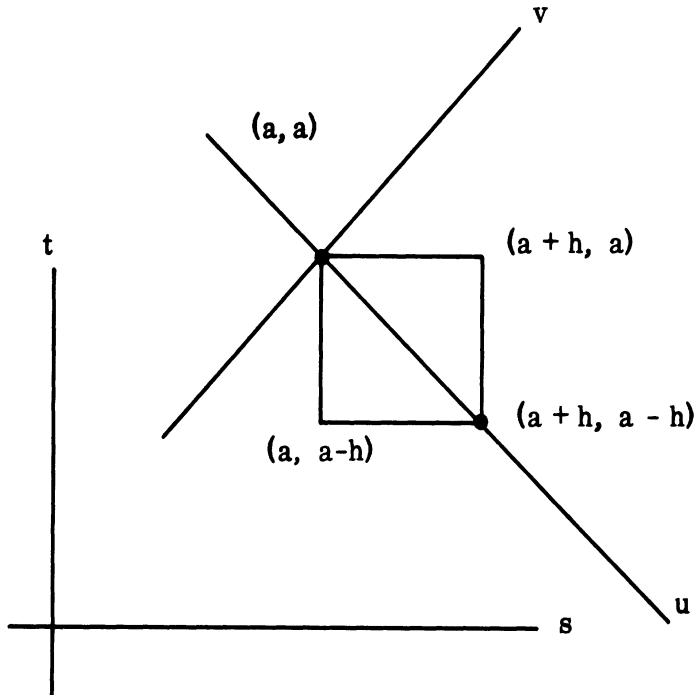
FIG. 3-15: COORDINATE SYSTEM.

Hence,

$$I^1_{a, a-h} = \int_{-\frac{h}{\sqrt{2}}}^{0} dv \int_{-v}^{v+\sqrt{2}\,h} du\ G(u, v)\ \ell n\sqrt{2}\ |v|$$

$$+ \int_{0}^{h/\sqrt{2}} dv \int_{v}^{-v+\sqrt{2}\,h} du\ G(u, v)\ \ell n\sqrt{2}\ |v| \qquad (3.194)$$

In the first term of (3.194) we let $v \rightarrow -v$;

$$I^1_{a,\,a-h} = \int_0^{h\sqrt{2}} dv \int_{-v}^{v+\sqrt{2}\,h} du \left[G(u,v) + G(u,-v) \right] \ln\sqrt{2}\, v. \quad (3.195)$$

Now put

$$v = h/\sqrt{2}\; x \;, \qquad u = h/\sqrt{2} \left[(1+x)y + 1 \right] \quad (3.196)$$

so that

$$I^1_{a,\,a-h} = \frac{h^2}{2} \int_0^1 dx(1+x)\ln hx \int_{-1}^1 dy \left\{ G\left(\frac{h}{2}\left[(1+x)y+1\right], \frac{h}{\sqrt{2}}\,x \right) \right.$$

$$\left. + \; G\left(\frac{h}{2}\left[(1+x)y+1\right], -\frac{h}{2}\,x \right) \right\}$$

$$= \frac{h^2}{2} \int_0^1 dx\,(1+x)\ln hx \int_{-1}^1 dy \left\{ F\left[s(x,y),\, t(x,y) \right] \right.$$

$$\left. + \; F\left[t(x,y),\, s(x,y) \right] \right\} \quad (3.197)$$

where

$$s(x,y) = \frac{h}{2}\left\{ (1+x)y + (1-x) \right\} + a$$

$$\left. \right\} . \quad (3.198)$$

$$t(x,y) = \frac{h}{2}\,(1+x)(1+y) + a$$

(U) As in the previous case, I^1_{aa}, the y-integration is to be done using a Gauss-Legendre scheme; the x-integration using a Gauss scheme with the weight $(1+x)\ln hx$ (section e). The resulting approximation is then of the form

$$I^1_{a,\,a-h} = \frac{h^2}{2} \sum_{\substack{i=1 \\ j=1}}^{\substack{j=M \\ i=N}} B_{ij} \left[F(s_{ij},\, t_{ij}) + F(t_{ij},\, s_{ij}) \right] \,. \tag{3.199}$$

(U) For $a = b = 0$ or $a = b = 1 - h$ we need consider integrals of the form

$$I_c = \iint_0^h F(s,t)\, \underline{P}\, \left(\frac{|s-t|}{s+t} \right) \frac{1}{s+t}\, ds\, dt \,. \tag{3.200}$$

On rotating $\pi/4$ about the origin,

$$s = \frac{u-v}{\sqrt{2}} \,, \qquad t = \frac{u+v}{\sqrt{2}} \tag{3.201}$$

and

$$I_c = \int_0^{h/\sqrt{2}} du \int_{-u}^{u} dv\, \frac{1}{\sqrt{2}\, u}\, P\left(\frac{|v|}{u} \right) G(u,v)$$

$$+ \int_{h/\sqrt{2}}^{\sqrt{2}\, h} du \int_{-(\sqrt{2}\, h - u)}^{\sqrt{2}\, h - u} dv\, \frac{1}{\sqrt{2}\, u}\, P\left(\frac{|v|}{u} \right) G(u,v)$$

$$\equiv I_c^{(1)} + I_c^{(2)} \,. \tag{3.202}$$

(U) The first term in (3.202) we transform by

$$u = h/\sqrt{2}\; x \,, \qquad v = uy = h/\sqrt{2}\; xy \,. \tag{3.203}$$

Hence,

$$I_c^{(1)} = \frac{h}{2} \int_0^1 dx \int_{-1}^1 dy \, P(|y|) \, G\left(\frac{h}{\sqrt{2}} x, \frac{h}{\sqrt{2}} xy\right).$$

(3.204)

(U) Since in our case

$$P(|y|) = K\left(\sqrt{1 - y^2}\right)$$

we use $K\left(\sqrt{1 - y^2}\right)$ as the weight function in performing the y-integration in section f. For the x-integration we use a Gauss-Legendre scheme. We find

$$I_c^{(1)} = \sum_{\substack{i=1 \\ j=1}}^{\substack{j=M \\ i=N}} C_{ij} \left[F(s_{ij}, t_{ij}) + F(t_{ij}, s_{ij})\right].$$

(U) c) <u>Computation of the Fourier Coefficients of the Green's Function.</u>
Given the expression form (3.181)

$$G_m = \int_0^\pi \frac{e^{iKR}}{KR} \cos m \, \phi \, d\phi$$

$$= \frac{2K}{\Gamma R} \int_0^1 e^{i\Gamma dn(Kx)} \, T_{2m}\left[cn(Kx)\right] \, dx = \frac{2K}{R} \, g_m$$

we need to compute the elliptic functions $dn(Kx)$ and $cn(Kx)$ at the Legendre nodes $x = x_i$. Since the methods of computing the elliptic functions depends on $K(k)$ or k we need refer to the nodes of the subsequent integration in order to choose the appropriate method.

(U) The critical cases occur for the diagonal cells with the weight $(1 - x)\ln hx$. The calculation of the nodes shows that k is sufficiently different from zero so that the Fourier series expansion of the elliptic functions is applicable and, in fact, converges very rapidly. We have

$$dn\ u = \sqrt{\frac{1}{k}}\ \frac{\Theta\ (u + k)}{\Theta(u)}$$

where

$$\Theta\ (u) = 1 + 2 \sum_1^\infty (-)^n q^{n^2} \cos\ (n\pi u/K)$$

$$\Theta\ (u + K) = 1 + 2 \sum_1^\infty q^{n^2} \cos\ (n\pi u/K)$$

and

$$q = e^{-\pi \frac{K'(k)}{K(k)}}\ ; \quad K'(k) = K(k')\ .$$

Using this expression for $dn\,u$ and the identity

$$cn^2 u = \frac{1}{k^2}\ (dn^2 u - k'^2)$$

we approximate the g_m by a Gauss-Legendre scheme where the number of terms will depend upon m.

(U) d) <u>The Logarithmic Weight.</u> Consider the integral

$$\int_0^1 dw\ (1 - w)\ \ln f(w)\ .$$

Let

$$I_n = \int_0^1 dw\, \omega^n (1 - w)\, \ln hw$$

$$I_o = \frac{1}{2} \ln h - \frac{3}{4}$$

$$I_1 = \frac{1}{6} \ln h - \frac{5}{36}$$

$$I_2 = \frac{1}{12} \ln h - \frac{7}{144}$$

$$I_3 = \frac{1}{20} \ln h - \frac{9}{400} \; .$$

The polynomial for the Gaussian quadrature is of the form

$$P = w^2 + bw + c$$

and the orthogonality condition is

$$I_2 + bI_1 + cI_o = 0 \quad , \quad I_3 + bI_2 + cI_1 = 0 \; .$$

Hence for

$$\Delta = I_1^2 - I_2 I_o$$

we find

$$b = \frac{I_o I_3 - I_1 I_2}{\Delta} \quad , \qquad c = \frac{I_2^2 - I_1 I_3}{\Delta} \; .$$

This gives the nodes

$$w = \frac{-b + \sqrt{b^2 - 4c}}{2}$$

119

and the weight

$$A_k = \int_0^1 (1 - w)\ln hw \, \frac{P(w)}{(w - w_k) \, P'(w_k)}$$

where

$$A_1 = \frac{1}{w_1 - w_2} \left[I_1 - w_2 \, I_0 \right]$$

$$A_2 = \frac{1}{w_2 - w_1} \left[I_1 - w_1 I_0 \right]$$

with

$$w_1 = \frac{-b - \sqrt{b^2 - 4c}}{2}$$

$$w_2 = \frac{-b + \sqrt{b^2 - 4c}}{2}$$

$$A_1 + A_2 = -\frac{I_0}{v_1 - w_2} (w_1 - w_2) = I_0$$

$$A_1 - A_2 = \frac{2I_1}{w_1 - w_2} + \frac{I_0}{w_1 - w_2} \left[-w_2 - w_1 \right]$$

(U) e) <u>The Second Logarithmic Weight.</u> Consider the integral

$$I = \int_0^1 dx \, (1 + x) \, \ln hx \, F(x) \; .$$

This is approximated just as in d, with the changed moments

$$I'_0 = 1/2 \, \ln h + 3/4$$

$$I'_1 = 1/2 \, \ln h + 5/36$$

$$I'_2 = 1/12 \ln h + 7/144$$

$$I'_3 = 1/20 \ln h + 9/400$$

(U) f) <u>The Elliptic Integral Weight</u>. Consider the integral

$$I \int_{-1}^{1} dy \ K'(y) \ F(y) \ .$$

The moments using the weight $K'(y)$ are

$$I_n = \int_{-1}^{1} y^n \ K'(y) \ dy \ .$$

Since $K'(y)$ is even only the even moments are non-vanishing

$$I_o = \pi^2/2 \ , \qquad I_2 = \pi^2/8 \ , \qquad I_4 = 9/16 \ \pi^2 \ .$$

For a cubic polynomial approximation because of the even weight the function the polynomial must be of the form

$$P = y \, (y^2 - a^2) \ ,$$

hence, the nodes occur at

$$y = 0, \ \pm \ a$$

where

$$a = \sqrt{I_4/I_2} \ = \ 2/3 \sqrt{2} \ .$$

The approximation weights are

$$A_o = 2 \, I_o = \pi^2$$

$$A_1 = 1/a^2 (I_2 + aI_o) = \frac{9\pi^2}{16} \left[\frac{1}{4} - \frac{2}{3} \sqrt{2} \right]$$

$$A_{-1} = 1/a^2 (I_2 - aI_o) = \frac{9\pi^2}{16} \left[\frac{1}{4} + \frac{2}{3} \sqrt{2} \right]$$

where

$$y_o = 0 \; , \qquad y_1 = 2/3 \sqrt{2} \; , \qquad y_{-1} = -2/3 \sqrt{2} \; .$$

3.5 Plasma Re-entry Sheath (Task 3.1.5)

3.5.1 Introduction

(U) Work that has been completed under this task is given below. A review of the assumptions and basic equations for a re-entry sheath is given for the case of laminar flow. This study is a necessary preliminary to an investigation to determine whether the velocity and other effects play an important role. Then the efforts of temperature are briefly examined for a gradient type non-lossy sheath. The results indicate that temperature effects are important, and much more analysis should be attempted.

(U) The integral equation approach (given in the first Quarterly Report) was investigated. However, for simplification, the case of a non-homogeneous planar sheath was treated. Practical results came out of the analysis. Further work should be attempted to generalize the technique to curved surfaces.

(U) Surface wave modes were studied for a plasma sheathed cylinder. These results are to be correlated with future experiments. Experimental evidence based upon the flat plate type geometry indicate that the "leaky wave" type modes are important for a plasma, ablative-coated object. These types of modes will have to be investigated for cylindrical and conical geometries.

3.5.2 A Review of the Assumptions.

(U) The investigation of the re-entry problem involves the study of the formation of a plasma layer around a re-entering vehicle. As the vehicle speeds through the atmosphere, the shock wave generated around it heats up the atmosphere sufficiently to cause ionization which forms the plasma. The theory involved in this problem concerns several scientific disciplines, including gas dynamics, chemical kinetics, statistical mechanics and electrodynamics. The properties of the boundary layer, chemical kinetics of a multi-component reacting gas such as air constitute a complex system of coupled chemical reactions and reacting species that will require considerable sophistication in the approach to a solution.

(U) The method used to solve this type of problem involves the application of both the electrodynamic equation of electromagnetic theory and the kinetic equations of particle interaction. The electrodynamic equations determine the fields exist within the plasma and therefore the forces acting upon the particles of the plasma. Kinetic equations express the transport phenomena of a plasma by considering the forces of interaction between its constituents. Simultaneous solution of these sets of equations determines the properties of waves in plasma. However, the mathematical difficulties involved in a multi-component, nonequilibrium, hypersonic viscous flow over a re-entry vehicle (boundary layer) could be so enormous that simplifying assumptions have to be made to reduce the equations to manageable forms suitable for machine computation. This section is intended to review the assumptions used in arriving at the necessary equations.

(U) a) The Transport Phenomena of a Plasma (Bird, et al 1960; Hayes and Probstein, 1959; Hirschfelder, et al 1963). The phenomena of diffusion, viscosity and thermal conductivity experienced in plasmas all involve the transport of some physical property through the plasma. Ordinary diffusion is the transfer of mass from one region to another because of a gradient in the concentration; viscosity is the transfer of momentum through the gas because of a gradient in the velocity; and thermal conductivity is the transfer of thermal energy resulting from the existence of thermal gradients in the gas. The transport coefficients D, μ and k are found to be functions of the gas mixture temperture, gas-species molecular weights, and certain parameters of the interparticle force fields. They can best be described in terms of the kinetic theory of gases or gas dynamics.

(U) A mathematical theory can be developed which describes the macroscopic feature of a gas mixture (which is not in thermodynamic or chemical equilibrium) based upon a postulated microscopic behavior of the constituent gas particles. The technique is to represent the state of an ensemble of particles by a distribution function $f^N(\underline{r}^N, \underline{p}^N, t)$ in a phase space. Here $\underline{r}$ and $\underline{p}$ are the position and momentum vectors respectively and N is the number of particles. This distribution function is so chosen that averages over the ensemble are in exact agreement with the incomplete knowledge of the state of the system at some specific time. Then the probable behavior of the system at subsequent times is taken to be the average behavior of members of the respective ensemble. The variation of the distribution function $f^N(\underline{f}^N, \underline{p}^N, t)$ with time is described by the Liouville equation. It involves 6N variables and is usually difficult to solve. Fortunately, one is principally concerned with the lower-order distribution functions $f^{(1)}$ and $f^{(2)}$. For example, $f^{(1)}$ gives the proba-

bility of finding one particular molecule with the specified position and momentum and does not depend upon the relative positions of two or more molecules. The level of information corresponding to the use of $f^{(1)}$ alone is, however, sufficient for studying the behavior of a moderately dilute gas. One form of the equation for $f^{(1)}$ is the Boltzmann equation which has been successfully applied to plasma problems. The distribution $f^{(2)}$ should be written as $f^{(2)}(\underline{r}_1, \underline{r}_2, \underline{p}_1, \underline{p}_2, t)$ and it is the distribution function of pairs of particles in phase space. It applies to a system in which two-body forces can be assumed and is therefore applicable to gases at higher density.

(U) b) <u>The Boltzmann Equation</u> (Hirschfelder, et al 1963). The macroscopic behavior of a dilute monatomic gas mixture in a nonequilibrium state is usually described with sufficient accuracy by a distribution function of lower order such as $f_i^{(1)}$. Here the subscript i indicates the ith constituent of the gas mixture. The Boltzmann equation can be derived from the Liouville equation by integrating over the coordinates of (N - 1) molecules and introducing the concept of "molecular chaos". The general form of the Boltzmann equation is (omitting the superscript (1) on f_i)

$$\frac{\partial f_i}{\partial t} + \left(\underline{v}_i \cdot \frac{\partial f_i}{\partial \underline{r}}\right) + \frac{1}{m_i}\left(\underline{X}_i \cdot \frac{\partial f_i}{\partial \underline{v}_i}\right) = \left(\frac{\partial f_i}{\partial t}\right)_{coll} , \qquad (3.205)$$

where $X_i(r, t)$ is the external force, and $(\partial f_i/\partial t)_{coll}$ represents a term known as the collision integral. The external force is usually assumed to be much smaller than the forces which act on the molecules during an encounter. In the collision integral, binary collisions only are assumed.

(U) The simplest version of Eq. (3.205) represents a gas of collisionless states and with no external force. The velocity distribution function thus

obtained reduces to the Maxwellian distribution function $f_i = n_i (m_i/2\kappa T)^{3/2} \exp$ $(-m_i v_i^2/2\kappa T)$. Maxwellian distribution still prevails even if the gas is in a state collisional equilibrium. This is because, even if the velocities of individual particles continue to suffer abrupt changes due to collisions, in a state of collisional equilibrium, the same number of particles enter a given volume of phase space as leave it, so the distribution function is unchanged.

(U) Equation (3.205) in its most general form, is difficult to solve. However, one is usually interested in the properties of gases which are under conditions only slightly different from equilibrium. In this limit the distribution function is nearly Maxwellian, and the Boltzmann equation can be solved by a perturbation method which provides a series approximation to the distribution function such as

$$f_i = f_i^{[0]} + \epsilon f_i^{[1]} + \epsilon^2 f_i^{[2]} + \dots , \qquad (3.206)$$

where the perturbation parameter ϵ is chosen such that $1/\epsilon$ represents a measure of the frequency of collisions between particles of various kinds. The square bracket used in the superscript is meant to differentiate with the order of the distribution function introduced previously. The zeroth order approximation, which considers only the first term of the series, gives a distribution function which is locally Maxwellian. The equations of change derived from this approximation are the Euler equation of change. In the first-order approximation, one writes

$$f_i^{[1]}(\underline{r}, \underline{v}_i, t) = f_i^{[0]}(\underline{r}, \underline{v}_i, t) \, \phi_i (\underline{r}, \underline{v}_i, t) ,$$

where ϕ is a perturbation function. The resultant Boltzmann equation leads to the Navier-Stokes equations. A second-order approximation leads to the

Burnett equations. Higher order approximations contribute terms proportional to higher derivatives and power of the lower derivatives of the physical quantities and thus add to the complexity of the equations. Among the three approximations just mentioned, the Navier-Stokes equations are most widely used for solving problems involving nonequilibrium plasmas.

(U) The assumptions used to derive the Navier-Stokes equation (Dorrance, 1962) can be summarized as follows:

1. The gradients of the physical quantities, the variables of states, and the flow velocity are small. These equations are, strictly speaking, not applicable to a gas mixture in the immediate regions of a strong shock wave.

2. Only binary collisions are considered. This is to say that the gas density is moderately dilute. For high density gases where the three-body and higher-order collisions are not negligible, this theory does not apply.

3. The effective range of intermolecular or inter-particle forces is small compared with the mean free path.

4. Assume the gases have little or no internal degree of freedom.

5. The quantum mechanical effects are not important. The theory is inadequate for gases with very low density and low temperature (typically below 100°K).

6. The mean free path of the gas must be small compared with any physical dimensions of the boundaries so that equilibrium conditions within the gas are determined by gas-particle collisions.

(U) c) The Equations of Change. (Hirschfelder, et al 1963). The Boltzmann equation describes the time variation of the velocity distribution function. The macroscopic equations of the gas can then be obtained from the equations of change.

(U) If $\psi\,(\underline{r}_i,\ \underline{v}_i,\ t)$ is any function, the average values of ψ can be obtained by multiplying the distribution function by ψ and integrating over the velocity space, i.e.,

$$\int \psi \left(\frac{\partial f_i}{\partial t} + \underline{v}_i \cdot \frac{\partial f}{\partial \underline{r}_i} + \underline{X}_i \cdot \frac{\partial f_i}{\partial \underline{v}_i} \right)\, d^3v = \int \psi \left(\frac{\partial f_i}{\partial t} \right)_{coll} d^3v . \quad (3.207)$$

Moment equations are obtained by letting ψ take on values which are proportional to increasing powers of the velocity v_i. It is seen that setting $\psi = 1$ corresponding to taking the zeroth moment leads to the continuity equation; the first moment, obtained by setting $\psi = mv_j$, leads to the momentum equation; while setting $\psi = \frac{1}{2} mv_j^2$ leads to the energy equation.

(U) Thus far, the behavior of an individual species of a gas mixture has been described. It is now desired to derive a set of equations that will describe the behavior of the gas mixture as a whole, i.e., regarding the gas mixture as a fluid. Let v_i be the individual velocity of the ith species, $\bar{v}_i$ is the average of v_i. The mass average velocity of the fluid $v_o(\underline{r},\ t)$ is defined as

$$v_o\,(\underline{r},\ t) = \frac{1}{\rho} \sum_i m_i \int f_i\,\underline{v}_i\,d^3v. \quad (3.208)$$

where ρ is the mass density, m_i is the mass of one particle, the ith species. The peculiar velocity of the ith species is defined as $V_i = v_i - v_o$ and is the velocity of the ith species with respect to a coordinate system moving with the mass velocity v_o of the fluid, and $\bar{V}_i = \bar{v}_i - v_o$ is the mean peculiar velocity. Equations of change will be expressed in terms of these average velocities to account for the gas dynamics in a gas mixture.

(U) If the collisions in gas mixture result in a chemical reaction which creates more particles, then other complications follow. The right-hand side of the Boltzmann equation (3.205) (the collision integral), needs to be modified. Let K_i be the rate of change per unit volume of the number of particles due to chemical reaction, then the collision integral may be replaced by K_i provided that the mass is conserved throughtout the chemical reactions, i.e., $\sum_i K_i m_i = 0$. For a multi-component gas mixture such as air, where many chemical reactions can take place simultaneously, the calculation of K_i becomes a formidable problem.

(U) With these changes, the equations of change can be rewritten, in terms of the mean mass velocity and K_i in the following form. For example, for the individual species, the equation of continuity becomes

$$\frac{\partial n_i}{\partial t} + \left[\frac{\partial}{\partial \underline{r}} \cdot n_i (v_o + \overline{V}_i) \right] = K_i \quad . \tag{3.209}$$

The equation of continuity for the entire system becomes

$$\frac{\partial \rho}{\partial t} + \left(\frac{\partial}{\partial \underline{r}} \cdot \rho v_o \right) = 0 \ , \tag{3.210}$$

where n_i is the number density of the ith species and ρ is the mass density. The equation for the conservation of momentum becomes

$$\frac{\partial \underline{v}_o}{\partial t} + \left(\underline{v}_o \cdot \frac{\partial}{\partial \underline{r}} \underline{v}_o \right) = -\frac{1}{\rho} \left(\frac{\partial}{\partial \underline{r}} \cdot P \right) + \frac{1}{\rho} \sum_i n_i X_i \ , \tag{3.211}$$

where P is a pressure tensor. The equation for the conservation of energy becomes

$$\rho \hat{c}_V \left[\frac{\partial T}{\partial t} + \left(v_o \cdot \frac{\partial}{\partial \underline{r}} T \right) \right] = - \left(\frac{\partial}{\partial \underline{r}} \cdot q \right) - \left(P \cdot \frac{\partial}{\partial \underline{r}} v_o \right) +$$

$$+ \sum_i n_i (\bar{V}_i \cdot X_i) - \sum_i m_i K_i \hat{U}_i + \sum_i \hat{U}_i \left(\frac{\partial}{\partial \underline{r}} \cdot n_i m_i \bar{V}_i \right) , \quad (3.212)$$

where

$$\hat{c}_V = \frac{1}{\rho} \sum_i n_i m_i \left(\frac{\partial \hat{U}_i}{\partial T} \right)_V = \frac{1}{\rho} \sum_i n_i m_i (\hat{c}_V)_i$$

and is the average heat capacity per gram at constant volume.

$\hat{U}_i$ is the average internal energy per unit mass ,

q is the total head flux

and

$P : \dfrac{\partial}{\partial \underline{r}} v_o$ is a tensor product as $\displaystyle\sum_i \sum_j P_{ij} \dfrac{\partial}{\partial r_j} v_i$.

(U) Chemical reactions produce heat transfer. Internal energy may be converted into heat in an exothermic reaction, while the external translational energy may be converted into internal energy in endothermic reactions concurrently with the formation of new species. In computing the energy equation, the enthalphy of the gas mixture, and the rate and the gradient of the heat transfer have to be evaluated from the study of the thermo-chemistry processes involved (Lenard, 1964; and Bortner, 1963).

(U) d) <u>Reducing the Equations of Gas Dynamics to the Boundary Layer Equations</u> (Dorrance, 1962; Blottner, 1964; and Pallone et al, 1964). The equations of change stated in the previous section may now be reduced to boundary layer equations in order to apply to the re-entry plasma problem. It is postulated

that the effects of the transport phenomena in a dilute gas mixture are confined to a thin layer near the surface of the body over which the plasma fluid flows. It is also assumed that the head transfer from the boundary layer composed of a mixture of dissociating gases is independent of the location of the reaction zone within the boundary layer. Under this approximation, the transport properties are independent of the composition of the boundary-layer gas mixture. In other words, the chemical reactions as assumed to occur at the surface and the gas-phase reactions are frozen. Adopting Prandtl's boundary layer concept that

$$\delta(x) << x \quad \text{and} \quad \frac{\delta^2}{x} = O\left(1/R_e\right) ,$$

where $\delta(x)$ is the velocity boundary-layer thickness and $R_e = \rho_e u_e x / \mu_e$, the component equations of the equations of change can be expressed in terms of δ, R_e and a characteristic length L. By comparing the order or magnitude of the individual terms in the resultant equations, it is found that many terms can be neglected against the dominating terms. This order-of-magnitude analysis simplifies the equations considerably. Further simplifications are achieved by assuming that

1. All gas species considered behave as perfect gas species,
2. The flow is in a steady state,
3. The effects of radiation are neglected, and
4. The flow is two-dimensional or axially symmetric.

(U) e) <u>Reduce the Boundary-Layer Partial Differential Equations to Ordinary Differential Equations</u>. (Dorrance, 1962; Blottner, 1964). The boundary-layer equations stated in the previous sections are nonlinear partial differential equations which are difficult to solve except under special circum-

stances where enough terms can be dropped to reduce the equations to ordinary differential equations. Another circumstance under which the equations can be reduced to ordinary differential equations occurs where there exists a natural coordinate system (χ, η), related to the Cartesian coordinate system (x, y) through appropriate transformation in which the derivatives of the dependent variables become separable and ordinary differential equations result.

(U) To solve this set of differential equations for a particular boundary-layer problem, the boundary conditions must be known or assumed. There are two boundaries in this reduced two-dimensional problem: one at the wall of the body and the other at the outer edge of the flow. At the wall, it is assumed that both the normal and tangential velocities are zero, and that the temperature and the mass fraction of the species are specified. At the outer edge, a nonequilibrium inviscid flow condition is assumed. The boundary conditions on the species concentration at the wall are dictated by a degree of catalyticity of the wall material.

(U) Typical initial velocity and temperature profiles (Blottner, 1964) of a frozen flow is shown in Figs. 3-16 and 3-17 respectively. These initial conditions are used to calculate the nonequilibrium species density, temperature and enthalpy profiles of the particular gas constituent at various altitudes. Results (Blottner, 1964; and Pallone, et al 1964) of these calculations indicate that the temperature profile does not vary much along the body of the vehicle. However, the electron density can vary several orders of magnitude along it.

(U) f) Waves in Plasma (Holt and Haskell, 1965; and Glick, 1962). To study the interaction of electromagnetic waves and plasmas, Maxwell's equations may be solved simultaneously with equations that describe the motion of plasma particles. For plasmas involving multi-component gases, a complete descrip-
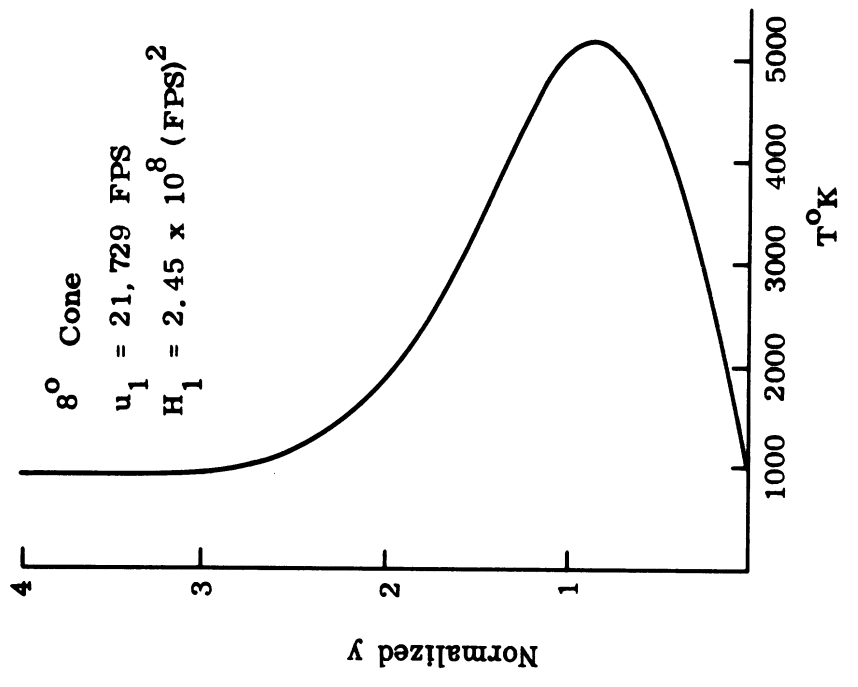
FIG. 3-17: INITIAL TEMPERATURE PROFILE
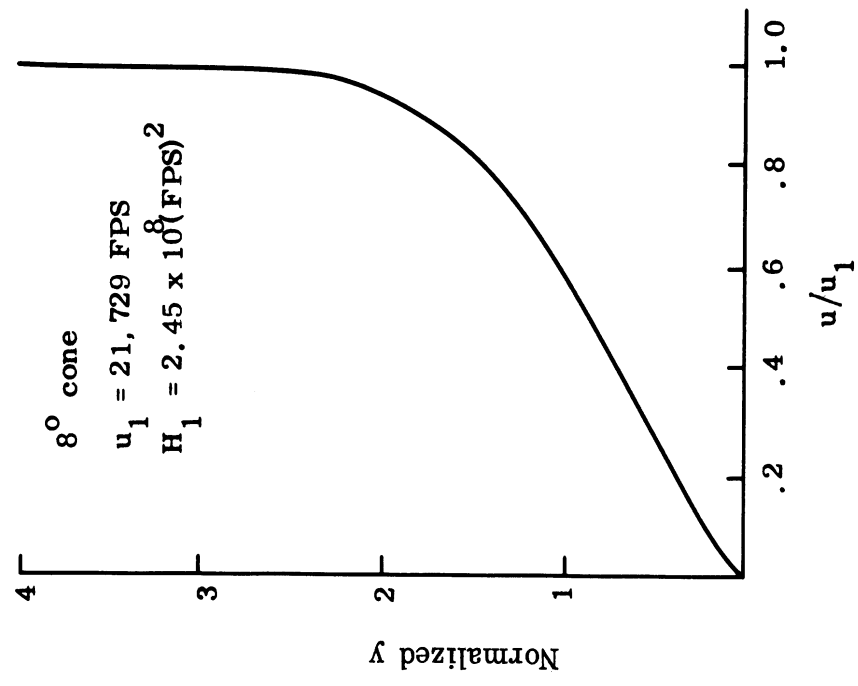
FIG. 3-16: INITIAL VELOCITY PROFILE

tion of the particle motion can be obtained by writing out a Boltzmann equation for each species. A typical example of this approach is given by the Vlasov equation in which the plasma is considered to be collisionless and the ions are considered motionless. Also used as an assumption is that in the external force term in the Boltzmann equation, only the longitudinal component of the electric field due to space charges is considered. The Boltzmann equation is then linearized by neglecting the higher-order derivatives and products terms introduced by perturbation function. On the other hand, the electron density and the charge density can be defined in terms of the perturbed distribution function. Upon substituting the charge density expression into the Poisson equation, the electric field can then be expressed in terms of the distribution function. Now, both the Boltzmann equation and the electric field equation containing the distribution function and the electric field can be solved to obtain a self-consistent solution. The procedure leads to the dispersion equation from which the wave phenomena in plasma can be investigated.

(U) For a chemically reacting multi-component plasma, severe difficulties in mathematical handling arise. Simplifying models of plasmas are frequently used for analysis. In the single-fluid model, only the motion of the electron is considered. In the two-fluid model, the motion of both the electrons and ions are considered. Likewise, a three-fluid model will consider the motion of electrons, ions and neutral particles. The appropriate continuity and momentum equations for each case are written. These equations are solved simultaneously with Maxwell's equations. The results is again the dispersion relation.

(U) Another approach that is frequently used in studying the properties of wave propagation in the ionosphere should also be mentioned. In this approach one derives a wave equation from Maxwell's equations as usual but characterizes the plasma either as a conductive or dielectric medium whose conductivity or dielectric constant (or complex tensor) is derived from the basic transport

equations describing the plasma. For a weakly ionized medium a simple form of the equation of motion, the Langevin equation, is used in conjunction with Maxwell's equations to describe the dynamics of plasmas.

(U) g) <u>Other Simplifying Assumptions</u>. In the preceding sections, assumptions are specified as various basic equations are introduced. These are general assumptions used to derive these basic equations. For a particular problem, further simplifications can be achieved by introducing more specific assumptions. For example, for a two-dimensional boundary-layer problem discussed in a previous section, besides the assumptions already stated, further simplifications in equations of momentum and energy can be made assuming the following (Bird, et al 1960)

1. The flow is laminar,

2. In the transport phenomena, only diffusions due to concentration and thermal gradients are considered,

3. A pressure gradient exists in the x-direction (along the vehicle body) only,

4. A temperature gradient exists in the y-direction (perpendicular to the surface of the vehicle body) only,

5. The external force is zero. Gravitational force applies equal to all species in all direction.

Many other assumptions can be added in dealing with chemical kinetics such as the following (Pallone et al, 1964)

1. A limited number of gas constituents.

2. Limited chemical reactions.

3. All gas species are coupled only at the wall.

4. Ionization energy is negligible.

5. Concentrations of certain constituent gases (particularly that of of N_2 and O_2 in atmospheric gas) at the wall and at the outer edge of the boundary layer are the same.

6. The mass flux is balanced by recombination at the wall.

3.5.3 Fields in a Warm Inhomogeneous Plasma Near the Plasma Frequency.

(U) Scattering of plane waves from planar, inhomogeneous cold plasmas has been studied at considerable length (Budden, K. G., 1961) in connection with ionospheric studies, and some interesting phenomena which are pertiment to the study of scattering from plasma clad objects have been noted. Specifically, incident plane waves with $\overline{E}$ polarized parallel to the plane of incidence ($\overline{E}$-waves) excite $\overline{E}$-waves in the plasma region which show a singularity in that region of the plasma where plasma frequency and incident wave frequency are equal. These cold plasma results are derived in subsection a, where it is shown that the x-component of the electric field goes as $1/x$ near $x = 0$, the position in the plasma at which the frequency of the incident radiation and the plasma frequency are equal, and that the y-component of the electric field goes as ℓnx near $x = 0$. The large fields which occur at $x = 0$ indicate that a non-linear analysis is required to adequately describe the behavior of the fields there. Such analysis have been made (Forsterling and Wüster, 1951) and seem to indicate that anomolous absorption and re-radiation of higher harmonics of the incident waves may occur when the frequency is near the plasma frequency. If such is the case, the determining factor in the scattering of E-waves from plasma sheath clad objects could be the outer underdense edge of the plasma sheath up to and including the neighborhood of the region in which the plasma frequency and incident wave frequency are equal. (See Fig. 3-18) The bulk of the plasma sheath and the wall region of the scatter may be largely shielded
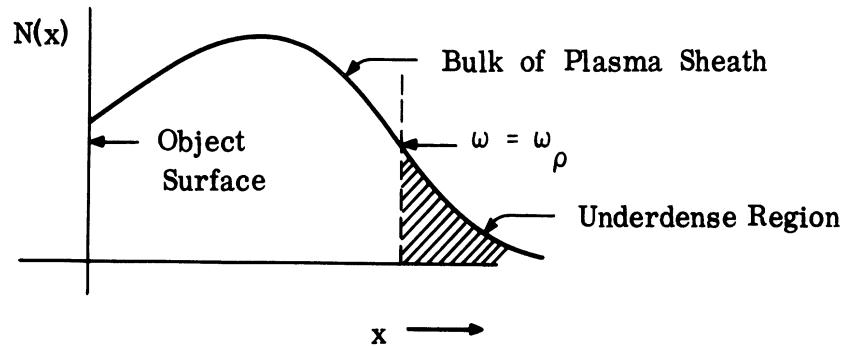
FIG. 3-18: THE PLASMA SHEATH

from incident radiation and, consequently, could play a secondary rather than their current primary role in the scattering phenomena. An interesting result would be an increase in the effective size of the scatterer for E-waves but not for H-waves which are not as sensitive to the critical region about the plasma frequency.

(U) The purpose of this study has been to re-examine the behavior of the fields in the neighborhood of the plasma frequency in the context of the more precise warm plasma model in an effort to determine whether or not singularities in the fields occur in the neighborhood of the plasma frequency and whether or not this region has a profound effect on the scattering of E-waves. The problem is approached via the hydrodynamic equations (Maxwell's equations and the first three moments of the Vlasov equation) which provide a good description of the warm plasma near the plasma frequency.[*] Static electric and magnetic fields are neglected as are collisions and the effect of ions and neu-

---

[*] The validity of this approach in the general case - at arbitrary density for a given frequency-has been a topic of much concern, at issue being the nature of the error incurred by neglecting the heat flow tensor in the third moment equation. However, it is generally agreed, and there are a number of arguements to demonstrate that the adiabatic assumption is a good approximation in the vicinity of $\omega = \omega_p$.

tral particles except insofar as they maintain a charge balance in the unperturbed plasma. The extension to take collisions into account is straight forward and does not have an essential effect on the results. In this report plasma streaming is also neglected although progress has already been made on inclusion of the effect of plasma flow in the analysis. Initially the equations will be derived for arbitrary geometry but the solution will eventually be carried out only for a two dimensional plasma ($\partial/\partial z = 0$) whose equilibrium properties vary only in the x-direction. Finally, a small signal analysis is assumed.

(U) The appropriate hydrodynamic equations are:

$$\nabla \times \bar{E} = -\frac{\partial \bar{B}}{\partial t} \tag{3.213}$$

$$\nabla \times \bar{H} = \bar{J} + \frac{\partial \bar{D}}{\partial t} \tag{3.214}$$

$$\nabla \cdot \bar{J} + \frac{\partial \rho}{\partial t} = 0 \tag{3.215}$$

$$N \left[\frac{\partial \bar{v}}{\partial t} + (\bar{v} \cdot \nabla) \bar{v} \right] + \frac{1}{M} \nabla p = \frac{N}{M} \bar{F} \tag{3.216}$$

$$p = 3KTN \quad . \tag{3.217}$$

These equations are linearized according to the following scheme:

$$\bar{E} = \bar{E}(\bar{r}) \, e^{-j\omega t}$$

$$\bar{H} = \bar{H}(\bar{r}) \, e^{-j\omega t}$$

$$\bar{v} = \bar{v}(\bar{r}) \, e^{-j\omega t}$$

$$N = N(\bar{r}) + \eta(\bar{r}) \, e^{-j\omega t} \quad ,$$

and the linearized equations are:

$$\nabla \times \overline{E} = j\omega\mu \ \overline{H} \tag{3.218}$$

$$\nabla \times \overline{H} = \overline{J} - j\omega\epsilon_o \ \overline{E} \tag{3.219}$$

$$\nabla \cdot \overline{J} - j\omega\rho = 0 \tag{3.220}$$

$$-j\omega \overline{J} + a\nabla\rho = \omega_p^2 \ \epsilon_o \ \overline{E} \tag{3.221}$$

where

$$\overline{J} = q \ N(\overline{r}) \ \overline{v} \ (\overline{r}) \ e^{-j\omega t}$$

$$\rho = q \ \eta \ (\overline{r}) \ e^{-j\omega t}$$

$$\omega_p^2 = \frac{q^2 N(\overline{r})}{M\epsilon_o}$$

$$a = \frac{3KT}{M} \quad .$$

It has been assumed in deriving equation (3.221) that the magnetic terms in the Lorentz force are neglible compared to the electric force terms.

(U) In subsection b, the linearized set of equations (3.218) through (3.221) are reduced to the following coupled set of second order partial differential equations:

$$\nabla^2 \overline{H} - K^2 \nabla \left(\frac{1}{K^2}\right) \times (\nabla \times \overline{H}) + K^2 \overline{H} = -\frac{a}{j\omega} K^2 \ \nabla\left(\frac{1}{K^2}\right) \times \nabla_\rho \tag{3.222}$$

$$a\nabla^2 \rho + aK^2 \nabla\left(\frac{1}{K^2}\right) \cdot \nabla\rho + c^2 K^2 \rho = j\omega K^2 \nabla\left(\frac{1}{K^2}\right) \cdot (\nabla \times \overline{H}) \tag{3.223}$$

where

$$K^2 = (\frac{\omega}{c})^2 \left[1 - (\frac{\omega_p}{\omega})^2 \right] \quad .$$

(U) Equations (3.222) and (3.223) are applicable to any geometry and to both E-waves and H-waves ($\overline{H}$ polarized parallel to the plane of incidence). However, to facilitate the solution, the problem will be specialized to that of the scattering of E-waves from a plane, stratified plasma. That is $\partial/\partial z = 0$ and the unperturbed plasma density, N, varies only in the direction perpendicular to the plane of the plasma, N = N(x). For this model, the H-waves, as is readily shown, do not couple to the plasma waves. Hence the solution for the H-waves is substantially the same as that for a cold plasma, a problem much discussed (Budden, 1961; Miller, G.F. 1962; and Taylor, L.S. 1961).

(U) From the boundary conditions on $\overline{E}$ and $\overline{H}$ it is obvious that $\partial/\partial y \rightarrow$ j (ω/c) sin θ where θ is the angle of incidence. Since interest is to be focussed on the region about $\omega = \omega_p$, one may let this point occur at x = 0 and expand $K^2\nabla(1/K^2)$ in a Maclaurin series. Keeping only the first non-zero terms $\left[K^2(0) = 0 \right]$ in the series and using $\partial/\partial y = j(\omega/c)$ sin θ, Eqs. (3.222) and (3.223) reduce to the following pair of coupled, ordinary linear differential equations:

$$\frac{d^2H}{dx^2} - \frac{1}{x} \frac{dH}{dx} + \left[\beta x - (\frac{\omega}{c} \sin \theta)^2 \right] H = \frac{a \sin \theta}{cx} \rho \tag{3.224}$$

$$a \frac{d^2\rho}{dx^2} - \frac{a}{x} \frac{d\rho}{dx} + \left[c^2 \beta x - a (\frac{\omega}{c} \sin \theta)^2 \right] \rho = \frac{\omega^2 \sin \theta}{cx} H \tag{3.225}$$

where

$$\beta = \frac{\partial K^2}{\partial x} \bigg|_{x = 0} \quad .$$

(U) Since the singularity that occurs at $x = 0$ appears to be regular, a solution in the form of a power series is attempted. The solutions written below are derived in subsection c.

$$H_1 = Ax^2 \left[1 + \frac{1}{6} (\frac{\omega}{c} \sin \theta)^2 x^2 - \frac{\beta}{15} x^3 + \ldots \right] +$$
$$+ \frac{a \sin \theta}{3c} Bx^3 \left[1 + \frac{1}{10} (\frac{\omega}{c} \sin \theta)^2 x^2 + \ldots \right] \qquad (3.226)$$

$$\rho_1 = Bx^2 \left[1 + \frac{1}{6} (\frac{\omega}{c} \sin \theta)^2 x^2 - \frac{c^2 \beta}{a} x^3 + \ldots \right] +$$
$$+ \frac{\omega^2 \sin \theta}{3ac} Ax^3 \left[1 + \frac{1}{10} (\frac{\omega}{c} \sin \theta)^2 x^2 + \ldots \right] \qquad (3.227)$$

$$H_2 = C \left[1 - \frac{\beta}{3} x^3 - \frac{1}{24} (\frac{\omega}{c} \sin \theta)^4 x^4 + \ldots \right] -$$
$$- a \frac{\sin \theta}{c} Dx \left[1 + \frac{1}{3} (\frac{\omega}{c} \sin \theta)^2 x^2 - \frac{\beta}{24} (3 - \frac{c^2}{a}) x^3 + \ldots \right] (3.228)$$

$$\rho_2 = D \left[1 - \frac{c^2 \beta}{3a} x^3 - \frac{1}{24} (\frac{\omega}{c} \sin \theta)^4 x^4 + \ldots \right] -$$
$$- \frac{\omega^2 \sin \theta}{ac} Cs \left[1 + \frac{1}{3} (\frac{\omega}{c} \sin \theta)^2 x^2 - \frac{\beta}{24} (\frac{3c^2}{a} - 1) x^3 + \ldots \right] . (3.229)$$

The complete solutions for H and ρ are:

$$H = c_1 H_1 + c_2 H_2$$

$$\rho = c_3 \rho_1 + c_4 \rho_2 \quad .$$

(U) The electric field is given by Eq. (3.246) (subsection b) which can be rewritten in component form near $x = 0$ (i.e. $K^2 = \beta x$) as:

$$E_x = - \frac{\mu}{\beta x} \left[\frac{\omega^2 \sin \theta}{c} H + a \frac{\partial \rho}{\partial x} \right]$$

$$E_y = - j \frac{\mu}{\beta x} \left[\omega \frac{\partial H}{\partial x} + \frac{a \omega \sin \theta}{c} \rho \right] .$$

Substituting the power series solutions in for H and ρ one finds

$$E_{x_1} = - \frac{2 \mu a}{\beta} B - \frac{2 \mu}{\beta} \left[\frac{\omega^2 \sin \theta}{c} \right] Ax$$

$$+ \text{(Terms of higher order in } x) \tag{3.230}$$

$$E_{x_2} = \frac{\mu a}{\beta} \left[\frac{\omega \sin \theta}{c} \right]^2 D + \frac{\mu}{\beta} \left[c^2 \beta D + \omega \left(\frac{\omega \sin \theta}{c} \right)^3 C \right] x$$

$$+ \text{(Terms of higher order in } x) \tag{3.231}$$

$$E_{y_1} = - j \frac{2 \omega \mu}{\beta} A - j \frac{2 \mu}{\beta} \left[\frac{a \omega \sin \theta}{c} \right] Bx$$

$$+ \text{(Terms of higher order in } x) \tag{3.232}$$

$$E_{y_2} = - j \frac{\omega^2 \epsilon_o \sin \theta}{\beta} C + j \frac{\mu}{\beta} \omega \left\{ BC + \frac{a}{\omega} \left(\frac{\omega \sin \theta}{c} \right)^3 D \right\} x$$

$$+ \text{(Higher order terms in } x) . \tag{3.233}$$

(U) A study of Eqs. (3.230) through (3.233) indicates that neither of the singularities that occur in the cold plasma are predicted by the warm plasma theory. That none of the components of electric field go as $1/x$ is obvious upon inspection of Eqs. (3.230) through (3.233) because there are no negative powers of x involved. This is to be expected because a singularity which goes as $1/x$ also leads to a singularity in the energy density and is, therefore, not physically realizeable (Meixner, J., 1949). That no other type of singularity exists at $x = 0$ is apparent from the form of the expressions for the components of the electric field: Each component of $\bar{E}$ is in the form of a series of the form

$$\sum_{0}^{\infty} b_n x^n \quad .$$

Consequently, as long as all of the b_n are finite this series must converge at $x = 0$. In particular, it can't be logarithmic at $x = 0$.

(U) At first glance all the b_n appear to be bounded; however, this has yet to be established rigorously and some problems are already apparent. In particular, the coefficients, b_n, are not finite in the limit of zero temperature. This is to be expected in order to provide the transition from the non-singular warm plasma case $(T \neq 0)$ to the singular cold plasma case $(T = 0)$, but it opens questions regarding the convergence of the solutions in the limit of low temperture. The behavior of the series solutions in the limit of low temperature is not transparent and it is not obvious that they converge to the proper cold plasma result.

Page number 144 was not used in this report.

(U) Hence continuing study is required. In particular the series must be investigated more closely to prove rigorously that no singularity occurs in the warm plasma fields and it must be shown that the warm plasma solutions reduce to the cold plasma solutions in the limit of zero temperature. Once this has been done a final assesment of the importance of that portion of the plasma about $\omega = \omega_p$ on the scattering of E-waves can be made and the analysis can be extended to include such factors as plasma flow and collisions. If the fields prove to be singular an extension of the investigation to include a non-linear analysis will be required at $x = 0$.

(U) In the following subsections some of the details refered to in the preceeding paragraphs are supplied. In the first part, subsection a, a brief derivation of the pertinent cold plasma results is sketched. In subsection b the two coupled, partial differential equations for the magnetic field and plasma density, Eqs. (3.222) and (3.223) are derived from the hydromagnetic equations. In the last part, subsection c, the power series solution of Eqs. (3.224) and (3.225) is derived.

(U) a) The fields in an inhomogeneous cold plasma are obtained from the solution to the following equation:

$$\nabla^2 \overline{H} - K^2 \nabla (1/K^2) \times (\nabla \times \overline{H}) + K^2 \overline{H} = 0 \qquad (3.234)$$

where

$$K^2 = (\omega/c)^2 \left[1 - (\omega_p/\omega)^2 \right]$$

$$\omega_p^2 = \frac{q^2 N}{M \epsilon_0} \quad .$$

In the particular case of a two dimensional plasma whose density, N, varies

only in the direction perpendicular to the plane of the plasma, the x-direction, one has $\partial/\partial z = 0$, $\partial/\partial y = j \frac{\omega}{c} \sin \theta$ which follows from the boundary conditions, and $\nabla(1/K^2) = \frac{\partial}{\partial x}(1/K^2) \hat{x}$. Consequently, for E-waves Eq. (3.234) reduces to:

$$\frac{d^2 H}{dx^2} + K^2 \frac{\partial}{\partial x} (1/K^2) \frac{\partial H}{\partial x} + \left[K^2 - (\frac{\omega}{c} \sin \theta)^2 \right] H = 0 \quad . \quad (3.235)$$

Letting $x = 0$ be the position at which $\omega = \omega_p$ one may expand K^2 in a Maclaurin series to obtain the solution for H near $x = 0$. The resultant equation is:

$$\frac{d^2 H}{dx^2} - \frac{1}{x} \frac{dH}{dx} + \left[\beta x - (\frac{\omega}{c} \sin \theta)^2 \right] H = 0 \quad (3.236)$$

where

$$\beta = \left. \frac{\partial K^2}{\partial x} \right|_{x = 0} \quad .$$

It is interesting to note that although Eq. (3.236) is valid only near $x = 0$ for general density gradients, it happens to be correct for all x for linear gradients. If the slope is $1/L$ then $\beta = (-\omega^2/c^2 L)$.

(U) Equation (3.236) is an ordinary linear differential with a regular singular point at $x = 0$. Guessing a power series solution of form

$$H_1 = \sum_{n = 0}^{\infty} a_n x^{n + p}$$

leads to only one independent solution. The second is found by guessing

$$H_2 = H_1 \ell n x + \sum_{n=0} a_n x^n .$$

Carrying out the algebra one obtains:

$$H_1 = x^2 \left[1 + \frac{1}{8} (\frac{\omega}{c} \sin \theta)^2 x^2 - \frac{\beta}{15} x^3 + \ldots \right] \qquad (3.237)$$

$$H_2 = \frac{1}{2} (\frac{\omega}{c} \sin \theta)^2 H_1 \ell n x - \left[1 - \frac{\beta}{3} x^3 - \frac{3}{64} (\frac{\omega}{c} \sin \theta)^4 x^4 \ldots \right] \qquad (3.238)$$

and

$$H = AH_1 + BH_2 .$$

(U) The electric fields are found from Maxwell's equations and in particular from

$$\nabla \times \overline{H} = - j \omega \epsilon_0 \left[1 - (\omega_p / \omega)^2 \right] \overline{E} .$$

Thus, near $x = 0$, one obtains

$$E = \frac{j \omega \mu}{\beta x} \nabla \times \overline{H}$$

and

$$E_x = \frac{j \omega \mu}{\beta x} \frac{\partial H}{\partial y}$$

$$E_y = - \frac{j \omega \mu}{\beta x} \frac{\partial H}{\partial x} .$$

Keeping only first order terms in x one obtains

$$E_x = + \frac{\omega^2 \mu \sin \theta}{c\beta} \; B_x \tag{3.239}$$

$$E_y = \frac{j\omega\mu}{\beta} \left[A + (\frac{\omega}{c} \sin \theta)^2 \, B \, \ell nx \right] \tag{3.240}$$

Hence, both E_x and E_y become very large at $x = 0$, E_x going as $1/x$ and E_y getting large as ℓnx. However, these results are not strictly valid at $x = 0$, because the analysis that led to Eq. (3.234) was based on a small signal assumption. Consequently, Eqs. (3.239) and (3.240) should be interpreted to mean that a more precise non-linear analysis is required in the cold plasma model at $x = 0$.

(U) b) In this subsection Eqs. (3.222) and (3.223) are derived from the linearized hydromagnetic equations, Eqs. (3.218) through (3.221). These equations are rewritten below in slightly modified form.

$$\nabla \times \overline{E} = j\omega\mu \overline{H} \tag{3.241}$$

$$\nabla \times \overline{H} = \overline{J} - j\omega \epsilon_o \overline{E} \tag{3.242}$$

$$\nabla \cdot \overline{J} = j\omega \rho \tag{3.243}$$

$$\overline{J} = -\frac{1}{j\omega} \left[\omega_p^2 \, \epsilon_o \, \overline{E} - a \nabla \rho \right]. \tag{3.244}$$

Eliminating $\overline{J}$ from (3.242), the two Maxwell's equations (3.241) and (3.242) become:

$$\nabla \times \overline{E} = j\omega\mu \, H \tag{3.245}$$

$$\overline{E} = -\frac{\mu}{K^2} \left[-j\omega \nabla \times \overline{H} + a \nabla \rho \right] \tag{3.246}$$

where

$$K^2 = \left[\frac{\omega}{c}\right]^2 \left[1 - \frac{\omega_p^2}{\omega^2}\right] .$$

(U) An equation for $\overline{H}$ is found by taking the curl of Eq. (3.246) and then using Eq. (3.245)

$$\nabla \times \overline{E} = j \omega \mu \overline{H} = -\mu \nabla \times \left[\frac{1}{K^2} (-j \omega \nabla \times \overline{H} + a \nabla \rho)\right]$$

$$= j \omega \mu \frac{1}{K^2} \nabla \times \nabla \times \overline{H}$$

$$+ j \omega \mu \nabla (1/K^2) \times (\nabla \times H) - \mu a \nabla (1/K^2) \times \nabla \rho$$

and solving for $\overline{H}$

$$\nabla^2 \overline{H} - K^2 \nabla (1/K^2) \times (\nabla \times \overline{H}) + K^2 \overline{H}$$

$$= j \frac{a}{\omega} K^2 \nabla (1/K^2) \cdot \nabla \rho . \tag{3.247}$$

(U) The equation for ρ is obtained by taking the divergence of Eq. (3.246) and making used of $\nabla \cdot \overline{E} = \rho/\epsilon_0$ which can be derived from Eqs. (3.246) and (3.243)

$$\nabla \cdot \overline{E} = \frac{\rho}{\epsilon_0} = -\mu \nabla \cdot \left[\frac{1}{K^2} (-j\omega \nabla \times H + a \nabla \rho)\right]$$

$$= j \omega \mu \nabla (1/K^2) \cdot (\nabla \times \overline{H})$$

$$- a \mu \nabla (1/K^2) \cdot \nabla \rho - a \mu (1/K^2) \nabla^2 \rho .$$

149

Solving for ρ on obtains:

$$a \nabla^2 \rho + a K^2 \nabla (1/K^2) \cdot \nabla\rho + c^2 K^2 \rho$$

$$= j \omega K^2 \nabla(1/K^2) \cdot (\nabla \times \overline{H}) . \tag{3.248}$$

(U) c) In this subsection the power series solution for the warm plasma problem, Eqs. (3.244) and (3.245) is derived. Equations (3.244) and (3.245) are rewritten below where the substitutions $\alpha = - \left[(\omega/c)\sin \theta\right]^2$ and $\delta = (\sin \theta/c)$ have been made:

$$\frac{d^2 H}{dx^2} - \frac{1}{x} \frac{dH}{dx} + (\alpha + \beta x) H = \frac{a\delta}{x} \rho \tag{3.249}$$

$$a \left(\frac{d^2 \rho}{dx^2} - \frac{1}{x} \frac{d\rho}{dx} \right) + (a \alpha + c^2 \beta x) \rho = - \frac{\alpha}{\delta x} H \tag{3.250}$$

and solution is attempted in the form of a power series

$$H = \sum_n a_n x^{n+p} \tag{3.251}$$

$$\rho = \sum_n b_n x^{n+p} . \tag{3.252}$$

The multiplicative factor x^p does not have to be the same for H and ρ but is assumed so far convenience as choosing different factors eventually leads to the same results. Substituting (3.251) and (3.252) into (3.249) and (3.250) one obtains

$$\sum_{o} (n + p)(n + p - 2)\, a_n\, x^{n + p - 2} + (\alpha + \beta x) \sum_{o} a_n\, x^{n + p}$$

$$- a\, \delta \sum_{o} b_n\, x^{n + p - 1} = 0 \;,$$

$$a \sum_{o} (n + p)(n + p - 2)\, b_n\, x^{n + p - 2} + (a\alpha + c^2\beta x) \sum_{o} b_n x^{n + p}$$

$$+ \frac{\alpha}{\delta} \sum_{o} a_n\, x^{n + p - 1} = 0$$

which may be rewritten as:

$$p(p - 2)\, a_o\, x^{p - 2} + \left[(p + 1)(p - 1)\, a_1 - a\, \delta b_o \right] x^{p - 1}$$

$$+ \left[p\,(p + 2)\, a_2 + \alpha\, a_o - a\, \delta\, b_1 \right] x^p$$

$$+ \sum_{o} \Big\{ (n + p + 3)\,(n + p + 1)\, a_{n + 3} + \alpha\, a_{n + 1}$$

$$+ \beta\, a_n - a\, \delta\, b_{n + 2} \Big\} x^{n + p + 1} = 0$$

$$a p\,(p - 2)\, b_o\, x^{p - 2} + \left[a\,(p + 1)(p - 1)\, b_1 + \frac{\alpha}{\delta}\, a_o \right] x^{p - 1}$$

$$+ \left[a p\,(p + 2)\, b_2 + a\, \alpha\, b_o + \frac{\alpha}{\delta}\, a_1 \right] x^p \quad +$$

$$+ \sum_{0} \left\{ a(n+p+3)(n+p+1) b_{n+3} \right.$$

$$\left. + a\alpha b_{n+1} + c^2 \beta b_n + \frac{\alpha}{\delta} a_{n+2} \right\} x^{n+p+1} = 0 \quad .$$

Hence $p = 0, 2$ and one has the following sets of recursion relations:

Case I $p = 2$

$$a_1 = \frac{a\delta}{3} b_0 \tag{3.253}$$

$$a_2 = \frac{1}{8} \left[a\delta b_1 - \alpha a_0 \right] \tag{3.254}$$

$$(n+5)(n+3) a_{n+3} + \alpha a_{n+1} + \beta a_n - a\delta b_{n+2} = 0 \tag{3.255}$$

and

$$a b_1 = -\frac{1}{3} \frac{\alpha}{\delta} a_0 \tag{3.256}$$

$$a b_2 = -\frac{\alpha}{8} \left[a b_0 + \frac{1}{\delta} a_1 \right] \tag{3.257}$$

$$a(n+5)(n+3) b_{n+3} + a\alpha b_{n+1} + c^2\beta b_n + \frac{\alpha}{\delta} a_{n+2} = 0$$

Case II $p = 0$

$$a_1 = -a\delta b_0 \tag{3.258}$$

$$a_2 = \text{unspecified} \tag{3.259}$$

$$(n+3)(n+1)\,a_{n+3} + \alpha\,a_{n+1} + \beta\,a_n - a\,\delta\,b_{n+2} = 0 \tag{3.260}$$

and

$$a\,b_1 = \frac{\alpha}{\delta}\,a_o \tag{3.261}$$

$$b_2 = \text{unspecified} \tag{3.262}$$

$$a(n+3)(n+1)b_{n+3} + a\,\alpha\,b_{n+1} + c^2\beta b_n + \frac{\alpha}{\delta}\,a_{n+2} = 0 \;. \tag{3.263}$$

(U) It is interesting to note that if one lets $a = 0$ in Eqs. (3.253) through (3.257) the resultant recursion relation for H is just the same as for the cold plasma for $p = 2$ and reduces to the same relation for $p = 0$.

(U) When $a \neq 0$ one can solve the recursion relations to obtain the following independent series:

$$H_1 = a_o x^2 \left[1 - \frac{\alpha}{6}\,x^2 - \frac{\beta}{15}\,x^3 + \ldots \right] +$$

$$+ \frac{a\delta}{3}\,b_o\,x^3 \left[1 - \frac{\alpha}{10}\,x^2 + \ldots \right]$$

$$\rho_1 = b_o x^2 \left[1 - \frac{\alpha}{6}\,x^2 - \frac{\beta}{15}\,(c^2/a)\,x^3 + \ldots \right]$$

$$- \frac{\alpha}{36a}\,x^3 a_o \left[1 - \frac{\alpha}{10}\,x^2 + \ldots \right]$$

and

$$H_2 = a_o \left[1 - \frac{\beta}{3} x^3 - \frac{\alpha^2}{24} x^4 + \ldots \right]$$

$$- a \delta b_o x \left[1 - \frac{\alpha}{3} x^2 - \frac{\beta}{24} (3 - \frac{c^2}{a}) x^3 + \ldots \right]$$

$$\rho_2 = b_o \left[1 - \frac{\beta}{3} (c^2/a) x^3 - \frac{\alpha^2}{24} x^4 + \ldots \right]$$

$$+ \frac{\alpha}{a\delta} a_o x \left\{ 1 - \frac{\alpha}{3} x^2 - \frac{\beta}{24} \left[3(c^2/a) - 1 \right] x^3 + \ldots \right\} .$$

The general solution for H and ρ are:

$$H = c_1 H_1 + c_2 H_2$$

$$\rho = c_3 \rho_1 + c_4 \rho_2 .$$

3.5.4 The Integral Equation Approach

(U) In the last quarter, a general integral equation was developed for the fields generated by a plane wave incident upon a plasma-sheathed body. Before attempting to obtain analytical solutions based upon the principal of local analysis it is best to consider simple special cases first, and from these results attempt to find a generalization.

(U) The simplest case that should be considered first is of course the non-homogeneous slab backed by a perfect conductor, with the variation in the permittivity limited to a direction normal to the surface. This case is treated here for the two polarizations. It will be as shown that non-homogeneous thin sheaths of thickness δ, can be replaced by a homogeneous sheath of thickness

δ and "mean" relative permittivity ϵ_1 which is a function of the polarization. The results are important both from the theoretical and experimental stand-points, and would allow one to model a non-homogeneous thin slab by a homo-geneous slab.

(U) In the following analysis, the Cartesian coordinate system is oriented so that the positive z axis is normal to the sheath of thickness δ, with the z = 0 plane being the conducting surface. The angle of incidence is denoted by θ, with the plane of incidence being the x-z plane.

(U) a) <u>Polarization Perpendicular to the Plane of Incidence.</u> For this polarization the electric intensity has the general form

$$\underline{E} = \hat{y} \ e^{ikx \sin \theta} \ \zeta(z) .$$

Outside the slab $(z > \delta)$, the field is comprised of the incident wave and the reflected wave in which case $\zeta(z)$ has the explicit form

$$\zeta(z) = \exp(-ikz \cos \theta) + R \exp\left[ik (z - 2 \delta) \cos \theta \right]$$

where R is the reflection coefficient. In the slab, the function $\zeta(z)$ must satisfy the following differential equation which is derivable from Maxwell's equations

$$\frac{d^2 \zeta}{dz^2} + k^2 (\epsilon - \sin^2 \theta) \zeta = 0. \tag{3.264}$$

Associated with the differential equation are the boundary conditions $\zeta = 0$ at z = 0, which follows from the vanishing of the tangential electric field on the conducting surface, and ζ and $\frac{d\zeta}{dz}$ continuous at z = δ, which follows from

the continuity requirements on the tangential components of the field at the interface $z = \delta$. In order to express Eq. (3.264) in terms of an integral equation, the constant ϵ_1 will be introduced. The actual value of ϵ_1 will not be prescribed at this moment, however a criterion will be later introduced which will specify ϵ_1 as a "mean" value of relative permittivity of the sheath.

(U) Equation (3.264) can be expressed in the form

$$\frac{d^2 \mathscr{C}}{dz^2} + \kappa^2 \mathscr{C} = k^2 (\epsilon_1 - \epsilon) \mathscr{C} , \tag{3.265}$$

where

$$\kappa^2 = k^2 (\epsilon_1 - \sin^2 \theta) , \tag{3.266}$$

from which an integral equation satisfying the required boundary condition at $z = 0$ can be obtained

$$\mathscr{C}(z) = \mathscr{C}_0 \sin \kappa z + \frac{1}{\kappa} \int_0^z \sin \kappa (z - t) f(t) \, dt , \tag{3.267}$$

$$f(z) = k^2 \left[\epsilon_1 - \epsilon (z) \right] \mathscr{C} (z) .$$

The employment of the two continuity conditions at $z = \delta$ yields the following two equations involving the two unknown quantities $\mathscr{C}_0$ and R,

$$\mathscr{C}_0 \sin \kappa \delta + \frac{1}{\kappa} \int_0^\delta \sin \kappa (\delta - t) f(t) \, dt$$

$$= e^{-ik\delta \cos \theta} \left[1 + R \right] ,$$

$$\kappa \, \mathcal{E}_0 \cos \kappa \, \delta + \int_0^\delta \cos \kappa \, (\delta - t) \, f(t) \, dt$$

$$= e^{-ik \delta \cos \theta} \left[-1 + R \right] ik \cos \theta .$$

From these, the reflection coefficient R can be obtained as follows

$$- \int_0^\delta \sin (\kappa \, t) \, f(t) \, dt \; e^{ik \delta \cos \theta} = \left[\kappa \, \cos \kappa \, \delta \right.$$

$$\left. + ik \cos \theta \sin \kappa \delta \right] + R \left[\kappa \, \cos \kappa \delta - ik \cos \theta \sin \kappa \delta \right] . \tag{3.268}$$

· The mean relative permittivity ϵ_1, will be chosen so that the reflection coefficient associated with a uniform slab of thickness δ and permittivity ϵ_1, will be the same as the reflection coefficient given by Eq. (3.268) for the non-uniform case. The expression corresponding to Eq. (3.268) for the uniform case is identical to Eq. (3.268) except that the left-hand side will be zero. Thus the constant ϵ_1 will be chosen so that the left-hand side of Eq. (3.268) is zero, yielding

$$\int_0^\delta \sin (\kappa \, t) \left[\epsilon_1 - \epsilon(t) \right] \widetilde{\mathcal{E}} (t) \, dt = 0 \tag{3.269}$$

where $\mathcal{E}(z)$ is normalized such that

$$\mathcal{E}(z) = \mathcal{E}_0 \, \widetilde{\mathcal{E}}(z) .$$

The appropriate form for $\widetilde{\mathscr{E}}(z)$ is found by iterating Eq. (3.267)

$$\widetilde{\mathscr{E}}(z) = \sin \kappa z + \int_0^z K(z, t) \sin \kappa t \, dt$$

$$+ \int_0^z K(z, t) \int_0^t K(t, r) \sin \kappa r \, dr \, dt + \ldots \qquad (3.270)$$

with

$$K(z, t) = \frac{k^2}{\kappa} \left[\epsilon_1 - \epsilon(t) \right] \sin \kappa (z - t) . \qquad (3.271)$$

Substitution of expression (3.270) into Eq. (3.269) will give a transcendental equation which will determine the appropriate value of ϵ_1.

(U) A simple solution can be obtained for sheaths thin enough such that $|\kappa \delta| < 1$, in which case $\mathscr{E}(t)$ will be given by the first approximation to Eq. (3.270)

$$\mathscr{E}(z) \sim \kappa z . \qquad (3.272)$$

On applying the approximation (3.272) to Eq. (3.269) one obtains the relation

$$\epsilon_1 = (3/\delta^3) \int_0^\delta t^2 \, \epsilon(t) \, dt \qquad (3.273)$$

which determins the "mean" value ϵ_1 of relative permittivity of the sheath.

(U) b) <u>Polarization in the Plane of Incidence.</u> For this polarization, the magnetic field has the general form

$$\underline{H} = \hat{\underline{y}} \, e^{ik x \sin \theta} \, H(z) .$$

Outside the slab $(z > \delta)$, the field is comprised of the incident and reflected wave in which case $H(z)$ has the explicit form

$$H(z) = \exp \left[- ik z \cos \theta \right] + R \exp \left[ik (z - 2\delta) \cos \theta \right] .$$

In the slab the function $H(z)$ must satisfy the following differential equation

$$\epsilon \, \frac{d}{dz} \left[\frac{1}{\epsilon} \frac{dH}{dz} \right] + k^2 (\epsilon - \sin^2 \theta) \, H = 0 \qquad (3.274)$$

subject to the boundary conditions $\frac{dH}{dz} = 0$ at $z = 0$ and H and $\frac{1}{\epsilon} \frac{dH}{dz}$ are continuous at $z = \delta$. Proceeding in a somewhat similar manner to that employed for the other polarization, Eq. (3.274) can be placed in the following integral equation form

$$H(z) = H_0 \cos \kappa \, \zeta + \frac{1}{\kappa} \int_0^\zeta \sin \kappa \, (\zeta - t) \, f(t) \, dt \qquad (3.275)$$

where

$$\zeta = \int_0^z \epsilon(t) \, dt$$

$$\kappa^2 = k_0^2 \left[\frac{\epsilon_1 - \sin^2 \theta}{\epsilon_1^2} \right]$$

$$f(\zeta) = \left[\kappa^2 - k_o^2 \left(\frac{\epsilon(z) - \sin^2\theta}{\epsilon^2(z)}\right)\right] H \quad .$$

The application of the two continuity conditions at $z = \delta$ yields the following two equations

$$H_o \cos \kappa \, \zeta_1 + \frac{1}{\kappa} \int_0^{\zeta_1} \sin \kappa(\zeta_1 - t) \, f(t)dt = e^{-ik\delta\cos\theta}\left[1 + R\right] ,$$

$$-\kappa \, H_o \sin \kappa \, \zeta_1 + \int_0^{\zeta_1} \cos \kappa \, (\zeta - t) \, f(t) \, dt$$

$$= e^{-ik\,\delta\cos\theta} \, ik \cos \theta \left[-1 + R\right]$$

where ζ_1 is the value of ζ at $z = \delta$. The reflection coefficient R can be immediately obtained

$$\int_0^{\zeta_1} \cos \kappa \, t \, f(t) \, dt \, e^{ik\,\delta\cos\theta} = \left[\kappa \sin \kappa \, \zeta_1 - ik \cos \theta \cos \kappa \, \zeta_1\right]$$

$$+ R \left[\kappa \sin \kappa \, \zeta_1 + ik \cos \theta \cos \kappa \, \zeta_1\right] .$$

The "mean" value ϵ_1 will be chosen so that the reflection coefficient is the same as that of a homogeneous slab of thickness δ and relative dielectric constant ϵ_1. Thus it follows that

$$\int_0^\delta \cos \left(\kappa \int_0^t \epsilon \, dt \right) \left\{ \epsilon(t) \, \kappa^2 - k_0^2 \, \frac{[\epsilon(t) - \sin^2\theta]}{\epsilon(t)} \right\} \tilde{H} \, dt = 0 . \qquad (3.276)$$

H, the normalized version of H, is found by iterating Eq. (3.275) with $H_0 = 1$, yielding

$$\tilde{H}(z) = \cos \kappa \, \zeta + \frac{1}{\kappa} \int_0^\zeta \sin \kappa \, (\zeta - t) \cos \kappa t \, dt + \ldots . \qquad (3.277)$$

Substitution of expression (3.277) into Eq. (3.276) gives a transcendental equation that determines the "mean" value ϵ_1.

(U) A simple solution can be obtained for thin slabs for which

$$(\kappa \, \zeta_1) = \left| \kappa \int_0^\delta \epsilon(t) \, dt \right| < 1 ,$$

in which case a first approximation to H is given by

$$\tilde{H}(z) \sim 1 + 0 \, (\zeta^2) .$$

(U) In this case the appropriate equation for ϵ_1 derived from Eq. (3.276) becomes

$$(\epsilon_1 - \sin^2\theta) \int_0^\delta \epsilon(t) \, dt = \epsilon_1^2 \int_0^\delta \left[1 - \sin^2\theta / \epsilon(t) \right] dt \qquad (3.278)$$

which is a quadratic equation in ϵ (except for normal incidence). Unlike the other polarization, the first approximation to ϵ_1 for this polarization is de-

pendent upon the angle of incidence. However if

$$\left| \int_0^\delta \epsilon(t)\, dt \right| > \delta$$

$$\left| \int_0^\delta \frac{1}{\epsilon(t)}\, dt \right| < 1$$

then the mean value of ϵ_1 is independent of angle of incidence and is given by the relation

$$\epsilon_1 \sim \frac{1}{\delta} \int_0^\delta \epsilon(t)\, dt \quad .$$

This will only hold if $\left| \kappa \zeta_1 \right| < 1$, implying that $\left| \sqrt{\epsilon_1}\, k\delta \right| < 1$.

3.5.5 Mode Study for Simulated-Plasma Experiment

(U) As a prelude to the experimental investigation of simulated plasmas on cylinders and cones we have begun a theoretical study of the surface-wave modes that may be supported by such complicated guiding structures. In particular, we are examining the wave modes that may be sustained by an infinite conducting cylinder surrounded by a thin inductive sheath with an air gap separating the sheath from the conducting cylindrical core. The tangential fields on the infinitesimally thin sheath are assumed to satisfy the following boundary conditions:

$$\vec{E}_{tan}^{(1)} = \vec{E}_{tan}^{(2)} \quad ,$$

$$\vec{E}_{tan}^{(1)} = Z_s\, \hat{n} \wedge (\vec{H}_{tan}^{(1)} - \vec{H}_{tan}^{(2)}) \quad ,$$

where the affix (1) refers to the free-space region exterior to the cylindrical structure and the affix (2) refers to the free-space air gap. The complex constant Z_s is a jump impedance describing the effect of the sheath and the unit normal vector $\hat{n}$ is pointing into the exterior region (1). The time dependence is taken as $e^{-i\omega t}$ and the impedance Z_s will be assumed to be purely inductive, $Z_s = -i\,X_s,\ X_s > 0.$

(U) Before entering into the details concerning the surface-wave behavior of the inductive sheath structure above, let us review the mode theory for scattering by long thin dielectric rods. The general approach, well known in the literature, is to consider the elongated dielectric structure as a passive traveling wave antenna in the manner suggested by Peters (1958) who derives the radar cross section in the form

$$\sigma = \frac{\lambda^2 G^2}{4\pi}\ \gamma^2\ ,$$

where $G = G(\theta, \phi)$ is the gain function of the device operating as an antenna and γ^2 is a power reflection coefficient describing the rear termination. Now it has been found experimentally that a suitably proportioned dielectric rod can act as an efficient end-fire antenna (see e.g. Kiely, 1953), and several investigators (Horton and Watson, 1954; Peters, 1958; Howard and Thomas, 1963) have recognized that a dielectric rod antenna, properly shorted at the rear termination, becomes an unusually effecient radar reflector. This is principally due to the surface-wave modes excited on the dielectric structure and an understanding of the behavior of these modes is fundamental in order to assess the properties of the device.

(U) The surface wave on a dielectric rod carries its energy within a small distance from the dielectric-air interface. The proportion of energy flowing in the dielectric or in the external medium can be controlled by adjusting the physical parameters of the rod; however, radiation occurs in the presence of bends and discontinuities. That is, if the surface wave structure is curved in the direction of propagation, the surface-wave mode is perturbed into a complex mode that loses some energy by radiation. On the other hand, if the surface wave meets a discontinuity, such as the termination of the structure, radiation (and reflection) again takes place. This tendency toward radiation in a dielectric waveguide is turned to advantage in the dielectric antenna. By proper design, the dielectric guide produces a single lobe radiation pattern directed along the axis of the antenna, and in this respect it behaves as an end-fire array.

(U) In the case of the dielectric rod the cut-off frequency of the dominant mode (which is the hybrid HE_{11} mode) is zero. All higher order modes, including the symmetric H_{01} and E_{01} modes have non-zero cut-off frequencies. For the HE_{11} wave the electric field in a transverse plane normal to the axis has the same phase and one preferred direction. It is this phase equality and almost parallel nature of the field lines that make this mode in a dielectric rod suitable for use as a directional radiator. Most of the higher-order modes, including H_0 and E_0, possess a null in the end-fire direction in addition to multilobed patterns. Hence, from an antenna point of view, it is desirable to cut-off the higher modes. Further, in a scattering problem the dominant HE_{11} mode is the one that will be excited for nose-on plane-wave incidence; it has the correct azimuthal dependence.

(U) When used as an end-fire antenna, the dielectric rod is generally tapered in order to eliminate standing waves within the antenna and to suppress the side lobes appearing in the radiation pattern. Indeed, some of the most practical dielectric antennas are single taper structures that take the shape of a cone. It is not difficult to see that such a tapered dielectric structure of optimum design would behave as a good backscatterer if the base of the structure were electrically terminated in a short circuit by a conducting disc or coating. Thus, in studing the nose-on return from a cone-sphere surrounded by a plasma layer and perhaps by a dielectric ablative material, it is important to investigate the possibility of cross section enhancement due to the surface wave modes. There is also the possibility of cross section reduction if higher order modes are excited since these modes generally contribute a null in the end-fire direction.

(U) Let us now consider the modal behavior for the inductive sheath structure. We seek the waveguide modes with exponential dependence of the form e^{-ihz} corresponding to propagation along the axis of the cylindrical structure. To find these modes we must choose solutions of the source-free Maxwell equations such that the fields are finite everywhere, zero at infinite radial distance, and satisfy the boundary conditions at the sheath and at the conducting core. Since the solutions have no source within a finite length of the structure, we obtain an eigenvalue equation for the modes:

$$\left[A_n^{(0)} - A_n^{(1)} - \frac{Z_o}{iZ_s} \right] \left[\left(\frac{1}{A_n^{(0)}} - \frac{1}{B_n^{(1)}} \right)^{-1} + \frac{iZ_s}{Z_o} \right]$$

$$= \frac{n^2}{u^2} \left[1 + (ka/u)^2 \right] \quad ,$$

where

$$A_n^{(0)} = -\frac{ka}{u} \frac{K'_n(u)}{K_n(u)} \quad ,$$

$$A_n^{(1)} = -\frac{ka}{u} \frac{I'_n(u) K_n(pu) - I_n(pu) K'_n(u)}{I_n(u) K_n(pu) - I_n(pu) K_n(u)} \quad ,$$

$$B_n^{(1)} = -\frac{ka}{u} \frac{I'_n(u) K'_n(pu) - I'_n(pu) K'_n(u)}{I_n(u) K'_n(pu) - I'_n(pu) K_n(u)}$$

with I_n and K_n representing the modified Bessel functions of order n. The parameter a denotes the radius of the impedance sheath and $p = b/a$ denotes the ratio of the conducting core radius b to the sheath radius a. The unknown in the equation is the eigenvalue u which is related to the axial propagation constant h by the equation

$$u = a (h^2 - k^2)^{1/2} \quad .$$

Thus when u is found for a particular set of parameters, the guided wave-length λ_g may then be obtained from the relation

$$\frac{\lambda_g^2}{\lambda^2} = k^2/h^2 = \left[1 + (u/ka)^2 \right]^{-1} \quad .$$

(U) Consider first the symmetric modes corresponding to n = 0. The eigenvalue equation then uncouples into two equations, one for the E_0 mode and one for the H_0 mode:

$$\frac{iZ_s}{Z_o} = \frac{u^2}{ka} \left[K_o(u) \right]^2 \left\{ \frac{I_o(u)}{K_o(u)} - \frac{I_o(pu)}{K_o(pu)} \right\} \quad (E_0 \text{ mode})$$

$$\frac{iZ_s}{Z_o} = - ka \left[K_1(u) \right]^2 \left\{ \frac{I_1(u)}{K_1(u)} - \frac{I_1(pu)}{K_1(pu)} \right\} \quad (H_0 \text{ mode}) \quad .$$

For an inductive sheath, $Z_s = - i X_s$, $X_s > 0$; hence, the left-hand sides of the equations are positive. Now the ratio $I_n(u)/K_n(u)$ is a monotonically increasing function with increasing u since, by use of the Wronskian relation,

$$\frac{d}{du} \frac{I_n(u)}{K_n(u)} = \left[K_n(u) \right]^{-2} \left\{ K_n(u) I'_n(u) - K'_n(u) I_n(u) \right\}$$

$$= \frac{1}{u} \left[K_n(u) \right]^{-2} > 0 \quad .$$

Thus, because $u > (pu)$, the quantities in $\left\{ \ \right\}$ above are positive and roots can exist only for the E_0 mode. We have, then an E_0 mode possible but no H_0 mode. This is in contrast with the ordinary dielectric rod waveguide for which both modes are possible.

(U) The E_0 mode here has no cut-off frequency. To show this, consider the eigenvalue equation for this mode

$$\frac{ka}{u} \frac{X_s}{Z_o} = u \left[K_o(u) \right]^2 \left\{ \frac{I_o(u)}{K_o(u)} - \frac{I_o(pu)}{K_o(pu)} \right\} \quad .$$

As $u \to 0$ we have

$$\frac{ka}{u} \frac{X_s}{Z_0} \sim - u \log u \left[1 - \frac{\log u}{\log pu} \right] \sim \begin{cases} - u \log (p), & p \neq 0 \\ \\ - u \log (u), & p = 0. \end{cases}$$

In either case the ratio (ka/u) goes to zero and therefore $(\lambda_g/\lambda) \rightarrow 0$ along with $(ka) \rightarrow 0$. There is no cut-off for the E_0 mode. This also is in contrast with the ordinary dielectric rod waveguide.

(U) The modes corresponding to $n \geq 1$ are coupled or hybrid EH modes. For $n > 1$ the modes possess a cut-off frequency that can be determined by taking the limit $u \rightarrow 0$ in the eigenvalue equation. In this limit the equation may be put in the form

$$(ka)^2 \left\{ \frac{1}{2} \frac{n}{n^2 - 1} \left[1 + \frac{1}{n} p^{2n+2} \right] \right\} + (ka) \left\{ \frac{X_s}{Z_0} - \frac{Z_0}{X_s} \frac{1}{4} \left[1 - p^{2n} \right]^2 \right\} - \left\{ \frac{n}{2} \left[1 - p^{2n} \right] \right\} = 0$$

and the positive root for ka determines the cut-off frequency. For $n = 1$ the cut-off frequency is zero as in the ordinary dielectric rod case.

(U) The general eigenvalue equation has been programmed for the computer and the guided wavelengths have been determined for a variety of parameters. In Fig. 3-19, for example, we present (λ_g/λ) versus (ka) for $n = 0$, 1, 2, 3 and for the choice of parameters $X = (X_s/Z_0) = 1$, $p = 0.1$. In this figure we observe the cut-off behavior characteristic of the modes for $n > 1$, while the modes for $n = 0$, 1 have no cut-off. To illustrate the behavior of the $n = 1$ mode, which is the important mode for nose-on incidence, we present in Fig. 3-20, the result for $p = 0.5$ and differing X, and in Fig. 3-21 the results for $X = 1$ with differing p.
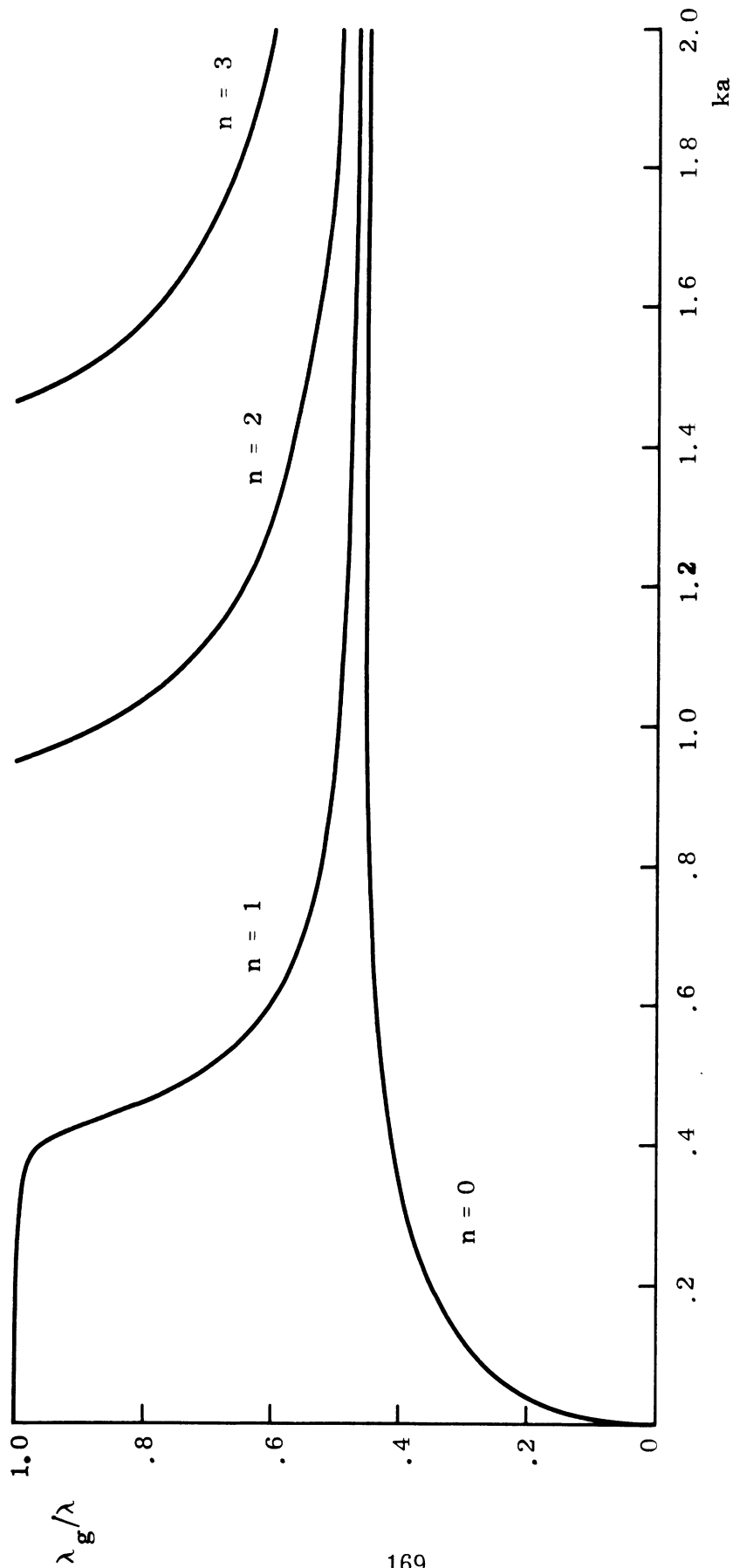
FIG. 3-19: COMPUTER SOLUTIONS FOR THE MODES n = 0, 1, 2, 3 WITH X = 1 AND p = 0.1.
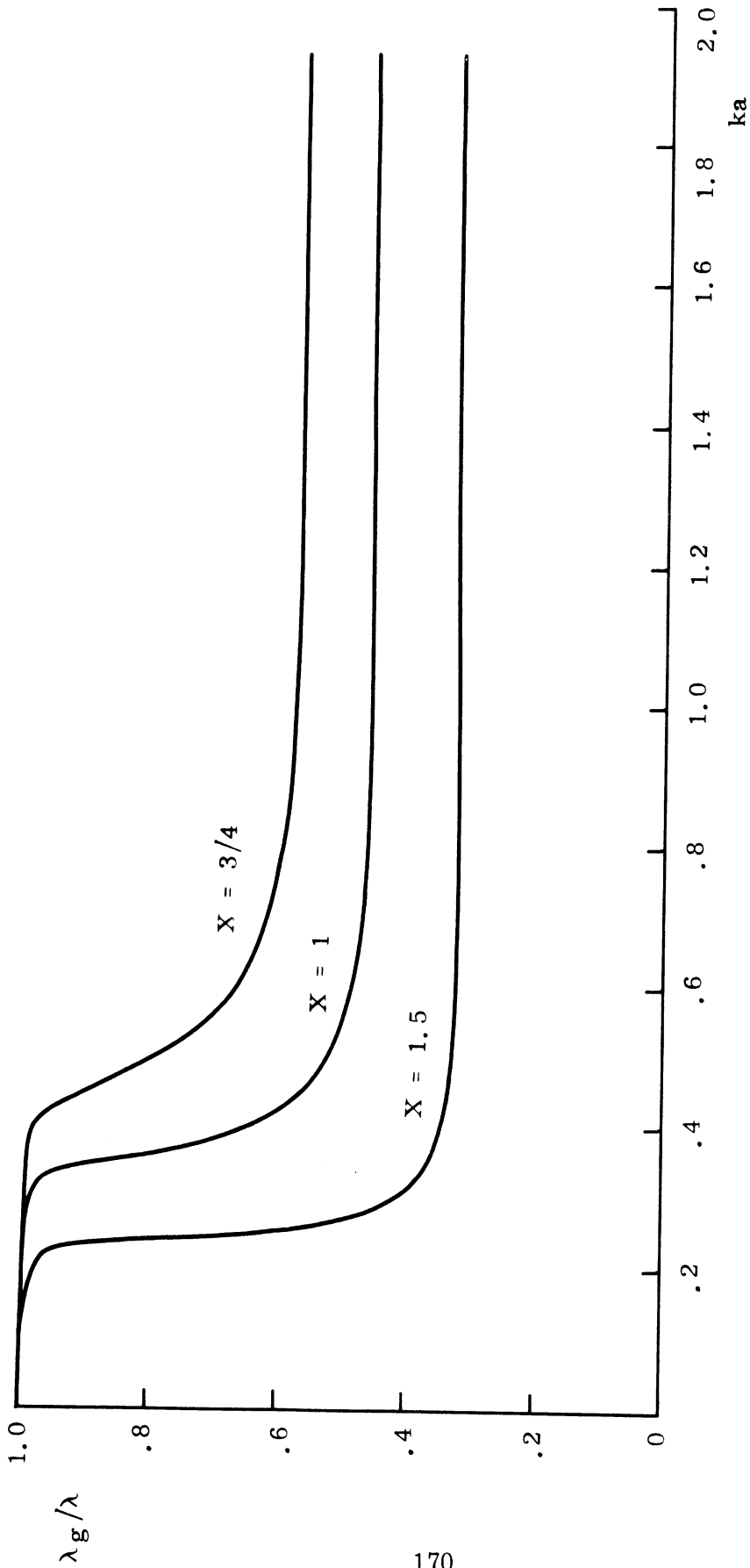
FIG. 3-20: COMPUTER SOLUTIONS FOR THE n = 1 MODE WITH
p = 0.5 AND DIFFERING X.
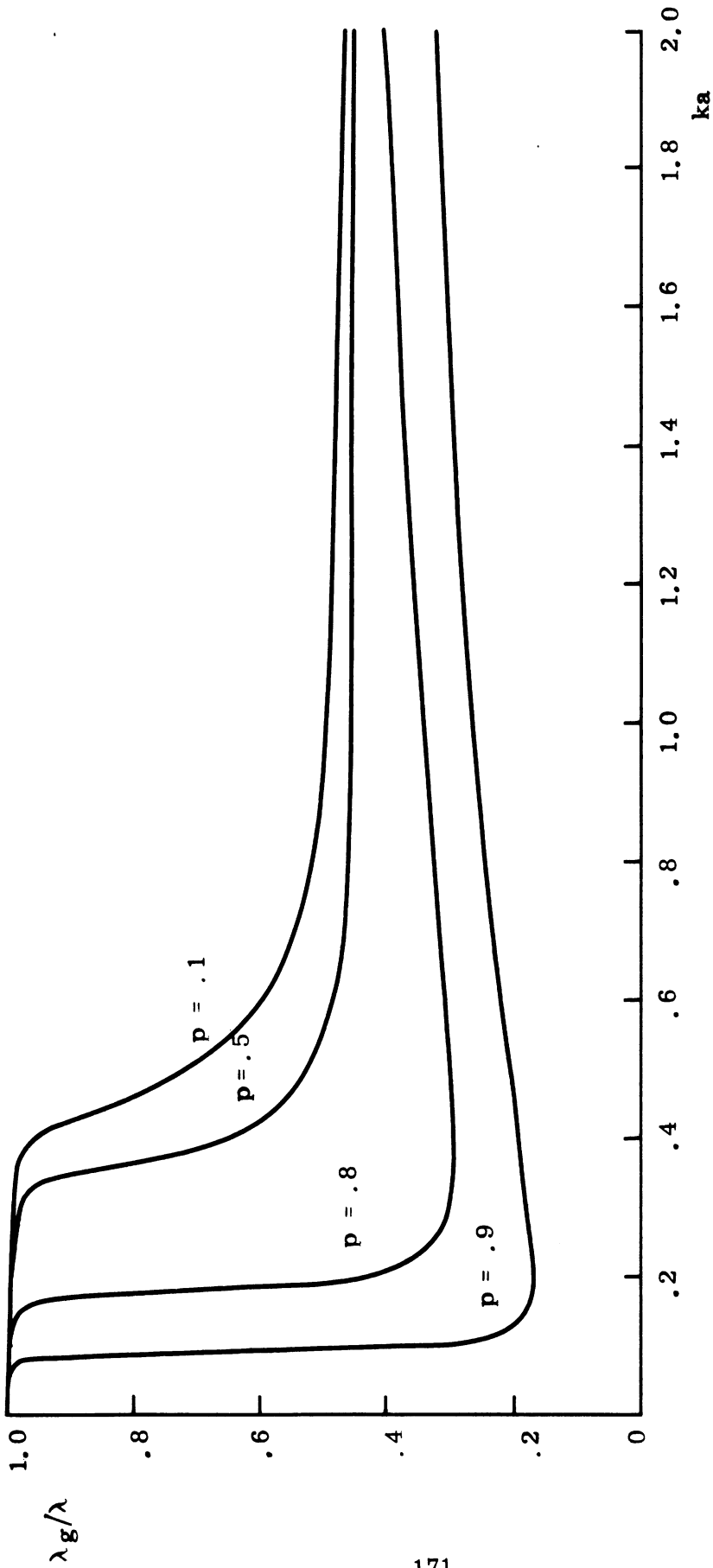
FIG. 3-21: COMPUTER SOLUTIONS FOR THE n = 1 MODE WITH X = 1 AND DIFFERING p.

(U) More complete numerical results are available; the results displayed in the figures have been chosen merely to illustrate the general nature of the model solutions. In the future these results will play an important role in design of the simulated plasma experiments concerning cylinders and cones. The considerations involved will be similar to those involved in the design of dielectric rod antennas; however, it is premature to enter into these considerations until the plasma sheath experiments on flat surfaces have provided a positive verification of the theoretical model.

3.6 **Analysis of Experimental Data**

(U) In this section, some of the experimental data is examined and some comparisons are made with theoretically derived formulas.

3.6.1 **Backscattering Characteristics of Models ID-1 and ID-2**

(S) Section 2.3 describes measurements of the backscattering patterns of a second metallic cone-sphere model with an indented back (Model ID-2).
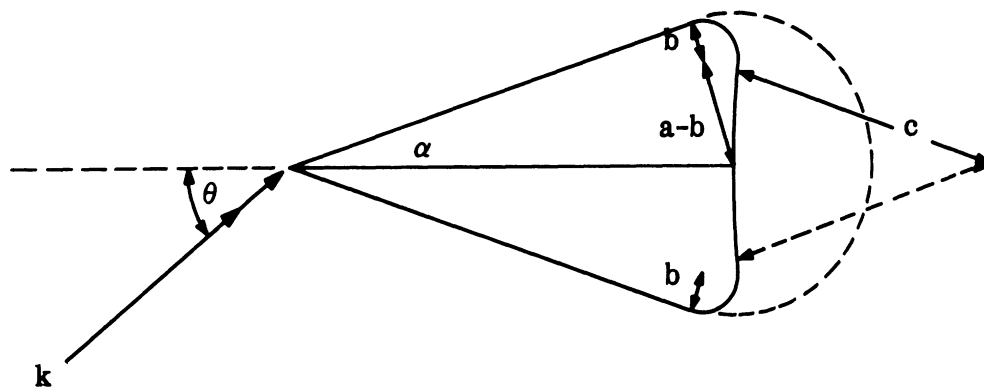
FIG. 3-22: CONE-SPHERE WITH CONCAVE INDENTATION
IN REAR CAP.

(S) For Models ID-1 and ID-2, three specific parameters: half-angle (α), radius of original spherical cap (a) and radius of curvature (b) at join are identical; only the radius of curvature (c) of the concave indentation serves to distinguish them. For symmetric illumination the theoretical estimate of the creeping wave contribution to the backscattering depends on the radius of curvature (b) of the toroidal segment at the join but is independent of c. Therefore, the nose-on cross sections of the two models should be the same. Moreover, a strong similarity should persist for all angles of incidence at least out to the specular flash $(\theta = 90^\circ - \alpha)$.

(S) Since backscattering measurements of Model ID-1 are already available it is of interest to compare them with those of Model ID-2. Figure 3-23 shows the empirical curve for the radar cross section of Model ID-2. On it are also displayed the corresponding measurements from ID-1 (which are listed in Table 3-I). The agreement is very good and thus provides a measure of confirmation of the expected behavior.

(S) On the basis of theoretical estimates provided in 7741-4-T (Final Report BSD-TR-67-140) the nose-on backscattering cross section for Model ID-2 (or ID-1) is given by

$$\sigma/\lambda^2 = \frac{1}{\pi} \left| S_1 + S_2 + S_3 \right|^2$$

where

$$S_1 = -\frac{i}{4} \frac{\tan^2 \alpha}{(1 - \sec^2 \alpha)^{3/2}} e^{-2ik(a \cot \alpha \cos \alpha + b \sin \alpha)}$$

is the tip contribution,

$$S_2 = \frac{i}{4} \sec^2 \alpha \, e^{-2ikb \sin \alpha}$$
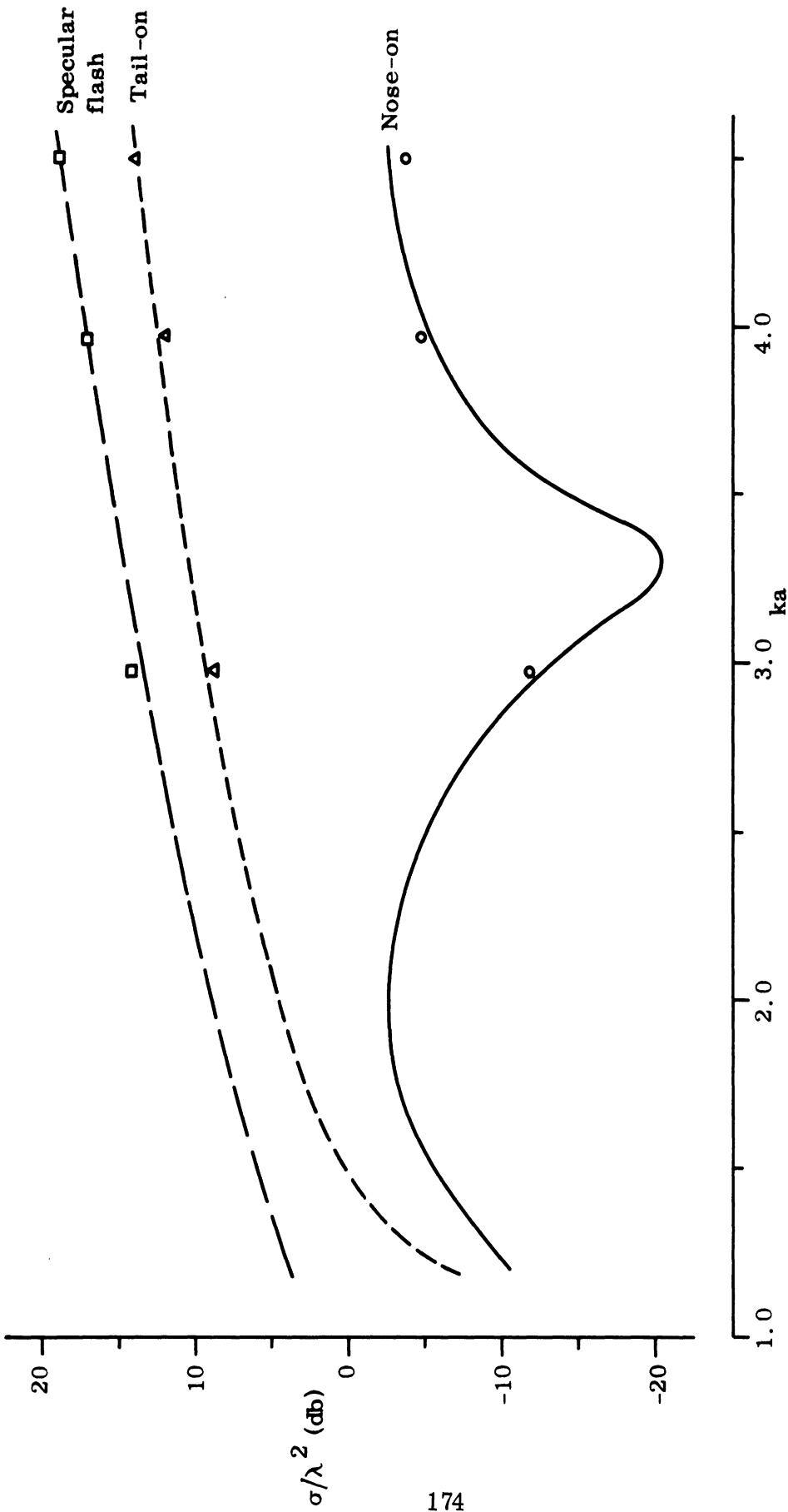
FIG. 3-23: COMPARISON OF EXPERIMENTAL CROSS SECTION OF MODELS ID-2 AND ID-1.

174

is the join contribution and the creeping wave contribution is given by

$$S_3 = \frac{i\pi\ ka\ e^{ik\left[\pi\,b\,+\,2(a\,-\,b)\right]}}{\sqrt{2k\ (a\,-\,b)}} \cdot \left\{ \hat{q}\left[\frac{\pi}{2}\ (kb/2)^{1/3}\right]\right.$$

$$+ \frac{1}{\sqrt{\pi}}\ e^{i\pi/6}\ \frac{2^{1/3}}{(kb)^{2/3}}\ \sum_S\ \exp\left\{ ie^{i\pi/3}\ \xi\,\alpha_s\right\}$$

$$\left. \cdot\ \frac{1}{\alpha_s\left[Ai\,(-\alpha_s)\right]^2}\ \left[(\alpha_s/30) + (1/10\alpha_s^2)\right]\right\}^2$$

in which

$$\xi = (kb/2)^{1/3}\ \frac{\pi}{2}\ ,$$

α_2 is a root of

$$Ai'\ (-\alpha_s) = 0\ , \quad \text{and} \quad \hat{q}(\xi) = \hat{q}^{(0)}(\xi)$$

is tabulated in Table T, pp. 8-18 of "General Research in Diffraction Theory" by N. A. Logan, LMSD 288088.

(S) In the explicit expressions for the backscattering contributors it should be noted that the shadow boundary was chosen as the phase origin. The cross section estimate was computed for a selection of twenty-two values of ka in the range 1 < ka < 7 and are listed in Table 3-II. Figure 3-24 shows the theoretical extimate compared to the experimentally measured cross sections for Model ID-2.

TABLE 3-I: Model ID-1, Backscattering Data

Pattern No.	Freq. GHz	ka	Measured Cross Sections σ/λ^2 (db)		
			Nose-on	Tail-on	Specular Flash
3969	2.53	2.98	-11.8	9.0	14.2
3978	3.37	3.96	- 4.8	12.1	16.9
3980	3.83	4.51	- 3.6	14.0	18.5
3962	5.73	6.74	- 0.4	19.8	23.1

TABLE 3-II: Nose-on Backscattering Data for
Model ID-2 (Calculated).

ka	σ/λ^2	σ/λ^2 (db)
1.25	.04749	-13.23
1.5	.03435	-14.64
1.8	.06094	-12.15
2.0	.09605	-10.18
2.5	.16797	- 7.75
2.8	.17594	- 7.55
3.0	.15960	- 7.98
3.2	.12995	- 8.89
3.5	.07621	-11.18
3.8	.02948	-15.31
4.0	.01181	-19.28
4.15	.01015	-19.93
4.5	.03438	-14.64
4.75	.06670	-11.76
5.0	.09965	-10.02
5.25	.12497	- 9.03
5.5	.12644	- 8.98
5.75	.11033	- 9.57
6.0	.08089	-10.92
6.3	.03993	-13.99
6.55	.01261	-18.99
6.74	.00368	-24.32

ooo   Experimental Points

—— Empirical Curve

xxx   Theoretical Points
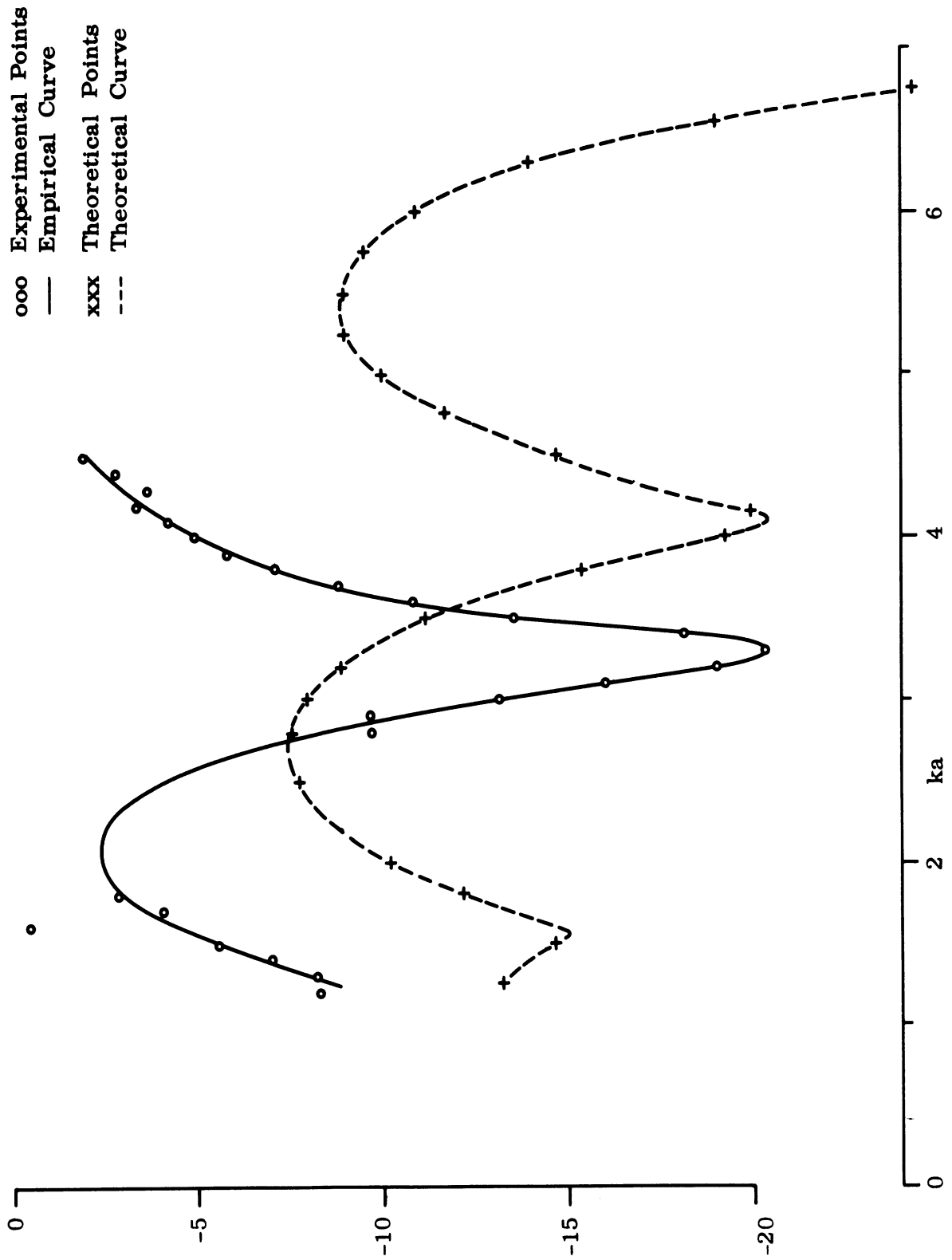
– – – Theoretical Curve

FIG. 3-24: MODEL ID-2 BACKSCATTERING CROSS SECTION (NOSE-ON).

177

(S) It is observed that the theoretical estimates follow a curve which has a shape similar to, but slightly displaced from, the empirical curve. The theoretical values also tend to lie below (on the order of 5 to 6 db) the measured data — if a slight translation of the theoretical curve is permitted in order to obtain agreement between the lobe structure of the empirical curve and theoretical estimates.

(S) Both these features are not unexpected: In an earlier study (Senior, 1965) it was shown that, for a sphere, the geometrical theory of diffraction gives estimates of the creeping wave contribution to the backscattering which differ from the exact value. The amount of difference depends on ka. For example, for ka = 3, the first order geometrical theory of diffraction underestimates the modulus of the creeping wave term by a factor of (about) two and it differs in phase from the exact value by (about) 30°. Since it is the square of the modulus which gives the cross section, the above factor of two would correspond to a cross section augmented by 2^2 = 4 or 6 db which is of the same order of magnitude as that observed.

(S) The displacement of the minima (or maxima) of the experimental relative to the theoretical is not as well covered by the 30° phase difference noted, but within the limits that Fig. 3-24 can be read, the lobe structures seem to be compatible. Table 3-III lists these locations and it is clear that the relative shift ($\cong$ 0.65) is reasonably constant, although considerably larger than the $\Delta(ka) \cong \pi/12$ = 0.26 obtained from a 30° phase shift. However, if it is the curvature along the geodesic beyond the join rather than the radius of curvature of the rear cap which is the more important for the determination of the phase displacement, then, using kb rather than ka, the geometrical theory of diffraction differs in phase from the exact value by about 50° and this leads to the estimate $\Delta(ka) \cong$ 0.45 for the relative shift.

TABLE 3-III: Model ID-2 Cross Section Comparison

Description	Location (ka)	Displacement
Exp. Max.	2.05	
Theor. Max.	2.70	$\Delta = 0.65$
Exp. Min.	3.35	
Theor. Min.	4.05	$\Delta = 0.70$
Exp. Max.	(est) 4.75	
Theor. Max.	5.40	$\Delta = 0.65$

3.6.2 Cone-spheres with Concave Indentations and a Coating.

(S) A metallic cone-sphere of half angle $\alpha = 7\ 1/2^\circ$ and base radius a = 2.21" had its rear spherical cap reformed to exhibit a concave indentation of radius c so that the resulting form had a smooth tangent. Three indentations, c, were used. A 1/4" coating of LS-26 was applied uniformly over the surface, excluding the portion of the concave indentation where the coating did not follow the concavity but a straight line as shown in the sketch below.
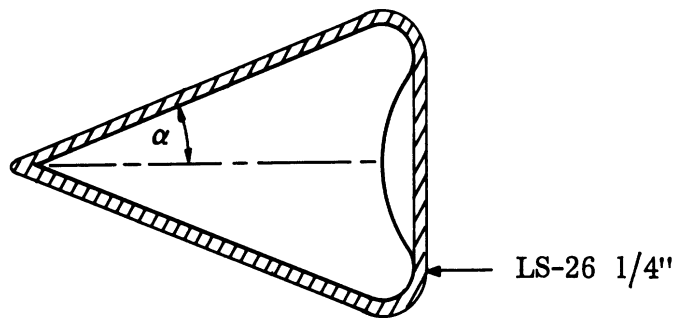
FIG. 3-25: INDENTED VEHICLE SHOWING
COATING CONFIGURATION.

(S) The azimuthal component of the magnetic field, H_ϕ, was measured at four frequencies: 0.935, 2.55, 4.25 and 6.799 GHz which correspond respectively to ka = 1.1, 3.0, 5.0 and 8.0. In the four figures 3-26 to 3-29 which follow, two conclusions are immediate. (1) The effect of the coating is to mask the differences in the surface fields supported on each of the models and, for all practical purposes, the surface fields are identical. This suggests that the scattering from such coated perturbed cone-spheres should be very similar. (2) As ka increases the effect of this thickness of coating is to modify the fields in a way identical to that observed on metallic cone-spheres, i.e. for ka small (say, less than 3) the fields are not substantially different from those supported on uncoated models; for ka $\geq$ 5 approximately the field is characterized by a build-up away from the tip followed thereafter by a steady decay out to the join.

(S) There are two areas in which the behavior is not completely regular: in the immediate vicinity of the tip, and over the concave indentation.

ka = 1.1, scale 5 units, full scale

ID-1 ——
ID-2 ‑‑‑
ID-3 —‑—

FIG. 3-26: ID SURFACE FIELD DATA FOR ka = 1.1

ka = 3.0, Scale 2.5 units, full scale

ID-1 ———
ID-2 – – –
ID-3 —––—
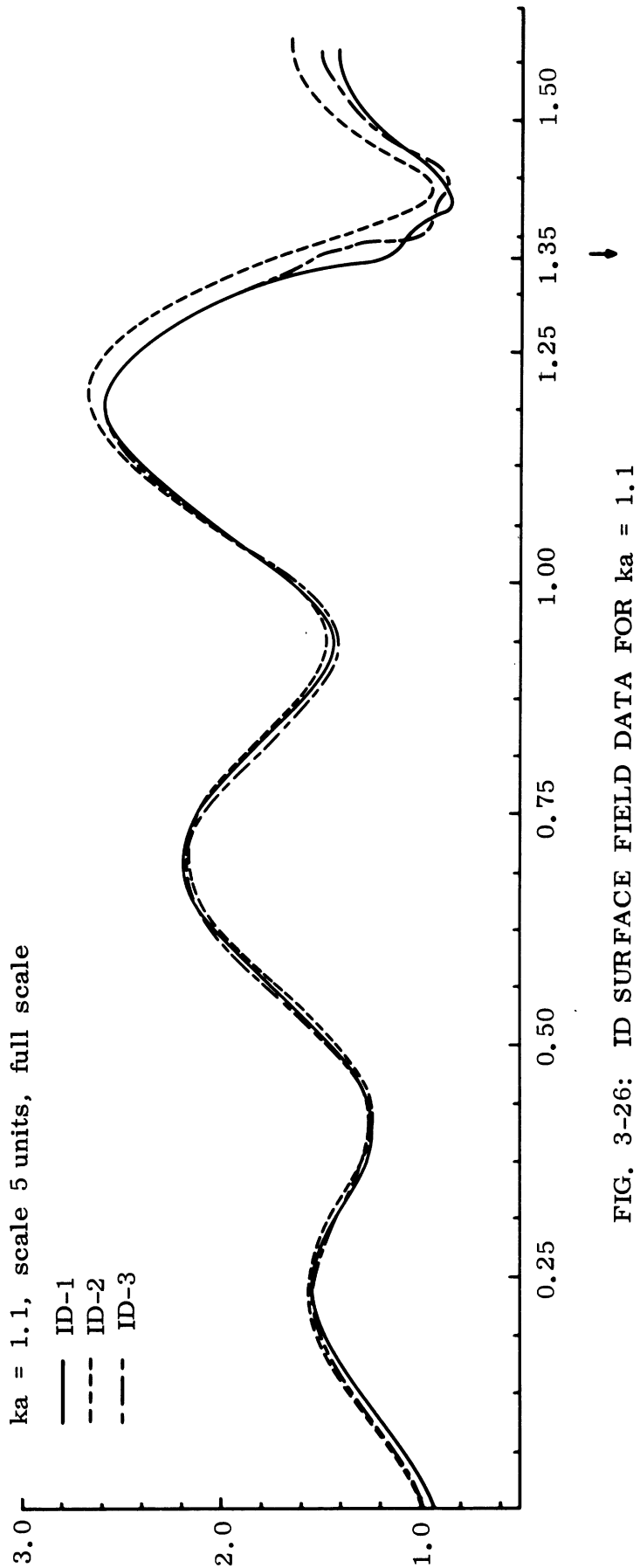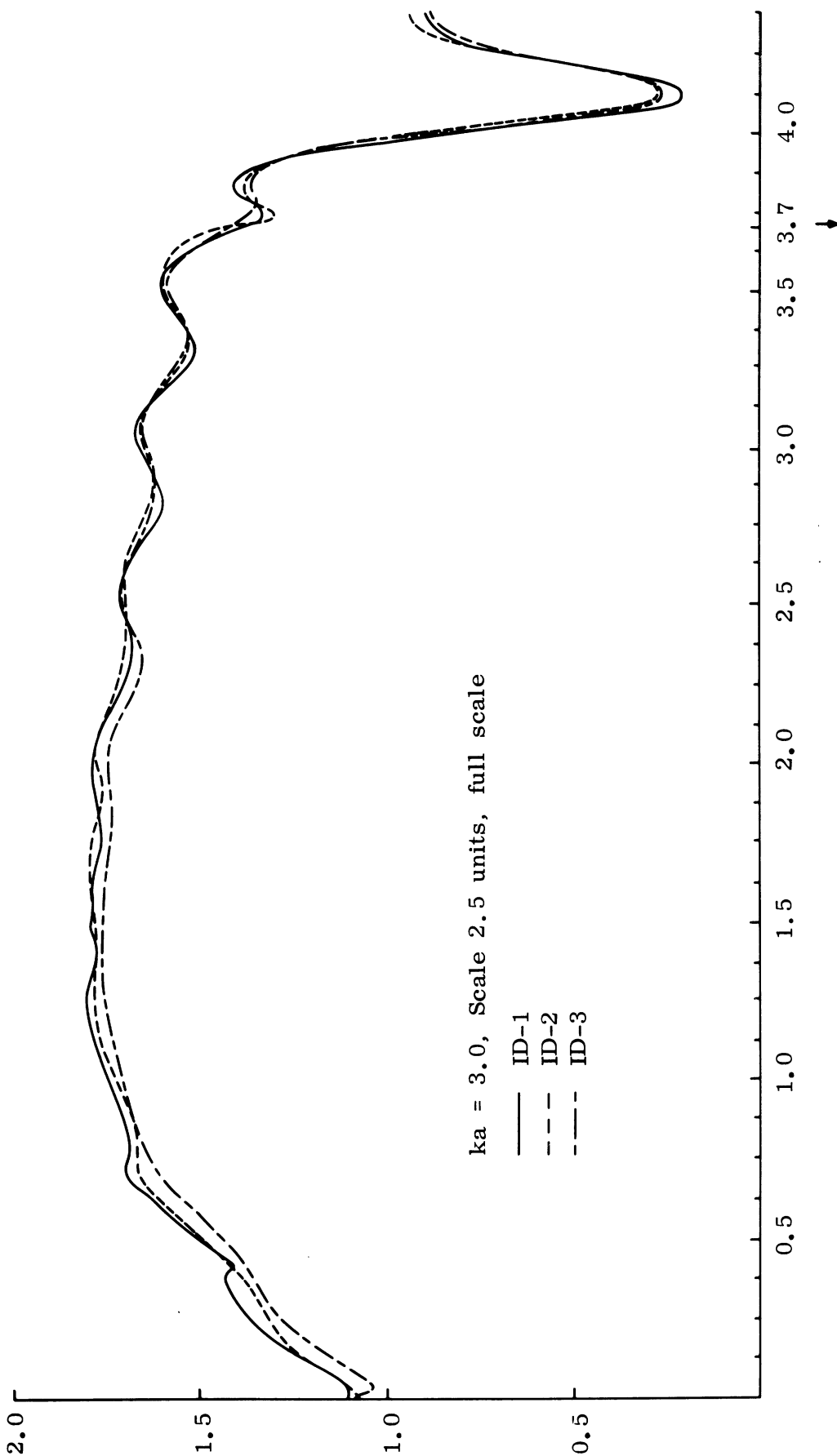
FIG. 3-27: ID SURFACE FIELD DATA FOR ka = 3.0.

182

ka = 5.0, Scale 2.5 units, full scale

ka = 5.0

——— ID-1

— — ID-2

- - - ID-3
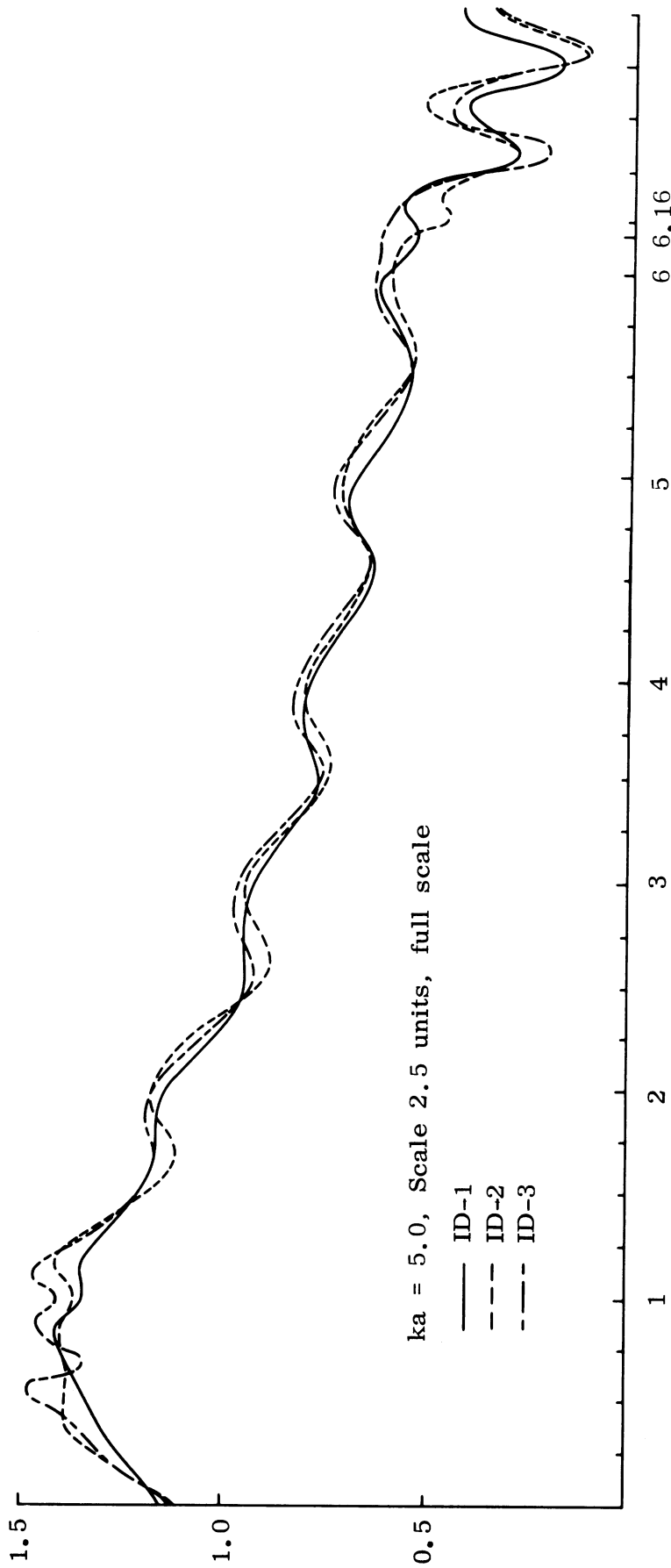
FIG. 3-28: ID SURFACE FIELD DATA FOR ka = 5.0

ka = 8.0 Scale: 2.5 units, full scale

ID-1 ————
ID-2 ——‑——
ID-3 —‑—‑—

9.84
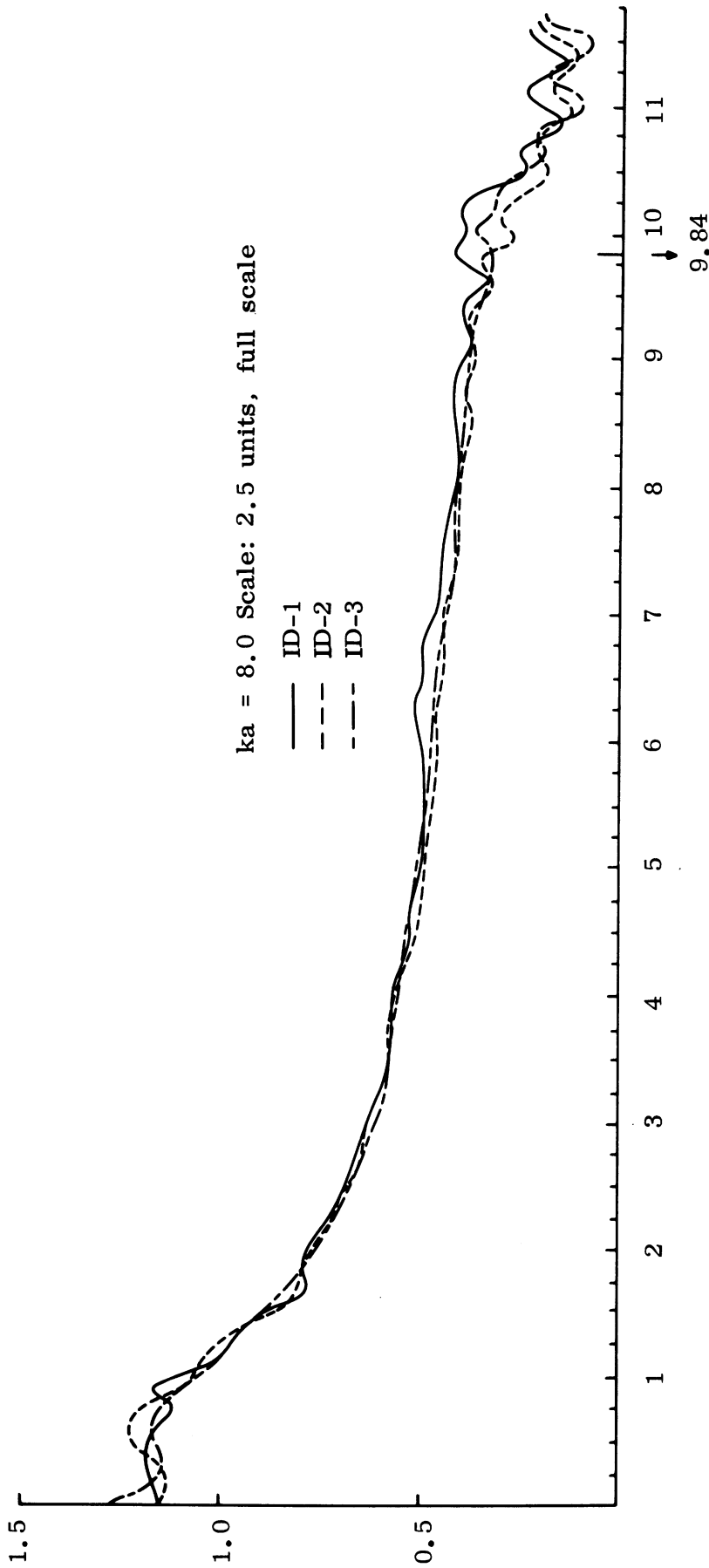
FIG. 3-29: ID SURFACE FIELD DATA FOR ka = 8.0

── THE UNIVERSITY OF MICHIGAN ──

8525-2-Q

IV

TASK 4.0 SHORT PULSE INVESTIGATION

4.1 Introduction

(S) In pursuing the objectives of the short pulse investigation, i.e. determining the utility of these techniques for discrimination among low cross section targets, a vital requirement is a sufficiently accurate means of estimating the response of the targets of interest to short incident pulses. The first goal of this program is to provide theoretical methods of calculating the back scattered response of perfectly conducting targets to realistic incident pulses. This study includes evaluation of existing methods as well as the derivation of new techniques.

(U) As outlined in the previous quarterly report, the investigation is proceeding along a number of lines in an attempt to provide approximate results of necessarily limited validity as well as a rigorous description of pulse scattering on which to base more refined approximations. In this way it is hoped to develop theoretical methods which can not only be used to answer practical questions in today's short pulse system but can also serve future needs. For example, a secondary scattered pulse which is undetectable in today's system may prove to be an effective key to discrimination with more refined measurements. But while system capability may vary, the underlying theory does not. The development and application of this theory is a principal concern of this work.

(U) The effort has been divided into so-called direct methods, i.e. a direct attack on the time-dependent scattering problem, and indirect methods which involve the Fourier transform of solutions of scattering problems in the frequency domain. Actually, this characterization is a matter of convenience and is not precise since, as will be seen below, a "direct" method apparently leads into the frequency domain which requires a Fourier transform to return to the

time domain.   This is described in Section 4.2, which summarizes the progress to date on the attempt to characterize the pulse response as an expansion in time around the pulse front.   The incident and reflected rays admit of power series expansions whereas the diffracted or creeping waves do not.   How to account for these contributions in the time domain is still under investigation.

(U) Work has begun on a second "direct" method, this one directed toward the derivation of integral equations, analogous to those available in the frequency domain, governing the time-dependent field.   The goal here is two-fold since a tractable integral equation could be employed both analytically and numerically to obtain the pulse scattering characteristics of a given target. Work on this method, described in Section 4.3, has been of an essentially preliminary nature.

(U) As described in the previous quarterly report, the "indirect" method involves taking the Fourier transform of the product of the spectral function of the incident pulse and the field scattered by the target when illuminated by a monochromatic time harmonic plane wave.   The idea here is that while this scattered field may not be known over the entire frequency range, for relatively narrow banded incident pulses with high center frequency, it will be sufficient to know the scattered field at high frequencies.   Moreover, in this frequency range, the large body of available asymptotic theory may be employed to obtain sufficiently accurate estimates of the scattered field.

(U) The validity of this argument is being tested in a simple case where the exact solution is available.   The impulse response from a sphere has been computed from the exact solution.   This has been employed in a convolution integral to obtain the response to a more realistic incident pulse.   This same response was also calculated using the Fourier transform method described above and the results are in agreement.   This provides a reliable control with

UNCLASSIFIED

which the results of the approximation may be compared. These calculations and results are presented in detail in Section 4.4. Calculation of the approximate response for the same case where the exact response is available is now under way. Additional calculations of the exact response for different incident pulse characteristics are also being carried out.

4.2 Ray Optical Method

(U) The transient response $\mu^S(r, t)$ due to a short pulse incident upon a scatterer can be found from the CW solution $u^S(r, \omega)$ by the integration

$$\mu^S(r, t) = \int_{-\infty}^{\infty} F^i(\omega) u^S(r, \omega) e^{-i\omega t} d\omega \tag{4.1}$$

where $F^i(\omega)$ is the Fourier transform of the incident pulse as a function of time. If $u^S(r, \omega)$ is known only for relatively high frequencies, (4.1) is still useful if $F^i(\omega)$ can be adequately described by the range of frequencies for which the $u^S(r, \omega)$ approximate expression is valid.

(U) An alternate use of the high frequency approximation to $u^S(r, \omega)$ can be made if one is only interested in $\mu^S(r, t)$ for relatively short times after the pulse reaches the observer, at, say, $t = t_i$. One then connects these quantities by appropriate Abelian or Tauberian theorems. For example, one could use the theorem: If a one-sided original is represented asymptotically as $t \to 0+$ by some power series of not necessarily integral exponents exceeding -1, then the series obtained by transforming the original term represents the image asymptotically as $s \to \infty$.

(U) This section describes an approximation method which one can use when $u^S(r, \omega)$ is not known, namely the generalized optical method of J.B. Keller and coworkers. There remain quite a few unanswered questions and

187

unfinished tasks before this approach will be usable; thus what follows is to be taken simply as an interim or progress report.

4.2.1 Incident Pulse

(U) In the problem under consideration, a plane short pulse is incident upon a perfectly conducting, finite, three-dimensional convex body located in free space. The incident pulse length T is such that $cT << d$ where d is the maximum dimension of the scatterer in the direction of propagation. All time derivatives of the incident pulse are assumed to exist in the range between the leading and trailing edge of the pulse. The discontinuities which exist at the leading and trailing edges of the incident pulse are assumed finite and known. For convenience the origin of the reference system is located somewhere within the scattering body.

(U) A Taylor series expansion can be written for the incident pulse which will be a valid description of the pulse for a short interval behind the pulse front. Assuming a plane pulse traveling in the positive z-direction in the rectangular coordinate reference frame we may write:

$$\bar{E}^i(z,t) = \sum_{n=0}^{\infty} \frac{\partial^n \bar{E}^i(z,t)}{\partial t^n}\bigg|_{t=t_i} \frac{(t-t_i)^n}{n!} \quad , \quad t-t_i > 0$$

$$= 0 \; , \quad\quad\quad\quad\quad\quad\quad\quad\quad t-t_i < 0 \quad (4.2)$$

where t_i is the time that the pulse front passes the point of observation, and the superscript i indicates the incident pulse. Similarly,

$$\bar{H}^i(z,t) = \sum_{n=0}^{\infty} \frac{\partial^n \bar{H}^i(z,t)}{\partial t^n}\bigg|_{t=t_i} \frac{(t-t_i)^n}{n!} \quad , \quad t-t_i > 0$$

$$= 0 \; , \quad\quad\quad\quad\quad\quad\quad\quad\quad t-t_i < 0 \; . \quad (4.3)$$

Let

$$\overline{A}_n^i(z) \equiv \left. \frac{\partial^n \overline{E}^i(z,t)}{\partial t^n} \right|_{t=t_i} \quad ; \quad \overline{B}_n^i(z) \equiv \left. \frac{\partial^n \overline{H}^i(z,t)}{\partial t^n} \right|_{t=t_i} . \quad (4.4)$$

The derivatives are one-sided derivatives evaluated at the pulse front, the field and all derivatives in front of the pulse front ($t < t_i$) are assumed to be zero.

(U) In studying the scattering of this incident pulse we become interested in how the derivatives, i.e. the coefficients $\overline{A}_n$ and $\overline{B}_n$, are affected by the scattering process. Kline and Kay (1965) develop a transport equation which governs the behavior of these coefficients as they propagate along a geometrical optics ray. If the pulse fronts are described by

$$\psi(x, y, z) - ct = 0 \qquad (4.5)$$

then the direction of the rays at each point of the pulse front is $\hat{p} = \nabla \psi$. Let distance along such a ray be represented by τ; then the transport equations can be written:

$$\frac{\partial \overline{A}_n(\tau)}{\partial \tau} + \Delta \psi \, \overline{A}_n(\tau) = \Delta \, \overline{A}_{n-1}$$

$$\frac{\partial \overline{B}_n(\tau)}{\partial \tau} + \Delta \psi \, \overline{B}_n(\tau) = \Delta \, \overline{B}_{n-1}$$

$$(4.6)$$

where $n = 0, 1, 2, \ldots$, and $\overline{A}_{-1} = \overline{B}_{-1} = 0$.

(U) For the incident plane pulse traveling in the positive z-direction $\psi^i = z$ and

$$\frac{\partial \overline{A}_n^i(\tau)}{\partial \tau} = 0 \quad ; \quad \frac{\partial \overline{B}_n^i(\tau)}{\partial \tau} = 0 \qquad (4.7)$$

indicating that no change occurs in pulse shape along an incident ray at least until the pulse strikes the scattering body. The shape of the scattered pulse may be found in the following manner.

4.2.2 Reflected Pulses

(U) First recall that the scattered field can be decomposed into reflected and diffracted protions and that an observer at a given point in space will see reflected and/or diffracted pulse fronts pass him at different points in time. A Taylor expansion may be written to describe the field $\overline{E}^r$ immediately behind the reflected pulse front:

$$\overline{E}^r(\xi, \eta, \tau, t) = \sum_{n=0}^{\infty} \frac{\overline{A}_n^r(\xi, \eta, \tau)}{n!} (t - t_m)^n \tag{4.8}$$

where t_m is the time of arrival of the pulse front at the observation point, the superscript r indicates the reflected pulse, and the $\overline{A}_n^r(\xi, \eta, \tau)$ are the coefficients to be determined. The parameters ξ, η select the ray under consideration since the rays are a two-parameter family of curves. The diffracted pulse will be considered in Section 4.4.

(U) Consider now the determination of the reflected portion of the scattered pulse along a given ray (ξ, η), i.e. find $\overline{A}_n^r(\tau)$. This is an initial value problem which requires:

(a) Knowing the reflected front $\psi^r(x, y, z) - ct = 0$ and thus the reflected rays,

(b) determining the initial values of the reflected coefficients on the reflected rays,

(c) integration of the transport equation along the reflected ray to the observation point.

An expression for the reflected pulse front can be computed if the shape of the scattering body is known. In the general case we will assume $\psi^r(x, y, z)$ to be known. The parametric equation for the ray under consideration is also assumed known. For a given ξ, η the parametric equations of the ray become

$$x(\tau) , \qquad y(\tau), \qquad z(\tau) \tag{4.9}$$

so that the transport Eq. (4.6) can be written explicitly in terms of τ.

(U) The integration of the transport equation can be completed provided the initial values of the coefficients are available.

$$\overline{A}_n^r(\tau) \bigg|_{\tau = 0} = \overline{A}_n^r(0) , \qquad \overline{B}_n^r(\tau) \bigg|_{\tau = 0} = \overline{B}_n^r(0) . \tag{4.10}$$

Beginning with the discontinuity conditions derived by Kline and Kay (1965), we may write the initial values of the coefficients as:

$$\overline{A}_n^r(0) = c(\hat{p}^r \cdot \nabla \times \overline{B}_{n-1}) \, \hat{p}^r + \alpha_n^r \, \hat{N}^r + \beta_n^r \, \hat{S} \tag{4.11a}$$

$$\overline{B}_n^r(0) = - c(\hat{p}^r \cdot \nabla \times \overline{A}_{n-1})\hat{p}^r - \alpha_n^r \, \hat{N}^r - \beta_n^r \hat{S}$$

$$- c(\hat{p}^r \cdot \nabla \times \overline{B}_{n-1}) \, \hat{p}^r - c \, \nabla \times \overline{B}_{n-1} \tag{4.11b}$$

where the unit vectors are defined as follows:

$$\hat{S} = \hat{p}^i \times \hat{N}^s = \hat{p}^r \times \hat{N}^s \quad ; \quad \hat{N}^r = \hat{S} \times \hat{p}^r \quad ;$$

$$\hat{N}^i = \hat{S} \times \hat{p}^i \quad ; \quad \hat{N}^s = \text{Normal to scattering surface.} \tag{4.12}$$

All of the quantities on the right-hand side of (4.11) are known except for α_n^r, β_n^r. Note that the determination of the nth coefficient depends upon knowing the (n - 1)th coefficient, thus making an iterative procedure necessary in determening all of the coefficients for the expansion of the expansion of the reflected field.

(U) To compute α_n^r, β_n^r we begin by composing the incident coefficients into components in the directions $\hat{p}$, $\hat{N}$ and $\hat{S}$ as shown in Fig. 4-1
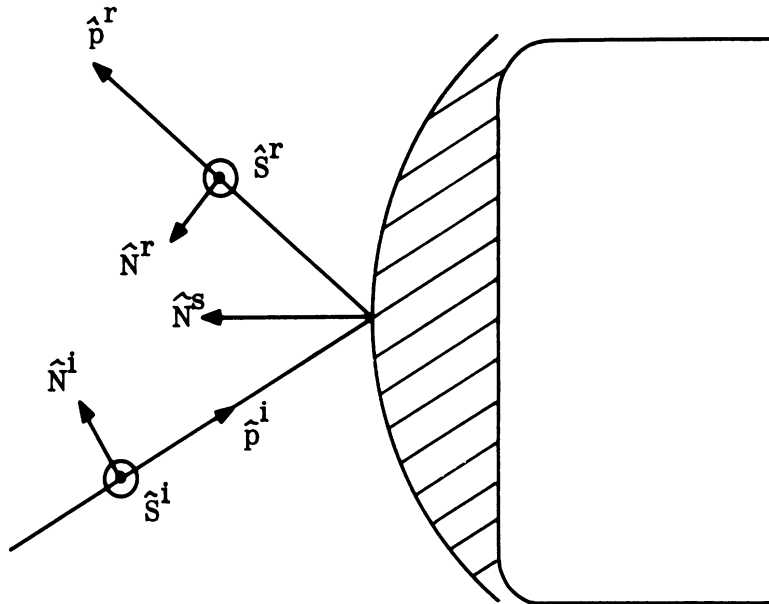

FIG. 4-1: COORDINATE SYSTEM.

where α_n^i, β_n^i are known. With the known boundary condition

$$\hat{N}^s \times (\overline{E}^i + \overline{E}^r) = 0 \qquad (4.14)$$

UNCLASSIFIED

we may write that

$$\hat{N}^s \times \left[\overline{A}_n^i(0) + \overline{A}_n^r(0) \right] = 0. \tag{4.15}$$

Substitution of (4.11a) and (4.13) into (4.15) leads to a system of equations which can be solved for α_n^r, β_n^r and results in known initial conditions (4.11).

4.2.3 Diffracted Pulse

(U)   a)   The Special Problems.   The diffracted pulse will not be expandable in a Taylor series in powers of t.   One can verify this by considering the knonw CW diffracted returns from edges, spheres and cylinders.   For example, a pulse which is a δ-function in time at a source located on a sphere yields a time variation elsewhere on the sphere which is of the form (see Levy and Keller, 1958)

$$u^d(t/T) \cong (T/t)^{3/2} \exp 3\left\{ \left[1 - (T/t)^{1/2} \right] \right\} \tag{4.16}$$

where T is a function of the angular separation between source and observation point.   This is only the first term in an expansion for small t and was determined by taking the Fourier transform of the dominant terms in the high frequency expansion of the CW field.   The corresponding function for more general bodies has not been worked out nor have the higher order terms.   The function (4.16) has an essential singularity at the wavefront which causes all of the time derivatives to vanish at that point.   Thus in the time domain we do not have the form of the time series to equation to (4.2) and hence no prescription as to how to determine the coefficients as was done for the reflected waves.

(U) Since there is presently no technique for the analysis of this problem in the time domain we shall make use of the Tauberian theorem and carry out the analysis in the frequency domain. The problem is thus converted to constructing a series representation for the high frequency CW diffracted field on the shadowed side of the diffracting object. The most general configuration of body shape and direction polarization of the incident wave for which such a solution is available will be discussed in the following section, which is based on the work of Hong (1966). To treat more general configurations one can use Hong's results together with the method of diffracted rays presented by Lewis and Keller (1964) with extensions as we shall discuss later. The method requires determination of sets of "scattering coefficients" which is done by comparison with known solutions. In the present analysis, we shall use Hong's results; then the Lewis and Keller method can be applied to those more general configurations for which Hong's configuration is a canonical form in a sense to be described below.

(U) b) The "Hong Configuration". The most general configuration of scattering body and incident field for which the surface electromagnetic fields have been determined by means of large k asymptotic expansion of the exact solution is the highly symmetric one where the object is symmetric about an axis and irradiated by a plane wave directed along this symmetry axis. The results in this case are given by Hong (1966) and from his results we can approximate the lower order coefficients. Before doing this let us first summarize the additional restrictions made on the analysis as well as point out in what sense his results are general. To do this it is necessary to introduce a coordinate system on the surface. The shadow boundary was taken by Hong as a coordinate curve $u = 0$ and the geodesics on the surface which intersect the shadow boundary orthogonally form one set of coordinate curves, $v = $ constant.

Their orthogonal trajectories, labeled u = constnat, form the other set of co-ordinate curves. These curves are chosen, as is always possible when one set are geodesics, so that a line element on the surface has length

$$ds = \left[du^2 + G \, dv^2 \right]^{1/2} \, .$$

In general, G would be a function of u and v but only the limited case where G depends on u alone was considered by Hong. Recall that by definition geodesics are curves of zero geodesic (tangential) curvature; their curvature vector K_g therefore lies in the direction of $\pm n$ where n is the surface normal.

(U) Hong did not explicitly require the high degree of symmetry mentioned above but restricted his work to cases where the geodesic curves also have zero torsion from which one concludes immediately that the geodesics admitted are plane curves, each plane containing all the surface normals along the geodesic in that plane. It is this property which forces the cylindrical symmetry; the zero torsion requirement is thus an implicit way of requiring this symmetry. An additional result of the zero torsion requirement is that G is a function of u only.

(U) Hong has also required a degree of fore and aft symmetry at the shadow boundary; i.e.,

$$\left. \frac{\partial K_g}{\partial u} \right|_{u \, = \, 0} = 0.$$

(This assumption is apparently not a fundamental restriction which implies his derivation could be reworked without this condition in a straightforward way.)

(U) The u = constant lines have both normal and tangential curvature components. Let their curvature at a point be given by $\overline{K}_t$; then

$$\vec{K}_t = K_{tn} \hat{n} + K_{tt} \hat{t}$$

where t is the direction of the unit bi-normal of u = constant which is the direction of the tangential vector to the geodesic intersecting at that point. Hong also assumed that the curvatures are "slowly varying" functions of u and v.

(U) The following additional notation is useful to describe the quantities which will be needed; from Hong's results:

$$\rho_g = 1/K_g \quad , \quad \rho_t = 1/K_t$$

and

$$\omega(p) = i \sqrt{\pi} \left[A_i(p) - i B_i(p) \right] \quad \text{where} \quad A_i(p) \text{ and } B_i(p)$$

are the Airy functions. In addition, the polarization angle θ_0 of the incident plane wave H_0 is defined by $0 < \theta < \pi/2$ and $\sin \theta = \hat{n}(0,0) \times \overline{H}_0$.

(U) Because of the cylindrical symmetry one can consider any typical plane through the symmetry axis and denote the geodesic in this plane by v = 0. Hong's results give the surface current density $\left[\overline{J}(u,0) = J_u \hat{u} + J_v \hat{v} \right]$. The tangential H field is $\hat{n} \times \overline{J}$ at the surface while the normal H field is zero. Thus at the shadow boundary the field is $H_u = J_v \hat{u}$, $H_v = J_u \hat{v}$. These components are directly available from Hong's results. For the electric field one must use Maxwell's equation

$$\text{curl } \overline{H} = j \omega \epsilon \overline{E}$$

$$
\begin{bmatrix} E_u \\ \\ E_v \\ \\ E_n \end{bmatrix} = \frac{1}{j\omega\epsilon} \begin{bmatrix} \dfrac{\partial H_v}{\partial n} \\ \\ \dfrac{\partial H_u}{\partial n} \\ \\ \dfrac{\partial H_v}{\partial u} + \dfrac{\partial H_u}{\sqrt{G'}\,\partial v} \end{bmatrix}.
$$

Thus determination of $\overline{E}$ on the surface requires a knowledge of $\overline{H}$ off the surface. This will require considerable extension of Hong's results. We consider therefore only H_u and H_v in this report.

(U) c) <u>The Diffracted Ray Method Applied to the Pulse Problem</u>. The incident pulse $\overline{E}^i(r, t)$ is given by Eq. (4.2). The Fourier transform of $E^i(r, t)$ is of the form

$$
\overline{F}^i(r, \omega) = \overline{A}^i(\omega)\, e^{ik\psi^i} \sim \sum \frac{\overline{A}_n^i}{(i\omega)^{n+1}}\, e^{ik\psi^i} \tag{4.17}
$$

Here, $\overline{F}$ will represent either $\overline{E}$ or $\overline{H}$.

(U) We consider the incident field as striking the object at point P and launching creeping waves which travel through the shadow region along a geodesic or surface ray to the point Q where the diffracted field originates which propagates along the diffracted ray to the point of observation (Fig. 4-2). We will neglect creeping waves which travel all the way around the surface one or more times since it can be verified that there is an exponential decay of the amplitude of the creeping waves with path length which renders these contributions negligible. The surface field engendered by a unit amplitude CW incident wave is shown by Hong (1966) to behave as an infinite sum of creeping
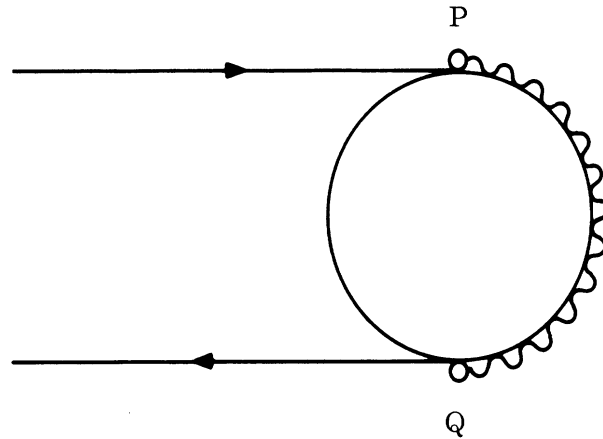
P

Q

FIG. 4-2: COORDINATE SYSTEM

waves. Specifically, Hong showed that an incoming CW wave of polarization

$$\hat{H}^i = -\cos\theta \,\hat{v} + \sin\theta \,\hat{n} \tag{4.18}$$

and zero phase at the plane of the shadow boundary generates a surface field

$$H^c = \left[A_0^c \,\hat{u} + \frac{A_1^c}{(i\omega)^{1/3}} \,\hat{v} + \frac{A_2^c}{(i\omega)^{2/3}} \,\hat{u} + O\,(1/\omega) \right] e^{iku} \,. \tag{4.19}$$

Furthermore from his derivation one learns that to this accuracy the $\hat{v}$-component of $\overline{H}^c$ is associated solely with the $\hat{n}$-component of $\overline{H}^i$, the $\hat{u}$-component of $\overline{H}^c$ with the $\hat{v}$-component of $\overline{H}^i$. Thus if we assume linear (for fixed ω) relationships between induced and incident fields, one way to introduce launching coefficients d_n and D_n is by

$$-\cos\theta_0 \,d_n^{(\omega)} \,\frac{A_n^i}{(i\omega)^{n+1}} \cong \frac{A_1^c}{(i\omega)^{1/3}}$$

$$-\sin\theta \,D_n^{(\omega)} \,\frac{A_n^i}{(i\omega)^{n+1}} \cong A_0^c + \frac{A_2^c}{(i\omega)^{2/3}} \tag{4.20}$$

198

where

$$\bar{A}_0^c(0) = \hat{u}\left\{\frac{\cos\theta_0}{\sqrt{\pi}}\int_{-\infty}^{\infty}\frac{dp}{\omega(p)}\right\} \tag{4.21}$$

$$\bar{A}_1^c(0) = \hat{v}\left\{\frac{i\,2^{1/3}\cos\theta_0}{\rho_g^{1/3}\sqrt{\pi}}\int_{-\infty}^{\infty}\frac{dp}{\omega(p)}\right\} \tag{4.22}$$

$$\bar{A}_2^c(0) = \hat{u}\left\{\frac{2^{2/3}\cos\theta_0}{\sqrt{\pi}\,\rho^{2/3}}\int_{-\infty}^{\infty}dp\left[\frac{dp}{\omega(p)}\left\{-\frac{2}{15}\right.\right.\right.$$

$$\left.+\frac{17}{15}\rho_g\frac{d^2\rho_g}{du^2}+\frac{\rho_g}{\rho_{tn}}\right\}+\frac{\omega(p)}{[\omega(p)]^2}\left\{-\frac{1}{5}+\frac{\rho^3}{30}\right.$$

$$\left.+\rho_g\frac{d^2\rho_g}{du^2}\left(\frac{8}{15}-\frac{6}{5}p^3\right)\right\}-\frac{p\omega(p)^2}{[\omega(p)]^3}\left\{\frac{7}{3}\rho_g\frac{d^2\rho_g}{du^2}\right.$$

$$\left.\left.+\frac{\rho_g}{\rho_{tr}}\right\}+\frac{4p[p\omega(p)]^3\,\rho_g\frac{d^2\rho_g}{du^2}}{3[\omega(p)]^4}\right]_{u=0}\right\} \tag{4.23}$$

One notes that the launching coefficients depend only on the Gaussian curvature of the body at the shadow boundary. Thus one can consider the Hong configuration as canonical in less symmetrical situations where the Gaussian curvature changes only slowly along the shadow boundary and use the same launching coefficients. Thus for the canonical problem with known $A_n^c(0)$ the $d_n(p)$

and $D_n(p)$ may be evaluated. The launching ciefficients d_o and D_o give the launching of the leading edge of the pulse discontinuity, d_1 and D_1 the launching of the discontinuity in the first derivative, etc.

(U) The asymptotic expansion for the surface field, in cases where the solution is not available via some other method, can be constructed for any point u along a surface ray by integration of a surface transport equation using the $A_n^c(0)$ from (4.20) as an initial value. For the scalar case this equation is given in Lewis and Keller (1964) but is not valid near the focus of the surface rays on the back; the behavior of the field there must still be studied.

(U) A similar procedure can be used to go from the surface field to the diffracted field once the diffraction factor for this situation is known. In this case the diffraction factors will be noted by $d_{2n}(Q)$ and $D_{2n}(Q)$. Once the surface transport equation is integrated to yield an expression for the creeping wave at point Q, the factors $d_{2n}(Q)$ and $D_{2n}(Q)$ can be utilized to obtain initial values of the coefficients in the series for the diffracted field. Integration of another transport equation along the diffracted ray then yields the desired diffracted field at the point of observation.

(U) In the application to date of this type of approach (Lewis and Keller, 1964) only the leading term in the expansion has been considered and $d_{10}(P)$ and $d_{20}(Q)$ were assumed to be of the same functional form. We will make the same assumption (at least as an interim measure) for the $d_{2n}(Q)$, i.e., that $d_{2n}(Q) = d_{1n}(Q)$.

(U) d) <u>Uncompleted Problems in Applying the Method of (c)</u>. To apply the method outlined above it will be necessary to determine

      (a) the vector surface transport equations,

      (b) the field variation at the focus on the shadow side where the Lewis-Keller surface transport equations are not valid and where Hong also has no solution for fields,

(c) the launching factors for the electric field using the Hong configuration.

Apart for applying the method, the validity or extent of approximation involved in the various assumptions should be investigated if possible; namely that

(a) equation (4.19) provides a reasonable approximation method,

(b) $d_{2n}(Q) = d_{1n}(Q)$,

(c) the Hong configuration is canonical for bodies with slowly varying Gaussian curvature along the shadow boundary.

(U) Generalizations of the above procedure to highly unsymmetric configurations for which the Hong configuration is clearly not canonical, and consideration of non-perfect conductors constitute further (major) problems for the more distant future.

4.3 Integral Equation Formulation of Time-Dependent Scattering Problems

(U) Our object is to formulate the time-dependent scalar and electromagnetic scattering problems with the help of integral equations which hold for surface coverings (the field or its normal derivative on the surface of the scatter). If this object is achieved, we shall apply the results to solve the problems of short pulse scattering. A significant advantage of this integral equation formulation is that the scattering problems for the scattering surfaces for which the wave operator is non-separable can be solved, at least numerically. The above-mentioned formulation is given by Maue (1949) for the reduced wave equation. We shall try to parallel his procedure as far as possible.

(U) In what follows we give some of the pertinent preliminaries. We have the wave equation

$$\nabla^2 \psi - \frac{1}{c^2} \frac{\partial^2 \psi}{\partial t^2} = - 4\pi \, f(\underline{x}, \, t) \tag{4.24}$$

where f is a known source distribution, c is the velocity of propagation in the medium, and $\underline{x}$ the vector corresponding to a point in 3-space. The Green's function for (4.24) satisfies

$$\left[\nabla_x^2 - (1/c^2)(\partial^2/\partial t^2)\right] G(\underline{x}, \ t; \ \underline{x}', \ t') = -4\pi \ \delta(\underline{x} - \underline{x}')\delta(t - t') \ . \qquad (4.25)$$

(U) We first need the solution of (4.24) for the infinite space with no boundaries which is given by

$$\psi(\underline{x}, \ t) = \int G(\underline{x}, \ t); \ \underline{x}', \ t) \ f(\underline{x}', \ t') \ d^3x' \ dt' \qquad . \qquad (4.26)$$

Here

$$x = (x, \ y, \ z) = \rho \ (\sin \theta \cos \phi, \ \sin \theta \sin \phi, \ \cos \theta),$$

$$d^3x = dx \ dy \ dz = \rho^2 \sin \theta \ d\rho \ d\theta \ d\phi,$$

$$k = (k_x, \ k_y, \ k_z) = k \ (\sin \theta_k \cos \phi_k, \ \sin \theta_k \sin \phi_k, \ \cos \theta_k),$$

$$d^3k = dk_x \ dk_y \ dk_z = k^2 \sin \theta_k \ dk \ d\theta_k \ d\phi_k \ .$$

(U) We have the usual representation

$$\delta(\underline{x} - \underline{x}') \delta(t - t') = \frac{1}{(2\pi)^4} \int d^3k \int d\omega \ e^{i\underline{k} \cdot (\underline{x} - \underline{x}')} e^{-i\omega(t-t')} \qquad (4.27)$$

$$G(\underline{x}, \ t; \ x', t') = \int d^3k \int d\omega \ g(\underline{k}, \ \omega) \ e^{i\underline{k} \cdot (\underline{x} - \underline{x}')} e^{-i\omega(t - t')} \qquad (4.28)$$

where $g(\underline{k}, \ \omega)$, the Fourier transform of G, is to be determined. Substituting (4.27), (4.28) into (4.25) we obtain

$$g(\underline{k}, \omega) = \frac{1}{4\pi^3} \frac{1}{k^2 - (\omega^2/c^2)} \quad , \tag{4.29}$$

so that

$$G(\underline{x}, t; \underline{x}', t') = \frac{1}{4\pi^3} \int d^3k \int d\omega \frac{1}{k^2 - (\omega^2/c^2)} e^{i\underline{k}\cdot(\underline{x}-\underline{x}')} e^{-i\omega(t-t')} \tag{4.30}$$

The integrand has poles at $k^2 = \omega^2/c^2$ in the ω-plane. We now proceed to provide a rule to handle these singularities which come from physical considerations. The Green's function satisfying (4.25) represents the wave disturbance caused by a point source at $\underline{x}'$ which is turned on only for an infinitesimal time interval at $t' = t$. We know that such a wave disturbance propagates outwards as a spherically diverging wave with a velocity c. So we demand that (a) $G \equiv 0$ everywhere for $t < t'$, (b) G represent outgoing wave for $t > t'$. Now consider the ω-integration; $g(\underline{k}, \omega)$ has its singularities at $\omega \mp ck$. For $t > t'$ the integral along the real axis in (4.30) is equivalent ot the contour integral around the path C, (see Fig. 4-3), closed in the lower half-plane since the contribution on the semicircle at infinity vanishes exponentially. On the other hand, for $t' > t$, the contour must be closed in the upper half-plane.

(U) In order to make G vanish for $t < t'$ we must imagine that the poles at $\omega = \pm ck$ are displaced below the real axis. Then the integral over C for $t > t'$ will give non-vanishing contribution, while the integral over C' for $t < t'$ will vanish. So

$$G(\underline{x}, t; \underline{x}', t') = \frac{1}{4\pi^3} \int d^3k \int d\omega \frac{e^{i\underline{k}\cdot\underline{R} - i\omega\tau}}{k^2 - \frac{1}{c^2}(\omega + i\epsilon)^2} \tag{4.31}$$
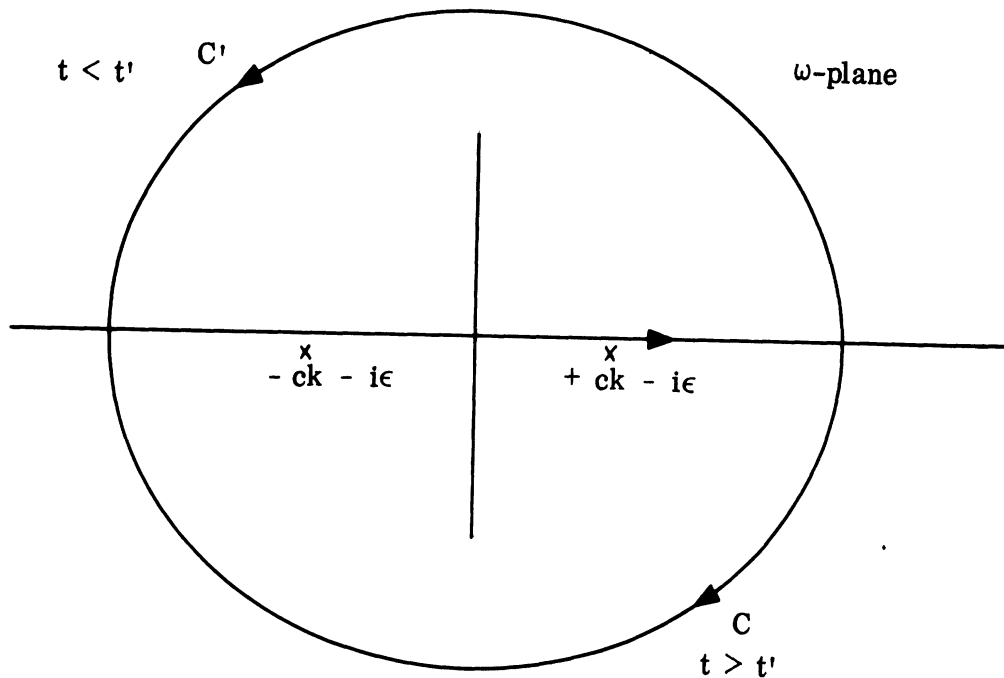
203

FIG. 4-3: COMPLEX ω-PLANE WITH CONTOUR C FOR
$t > t'$ AND CONTOUR C' FOR $t < t'$.

where $\underline{R} = \underline{x} - \underline{x}'$, $\tau = t - t'$, $\epsilon > 0$. The integration over ω for $\tau > 0$ around the contour C yields

$$G = \frac{c}{2\pi^2} \int d^3k \; e^{i\underline{k} \cdot \underline{R}} \; \frac{\sin (c \tau k)}{x}. \tag{4.32}$$

(U) The integration over d^3k can be accomplished by first integrating over angles, yielding

$$G = \frac{2c}{\pi R} \int_{-\infty}^{\infty} dk \; \sin (kR) \sin (c\tau k). \tag{4.33}$$

Since the integrand is even in k, the integral can be written over the whole interval, $-\infty < k < \infty$. With $x = ck$, (4.33) becomes

$$G = \frac{1}{2\pi R} \int_{-\infty}^{\infty} dx \left(e^{i\left[\tau - (R/c)\right]x} - e^{i\left[\tau + (R/c)\right]x} \right) \tag{4.34}$$

Since $\tau > 0$, (4.34) yields

$$G = \frac{1}{R} \delta\left(\tau - \frac{R}{c}\right) = \frac{\delta\left(t' + \frac{|\underline{x} - \underline{x}'|}{c} - t\right)}{|\underline{x} - \underline{x}'|} \ . \tag{4.35}$$

Therefore, the "retarded solution" is

$$\psi(\underline{x}, t) = \int \frac{\delta\left(t' + \frac{|\underline{x} - \underline{x}'|}{c} - t\right)}{|\underline{x} - \underline{x}'|} f(\underline{x}', t') \, d^3x' \, dt'$$

$$= \int \frac{\left[f(\underline{x}', t')\right]_{ret}}{|\underline{x} - \underline{x}'|} \, d^3x' \ , \tag{4.36}$$

where $\left[\ \right]_{ret}$ means that the time t' is to be evaluated at the retarded time,
$t' = t - \dfrac{|\underline{x} - \underline{x}'|}{c}$.

(U) Next we consider the initial boundary value problem. We apply the Green's theorem to ψ and G in the volume V bounded by the scattering surface S and the large sphere S_∞, and integrate over time from $t' = t_o$ to $t' = t_1 > t$:

$$\int_{t_o}^{t_1} dt' \int_V d^3x' \, (G\nabla'^2 \psi - \psi\nabla'^2 G) = \int_{t_o}^{t_1} dt'$$

$$\int_{S + S_\infty} d\sigma' \ \left(G \frac{\partial \psi}{\partial n'} - \psi \frac{\partial G}{\partial n'}\right) \tag{4.37}$$

If there are no sources at infinity the contribution from the integral over S_∞ as $R \to \infty$ vanishes; using (4.24) and (4.25), and the fact that $G \equiv 0$ at $t_1 > t$, we arrive at the Kirchhoff's representation

$$\psi(\underline{x}, t) = \int_V d^3x' \frac{\left[f(\underline{x}', t') \right]_{ret}}{\left| \underline{x} - \underline{x}' \right|} + \frac{1}{4\pi c^2} \int_V d^3x' \left(G \frac{\partial \psi}{\partial t'} - \psi \frac{\partial G}{\partial t'} \right)_{t'=t_o}$$

$$+ \frac{1}{4\pi} \int_{t_o}^{t_1} dt' \int_S d\sigma' \left(G \frac{\partial \psi}{\partial n'} - \psi \frac{\partial G}{\partial n'} \right) . \qquad (4.38)$$

(U) If we assume that there are no sources in V and that the initial values of ψ and $\partial \psi / \partial t$ vanish, then (4.38) reduces to

$$\psi(\underline{x}, t) = \frac{1}{4\pi} \int_{t_o}^{t_1} dt' \int_S d\sigma' \left(G \frac{\partial \psi}{\partial n'} - \psi \frac{\partial G}{\partial n'} \right) . \qquad (4.39)$$

(U) Now our main concern is to set up integral equations, if we can, governing the "coverings" or "layers", $\psi \big|_S$ and $\partial \psi / \partial n \big|_S$.

4.4 Pulse Scattering from a Perfectly Conducting Sphere

(U) A perfectly conducting sphere of radius a is considered and the back scattering integral field expressions for arbitrary incident pulses are formulated. The sphere is regarded as being a linear time-invarient system in the back scattering direction, so that the impulse response being known, solutions to other incident pulses can be constructed by a convolution or an inverse Fourier transform integral. The integral expressions for the back scattered pulse are then computed for particular incident pulses, indicating very close agreement in specular and creeping wave return ranges. Other computations which may prove useful are discussed.

4.4.1 The Impulse Response

(U) Assume a plane wave incident on a perfectly conducting sphere as shown in Fig. 4-4. The plane wave is taken with the electric field linearly
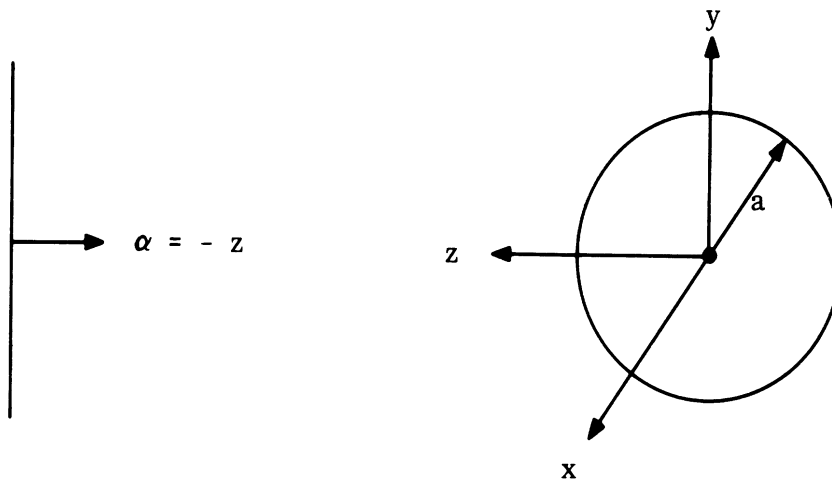

FIG. 4-4: COORDINATE SYSTEM.

polarized in the x-direction and it is given by

$$\underline{E}^i(r, \omega) = \hat{x}\, E_0\, e^{i\left(\frac{\hat{\alpha}\,\cdot\,\hat{r}}{c}\right)\omega} \tag{4.40}$$

where α = unit vector in the direction of propagation, $\hat{r}$ a vector in the radial direction, measured positively away from the origin. The superscript i indicates incident, while a superscript s will be used to indicated the scattered fields. Capital letters will indicate field expressions in the frequency domain while script will be used to represent the corresponding time domain expressions. Defining the Fourier and inverse Fourier transform integrals as

$$E^i(r, \omega) = \frac{1}{2\pi} \int_{-\infty}^{\infty} \mathcal{E}^i(r, t) \, e^{i\omega t} \, dt \qquad (4.41a)$$

and

$$\mathcal{E}^i(r, t) = \int_{-\infty}^{\infty} E^i(r, \omega) \, e^{-i\omega t} \, d\omega \qquad (4.41b)$$

the plane wave, (4.40) is represented in the time domain by

$$\mathcal{E}^i(r, t) = \hat{x} \; 2\pi \; E_o \; \delta\left(\frac{\hat{a} \cdot \bar{r}}{c}\right) - t \qquad (4.42)$$

i.e. an impulse function.

(U) According to our assumption of linearity and time invariance of the perfectly conducting sphere, the back scattered response to an incident pulse of the form of (4.42) will be a function characteristic of the back scattering properties of the sphere and will serve as a tool in constructing solutions for other incident pulses. Equivalent to this of course is to know the back scattered response of the incident plane wave given by (4.40), since the frequency and time domain solutions are connected by (4.41). The time harmonic response in the far zone backscattering direction of the perfecting conducting sphere for an incident plane wave is the well-known expression

$$E_\infty^s(r, \omega) = \hat{x} \, E_o \, i \, \frac{e^{i(\omega/c)r}}{(\omega/c)r} \sum_{n=1}^{\infty} (-i)^n (2n+1) \left\{ \frac{j_n(\omega a/c)}{h_n^{(1)}(\omega a/c)} \right.$$

$$\left. - \frac{\left[\frac{\omega a}{c} j_n(\omega a/c)\right]'}{\left[\frac{\omega a}{c} h_n^{(1)}(\omega a/c)\right]'} \right\} = \hat{x} \, E_o \, \frac{a}{2r} \, e^{i\frac{\omega}{c}[r - 2a]} \, G^*(\omega/c) \quad (4.43)$$

$$G^*(\omega a/c) = i \, \frac{e^{i2(\omega a/c)}}{(\omega a/c)} \sum_{n=1}^{\infty} (-i)^n (2n+1) \left\{ \frac{j_n(\omega a/c)}{h_n^{(1)}(\omega a/c)} \right.$$

$$\left. - \frac{\left[\frac{\omega a}{c} \, j_n(\omega a/c)\right]'}{\left[\frac{\omega a}{c} \, h_n^{(1)}(\omega a/c)\right]'} \right\} = S_1(\omega a/c) - iS_2(\omega a/c)$$

$$= \text{Mag } G^*(\omega a/c) \exp \left\{ -\tan^{-1} \left[\frac{S_2(\omega a/c)}{S_1(\omega a/c)} \right] \right\} \tag{4.44}$$

and it is tabulated (Bechtel, 1962) for $0 \leq \omega a/c \leq 50$ $\left[G^*(\omega a/c > 50) = -1.00 \right]$.

(U) Substituting (4.43) in (4.41b), the time-domain backscattered field $\underline{\zeta}^s(r,t)$ is

$$\underline{\zeta}^s(r, t) = \int_{-\infty}^{\infty} \underline{E}_\infty^s (r,\omega) \, e^{-i\omega t} \, d\omega$$

$$= 2 \, \text{Re} \int_0^{\infty} \underline{E}_\infty^s(r, \omega) \, e^{-i\omega t} \, d\omega \quad , \tag{4.45}$$

since

$$\underline{E}_\infty^s(r, \omega) = \underline{E}_\infty^s(r, \omega)^* \quad . \tag{4.46}$$

Considering (4.45) with (4.43),

$$\underline{\zeta}^s(r,t) = \hat{x} \, E_o \, \frac{c}{r} \, \text{Re} \int_0^{\infty} e^{-i(\omega a/c)\tau} \, G^*(\omega a/c) \, d(\omega a/c) \tag{4.47}$$

results where

$$\tau = \frac{ct}{a} + 2 - \frac{r}{a} \ .$$

Expression (4.47) may be rewritten as follows:

$$\underline{\zeta}^s(r, t) = \hat{x} \, E_o \, \frac{c}{r} \, \text{Re} \left\{ \int_0^{50} e^{-i(\omega a/c)\tau} \, G^*(\omega a/c) \, d(\omega a/c) \right.$$

$$+ \int_{50}^{\infty} e^{-i(\omega a/c)\tau} \, G^*(\omega a/c) \, d(\omega a/c) \right\}$$

$$= \hat{x} \, E_o \, \frac{c}{r} \, \text{Re} \left\{ \int_0^{50} e^{-i(\omega a/c)\tau} \, G^*(\omega a/c) \, d(\omega a/c) \right.$$

$$\left. - \int_{50}^{\infty} e^{-i(\omega a/c)\tau} \, d(\omega a/c) \right\} = \hat{x} \, E_o \, \frac{c}{r} \left\{ \frac{\sin 50 \, \tau}{\tau} \right.$$

$$+ \text{Re} \int_0^{50} e^{-i(\omega a/c)\tau} G^*(\omega a/c) d(\omega a/c) - \pi \, \delta \, (\tau) \right\} \qquad (4.48)$$

where we have substituted $G^*(\omega a/c) = -1.00$ in the integral

$$\int_{50}^{\infty} e^{-i(\omega a/c)\tau} \, G^*(\omega a/c) \, d(\omega a/c)$$

to arrive at relation (4.48).

(U) Upon normalization of (4.48) with respect to $E_o c/r$ and considering scalar quantities only, one obtains the expression.

$$\mathscr{E}^S_N(r, t) = \frac{\mathscr{E}^S(r, t)}{E_o c/r} = \left\{ \frac{\sin 50\, \tau}{\tau} + \text{Re} \int_0^{50} e^{-i(\omega a/c)\tau} \right.$$

$$\left. G^*(\omega a/c)\, d(\omega a/c) - \pi\, \delta\, (\tau) \right\} . \qquad (4.49)$$

This form has been employed in numerical computations for $0 \leq \tau \leq 7$. The result is shown in graphical form in Fig. 4-5. The parameter τ is a function of the observation point, of the sphere radius and of real time. The above indicated range is dictated by the following considerations. Assume an observer at a distance r from the origin, in the far zone. Let $t = 0$ be the time the impulse coinsides with the plane through the origin normal to the observation direction (here we restrict our attention to backscattering). At $t = 0$ the specular return is at a distance $r - 2a$ from the observer, thus $t = \frac{r - 2a}{c}$ is the time for the specular return to arrive at the observation point r. At this instant

$$\tau = \frac{c}{a} \left(\frac{r - 2a}{c} \right) + 2 - \frac{r}{a} = 0.$$

Again, at $t = 0$ the first creeping wave return is at a distance $\pi a + r$ from the observer. If it is assumed that v_{cr} = the velocity of the creeping wave in the umbra and penumbra regions $(\pi/2 < \theta < \pi)$ then the time which lapses for the first creeping wave to arrive at the observation point is $t = \frac{\pi a}{v_{cr}} + \frac{r}{c}$ then $\tau = \frac{c}{a} (\pi a/v_{cr}) + \frac{r}{a} + 2 - \frac{r}{a} = \frac{\pi c}{v_{cr}} + 2.$ For the computations it was
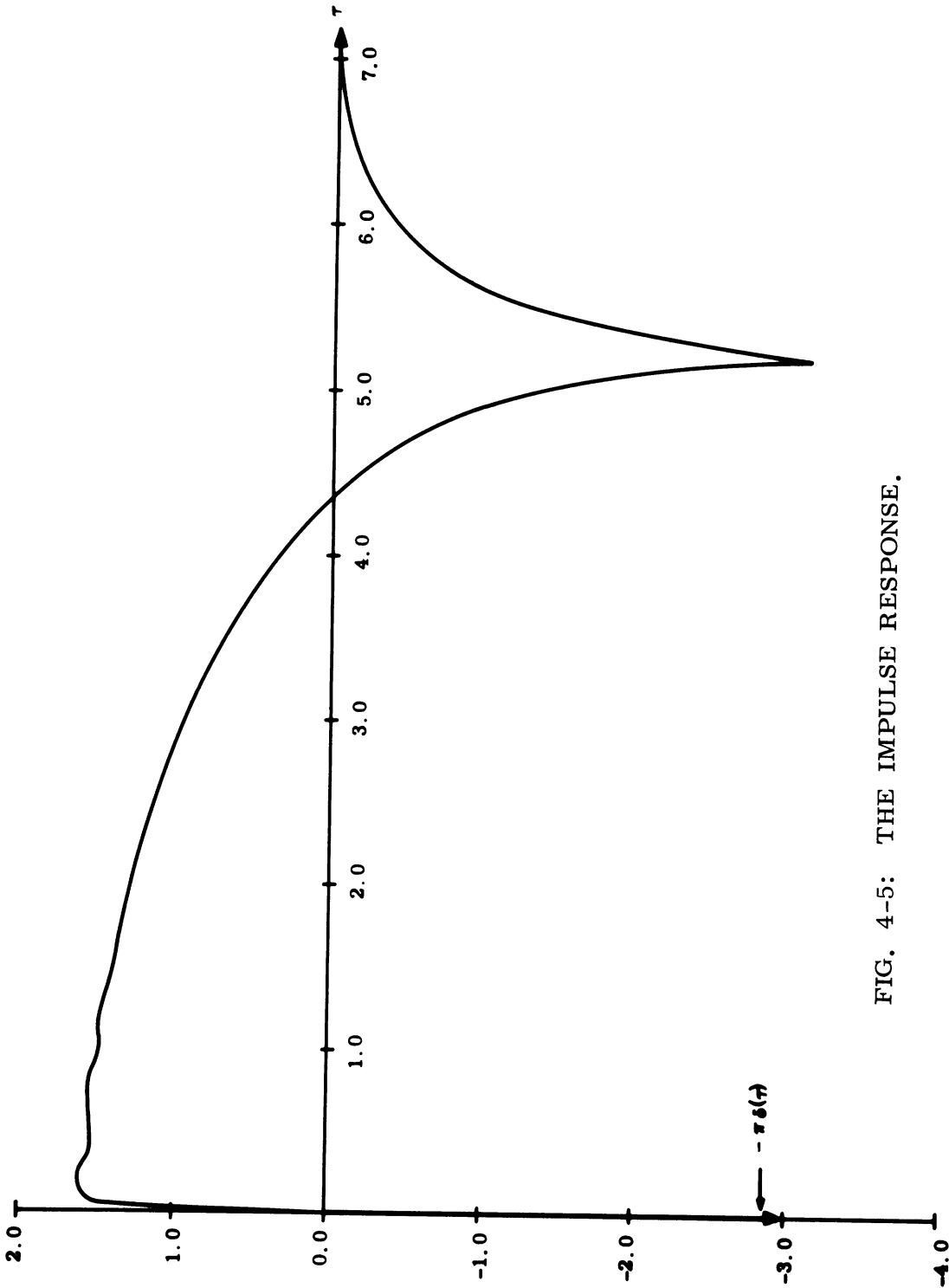
FIG. 4-5: THE IMPULSE RESPONSE.

assumed that $0.7c \leq v_{cr} < c$ and therefore the upper value of $\tau \doteq 7.00$ was used. However, as it can be seen in Fig. 4-5, the peak of the first creeping wave return at the observation point occurred at $\tau \doteq 5.1998$. This value of τ in the equation $\tau = \frac{\pi c}{v_{cr}} + 2$ implies that the creeping wave velocity in the umbra and penumbra regions $(\pi/2 \leq \theta \leq \pi)$ is approximately $v_{cr} \doteq 0.98c$. As it would be expected the specular return is π radians out of phase with the incident impulse (see Fig. 4-5).

4.4.2 Backscattering of Arbitrary Incident Pulses

(U) Having previously characterized the perfectly conducting sphere by its impulse response the backscattering integral expressions for arbitrary incident pulses are given by

$$f^S(r,t) = f^i(r,t) \circledast \mathcal{L}^S(r,t) = \frac{1}{2\pi} \int_{-\infty}^{\infty} \mathcal{L}^S(r,y) \, f^i(r,\,t-y) \, dy \qquad (4.50)$$

or

$$f^S(r,\,t) = \int_{-\infty}^{\infty} F^S(r,\,\omega) \, e^{-i\omega t} \, d\omega$$

with

$$F^S(r,\omega) = F^i(r,\,\omega) \, E^S(r,\,\omega) \,, \qquad (4.51)$$

where $f^i(r,\,t)$ is the incident pulse, $f^S(r,t)$ the backscattered pulse and $F^i(r,\omega)$, $F^S(r,\omega)$ their corresponding Fourier transforms. The symbol $\circledast$ clearly indicates a convolution process.

(U) a) <u>The Convolution Integral</u>. Rewriting (4.50) as

$$f^S(r,t) = \frac{1}{2\pi} \int_{-\infty}^{\infty} \zeta^S(r,y) \, f^i(r, t-y) \, dy$$

$$= \frac{a}{2\pi c} \int_{-\infty}^{\infty} \zeta^S(r,x) \, f^i\left(r, \frac{a}{c}[\tau - x]\right) dx \qquad (4.52)$$

(after having made the substitution $y = \frac{a}{c} x - \frac{2a}{c} + \frac{r}{c}$), and considering incident pulses of the form $f^i(r,x) = e(x) \cos \omega_o x$, such that $e(x) = 0$ whenever $x > T/2$, it follows that

$$f^i\left(r, \frac{a}{c}[\tau - x]\right) = 0$$

if $x - \tau > cT/2a$, and therefore

$$f^S(r,t) = \frac{a}{2\pi c} \int_{\tau - \frac{cT}{2a}}^{\tau + \frac{cT}{2a}} \zeta^S(r,x) \, f^i\left(r, \frac{a}{c}[\tau - x]\right) dx$$

$$= \frac{a}{2\pi c} \int_{-cT/2a}^{cT/2a} \zeta^S(r, x+\tau) \, f^i\left(r, -\frac{a}{c} x\right) dx$$

$$= \frac{a}{2\pi c} \int_{-cT/2a}^{cT/2a} \zeta^S(r, x+\tau) \, e\left(-\frac{a}{c} x\right) \cos \frac{\omega_o a}{c} x \, dx \qquad (4.53)$$

Upon introducing the change of variables, $\psi = \dfrac{2a}{cT} x = x/\ell$ with $\ell = \dfrac{cT}{2a}$, the backscattered response is finally given by

$$f^S(r, t) = \frac{T}{4\pi} \int_{-1}^{+1} {}^S(r, \tau + \ell\psi) \, e^{\left[-\frac{T\psi}{2}\right]} \cos \frac{\omega_o T}{2} \, \psi \, d\psi \qquad (4.54)$$

In relation (4.54), $\omega_o T$ fixes the number of cycles contained in one pulse, i.e. $\omega_o T = 2n\pi$, n = number of cycles. The parameter ℓ is dimensionless and it gives the ratio of pulse length to sphere diameter. The range of τ is $-\ell \leq \tau \leq 7.0$ with $\tau = -\ell$ corresponding to the instant of time the front of the pulse of the specular return arrives at the observation point. In this case of arbitrary incident pulses the reference point $t = 0$ coincides with the instant the center of the pulse coincides with a plane through the origin as shown in Fig. 4-6.
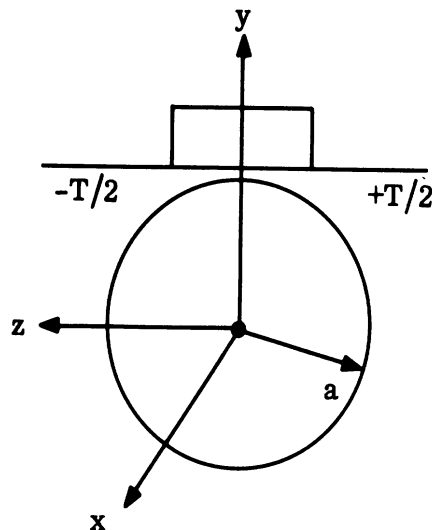

FIG. 4-6: THE INCIDENT PULSE IS ASSUMED SQUARE ENVELOPED.

Substituting in (4.54) the corresponding expression for $\xi^S(r, \tau + \ell\ \psi)$ the result is

$$
f^S(r, t) = \frac{E_o c}{r} \frac{T}{4\pi} \int_{-1}^{+1} \left\{ \frac{\sin 50\ (\tau + \ell\ \psi)}{\tau + \ell\psi} + \text{Re} \int_0^{50} \exp \right.
$$

$$
\left\{ - i(\omega a/c) \left[\tau + \ell\ \psi\right] \right\} G^*(\omega a/c)\ d(\omega a/c)
$$

$$
\left. - \pi\ \delta\ \left[\tau + \ell\psi\right] \right\} \cos n\pi\ \psi\ d\psi \tag{4.55}
$$

For computation the normalized expression

$$
f^S_N(r, t) = \frac{f^S(r, t)}{E_o cT/4\pi r} = \int_{-1}^{+1} \left\{ \frac{\sin 50\ (\tau + \ell\psi)}{\tau + \ell\psi} \right.
$$

$$
+ \text{Re} \int_0^{50} \exp \left\{ - i(\omega a/c)\ (\tau + \ell\ \psi) \right\} G^*(\omega a/c) d(\omega a/c)
$$

$$
\left. - \pi\delta \left[\tau + \ell\ \psi\right] \right\} \cos n\pi\ \psi\ d\psi \tag{4.56}
$$

is used.

(U) b) <u>The Inverse Fourier Integral.</u> The backscattered field $f^S(r, t)$ can also be computed by

$$
f^S(r, t) = \int_{-\infty}^{\infty} F^S(r, \omega)\ e^{-i\omega t}\ d\omega
$$

with

$$
F^S(r, \omega) = F^i(r, \omega)\ E^S(r, \omega) \quad . \tag{4.51}
$$

Since $F^S(r, \omega) = F^S(r, -\omega)^*$, we rewrite (4.51) as

$$f^S(r, t) = 2 \, \text{Re} \int_0^\infty F^i(r, \omega) \, E^S(r, \omega) \, d^{-i\omega t} \, d\omega \quad . \qquad (4.57)$$

where Re denotes the real part. Now substitute expression (4.43) for $E^S(r, \omega)$ in (4.53) and note that $F^i(r, \omega)$ is the Fourier transform of

$$f^i(r, t) = \begin{cases} e(t) \cos \omega_0 t & ; \quad |t| < T/2 \\ \\ 0 & \quad |t| > T/2 \end{cases} \quad ,$$

that is

$$F^i(r, \omega) = (T/4\pi) \left\{ \epsilon(\omega) \circledast \bar{\Phi} \, (\omega a/c, \, \ell, \, n) \right\} \qquad (4.58)$$

where $\epsilon(\omega)$ is the Fourier transform of $e(x)$ and

$$\bar{\Phi} \, (\omega a/c, \, \ell, \, n) = \frac{\sin \left[\dfrac{\omega a}{c} \ell + n\pi \right]}{\left[\dfrac{\omega a}{c} \ell + n\pi \right]} + \frac{\sin \left[\dfrac{\omega a}{c} \ell - n\pi \right]}{\left[\dfrac{\omega a}{c} \ell - n\pi \right]}$$

is the Fourier transform of $\cos \omega_0 t$ normalized by $T/4\pi$. The resulting expression for the scattered pulse is

$$f^S(r, t) = \frac{E_0 c}{r} \frac{T}{4\pi} \, \text{Re} \int_0^\infty \left[\epsilon(\omega) \circledast \bar{\Phi} \, (\omega a/c, \, \ell, \, n) \right]$$

$$e^{-i(\omega a/c)\tau} \, G^*(\omega a/c) \, d \, (\omega a/c) \quad . \qquad (4.59)$$

Normalizing $f^S(r, t)$ with $\dfrac{E_o c}{r} (T/4\pi)$ yields the final expression

$$f^S_N(r, t) = \text{Re} \int_0^\infty \left[\epsilon(\omega) \circledast \Phi\left(\frac{\omega a}{c}, \ell, n\right)\right] e^{-i(\omega a/c)\tau}$$

$$G^*(\omega a/c) \, d \,(\omega a/c) \quad . \tag{4.60}$$

4.4.3 Computations

(U) The integral expression (4.56) and (4.60) have been used for numerical computations for an incident-pulse of the form

$$f^i(r, t) = \begin{cases} \cos \omega_o t & ; \quad |t| < T/2 \\[2ex] 0 & ; \quad |t| > T/2 \end{cases} \quad .$$

The convolution integral in this case becomes

$$f^S_N(r, t) = \int_{-1}^{+1} \frac{\sin 50 \,(\tau + \ell\psi)}{\tau + \ell\,\psi} \cos n\pi\,\psi \, d\psi$$

$$+ \int_{-1}^{+1} \left[\int_0^{50} \left\{ \cos\left[(\omega a/c)\,(\tau + \ell\,\psi)\right] \, S_1(\omega a/c) \right.\right.$$

$$\left.\left. + \sin\left[(\omega a/c)\,(\tau + \ell\,\psi)\right] \, S_2(\omega a/c) \right\} \, d\,(\omega a/c) \right]$$

$$\cdot \cos n\,\pi\,\psi \, d\psi - \begin{cases} \dfrac{\pi}{\ell}\cos\,(n\pi/\ell)\tau & ; \quad |\tau| < \ell \\[1ex] 0 & ; \quad |\tau| > \ell \\[1ex] \dfrac{\pi}{2\ell}\cos n\pi & ; \quad |\tau| = \ell \end{cases} \tag{4.61}$$

The inverse Fourier integral yields, in this case

$$f^S_N(r, t) = Re \int_0^\infty \oint (\frac{\omega a}{c}, \ell, n) e^{-i(\omega a/c)\tau} G^*(\omega a/c)d(\omega a/c) \qquad (4.62)$$

since

$$\left[\epsilon(\omega) \circledast \oint (\frac{\omega a}{c}, \ell, n)\right] = \left[\delta(\omega) \circledast \oint (\frac{\omega a}{c}, \ell, n)\right] = \oint (\frac{\omega a}{c}, \ell, n) \qquad (4.63)$$

The integrals (4.61) and (4.62) were programmed and evaluated for the case of $\ell = 1/4$, $n = 4$ and for $-1/4 \leq \tau \leq 7.0$. The results are shown in Figs. 4-7, 4-8 and 4-9. The two methods agree very closely with the inverse Fourier integral method, being much shorter in computer time (by a factor of about 3).

(U) In Fig. 4-7 the specular pulse return is graphed for $|\tau| \leq 1/4$, and it shows slight distortion as τ approaches $\pm 1/4$. Figure 4-8 indicates that the creeping wave return has considerably deteriorated from the original incident pulse shape, however it still exhibits four oscillations clearly ($n = 4$). Figure 4-9 shows the intermediate range as evaluated by the Fourier integral for $1/4 < \tau < 4.5$. It should be noted that in Fig. 4-8 more points were available for the convolution integral computation which could very well explain some of the apparent discrepancies between the inverse Fourier integral and convolution integral plots.

(U) Due to the advantage of shorter time for computations, the inverse Fourier integral was used for $\ell = 1/4$, $n = 1$ and $-1/4 \leq \tau \leq 7.0$ (Figs. 4-10, through 4-13). This computation was performed to check with the corresponding case of J. Rheinstein (1966) and the agreement was found to be very close. Note that as n increases the amplitude of the creeping wave decreases very considerably (this may be observed in both our results and Rheinstein's). This
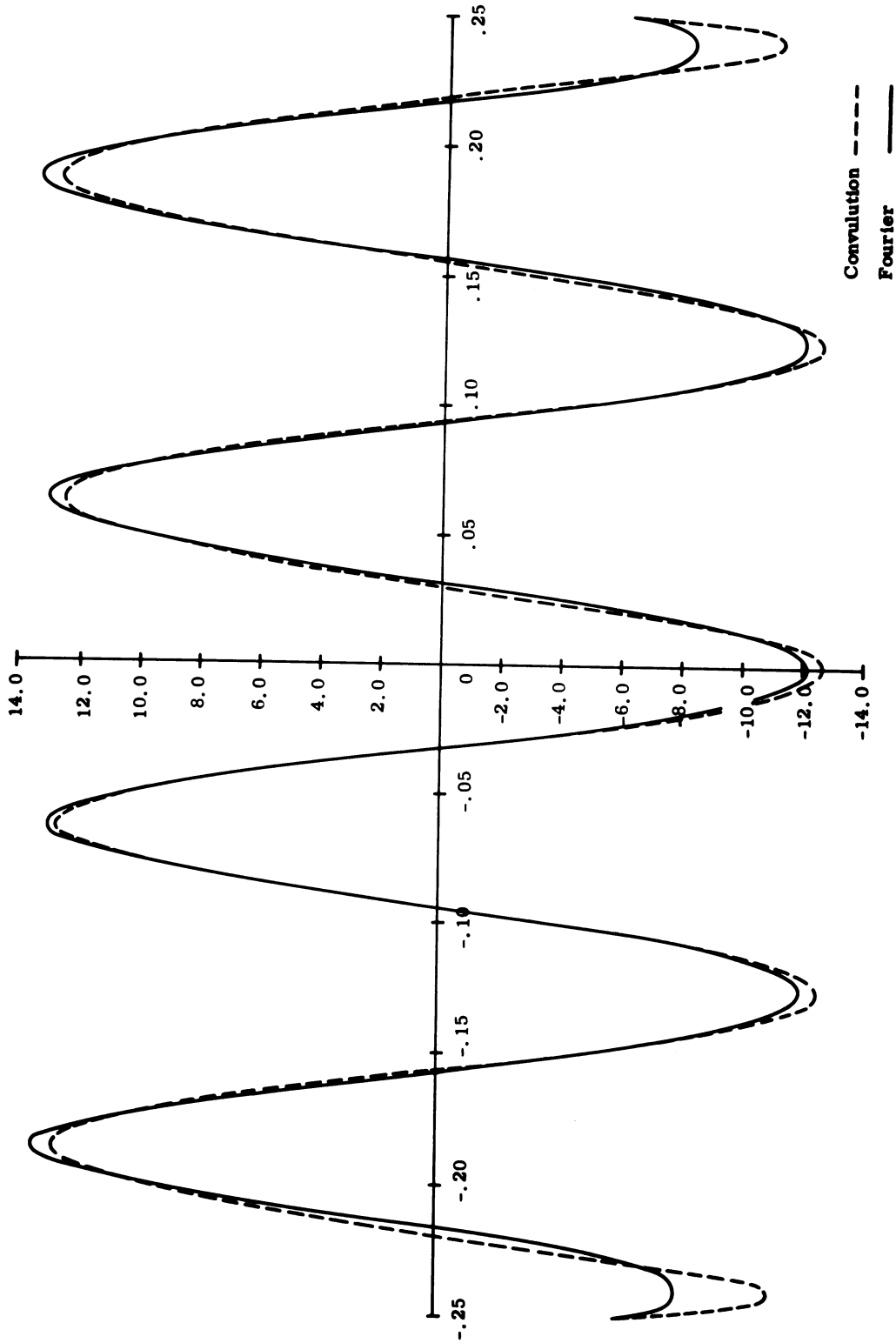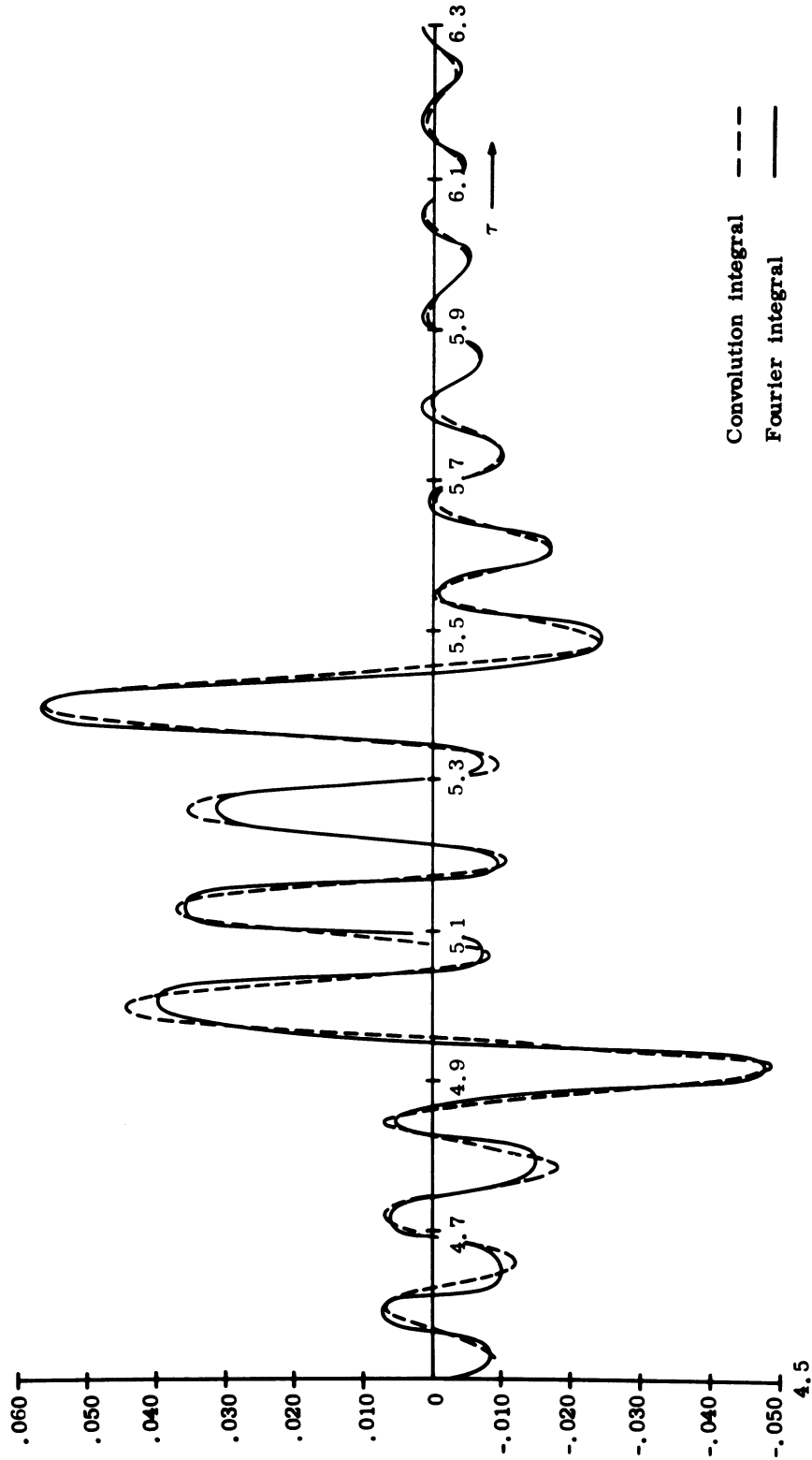
FIG. 4-7: SPECULAR RETURN (n = 4, ℓ = 1/4).
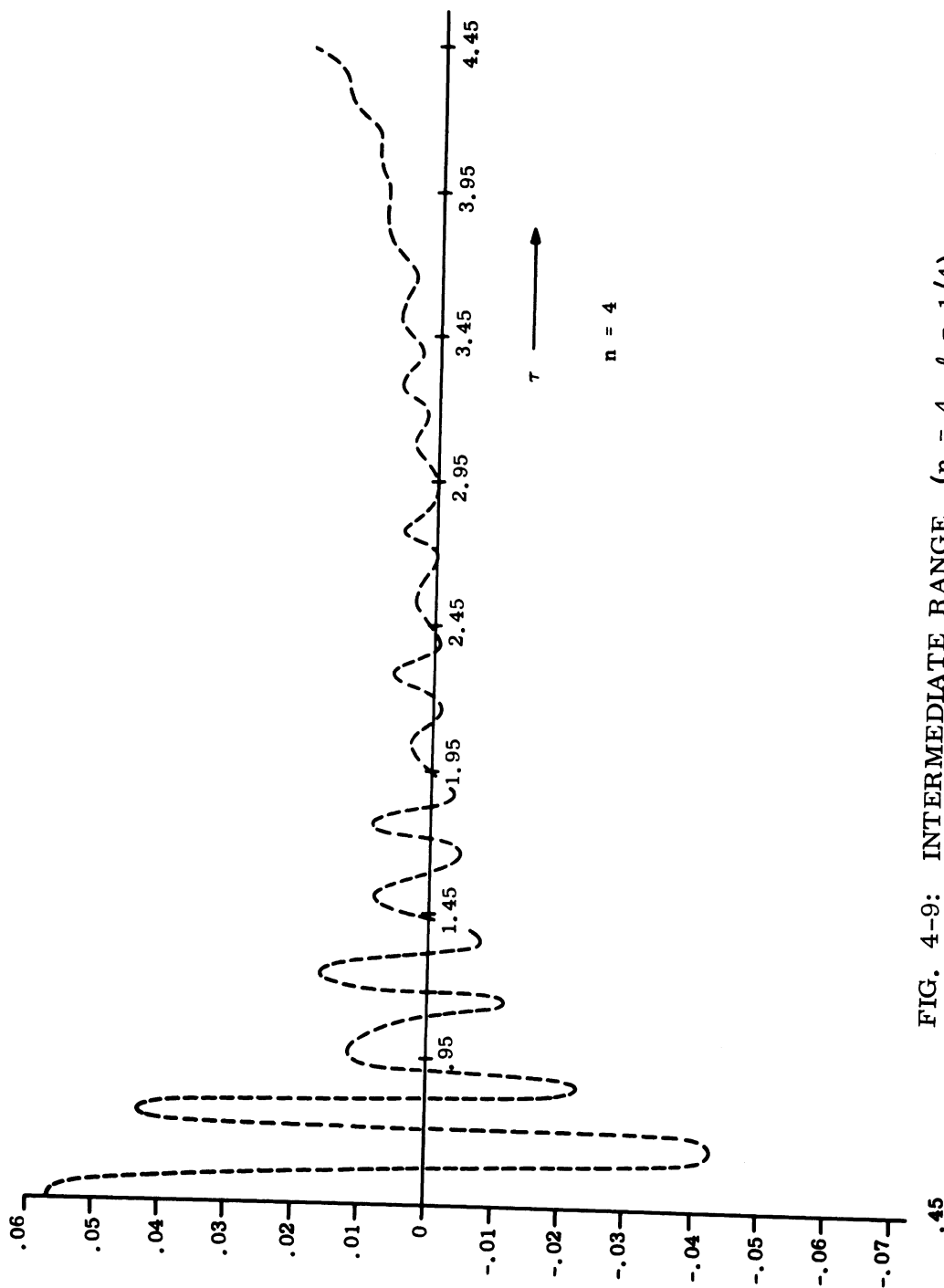
FIG. 4-8: CREEPING WAVE RETURN, (n = 4, ℓ = 1/4).
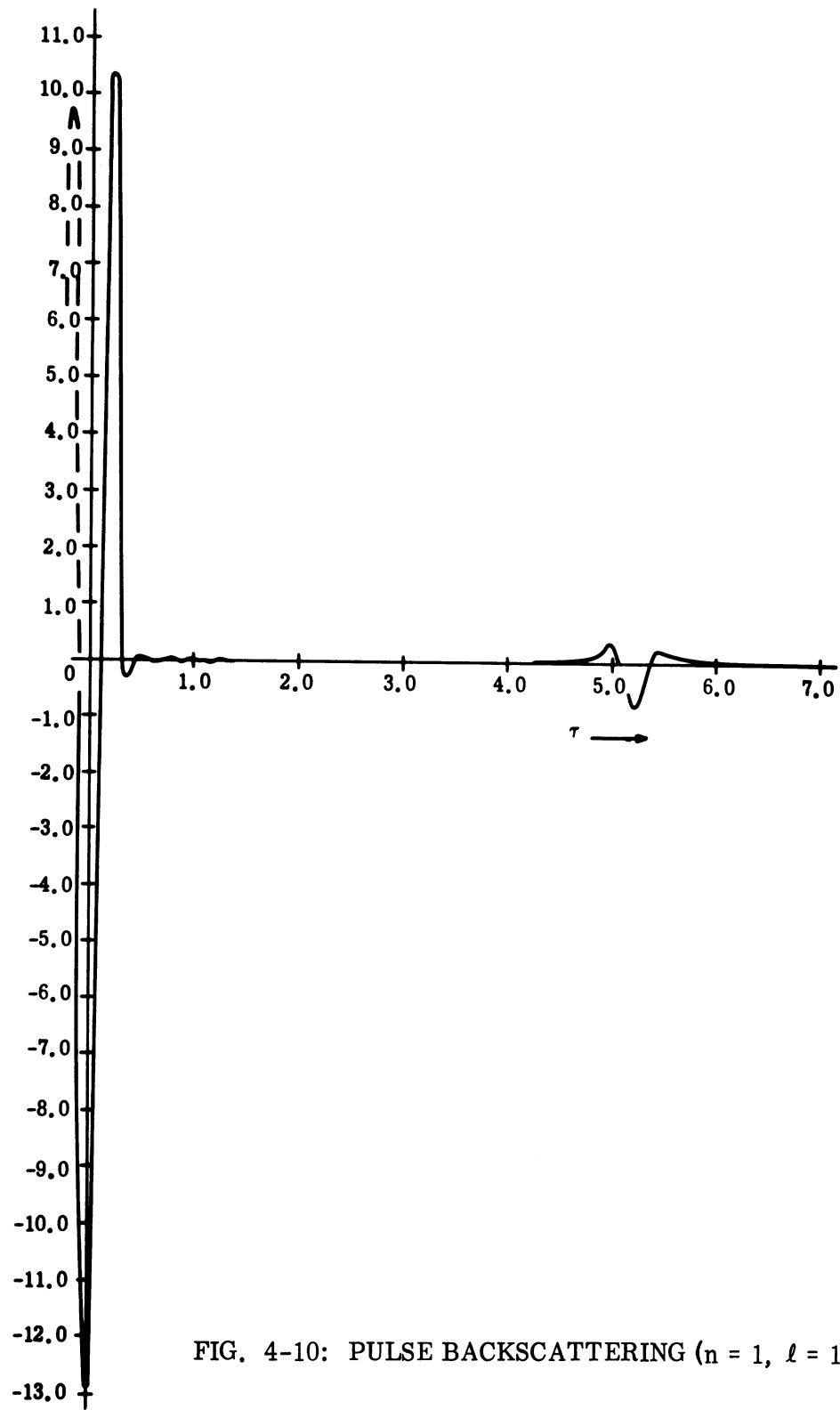
FIG. 4-9: INTERMEDIATE RANGE, (n = 4, ℓ = 1/4).

FIG. 4-10: PULSE BACKSCATTERING ($n = 1$, $\ell = 1/4$).
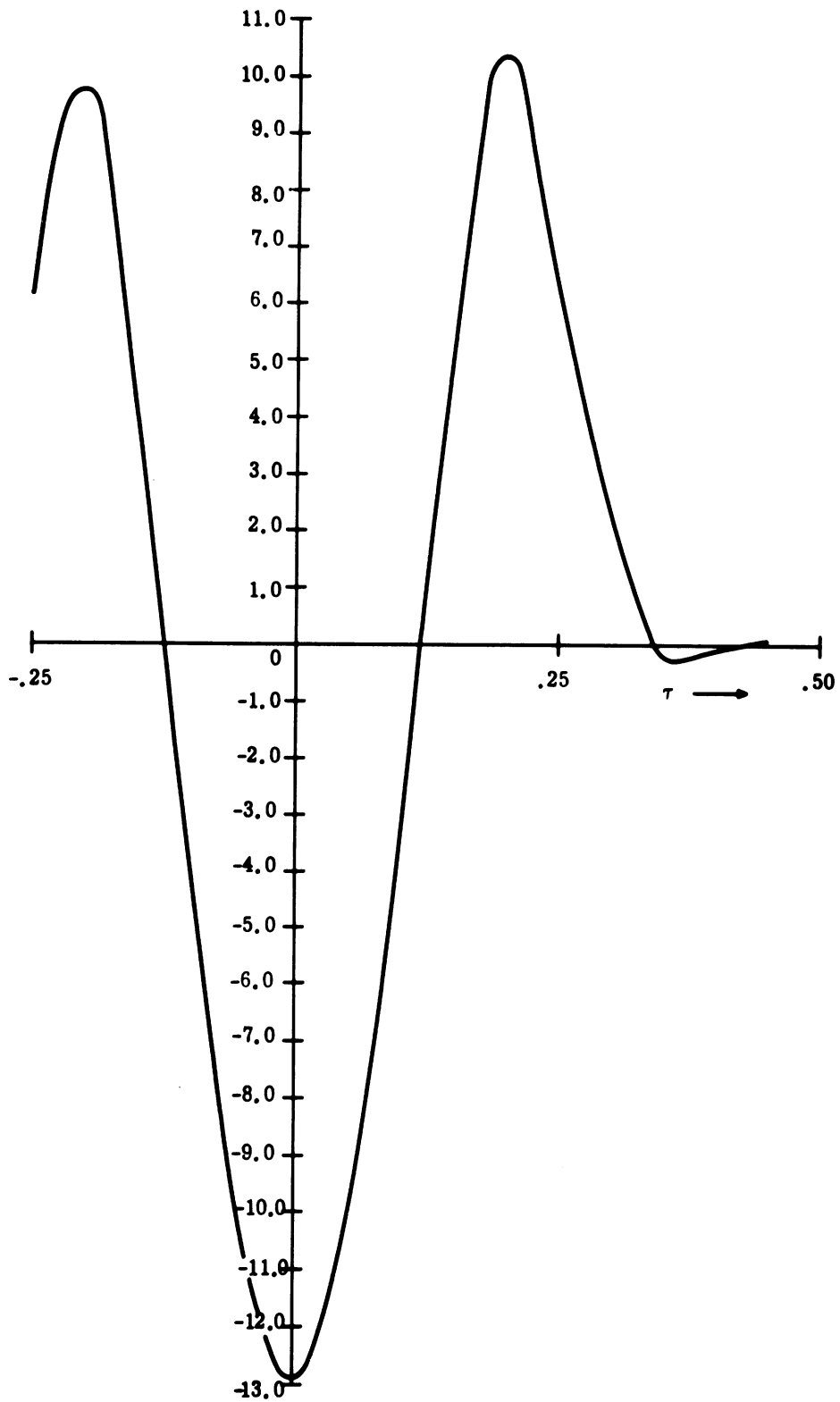
FIG. 4-11: SPECULAR RETURN, (n = 1, ℓ = 1/4).

224
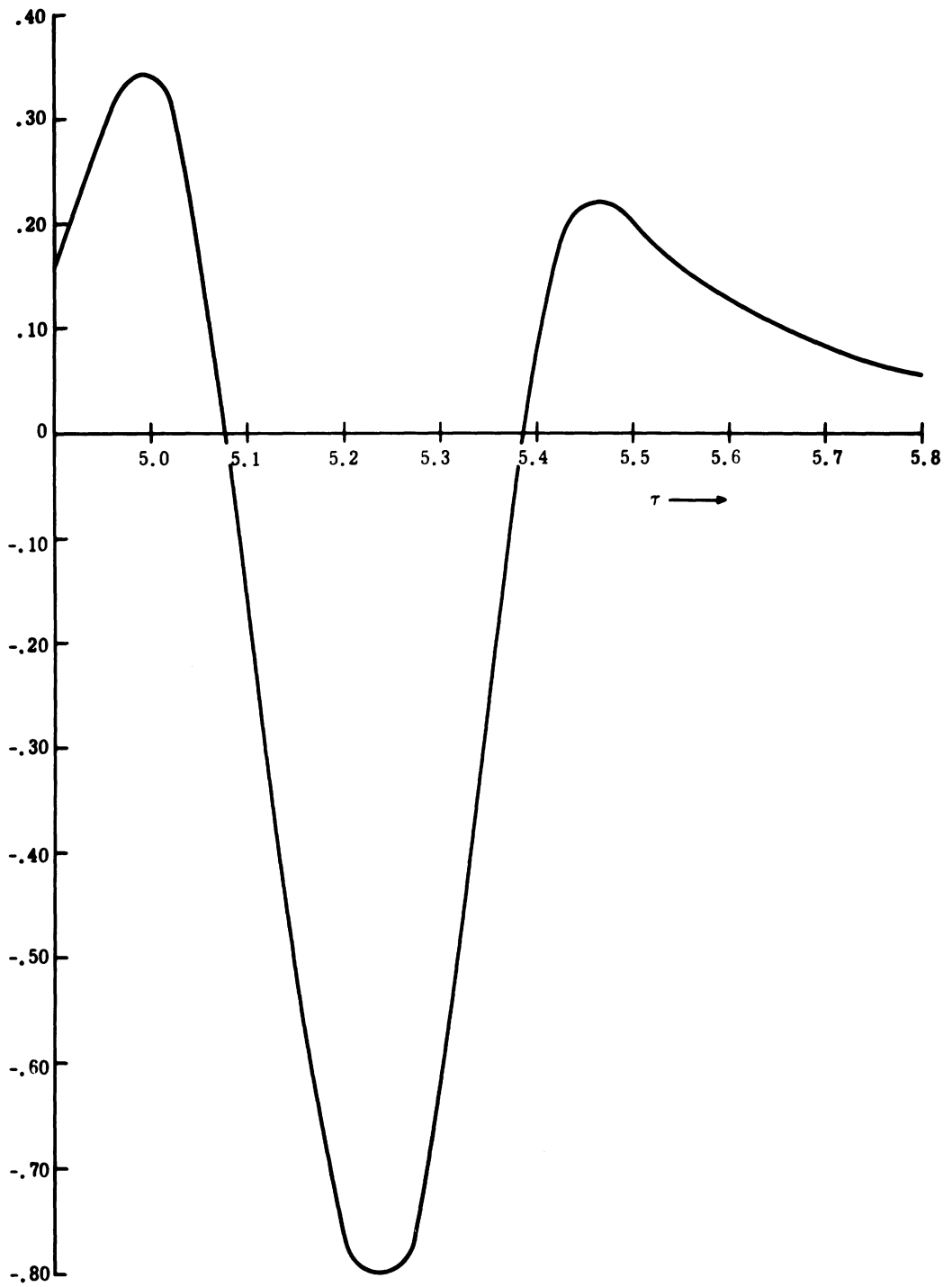
FIG. 4-12: CREEPING WAVE RETURN, (n = 1, ℓ = 1/4).
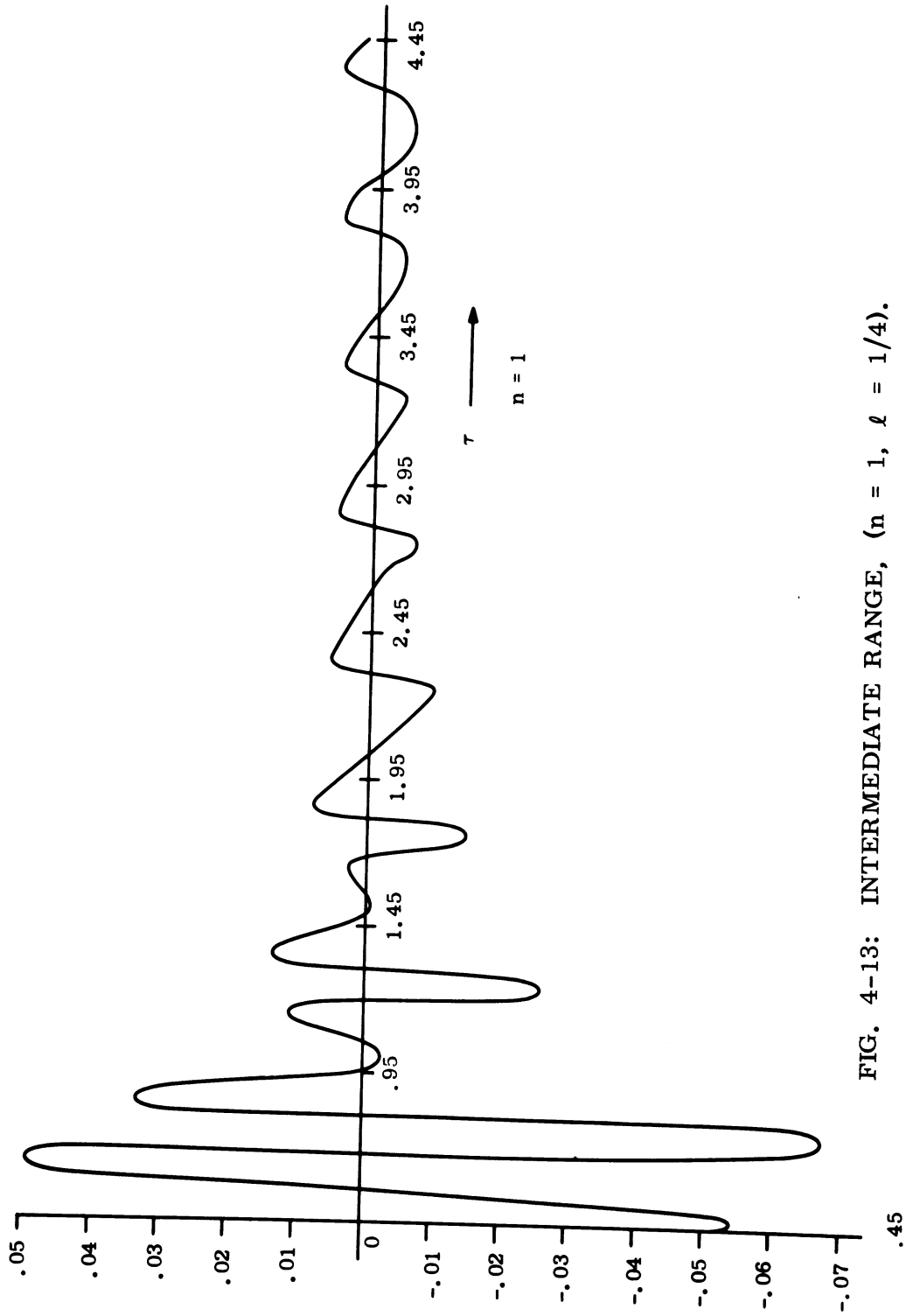
FIG. 4-13: INTERMEDIATE RANGE, (n = 1, ℓ = 1/4).

means not only that the creeping wave amplitude decays as frequency increases for a fixed sphere and pulse width (which is to be expected) but also that this amplitude decreases as pulse width increases for a fixed sphere and constant center frequency.

V

ACKNOWLEDGEMENTS

(U) In addition to the work of the principal authors, the report contains
contributions or summarizes the work of the following investigators:

1. Experimental Investigations

D. Brandenburg
L. Brown
E. Bublitz
C. Grabowski

2. Surface Field Analysis

C. Den
S-J Houng
T.B.A. Senior
L. Zukowski

3. Re-entry Plasma Investigation

J. Bowman
D. Levine
T. Smith
C. Yeh

4. Computer Programming

T. Boynton
R. Lyjak
F. Stenger
P. Wilcox

5. Short Pulse Investigation

N. Alexopoulos
E. Ar
J. Soper
H. Weil

This entire Appendix is Unclassified

APPENDIX A

A PERTURBATION SCHEME FOR THE DIFFRACTION OF EM WAVES BY AN IMPERFECTLY CONDUCTING BODY.

A. 1 Introduction

(U) In one of Maue's early papers (1949), he employed Franz's integral formulation (1948) for the electromagnetic field in free space bounded by a closed surface and derived two integral equations for the tangential electric and magnetic fields on the surface of the obstacle respectively. In this formulation the obstacle is assumed to be a perfect conductor. If the obstacle is not perfectly conducting, in general the interior problem as well as exterior problem of the obstacle must be considered. However, if only the field components exterior to the obstacle are of interest, we may assume that the tangential electric field and the tangential magnetic field on the surface of the obstacle satisfy the boundary condition

$$\underline{E} - (n \cdot \underline{E}) \, \hat{n} = \eta \, Z_o \, \hat{n} \times \underline{H}$$

i.e.,

$$\underline{E}_t = \eta \, Z_o \, \hat{n} \times \underline{H}_t \, , \tag{A.1}$$

and obtain integral equations for E_t and H_t. In Eq. (A. 1) $\eta \, Z_o$ denotes the surface impedance, Z_o, the free space intrinsic impedance and n, the outward normal from the surface of the obstacle. This approach theoretically, is only approximately correct since condition (A. 1) is also an approximation (Senior, 1961). In the next two sections, we will obtain an integral equation for H_t and then propose a scheme to decompose this integral equation to an infinite set of integral equations. In Section A.4, as an example, a justification of the scheme is illustrated by applying it to diffraction from a cylinder of finite conductivity.

A.2   Formulation of Integral Equation

(U) In an empty space bounded by a closed surface S_o, Maxwell's equation can be written as

$$\nabla \times \vec{E} = i\omega\mu_o \vec{H} \quad , \quad \nabla \times \vec{H} = -i\omega\epsilon_o \vec{E}$$

and the integral presentations of the E and H fields are of the form

$$\vec{E}(\vec{r}') = \oiint_{S_o} \nabla g_o \times (\vec{E} \times \hat{n}) \, ds$$

$$- \frac{1}{i\omega\epsilon_o} \nabla' \times \oiint_{S_o} \nabla g_o \times (\vec{H} \times \hat{n}) \, ds \quad , \qquad (A.2)$$

and

$$\vec{H}(\vec{r}') = \oiint_{S_o} \nabla g_o \times (\vec{H} \times \hat{n}) \, ds$$

$$+ \frac{1}{i\omega\mu_o} \nabla' \times \oiint_{S_o} \nabla g_o \times (\vec{E} \times \hat{n}) \, ds \qquad (A.3)$$

respectively, where the prime system indicates the coordinates of observation, the unprime system denotes the coordinates of integration and g_o is the free space Green's function given by

$$g_o = \frac{1}{4\pi} \frac{e^{ik\,r_{pQ}}}{r_{pQ}} \qquad (A.4)$$

230

where

$$r_{pQ} = \left| \underrightarrow{r'} - \underrightarrow{r} \right| \quad . \tag{A.5}$$

One may regard that the surface S_o consists of three parts; i.e., the source, the obstacle and surface at infinity and then (A.2) and (A.3) reduce to the form

$$\underrightarrow{E}(\underrightarrow{r'}) = \underrightarrow{E}_o(\underrightarrow{r'}) - \frac{1}{i\omega\epsilon_o} \nabla' \times \oiint_S \nabla g_o \times (\underrightarrow{H} \times \hat{n}) \, ds$$

$$+ \oiint_S \nabla g_o \times (\underrightarrow{E} \times \hat{n}) \, ds \quad , \tag{A.6}$$

and

$$\underrightarrow{H}(\underrightarrow{r'}) = \underrightarrow{H}_o(\underrightarrow{r'}) + \oiint_S \nabla g_o \times (\underrightarrow{H} \times \hat{n}) \, ds$$

$$+ \frac{1}{i\omega\mu_o} \nabla' \times \oiint_S \nabla g_o \times (\underrightarrow{E} \times \hat{n}) \, ds \tag{A.7}$$

where $\underrightarrow{E}_o(\underrightarrow{r'})$ and $\underrightarrow{H}_o(\underrightarrow{r'})$ are the electric vector and the magnetic vector of the incident wave, and S represents the surface of the obstacle. If we let

$$\underrightarrow{F} = \hat{n} \times \underrightarrow{H} \quad \text{on } S \tag{A.8}$$

and substitute (A.1) in (A.6) and (A.7), we arrive at

$$\underrightarrow{E}(\underrightarrow{r'}) = \underrightarrow{E}_o(\underrightarrow{r'}) + \frac{1}{i\omega\epsilon_o} \nabla' \times \oiint_S \nabla g_o \times \underrightarrow{F} \, ds$$

$$- \eta \, Z_o \oiint_S \nabla g_o \times (\hat{n} \times \underrightarrow{F}) \, ds \tag{A.9}$$

and

$$H(r') = H_0(r') - \oiint_S \nabla g_0 \times F \, dS$$

$$- \frac{n}{ik} \nabla' \times \oiint_S \nabla g_0 \times (n \times F) \, dS \quad . \tag{A.10}$$

It is seen from (A.9) and (A.10) that the field at any point r' except on the surface S is determined if F can be found by some means.

(U) We note that in Eqs. (A.2) and (A.3), the field point $P(r')$ is arbitrary but not on the surface S_0. Now if we let P approach towards that surface, the left hand side of (A.2) and (A.3) will be reduced by one half. For this reason, in Eq. (A.10), we choose $P(r')$ on S and cross multiply the whole equation with $\hat{n}'$, then we obtain

$$\frac{1}{2} F(r') = - H_0(r') \times \hat{n}' + \oiint_S (\nabla g_0 \times F) \times \hat{n}' \, ds$$

$$- \frac{n}{ik} \hat{n}' \times \nabla' \times \oiint_S \nabla g_0 \times (\hat{n} \times F) \, ds. \tag{A.11}$$

Equation (A.11) is an integral equation of second kind with $F(r')$ as the function to be determined.

(U) From Eq. (A.8), one notes that if the material making up the obstacle is of infinite conductivity, F represents the surface current. If the obstacle is not a perfect conductor, strictly speaking, there is no surface cur-

rent, however, since we employ the impedance boundary condition (A.1), we may disregard the fields inside the surface, and assume an equivalent surface current at the interface to support the outside magnetic field.

A.3 Perturbation Scheme

(U) In the previous analysis, we have implicitly used the assumption that the material making up the obstacle is homogeneous and isotropic. Under that assumption we see that η is independent of the spatial variable and if we set

$$\vec{F} = \vec{F}_0 + \eta \vec{F}_1 + \eta^2 \vec{F}_2 + \eta^3 \vec{F}_3 + \ldots \tag{A.12}$$

then all the vectors $\vec{F}$, $\vec{F}_0$, $\vec{F}_1$, ... are in the same direction. Furthermore $\vec{F}$ will approach $\vec{F}_0$ as $\eta \to 0$. The last statement implies that one may call $\vec{F}_0$ the surface current density of a perfectly conducting obstacle.

(U) Upon substituting (A.12) in (A.11) and equating the coefficients of like power of η we obtain

$$\frac{1}{2} \vec{F}_0(\vec{r}') - \iint_S (\nabla g_0 \times \vec{F}_0) \times \hat{n}' \, ds = - \vec{H}_0(\vec{r}') \times \hat{n}' \, , \tag{A.13}$$

and

$$\frac{1}{2} \vec{F}_n(\vec{r}') - \iint_S (\nabla g_0 \times \vec{F}_n) \times \hat{n}' \, ds$$

$$= - \frac{1}{ik} \hat{n}' \times \left[\nabla' \iint_{S_0} \nabla g_0 \times (\hat{n} \times \vec{F}_{n-1}) \, ds \right] . \tag{A.14}$$

$$n = 1, 2, \ldots$$

The set of integral equations (A.13) and (A.14) are of the same form as Maue's integral equation. In fact, Eq. (A.13) is exactly Maue's integral equation. It appears that if one knows how to solve Maue's integral equation for the obstacle of a specific geometrical configuration, one also knows how to solve the higher order correction terms. In the following section, we will justify the above statements with an example.

A.4 Diffraction from a Cylinder of Finite Conductivity.

(U) We consider an infinitely long circular cylinder of finite conductivity exposed to a plane electromagnetic wave at normal incidence. The cylinder is so oriented that its axis is parallel to the magnetic field of the incident wave. We further assume that the use of the boundary condition (A.1) takes care of the effect that the cylinder is an imperfect conductor. Let the radius of the cylinder be a and its axis be the z-axis of the cylindrical coordinates. Evidently, the only non-zero field components are H_z, E_ϕ and E_r. Thus the equivalent surface current density $\underline{F}$ becomes $F = -\hat{y}\, F_\phi$ where F is the sum of a series of the form

$$F = F_{o\phi} + \eta\, F_{1\phi} + \eta^2\, F_{2\phi} + \ldots \quad .\tag{A.15}$$

Because H_z is independent of z, the function $F_{n\phi}$ is also independent of z. Applying (A.13) and (A.14) to the above problem, this set of integral equation yield to the forms

$$F_{o\phi} - \frac{ia}{2} \int_0^{2\pi} F_{o\phi}\, \frac{\partial}{\partial r}\, H_o^{(1)}(k\rho_{pQ}) \Bigg|_{r = r' = a} d\phi$$

$$= -2\, H_o(a,\, \phi') \quad ,\tag{A.16}$$

and

$$F_{n\phi} - \frac{ia}{2} \int_0^{2\pi} F_{n\phi} \frac{\partial}{\partial r} H_o^{(1)} (k \rho_{pQ}) \bigg|_{r = r' = a} d\phi$$

$$= - \frac{ka}{2} \int_0^{2\pi} F_{n-1, \phi} \sum_{m=0}^{\infty} \epsilon_n J_m(k_o a) H_m^{(1)} I(k_o a) \cos m (\phi - \phi) d\phi \tag{A.17}$$

where

$$\rho_{pQ} = \sqrt{r^2 + r'^2 - 2 rr' \cos (\phi' - \phi)} \ . \tag{A.18}$$

Since $H_o^{(1)}(k\rho_{pQ})$ is symmetric with respect to r and r', for $r = r' = a$

$$\frac{\partial}{\partial r} H_o^{(1)}(k_o \rho_{pQ}) = \frac{\partial}{\partial r'} H_o^{(1)}(k_o \rho_{pQ}) = \frac{1}{2} \frac{\partial}{\partial a} H_o^{(1)}(k\rho_{pQ}) \ .$$

Assuming that

$$F_{n\phi} = \sum_{m=0}^{\infty} C_m^{(n)} \cos m\phi \ , \ n = 0, 1, 2, \ldots, \tag{A.19}$$

and using the well known addition formula

$$H_o^{(1)}(k_o \rho_{pQ}) = \sum_{m=0}^{\infty} \epsilon_m J_m(k_o r) H_m^{(1)}(k_o r') \cos m (\phi' - \phi) \ , \tag{A.20}$$

for $r' > r$

Eqs. (A.16) and (A.17) become

$$\sum_{m=0}^{\infty} C_m^{(n)} \left[1 - \frac{i\pi a}{2} \frac{\partial}{\partial a} \left[J_m(k_o a) H_m^{(1)}(k_o a) \right] \right] \cos m\phi'$$

$$= - 2 H_o (a, \phi') \text{ for } n = 0$$

$$= - \pi k_o a \sum_{m=0}^{\infty} C_m^{(n-1)} J_m(k_o a) H_m^{(1)}(k_o a) \cos m\phi', \qquad (A.21)$$

for $n \neq 0$.

Employing the Wronskian

$$J_m(k_o a) H_m^{(1)}(k_o a) - J_m'(k_o a) H_m^{(1)}(k_o a) = \frac{2i}{\pi k_o a} \qquad (A.22)$$

and assuming that the magnetic vector of the incident wave is of the form

$$H_o(a, \phi) = e^{jka \cos \phi'} = \sum_{m=0}^{\infty} \epsilon_m i^m J_m(k_o a) \cos m\phi' \qquad (A.23)$$

then Eq. (A.21) yields to a form as

$$\sum_{M=0}^{\infty} C_m^{(n)} J_m(k_o a) H_m^{(1)'}(k_o a) \cos m\phi'$$

$$= - \frac{2i}{\pi k_o a} \sum_{m=0}^{\infty} \epsilon_m J_m(k_o a) \cos m\phi', \quad n = 0$$

$$= - i \sum_{m=0}^{\infty} C_m^{(n-1)} J_m(k_o a) H_m^{(1)}(k_o a) \cos m\phi'. \quad n \neq 0 \quad (A.24)$$

From the last expression, we obtain the recurrence formula for the unknown coefficients $C_m^{(n)}$ as

$$C_m^{(0)} = -\frac{2i}{\pi k_o a} \frac{1}{H_m^{(1)'}(k_o a)}$$

$$C_m^{(n)} = -i \frac{H_m^{(1)}(k_o a)}{H_m^{(1)'}(k_o a)} C_m^{(n-1)} \quad , \quad n \neq 0 \quad . \tag{A.25}$$

(U) The conventional method gives

$$F_y = -\frac{2i}{\pi k_o a} \sum_{m=0}^{\infty} \epsilon_m i^m \frac{\cos m y'}{H_m^{(1)'}(k_o a) + i \eta H_m^{(1)}(k_o a)} \quad . \tag{A.26}$$

if

$$\left| i \eta \frac{H_m^{(1)}(k_o a)}{H_m^{(1)'}(k_o a)} \right| < 1$$

employing the binomial expansion, we obtain

$$F_y = -\frac{2i}{\pi k_o a} \sum_{m=0}^{\infty} \frac{\epsilon_m i^m \cos m y}{H_m^{(1)'}(k_o a)} \left[\sum_{n=0}^{\infty} (-i \eta \frac{H_m^{(1)}(k_o a)}{H_m^{(1)'}(k_o a)})^n \right] \tag{A.27}$$

We note that the result given by (A.27) agrees with the result by the previous method.

REFERENCES

Abramowitz, M. and I.A. Stegun (1964) Handbook of Mathematical Functions with Formulas, Graphs and Mathematical Tables, NBS Appl. Math. Series 55, Washington D.C. p. 256.

Bechtel, M.E. (1962) "Scattering Coefficients for the Backscattering of Electromagnetic Waves from Perfectly Conducting Spheres," Cornell Aeronautical Laboratory, Inc., Cornell University.

Bird, R.B., W.E. Steward, and F.N. Lightfoot, (1960) Transport Phenomena, John Wiley and Sons Co., Inc., New York.

Blottner, F.G. (1964) "Nonequilibrium Laminar Boundary-Layer Flow of Ionization," AIAA J. 2, pp. 1921-1927.

Bortner, M.H., (1963) "Chemical Kinetics in a Re-entry Flow Field," G.E. Tech. Information Series R635D63.

Brekhovskikh, L.M. (1960) Waves in Layered Media, Academic Press, New York, Chapter IV.

Budden, K.G. (1961) Radio Waves in the Ionosphere, University Press, Cambridge, Great Britain.

Castellanos, D. (1966) "Notes on Electromagnetic Scattering from Rotationally Symmetric Bodies with an Impedance Boundary Condition," The University of Michigan Radiation Laboratory Report No. 7741-1-T.

Den, Chi-Fu (1967) "A Perturbation Scheme for the Diffraction of EM Waves by an Imperfectly Conducting Body," The University of Michigan Radiation Laboratory Memorandum 8525-514-M (Appendix A).

Dorrance, W.H. (1962) Viscous Hypersonic Flow, McGraw-Hill Book Co., Inc. New York.

Franz, W. (1948) "Zur Formulierung des Huygensschen Prinzips," Z. Naturforsch. 3a 500-506.

Fock, V. (1946), "The Distribution of Currents Induced by a Plane Wave on the Surface of a Conductor," J. Phys., 10, p. 130.

Forsterling K. and H. Wüster (1951) "Uber die Enstehung von Oberwellen in der Ionosphere," Journal Atmos. Terr. Phys. 2, No. 1, pp. 22-31.

Glick, H.S. (1962) "Interaction of Electromagnetic Waves of Hypersonic Flows," ARS J. 32, pp. 1359-1364.

Goodrich, R.F., B.A. Harrison, R.E. Kleinman, and T.B.A. Senior, (1961) "Studies in Radar Cross Sections XLVII Diffraction and Scattering by Regular Bodies-I: The Sphere," The University of Michigan Radiation Laboratory Report No. 3648-1-T, AD 273006 UNCLASSIFIED.

Goodrich, R.F., B.A. Harrison, R.E. Kleinman, E.F. Knott, T.M. Smith and V.H. Weston (1967) "Investigation of Re-entry Vehicle Surface Fields (U)," The University of Michigan Radiation Laboratory Report No. 8525-1-Q, AD 382537-L SECRET-4.

Hayes, W.D. and R.F. Probstein, (1959) Hypersonic Flow Theory, Academic Press, New York.

Hirschfelder, J.O., C.F. Curtiss and R.B. Bird (1963) Molecular Theory of Gases and Liquids, John Wiley and Sons Co., Inc., New York.

Holt, E.H., and R.E. Haskell, (1965) Foundations of Plasma Dynamics, Macmillan Co., New York.

Hong, S. (August, 1966) "Asymptotic Theory of Diffraction by Smooth Convex Surfaces of Variable Curvature," The University of Michigan Radiation Laboratory Report No. 07741-2-T, AD 804916 UNCLASSIFIED.

Horton, C.W. and R.B. Watson (1954) "On the Backscattering of Radar Waves from the Traveling Edge of an Aircraft Wing," Texas J. Sci. 6, pp. 392-398.

Howard, D.D. and N.A. Thomas (1963) "The Dielectric Rod as an Unusually Effective Radar Reflector," Proc. NEC 19, pp. 72-78.

Ivanov, V.I., (1960) Radiotekhnika i elektronika, 5, 393.

Johnson, C.C. (1965) Field and Wave Electrodynamics, McGraw-Hill Book Co., Inc., New York, pp. 325-333.

Keller, J.B. (1956) "Diffraction by a Convex Cylinder," IRE. Trans. AP-4, p. 312.

Keller, J.B. and B.R. Levy (1959) "Decay Exponents and Diffraction Coefficients for Surface Waves on Surfaces of Nonconstant Curvature," IRE Trans. AP-7, S 52.

Kennaugh, E.M. (1961) "The Scattering of Transient Electromagnetic Waves by Finite Bodies," Final Engineering Report. The Antenna Laboratory, The Ohio State University.

Kiely, D.G. (1953), Dielectric Aerials, Matheuen's Monographs on Physical Subjects.

Kline M., and I.W. Kay (1965) Electromagnetic Theory and Geometrical Optics, Interscience Publishers, Chapters 5 and 6.

Lebedev, N.N. (1946) "Sur une Formule D'inversion" Comptes Rendus (Doklady) De l'Academie des Sciences de e'URSS Vol. 52, No. 8 pp. 655-658.

Lenard, M. (1964) "Chemically Reacting Boundary Layers," G.E. Tech. Information Series R645D14.

Levy, B.R. and J.B. Keller (January, 1958) "Propagation of Electromagnetic Pulses Around the Earth, IRE Trans. AP-6.

Lewis, R.M. and J.B. Keller (January, 1964), "Asymptotic Methods for Partial Differential Equations: The Reduced Wave Equation and Maxwell's Equations," New York University Research Report, EM-194.

Luke, Y. L. (1962) Integral of Bessel Functions, McGraw-Hill Book Company Inc., New York p. 325.

Magnus, W. (1941) "Ober die Beugung dektromagnetischer Wellen an einer Halbebene," Zeitschrift für Physik, B. 117 S. 168-179.

Maue, A.W. (1949) "On the Formulation of a General Diffraction Problem Through an Integral Equation," Zeitschrift fur Physik, Bd. 126 S. 601-618.

Meixner, J. (1949) "Die Kantenbedingung in der Theorie der Beugung electromagnetischer Wellen an Volkommen leitenden ebenen Schirmen, " Ann. der Physik, 6, pp. 2-9.

Miller, G. F. (August 1962) "Propagation of Electromagnetic Waves in a Nonuniformly Ionized Medium, " Physics of Fluids, 5, No. 8.

Oberhettinger, F. (1954) "Diffraction of Waves by a Wedge," Com. Pure and Appl. Math. Vol. 7, No. 3, pp. 551-563.

Oberhettinger, F. and T. P. Higgins (1961) Tables of Lebedev, Mehler, and Generalized Mehler Transforms. Boeing Scientific Research Laboratories.

Pallone, A.J., J.A. Moore, and J.I. Erdos, (1964) "Nonequilibrium, Nonsimilar Solutions of the Laminar Boundary Layer Equations, " AIAA J. 2, 1706-1713.

Peters, L. (1958) "End-fire Echo Area of Long Thin Bodies, " IRE. Trans. AP-6, pp. 133-139.

Rheinstein, J. (1966) "Backscatter from Spheres: A Short Pulse View, " Technical Report No. 414, Lincoln Laboratory, MIT.

Rice, S.O. (1954) "Communication in the Presence of Noise--Probability of Error for Two Encoding Schemes, " Bell System Tech. J. 33, 417.

Senior, T.B.A. (1961) "Impedance Boundary Conditions for Imperfectly Conducting Surfaces, " Appl. Sci. Res., Sec. B. Vol 8, pp. 418-436.

Senior, T.B.A. (1965) "Analytical and Numerical Studies of the Backscattering Behavior of Spheres, " The University of Michigan Radiation Laboratory Report No. 7030-1-T, AD 471260, UNCLASSIFIED.

Taylor, L.S. (1961) "RF Reactance of Plasma Sheaths, " Proc. IRE 99, No. 12.

Wait, J.R. (1960) "Propagation of EM Waves Along a Thin Plasma Sheet, " Can. J. of Phys., Vol. 38 pp. 1586-1594.

DISTRIBUTION LIST

Aerospace Corporation
ATTN: H.J. Katzman,
Bldg. 537, Room 1007
P.O. Box 1308
San Bernardino, CA 92402   Copies 1 - 10 (incl.)

Air Force Cambridge Research Laboratories
ATTN: R. Mack CRDG
L.G. Hanscom Field
Bedford, MA 01730   Copies 11, 12

Advanced Research Projects Agency
ATTN: W. Van Zeeland
The Pentagon
Washington, D.C. 20301   Copies 13, 14

Air University Library
ATTN: AU
Maxwell AFB, AL 36112   Copy 15

Air Force Avionics Laboratory
ATTN: William F. Bahret - AVWE - 2
Wright-Patterson AFB, OH 45433   Copy 16

Space and Missile Systems Organization
ATTN: Capt. J. Wheatley, BSYDP
Norton AFB, CA 92409   Copies 17, 18

Space and Missile Systems Organization
ATTN: BSYLD
Norton AFB, CA 92409   Copies 18, 20

Electronic Systems Division (AFSC)
ATTN: Lt. Nyman ESSXS
L.G. Hanscom Field
Bedford, MA 01730   Copy 21

8525-2-Q

Distribution List (Cont'd)

Institute for Defense Analyses
ATTN: Classified Library
400 Army-Navy Drive
Alexandria, VA 22202   Copy 22

MIT-Lincoln Laboratory Representative
P.O. Box 4188
Norton AFB, CA 92409   Copy 23

MIT-Lincoln Laboratory
BMRS Project Office
P.O. Box 73
Lexington, MA   02173   Copy 24

MIT-Lincoln Laboratory
ATTN: S. Borison
P.O. Box 73
Lexington, MA   02173   Copy 25

MIT-Lincoln Laboratory
ATTN: J. Rheinstein
P.O. Box 73
Lexington, MA 02173   Copy 26

MITRE Corporation
ATTN: P. Waterman
Bedford, MA 01730   Copy 27

North American Space
   and Information Systems
ATTN: S. Wozniak
Tulsa, OK 73100   Copy 28

Special Projects Office,
Bureau of Weapons
ATTN: M. Blum
Washington, D.C. 20301   Copies 29, 30, 31

Distribution List (Cont'd)

Northrop-Norair Division
ATTN: F.K. Oshiro
3901 W. Broadway
Hawthorne, CA 90250   Copy 32

DRC, Inc.
P.O. Box 3587
Santa Barbara, CA 93105   Copy 33

Ship Systems Analysis Branch
U.S. Naval Radiological Defense Lab.
ATTN: SABMIS
San Francisco, CA 94135   Copy 34

Defense Documentation Center
Cameron Station
Alexandria, VA 22314   Copies 35-54
                                                          (incl.)

. . . .

DOCUMENT CONTROL DATA - R&D

(Security classification of title, body of abstract and indexing annotation must be entered when the overall report is classified)

1. ORIGINATING ACTIVITY *(Corporate author)*	2a. REPORT SECURITY CLASSIFICATION
The University of Michigan Radiation Laboratory	SECRET
Department of Electrical Engineering	2b. GROUP
Ann Arbor, Michigan 48108	4

3. REPORT TITLE

Investigation of Re-Entry Vehicle Surface Fields (U)

4. DESCRIPTIVE NOTES *(Type of report and inclusive dates)*

Quarterly Report No. 2, 18 March through 18 June 1967

5. AUTHOR(S) *(Last name, first name, initial)*

Goodrich, Raymond F., Harrison, Burton A., Kleinman, Ralph E.

Knott, Eugene F., and Weston Vaughan H.

6. REPORT DATE	7a. TOTAL NO. OF PAGES	7b. NO. OF REFS
July 1967	241	48

8a. CONTRACT OR GRANT NO.	9a. ORIGINATOR'S REPORT NUMBER(S)
F 04694-67-C-0055	8525-2-Q
b. PROJECT NO.	
c.	9b. OTHER REPORT NO(S) *(Any other numbers that may be assigned this report)*
d.	BSD-TR-67-232

10. AVAILABILITY/LIMITATION NOTICES In addition to security requirements which apply to this document and must be met, this document is subject to special export controls and each transmittal to foreign governments or nationals may be made only with prior approval of SAMSO, SMSDI, Air Force Station, Los Angeles, CA 90045

11. SUPPLEMENTARY NOTES Further distribution by holder made only with specific prior approval of SAMSO, SMSDI, Air Force Station, Los Angeles, CA 90045	12. SPONSORING MILITARY ACTIVITY Hq. Space and Missile Systems Organization Air Force Systems Command Norton Air Force Base, CA 92409

13. ABSTRACT

SECRET

This is the Second Quarterly Report on Contract F 04694-67-C-0055 and covers the period 18 March to 18 June 1967. The report discusses work in progress on Project SURF and on a related short pulse investigation. Project SURF is a continuing investigation of the radar cross section of metallic cone-sphere shaped reentry bodies and the effect on radar cross section of absorber and ablative coatings, antenna and rocket nozzle perturbations, changing the shape of the rear spherical termination, and of the plasma reentry environment. The objective of the short pulse study is the determination of methods of modifying the short pulse signature of cone-sphere shaped reentry bodies and of decoys. SURF investigations make use of experimental measurements in surface field and backscatter ranges to aid in the analytical formulation of mathematical expressions for the computation of radar cross section. A computer program for determining the radar cross section of any rotationally symmetric body is being developed.

DD FORM 1 JAN 64 **1473**

14. KEY WORDS	LINK A		LINK B		LINK C	
	ROLE	WT	ROLE	WT	ROLE	WT
Radar Cross Sections						
Surface Field Measurements						
Cone-Sphere Re-entry Bodies						
Absorber Coatings						
Plasma Re-entry Environment						
Short Pulse Discrimination						

INSTRUCTIONS

1. ORIGINATING ACTIVITY: Enter the name and address of the contractor, subcontractor, grantee, Department of Defense activity or other organization (corporate author) issuing the report.

2a. REPORT SECURITY CLASSIFICATION: Enter the overall security classification of the report. Indicate whether "Restricted Data" is included. Marking is to be in accordance with appropriate security regulations.

2b. GROUP: Automatic downgrading is specified in DoD Directive 5200.10 and Armed Forces Industrial Manual. Enter the group number. Also, when applicable, show that optional markings have been used for Group 3 and Group 4 as authorized.

3. REPORT TITLE: Enter the complete report title in all capital letters. Titles in all cases should be unclassified. If a meaningful title cannot be selected without classification, show title classification in all capitals in parenthesis immediately following the title.

4. DESCRIPTIVE NOTES: If appropriate, enter the type of report, e.g., interim, progress, summary, annual, or final. Give the inclusive dates when a specific reporting period is covered.

5. AUTHOR(S): Enter the name(s) of author(s) as shown on or in the report. Enter last name, first name, middle initial. If military, show rank and branch of service. The name of the principal author is an absolute minimum requirement.

6. REPORT DATE: Enter the date of the report as day, month, year; or month, year. If more than one date appears on the report, use date of publication.

7a. TOTAL NUMBER OF PAGES: The total page count should follow normal pagination procedures, i.e., enter the number of pages containing information.

7b. NUMBER OF REFERENCES: Enter the total number of references cited in the report.

8a. CONTRACT OR GRANT NUMBER: If appropriate, enter the applicable number of the contract or grant under which the report was written.

8b, 8c, & 8d. PROJECT NUMBER: Enter the appropriate military department identification, such as project number, subproject number, system numbers, task number, etc.

9a. ORIGINATOR'S REPORT NUMBER(S): Enter the official report number by which the document will be identified and controlled by the originating activity. This number must be unique to this report.

9b. OTHER REPORT NUMBER(S): If the report has been assigned any other report numbers (either by the originator or by the sponsor), also enter this number(s).

10. AVAILABILITY/LIMITATION NOTICES: Enter any limitations on further dissemination of the report, other than those imposed by security classification, using standard statements such as:

(1) "Qualified requesters may obtain copies of this report from DDC."

(2) "Foreign announcement and dissemination of this report by DDC is not authorized."

(3) "U. S. Government agencies may obtain copies of this report directly from DDC. Other qualified DDC users shall request through
_____."

(4) "U. S. military agencies may obtain copies of this report directly from DDC. Other qualified users shall request through
_____."

(5) "All distribution of this report is controlled. Qualified DDC users shall request through
_____."

If the report has been furnished to the Office of Technical Services, Department of Commerce, for sale to the public, indicate this fact and enter the price, if known.

11. SUPPLEMENTARY NOTES: Use for additional explanatory notes.

12. SPONSORING MILITARY ACTIVITY: Enter the name of the departmental project office or laboratory sponsoring (paying for) the research and development. Include address.

13. ABSTRACT: Enter an abstract giving a brief and factual summary of the document indicative of the report, even though it may also appear elsewhere in the body of the technical report. If additional space is required, a continuation sheet shall be attached.

It is highly desirable that the abstract of classified reports be unclassified. Each paragraph of the abstract shall end with an indication of the military security classification of the information in the paragraph, represented as (TS), (S), (C), or (U).

There is no limitation on the length of the abstract. However, the suggested length is from 150 to 225 words.

14. KEY WORDS: Key words are technically meaningful terms or short phrases that characterize a report and may be used as index entries for cataloging the report. Key words must be selected so that no security classification is required. Identifiers, such as equipment model designation, trade name, military project code name, geographic location, may be used as key words but will be followed by an indication of technical context. The assignment of links, rules, and weights is optional.